



# **Preparation of Labeled Aromatic Amino Acids via Late-Stage $^{18}\text{F}$ -Fluorination of Chiral Nickel and Copper Complexes**

**In a u g u r a l - D i s s e r t a t i o n**

**zur**

**Erlangung des Doktorgrades  
der Mathematisch-Naturwissenschaftlichen Fakultät  
der Universität zu Köln**

**vorgelegt von**

**Austin Craig**

**aus Dublin, Irland**

**Köln, 2021**

Berichtersteller:

**Prof. Dr. Bernd Neumaier**

**Prof. Dr. Hans-Günther Schmalz**

Tag der mündlichen Prüfung: **03.07.2020**

## Abstract

$^{18}\text{F}$ -Labeled aromatic amino acids (AAA) are valuable tools for the detection of oncological and neurological disorders using positron emission tomography (PET). Despite their potential, only a minority of AAA tracers have been applied in clinical diagnostics due to the lack of efficient radiosynthetic protocols available. This work presents a practical procedure for the preparation of ten structurally diverse  $^{18}\text{F}$ -labeled AAA *via* alcohol-enhanced Cu-mediated radiofluorination of chiral Ni- or Cu-[(Benzylpropyl)amino]phenone-glycine/alanine (Ni/Cu-BPX) auxiliaries.

Herein, chiral Ni-BPX (also known as “Belokon”) complexes, which serve as easily-removable dual-protecting group functionalities, are demonstrated to be ideal for synthetic and radiosynthetic purposes. Accordingly, the application of (*S*)-Ni-BPX complexes towards several synthetically challenging  $\alpha$ -methyl-substituted-AAA ( $\alpha$ -Me-AAA) tracers is reported. In addition, the employment of (*R*)-Ni-BPX enabled the novel 3-(*R*)-[ $^{18}\text{F}$ ]fluorophenylalanine (3-(*R*)-[ $^{18}\text{F}$ ]FPhe) tracer to be accessed. The applicability of Cu-BPX complexes towards  $^{18}\text{F}$ -labeled AAA production has also been described for the first time. The application of Cu- instead of Ni-complexes in association with Cu-mediated radiofluorination advantageously requires only a single trace metal to be determined for  $^{18}\text{F}$ -labeled AAA products, in order to fulfill the requirements of current good manufacturing production (cGMP). The methodology, which furnishes  $^{18}\text{F}$ -labeled AAAs in high radiochemical yields (RCY), and excellent enantiomeric and radiochemical purities (RCP), provides significant advancements compared to literary procedures and paves the way for future AAA tracer preparations using the approach outlined herein.

In addition, 3-[ $^{18}\text{F}$ ]fluorophenylserine (3-[ $^{18}\text{F}$ ]FPheSer), a potential noradrenergic system imaging agent, was successfully prepared. As the noradrenergic system is adversely affected by neurological disorders, 3-[ $^{18}\text{F}$ ]FPheSer–PET may afford invaluable diagnostic information.

Finally, a one-step preparation of the promising prosthetic group 4-[ $^{18}\text{F}$ ]fluorophenylboronic acid ([ $^{18}\text{F}$ ]FPBA), previously demonstrated to be suitable for radiolabeling of biopolymers, has been developed.

## Kurzzusammenfassung

$^{18}\text{F}$ -Markierte aromatische Aminosäuren (AAS) sind zu wichtigen diagnostischen Instrumenten zur Erkennung von onkologischen und neurologischen Erkrankungen mit Hilfe der Positronen-Emissions-Tomographie (PET) geworden. Trotz ihres großen Potenzials fanden bisher nur wenige AAS-Tracer Anwendung in der klinischen Diagnostik, da effiziente Syntheseprotokolle für deren Herstellung fehlten. Das Ziel dieser Arbeit war daher die Entwicklung eines praktischen Verfahrens zur Herstellung von  $^{18}\text{F}$ -markierten AAS. Das Markierungsprotokoll basierte auf der alkoholverstärkten Cu-vermittelten Radiofluorierung von chiralen Ni- bzw. Cu-[(Benzylpropyl)amino]phenon-glycin/alanin (Ni/Cu-BPX) Auxiliaren. Mit dem etablierten Radiosyntheseprotokoll konnten insgesamt zehn verschiedene  $^{18}\text{F}$ -markierte AAS hergestellt werden.

Dabei haben sich vor allem chirale Ni-BPX-Komplexe (auch als "Belokon-Komplexe" bekannt), die als leicht entfernbare Dual-Auxiliar-Funktionalitäten dienen, für synthetische und radiosynthetische Zwecke als am besten geeignet herausgestellt. Dementsprechend wird in der vorliegenden Arbeit die Anwendung von (*S*)-Ni-BPX Komplexen auf mehrere, synthetisch anspruchsvolle  $\alpha$ -Me-AAS-Tracer beschrieben. Darüber hinaus ermöglicht der Einsatz von (*R*)-Ni-BPX den Zugang zu dem neuen, äußerst innovativen Tracer 3-(*R*)-[ $^{18}\text{F}$ ]Fluorphenylalanin (3-(*R*)-[ $^{18}\text{F}$ ]FPhe).

Des Weiteren wurde erstmals die Eignung von Cu-BPX-Komplexen für die Radiosynthese von  $^{18}\text{F}$ -markierten AAS beschrieben. Vorteilhaft für den Einsatz von Cu- anstelle von Ni-BPX-Komplexen ist, dass im Fall von Cu-vermittelten *c*GMP-Produktionen nur auf ein Übergangsmetall geprüft werden muss. Im Fall der Ni-BPX Komplexe muss sowohl auf Cu als auch auf Ni geprüft werden. Die beschriebene Methodik, die die Synthese von  $^{18}\text{F}$ -markierten AAS in hohen radiochemischen Ausbeuten (RCY) sowie enantiomeren und radiochemischen Reinheiten (RCP) ermöglicht, liefert bedeutende Fortschritte im Vergleich zu den in der Literatur beschriebenen Verfahren und ebnet den Weg für die eine verbreitete Nutzung von  $^{18}\text{F}$ -markierten AAS in der klinischen Diagnostik mittels PET.

Darüber hinaus wurde 3-[ $^{18}\text{F}$ ]Fluorphenylserin (3-[ $^{18}\text{F}$ ]FPheSer), ein potentieller PET-Ligand, für die Bildgebung des noradrenergen Systems hergestellt. Da das noradrenerge System häufig durch neurologische Erkrankungen geschädigt wird, hat der Radiotracer 3-[ $^{18}\text{F}$ ]FPheSer das Potenzial, wertvolle Informationen für die Diagnose von neurologischen Störungen zu liefern. Schließlich wurde eine einstufige Herstellung der vielversprechenden prosthetischen Gruppe

4- $^{18}\text{F}$ Fluorphenylboronsäure ( $^{18}\text{F}$ FPBA) entwickelt, die sich für die Radiomarkierung von Biopolymeren eignet.

In dieser Arbeit konnte eine innovative Herstellungsmethode für  $^{18}\text{F}$ -markierte AAS entwickelt werden, die die Herstellung der Vorläufer vereinfacht und sich zudem für die routinemäßige Herstellung für diagnostische Zwecke eignet. Darüber hinaus konnten effiziente Herstellungsverfahren für einen noradrenergen Tracer und eine prosthetische Gruppe etabliert werden.

## Acknowledgments

First and foremost, I wish to express my gratitude to my supervisors, Prof. Dr. Bernd Neumaier and PD Dr. Boris Zlatopolskiy, for their encouragement, dedication, and guidance throughout this project. Their consistent support inspired many of the successes of this work, and their continued advice perpetually motivated me throughout my doctorate. For the time and the opportunities they granted me, I am eternally grateful.

I am also thankful for the opportunity to initiate a collaboration with the research group of my second supervisor, Prof. Dr. Hans-Günther Schmalz, to whom I am very grateful for his expertise in organic chemistry, and his insightful contributions to my project.

I want to thank the Cologne research group for the many enjoyable experiences, such as Karnival, Christmas, St. Patrick's Day celebrations, and of course, the Lindenberg Cup. I particularly wish to thank Heike Endepols, for the advice, support, and friendly environment she provided. I specifically wish to thank Lukas, Steffi, Niklas, Philip, Nadine, Johannes, Elizaveta, Felicia, Britta, Julia, Olesia and Mehrab for their help throughout my project, their welcoming nature, and for the enjoyable lunchtime conversations. Furthermore, Niklas and Elizaveta have prepared some important compounds for this project. Additionally, I wish to thank the team at the Jülich research center for the relaxed atmosphere they provided.

A personal highlight of my Ph.D. experience was the opportunity to give an oral presentation of my research at the international symposium on radiopharmaceutical sciences (ISRS) in Beijing. There I had the chance to meet experts in my field, such as Tatsuo Ido (an [ $^{18}\text{F}$ ]FDG pioneer), explore the Forbidden City, and even walk along the Great Wall of China.

I am also very grateful to the German Academic Exchange Service (DAAD) for their generous funding of my short research stays to visit the group of Prof. Dr. Peter Scott at the University of Michigan, and the group of Dr. Raisa Krasikova at Russian Academy of Sciences in St. Petersburg. Both of these research groups have made significant contributions to the focus of my research project, and I learned a lot from both of these experiences.

Last but not least, I am humbled by the exceptional support I received from my family and close friends, who all had an essential role to play in sustaining my motivation throughout my Ph.D. experience. It is my hope that the successes of this project would make them all proud.

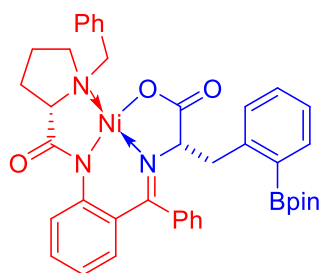
## Table of Contents

Abstract .....	I
Kurzzusammenfassung .....	II
Acknowledgments .....	IV
List of Ni/Cu-BPX-AAA Complexes .....	VIII
List of <sup>18</sup> F-Labeled Products .....	X
1. Introduction .....	1
1.1.1. The Tracer Principle .....	1
1.1.2. Positron Emission Tomography .....	2
1.1.3. Positron-Emitting Radionuclides .....	4
1.1.4. Introduction of Fluorine-18 .....	6
1.2. Radiofluorination Procedures .....	7
1.2.1. Electrophilic Radiofluorination .....	8
1.2.2. Nucleophilic Radiofluorination .....	10
1.2.3. Aliphatic <sup>18</sup> F-Substitution .....	11
1.2.4. Aromatic <sup>18</sup> F-Substitution .....	13
1.2.5. Radiofluorination via Isotopic Exchange .....	14
1.2.6. Radiofluorination via Quaternary Anilinium and Triarylsulfonium Salts .....	16
1.2.7. Radiofluorination Using Diaryliodonium Salts .....	16
1.2.8. The Minimalist Approach .....	19
1.2.9. Aromatic Transition Metal-Mediated Radiofluorination .....	20
1.2.10. Cu-Mediated Radiofluorination .....	22
1.2.10.1. Cu-Mediated Radiofluorination Towards <sup>18</sup> F-labeled AAA Preparations .....	25
1.2.11. Alcohol-Enhanced Cu-Mediated Radiofluorination .....	26
1.2.12. Cu-Mediated Radiofluorination Using Pyridine-Based Additives .....	27
1.2.13. Prosthetic Groups in Radiochemistry .....	29
1.3. Aromatic Amino Acids .....	32
1.3.1. Synthesis of Amino Acids .....	33
1.3.2. Ni- and Cu-BPB Complexes .....	34
1.4. Aromatic Amino Acids as PET Tracers .....	38
1.4.1. Aromatic Amino Acid Metabolism .....	39
1.4.2. The Noradrenergic System .....	41
1.4.3. <sup>18</sup> F-Labeled AAAs Towards Cerebral Tumor Imaging .....	42
1.4.4. Amino Acids as PET Tracers for Parkinson's Disease .....	43

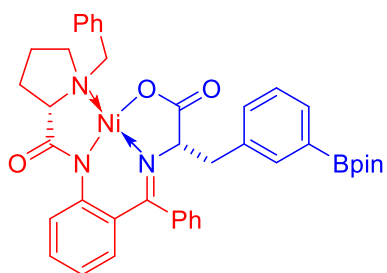
2.	Aims & Objectives.....	45
3.	Results & Discussion .....	47
3.1.	Preparation of Alkylating Agents .....	47
3.2.	Preparation of Reference Compounds .....	49
3.3.	Preparative Strategies Towards 6-[ <sup>18</sup> F]FDOPA Precursor .....	50
3.4.1.	Synthetic Route A .....	50
3.4.2.	Synthetic Route B .....	53
3.5.	Preparation of ( <i>R</i> )-AAA Tracer Precursor.....	55
3.6.	Preparation of ( <i>S</i> )-AAA Tracer Precursor Using Cu-BPB-Gly Complexes.....	56
3.7.	Preparations Towards [ <sup>18</sup> F]FPheSer .....	57
3.7.1.	Synthetic Route A .....	58
3.7.2.	Synthetic Route B .....	59
3.7.3.	Synthetic Route C .....	59
3.08.	Radiochemistry.....	61
3.08.1.	Cu-Mediated Radiofluorination.....	61
3.08.2.	Optimization of <sup>18</sup> F-Labeling Conditions.....	62
3.08.3.	Cu-Mediated Radiofluorination of Ni-BPX-AAA Complexes .....	64
3.08.4.	Optimization of Deprotection Conditions .....	65
3.08.5.	<sup>18</sup> F-labeled AAA Isolation & Purification.....	67
3.09.	General Overview of Radiosynthesis .....	67
3.10.	Preparation of <sup>18</sup> F-Labeled AAAs Using ( <i>S</i> or <i>R</i> )-Ni-BPX-AAA Complexes.....	68
3.11.	Preparation of <sup>18</sup> F-AAA Tracers Using a Cu-BPX-AAA Complex.....	69
3.12.	Preparation of 3-[ <sup>18</sup> F]FPheSer .....	70
3.13.	Preparation of 7-[ <sup>18</sup> F]FTrp.....	71
3.14.	Preparation of Prosthetic Group [ <sup>18</sup> F]FPBA.....	71
3.15.	Automated Synthesis .....	75
3.16.	<sup>18</sup> F-Labeled Product Analysis.....	76
3.17.	Carrier Amount & Specific Activity Determination .....	76
3.18.	Cu- and Ni-Content Determination .....	77
4.	Conclusion .....	78
5.	Experimental .....	80
5.1.	Organic Synthesis.....	80
5.1.1.	General Procedure for Alkylation Upon Ni/Cu-BPA-Gly or Ala (GP1).....	82
5.1.2.	General Procedure for Aldol Upon ( <i>S</i> )-Ni-BPB-Gly (GP2) .....	82
5.1.3.	General Procedure for Radical Bromination (GP3).....	82

5.1.4.	General Procedure for Suzuki-Miyaura Borylation (GP4) .....	83
5.1.5.	General Procedure for MOM-Protection (GP5).....	83
5.1.6.	General Procedure for Stannylation (GP6) .....	83
5.1.7.	General Procedure for Iodination (GP7).....	83
6.	NMR Spectra .....	118
6.1.2.	Mass Spectra.....	150
7.	Radiochemistry .....	153
7.1.1.	Radiochemical Terminology and Nomenclature .....	153
7.2.	General Information and Procedures .....	153
7.2.1.	Preprocessing of [ <sup>18</sup> F]Fluoride.....	154
7.2.2.	Synthesis of FET .....	154
7.3.	General Procedure for the <sup>18</sup> F-Labeling of Ni-BPB-AAAs (RGP1) .....	154
7.4.	Preparation of [ <sup>18</sup> F]FPBA (RGP2) .....	154
7.5.	HPLC .....	155
7.6.	Automated Synthesis of Radiofluorinated Amino Acids .....	156
8.	Radio HPLC Traces and RCC Data for <sup>18</sup> F-Labeled Products .....	158
9.	Quality Control of Products .....	164
10.	Determination of Enantiomeric Excess for AAA PET Tracers .....	174
11.	Supplementary Information: PET Evaluation.....	178
11.1.1.	2-[ <sup>18</sup> F]FPhe in Healthy Rats with/without Benserazide.....	178
11.2.2.	3-[ <sup>18</sup> F]FPhe in Healthy Rats with/without Benserazide.....	179
11.2.3.	3-(S)-[ <sup>18</sup> F]FPhe in Healthy Rats with/without Benserazide.....	180
11.2.4.	4-[ <sup>18</sup> F]FPhe in Healthy Rats without Benserazide.....	181
11.2.5.	α-Methyl-2-[ <sup>18</sup> F]FPhe in Healthy Rats with/without Benserazide .....	181
11.2.6.	α-Methyl-3-[ <sup>18</sup> F]FPhe in Healthy Rats with/without Benserazide .....	182
11.2.7.	α-Methyl-4-[ <sup>18</sup> F]FPhe in Healthy Rats with/without Benserazide .....	183
11.2.8.	7-[ <sup>18</sup> F]FTrp in Healthy Rats with Benserazide .....	184
11.2.9.	3-[ <sup>18</sup> F]FPheSer in Healthy Rats .....	185
11.2.10.	Tumor Model Mice .....	186
11.2.11.	Chicken Embryo PET with [ <sup>18</sup> F]FET and 3-[ <sup>18</sup> F]FPhe.....	187
12.	Appendix .....	189
13.	References .....	195
14.	Declaration .....	202
15.	Curriculum Vitae.....	203

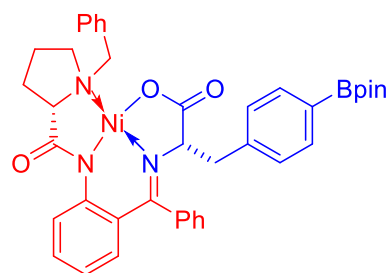
## List of Ni/Cu-BPX-AAA Complexes



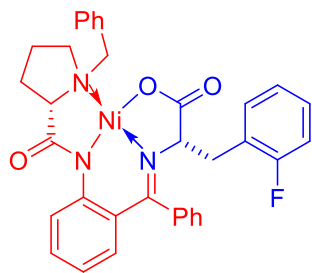
**127a**



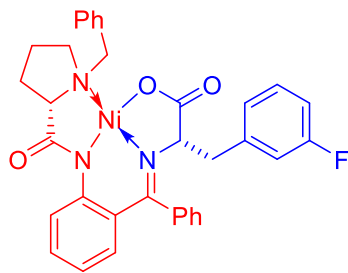
**127b**



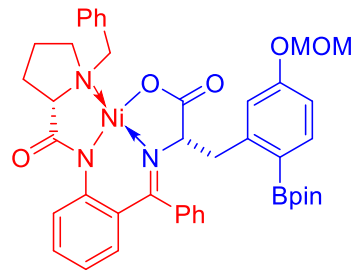
**127c**



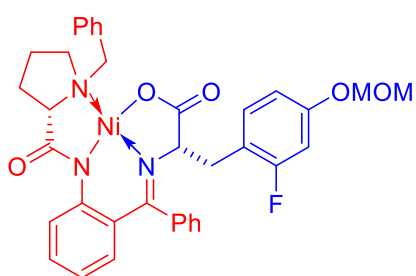
**134a**



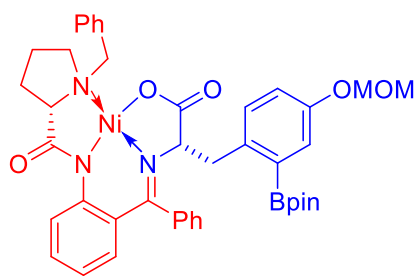
**134b**



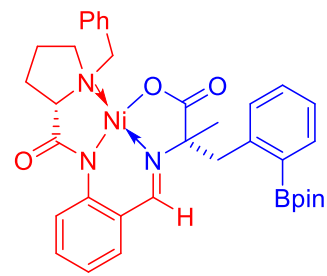
**127d**



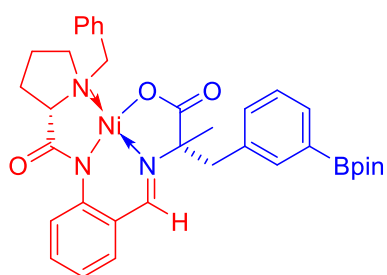
**134c**



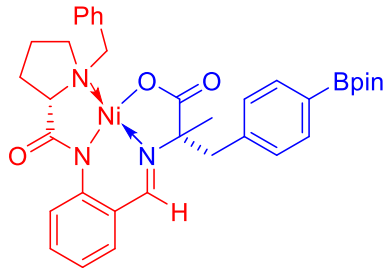
**127e**



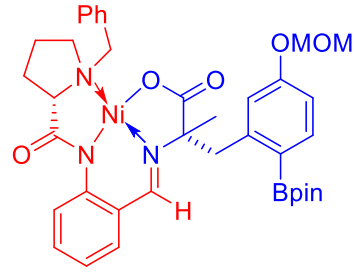
**127f**



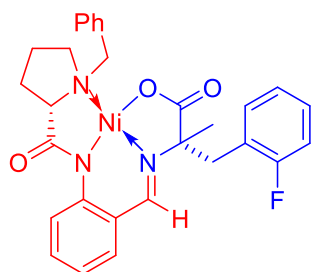
**127g**



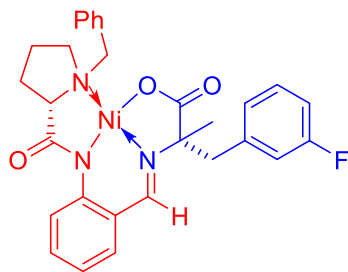
**127h**



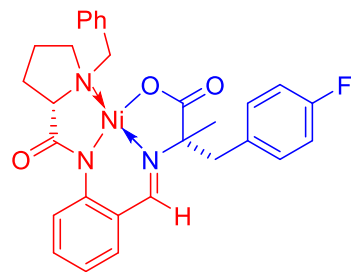
**127i**



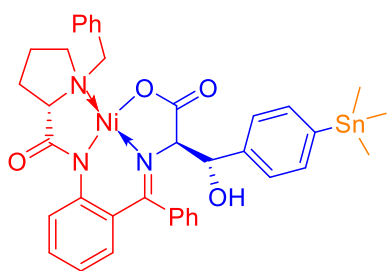
**134d**



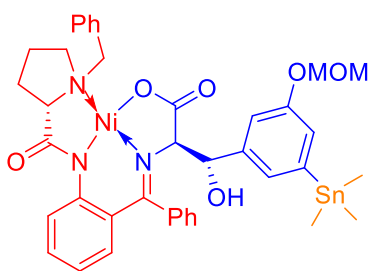
**134e**



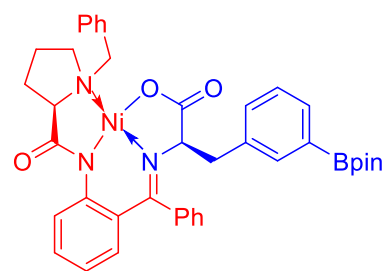
**134f**



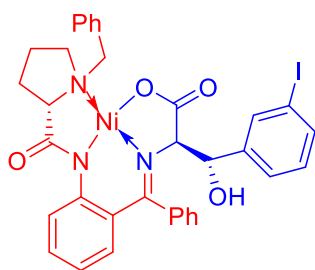
**167**



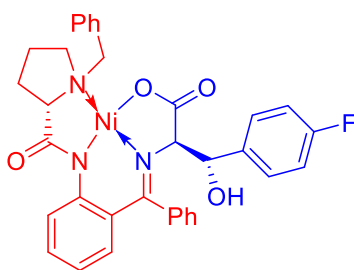
**168**



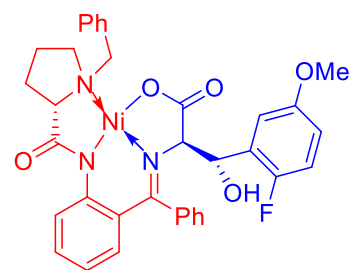
**152**



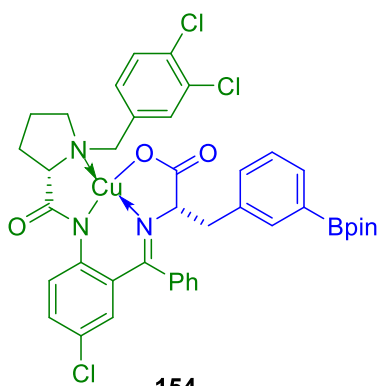
**160**



**156**

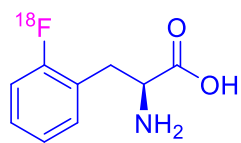


**158**

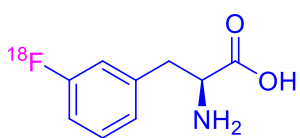


**154**

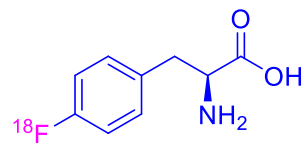
## List of $^{18}\text{F}$ -Labeled Products



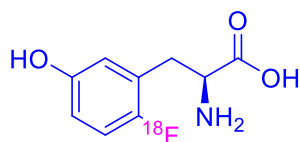
[ $^{18}\text{F}$ ]35



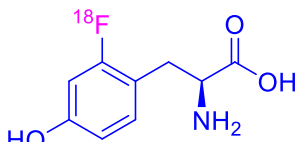
[ $^{18}\text{F}$ ]68



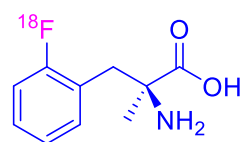
[ $^{18}\text{F}$ ]64



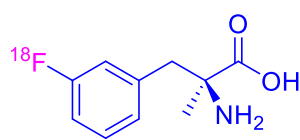
[ $^{18}\text{F}$ ]28



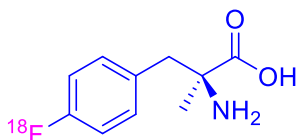
[ $^{18}\text{F}$ ]36



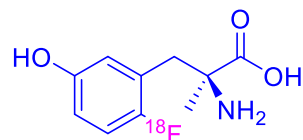
[ $^{18}\text{F}$ ]176



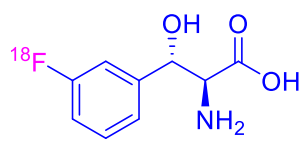
[ $^{18}\text{F}$ ]177



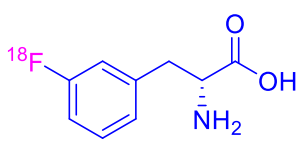
[ $^{18}\text{F}$ ]178



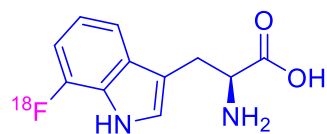
[ $^{18}\text{F}$ ]175



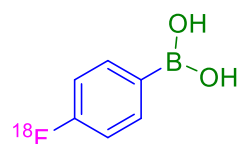
[ $^{18}\text{F}$ ]114



[ $^{18}\text{F}$ ]179



[ $^{18}\text{F}$ ]185

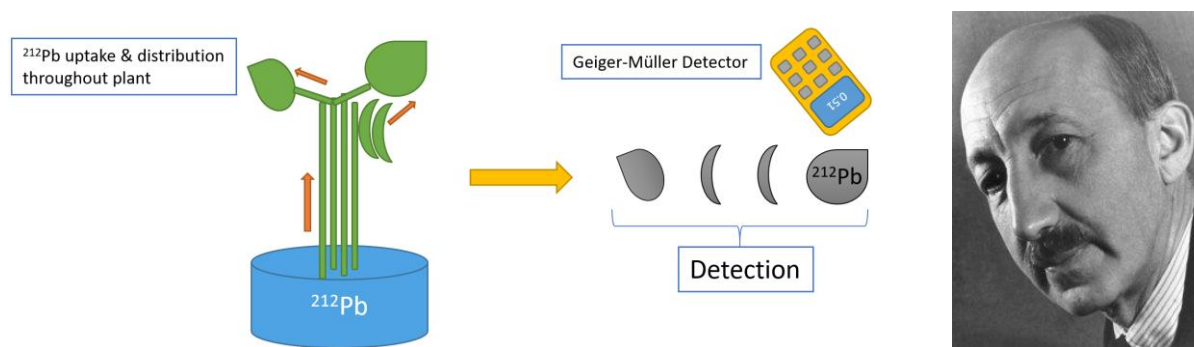


[ $^{18}\text{F}$ ]80

# 1. Introduction

## 1.1.1. The Tracer Principle

In 1923, George von Hevesy devised the first experiments using radionuclides to provide information on metabolic processes. In one of his most renowned experiments, he placed the roots of a bean plant, *Vicia Faba*, in an aqueous solution containing the radionuclide  $^{212}\text{Pb}$ . The uptake and distribution throughout the plant of the radionuclide  $^{212}\text{Pb}$  was subsequently determined by quantifying the amount of radioactivity detected from the ashes of the respective plant parts (Fig. 1).<sup>1</sup> For this seminal work and his use of the  $^{32}\text{P}$  radionuclide towards metabolic studies in animals, von Hevesy (Fig. 2) was awarded the Nobel prize and the Copley medal “For his distinguished work on the chemistry of radioactive elements and especially for his development of the radioactive tracer techniques in the investigation of biological processes”.<sup>2</sup>



Figures 1 & 2. George von Hevesy and his bean plant experiment.<sup>1,2</sup>

*George von Hevesy's Tracer Principles:*

1. Radioactive isotopes of an element behave identically as the non-radioactive isotopes of the same element.
2. The effect of radioactivity should not alter the chemical and physical properties in the environment of the experimental system.
3. Tracers should not have deleterious influences on the biological environment they are intended to study.
4. The tracer should be as analogous to the non-radioactive compound as possible.
5. Solely the radioactive isotope is traced, not the molecule.

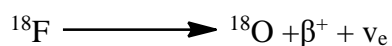
Today, von Hevesy's legacy remains in nuclear medicine through the tracer principles he first developed. The application of radiotracers is widely used for the diagnosis of a plethora of disorders and diseases and therefore plays an invaluable role in clinical practice. The tracer

principle is exploited by modern diagnostic methods such as PET and SPECT, which will be discussed in the following sections.<sup>3</sup>

### 1.1.2. Positron Emission Tomography

Carl David Anderson is credited with the discovery of the positron in 1932, for which he received the Noble Prize for Physics in 1936.<sup>4,5</sup> In Anderson's landmark manuscript, "The Positive Electron" the term "positron" was coined as an antonym of "electron" by the review editor.<sup>5</sup> Indeed, positrons ( $^+\beta$ ) can be thought of as positively-charged (anti-matter) electrons, considering their similar mass. A notable example of a positron-emitting radioisotope is the naturally occurring potassium-40 isotope ( $^{40}\text{K}$ ), which constitutes a tiny quantity (0.0117%) of potassium. Interestingly,  $^{40}\text{K}$  is the most abundant radioisotope found in humans, and it was found that approximately 4,400  $^{40}\text{K}$  nuclei undergo decay per second in the average human (weighing ca. 70 kg).<sup>6</sup>

Principally, positrons are generated following nuclear transmutation (radioactive decay) of proton-rich nuclei. Using  $^{18}\text{F}$ -decay as an example, we can observe how a proton is converted to a neutron in the nucleus of the atom producing the stable (non-radioactive)  $^{18}\text{O}$  nucleus, a positron and a neutrino (Scheme 1). The use of small molecular probes (or tracers) containing a positron-emitting radionuclide is the fundamental method by which positron emission tomography (PET) functions as a diagnostic tool.



*Scheme 1.  $^{18}\text{F}$  Decay*

PET is a non-invasive imaging technique that allows pathological and physiological processes to be visualized on a molecular level in real-time.<sup>7</sup> PET affords invaluable information concerning metabolic patterns, molecule-enzyme interactions, signal-transduction processes, receptor status, and transport to be identified. In contrast, medical imaging techniques such as magnetic resonance imaging (MRI), ultrasound (US), computed tomography (CT), and X-ray, provide only morphological and anatomical information.

Counterintuitively, it is not the emitted positrons that are being detected during a PET measurement, but the antiparallel gamma ( $\gamma$ ) quants released from the annihilation reactions that proceed positron-emission. As a positron is ejected from the nucleus following decay, the kinetic energy of the resulting positron (characteristic of the parent radioisotope) causes positron migration away from the nucleus. Ultimately, the kinetic energy of the positron is lost

following collisions with neighboring particles after deceleration, the positron combines with an electron under positronium formation.

A positronium is an unstable system where the mass of an electron and a positron is converted into energy and annihilate each other to release gamma-rays (Fig. 3). A positronium system can be classified as either a *para* or *ortho*-positronium depending on the relative orientations of the positron and electron spins. The *para*-positronium (*p*-Ps) has a mean half-time of 0.125 ns and decays into an even number (2, 4, 6) of antiparallel gamma quants (511 keV). *Para*-positronium systems typically release only two gamma quants, which allows the position of the annihilation event to be determined using PET. The *ortho*-positronium (*o*-Ps) has a mean half-time of 142.05 ns and decays preferentially into three gamma quants, making the *ortho*-positronium system less desirable for PET. The gamma-radiation produced from annihilation is released at an approximate 180° angle, and the coincident detection of this radiation is registered by the scintillation crystals in the surrounding PET detector units. The final PET image following measurement is reconstructed based on the quantity of coincident gamma-radiation over a specific time. Finally, from the PET image, the approximate localization and relative accumulation of the positron-emitting isotope can be determined *in vivo*.

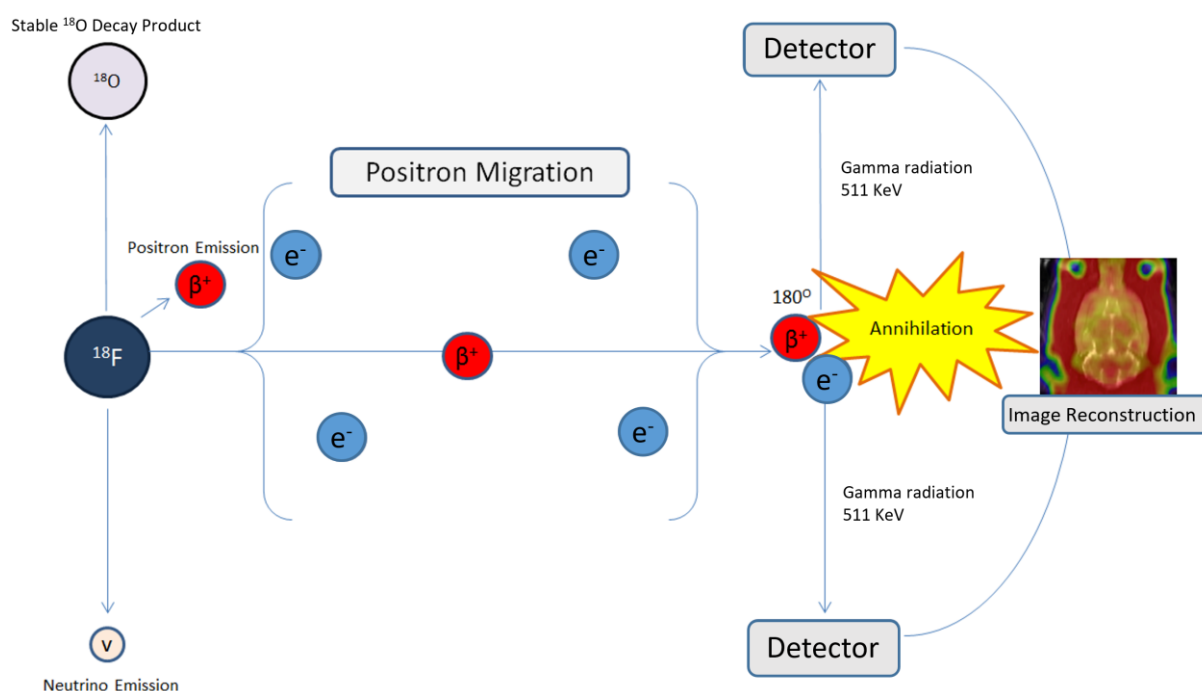


Figure 3. Schematic of major events during positron emission, thermalization, annihilation, and detection.

### 1.1.3. Positron-Emitting Radionuclides

The choice of radioisotope for PET imaging is not always an obvious one, with each radionuclide having respective advantages and limitations. Radiochemists must consider which radionuclides are most feasible for successful radiosynthesis and PET imaging experiments. The accessibility and physical properties of radionuclides such as half-life,  $\beta^+$ -intensity, and maximum positron energy are the most considered criteria prior to radiosynthesis. A table below displays some of the significant radionuclides for PET imaging studies (Tab. 1).

PET Radionuclide	Half-life ( $t_{1/2}$ )	$\beta^+$ -Intensity	Maximum Positron ( $\beta^+$ ) Energy (MeV)
$^{11}\text{C}$	20.4 min	( $\beta^+$ ) 99.9%	0.960
$^{13}\text{N}$	9.97 min	( $\beta^+$ ) 100%	1.199
$^{15}\text{O}$	2.04 min	( $\beta^+$ ) 99.9%	1.730
$^{18}\text{F}$	109.7 min	( $\beta^+$ ) 96.7%	0.634
$^{68}\text{Ga}$	67.6 min	( $\beta^+$ ) 88.9%	1.899
$^{64}\text{Cu}$	12.7 h	( $\beta^+$ ) 17.5%	0.653
$^{89}\text{Zr}$	78.4 h	( $\beta^+$ ) 22.7%	0.902
$^{124}\text{I}$	100.2 d	( $\beta^+$ ) 11.7%, 10.7%	1.535, 2.138

Table 1. Main short-lived positron-emitters and their respective physical properties.<sup>8</sup>

Generally, the accepted time for operations for a PET-isotope is three half-lives.<sup>9</sup> Therefore, short-lived isotopes such as  $^{11}\text{C}$ ,  $^{13}\text{N}$ , and  $^{15}\text{O}$  require an on-site cyclotron and rapid radiosynthesis protocols to be practical for PET imaging studies. Moreover, if we wished to observe a lengthy metabolic pathway *in vivo* using PET, radionuclides with relatively longer half-lives would be most suitable. In contrast to small molecules, which typically exhibit short clearance rates from the blood, the clearance of the biopolymers (e.g. proteins) is a considerably slower process. Accordingly, longer-lived positron-emitting radionuclides  $^{64}\text{Cu}$  and  $^{89}\text{Zr}$  are used for the radiolabeling of biopolymers.  $^{124}\text{I}$  is a positron-emitting radionuclide that can be used to trace even longer metabolic processes using PET imaging.

The  $\beta^+$ -intensity of a radionuclide is the probability of positron formation following radioactive decay. Generally, radionuclides with higher  $\beta^+$ -intensity values are preferable for PET imaging studies due to the greater magnitude of positrons produced, and the smaller amount of undesirable gamma quanta released. The latter feature reduces the amount of false-coincidence detections during a PET experiment and reduces associated radiation safety risks.

The maximum positron energy of the radionuclides provides us with information about the distance the positron will travel before losing kinetic energy and reacting with an electron in an annihilation reaction. Ideally, radionuclides would have a lower maximum positron energy, as the positron would have less kinetic energy to migrate away from the parent radionuclide, and therefore the position of annihilation would be closer to the place of the radioactive decay. The shorter the distance between the annihilation and location of the initial positron decay, the higher the image resolution obtained from a PET experiment. Various examples of PET tracers are shown in Fig. 4.

Notably,  $^{68}\text{Ge}/^{68}\text{Ga}$  generator enables the production of  $^{68}\text{Ga}$  in the absence of a cyclotron.<sup>10</sup> However, the incorporation of radiometals ( $^{68}\text{Ga}$ ,  $^{64}\text{Cu}$ , and  $^{89}\text{Zr}$ ) into precursor molecules requires the presence of chelators (e.g. HBED-CC, Fig. 4. **D**). This feature may result in the radiometals being unsuitable for small molecule radiolabeling.

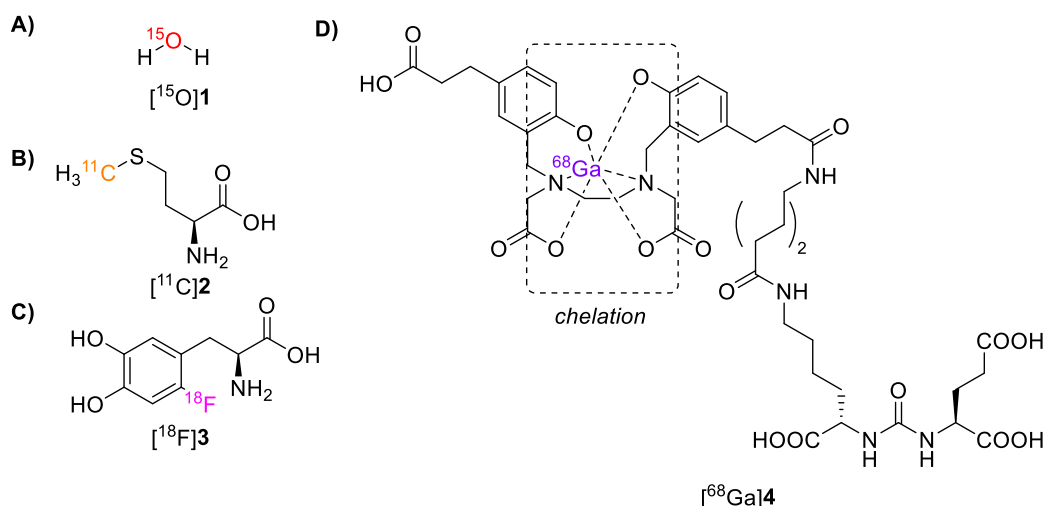


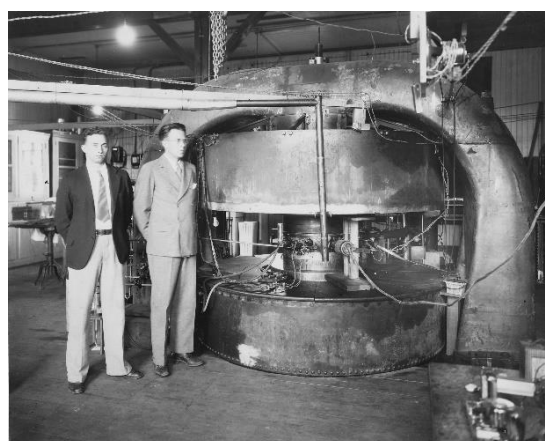
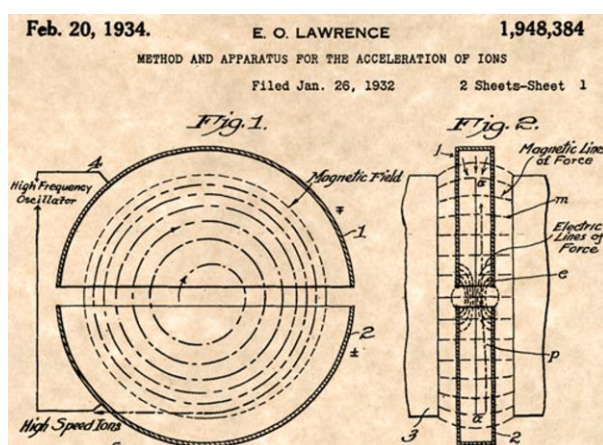
Figure 4. Examples of PET tracers: A)  $^{15}\text{O}\text{H}_2\text{O}$  ( $^{15}\text{O}$ 1), B)  $^{11}\text{C}$ C-methionine ( $^{11}\text{C}$ 2), C) 3,4-dihydroxy-6- $^{18}\text{F}$ fluoro-L-phenylalanine (6- $^{18}\text{F}$ DOPA, ( $^{18}\text{F}$ 3), and D)  $^{68}\text{Ga}$ Ga-PSMA-11 ( $^{68}\text{Ga}$ 4).

In summary, there are some criteria for positron-emitting radionuclides: For example, the half-life must be long enough to enable the tracing of the desired metabolic processes or target. Additionally, a longer half-life allows multi-step radiosynthesis and to trace the metabolism of tracers over a longer time frame, and may also permit transport to other clinical institutions. Another important criterion is the accessibility of the radionuclide. Most of the radionuclides in Table 1. are produced at a cyclotron.

#### 1.1.4. Introduction of Fluorine-18

The most prominent radionuclide for PET imaging studies,  $^{18}\text{F}$ , exhibits advantageous physical properties that satisfy many of the aforementioned criteria. For example, the half-life of  $^{18}\text{F}$  (109.7 min) poses fewer limitations on radiosynthesis times, permits tracer transport, and accommodates lengthy PET measurements. The low positron energy of  $^{18}\text{F}$  (0.635 MeV) affords desirable high-quality PET image resolution, and the high  $\beta^+$ -branching of fluorine-18 (96.9%  $\beta^+$ -emission) increases PET imaging sensitivity. Furthermore, approximately 20% of pharmaceuticals contain a fluorine atom, thereby facilitating tracer design. As fluorine is the most electronegative element, the introduction of fluorine into a molecule can have a dramatic effect on the overall physicochemical properties of the molecule. Accordingly, the *in vivo* distribution of an  $^{18}\text{F}$ -labeled molecule typically deviates somewhat from its unlabeled molecular counterpart. Although this contradicts one of the tracer principles, the latter feature may be exploited by radiochemists to enhance the binding affinity of a tracer or to confer stability to a molecule susceptible to metabolic degradation (e.g. 2- $^{18}\text{F}$ ]FDG).

Fluorine-18 is usually produced at a cyclotron. The first cyclotron was devised by Ernest Lawrence and Stanley Livingston in 1932 (Fig. 5 & 6).<sup>11</sup> Principally, a cyclotron is a machine that accelerates charged particles, such as hydrides, protons, or deuterons, to high energies which enable to induce nuclear reactions (Tab. 2). The acceleration of the charged particles can be achieved using a combination of an oscillating current and two powerful and oppositely charged magnets (Dees). The charged particle is accelerated until it reaches the desired energy to initiate a nuclear reaction with the target (e.g.  $^{18}\text{O}$ ]H<sub>2</sub>O).



Figures 5 & 6. (Left) Excerpt from the original cyclotron patent submitted by Ernest Lawrence (1934) depicting particle acceleration inside a cyclotron. (Right) Ernest Lawrence and Stanley Livingston with a cyclotron in 1932.<sup>11,12</sup>

The major production method of [ $^{18}\text{F}$ ] $\text{F}^-$  is the bombardment of  $^{18}\text{O}$ -enriched water ( $\text{H}_2^{18}\text{O}$ ) with protons using the  $^{18}\text{O}(\text{p},\text{n})^{18}\text{F}$  nuclear reaction. The highly efficient reaction permits the production of over 500 GBq of [ $^{18}\text{F}$ ]fluoride. It is important to consider whether electrophilic or nucleophilic [ $^{18}\text{F}$ ]fluorine is required for the radiosynthetic process. Either radiolabeling route will significantly impact the applicable  $^{18}\text{F}$ -fluorination procedures and specific activity ( $A_s$ ) of the final product.

Nuclear reaction	Target	Chemical Form of $^{18}\text{F}$	Molar Activity (Ci/mmol)
$^{16}\text{O}(^3\text{He},\text{p})^{18}\text{F}$	$\text{H}_2\text{O}$	$^{18}\text{F}^-_{(\text{aq})}$	$10^5$
$^{18}\text{O}(\text{p},\text{n})^{18}\text{F}$	$\text{H}_2^{18}\text{O}$	$^{18}\text{F}^-_{(\text{aq})}$	$10^5$
$^{18}\text{O}(\text{p},\text{n})^{18}\text{F}$	$^{18}\text{O}_2(0,1\% \text{F}_2)$	$[\text{F}^{18}\text{F}]_2$	1–10
$^{20}\text{Ne}(\text{d},\alpha)^{18}\text{F}$	$\text{Ne}(0,1\% \text{F}_2)$	$[\text{F}^{18}\text{F}]_2$	1–50

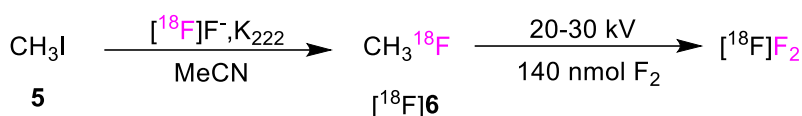
Table 2. Nuclear reactions generating  $^{18}\text{F}$ .<sup>13</sup>

## 1.2. Radiofluorination Procedures

The  $^{18}\text{F}$ -incorporation into a suitable precursor molecule is not always a trivial task. The relatively minute concentrations of [ $^{18}\text{F}$ ]fluorine used for radiofluorinations prohibits the transferability of standard fluorination procedures from organic synthesis to radiochemistry. The  $^{18}\text{F}$ -incorporation into a suitable precursor molecule proceeds by either electrophilic substitution of electron-rich systems or *via* nucleophilic aromatic substitution reactions of electron-poor systems. Radiochemists must contend with various challenges to achieve the highest RCYs and  $A_s$  values as possible. In order to minimize the effect of radioactive decay, radiofluorinations are carried out as rapidly as possible. Consequently,  $^{18}\text{F}$ -labeling often requires high reaction temperatures and is ideally carried out as late as possible in the tracer preparation. Therefore, an emphasis is often placed on “late-stage” or “direct radiofluorination” protocols, which are easier to implement into automated radiosynthesis modules. The latter is needed for *c*GMP production of PET tracers and routine clinical applications. Alternatively,  $^{18}\text{F}$ -labeled building blocks (prosthetic groups) are commonly employed towards the indirect radiolabeling of more complex molecules (see Section 1.2.14).

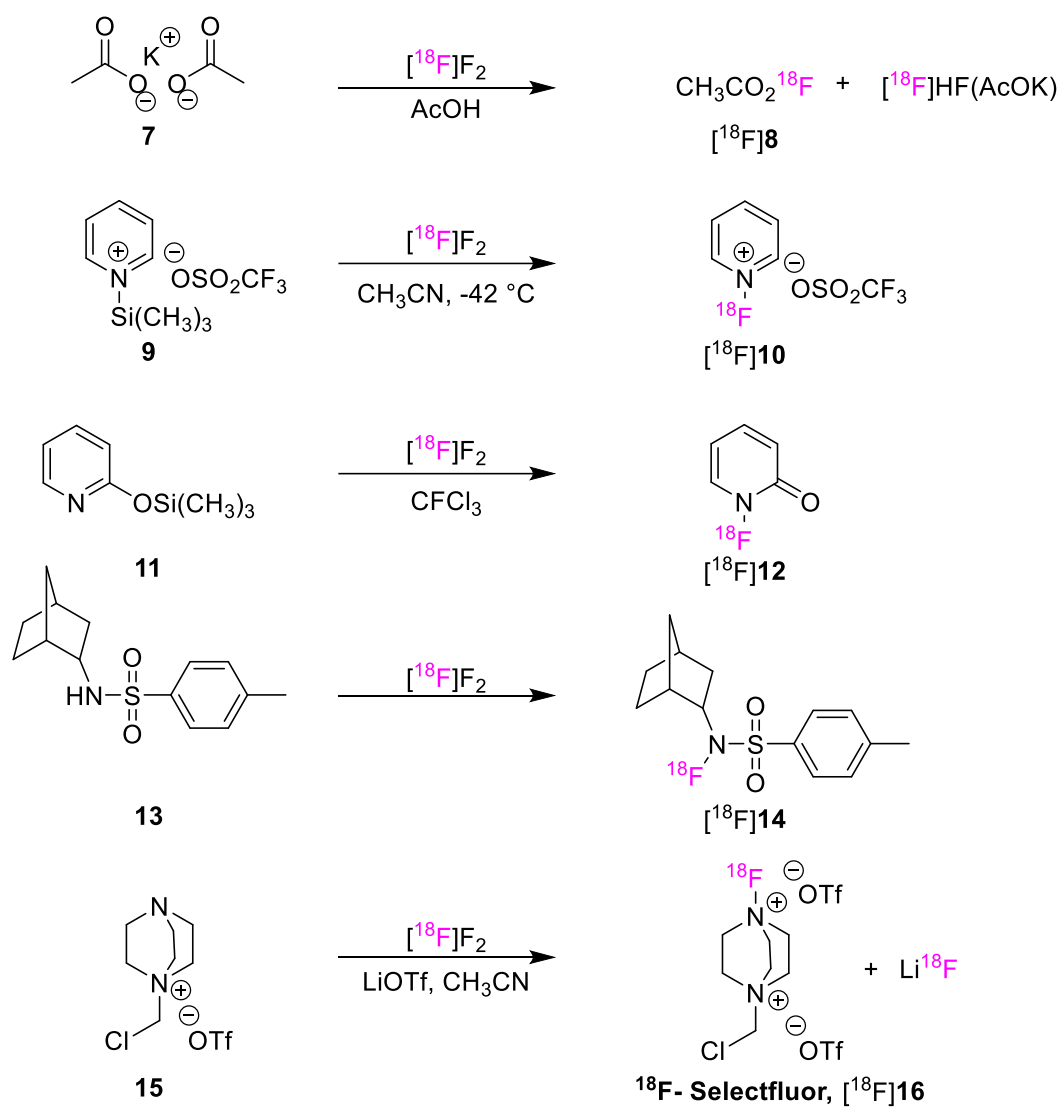
### 1.2.1. Electrophilic Radiofluorination

The preparation of [ $^{18}\text{F}$ ]F $_2$  gas *via*  $^{20}\text{Ne}(d,\alpha)^{18}\text{F}$  reaction (Tab. 2) is the primary method by which [ $^{18}\text{F}$ ]F $_2$  is produced for electrophilic radiofluorination. Alternatively, the  $^{18}\text{O}(\text{p},\text{n})^{18}\text{F}$  reaction using highly-enriched  $^{18}\text{O}_2$  in an Al target chamber can be used to generate [ $^{18}\text{F}$ ]F $_2$ .<sup>14</sup> In both instances, fluorine-18 adheres to the target walls and must be flushed with F $_2$  gas to initiate isotopic exchange responsible for the removal of [ $^{18}\text{F}$ ]F $_2$ . In this way, tracers produced by electrophilic radiofluorination may have lower molar activity ( $A_m$ ) due to the competing reaction of the precursor with  $^{19}\text{F}$ . Solen *et al.* reported the use of high  $A_s$  (30 GBq/ $\mu\text{mol}$ ) [ $^{18}\text{F}$ ]F $_2$  production by the electric discharge of [ $^{18}\text{F}$ ]CH $_3\text{F}$  (Scheme 2).<sup>14</sup> Furthermore, as the non-radioactive  $^{19}\text{F}$  isotope also has an equal possibility to react with the precursor compound as  $^{18}\text{F}$ , the theoretically achievable RCY *via* electrophilic radiofluorination using [ $^{18}\text{F}$ ]F $_2$  is 50%.



*Scheme 2. Preparation of electrophilic [ $^{18}\text{F}$ ]F $_2$  by electrical discharge.<sup>14</sup>*

A notable example of electrophilic radiofluorination was the first radiosynthesis of 2-[ $^{18}\text{F}$ ]FDG ([ $^{18}\text{F}$ ]**6**) by Ido *et al.* in 1976.<sup>15</sup> Although this seminal work provided a method for 2-[ $^{18}\text{F}$ ]FDG to be accessed, the lack of regioselectivity of the radiofluorination (due to the high reactivity of the electrophilic [ $^{18}\text{F}$ ]F $_2$ ) was a considerable disadvantage. This drawback gave rise to multiple unwanted radiofluorinated side-products. Taking into account that the  $A_s$  would also be very low, and the purification of the final tracer was challenging, improved radiosynthetic methods were highly sought after. A short overview of some notable examples of electrophilic radiofluorinations are presented in Scheme 3.



*Scheme 3. The preparations of electrophilic radiofluorination agents.<sup>16-20</sup>*

### 1.2.2. Nucleophilic Radiofluorination

Before successful nucleophilic radiofluorination, several pre-processing steps of [ $^{18}\text{F}$ ]fluoride must be carried out. The cyclotron produces [ $^{18}\text{F}$ ]F $^-$  in a solution of the previously bombarded  $\text{H}_2^{18}\text{O}$  sample. Consequently, the high solvation with neighboring water molecules severely hinders the ability of [ $^{18}\text{F}$ ]F $^-$  to act as a nucleophile. Typically, the irradiated water containing the [ $^{18}\text{F}$ ]F $^-$  is passed through an ion-exchange resin (e.g. QMA cartridge), allowing the water to pass through the resin, and trapping the [ $^{18}\text{F}$ ]fluoride. This allows for expensive target water ( $\text{H}_2^{18}\text{O}$ ) to be recycled. Thereafter, the [ $^{18}\text{F}$ ]F $^-$  may be eluted from the resin with a weak base such as  $\text{Cs}_2\text{CO}_3$ ,  $\text{Rb}_2\text{CO}_3$ ,  $\text{K}_2\text{CO}_3$ , or ammonium salt (Fig. 7). Following elution, a phase transfer catalyst such as Kryptofix-222 ( $\text{K}_{222}$ ) is added to the reaction vial, and the [ $^{18}\text{F}$ ]fluoride is repeatedly dried (two or three cycles) *via* azeotropic distillation with MeCN to remove remaining water traces. The resulting anhydrous [ $^{18}\text{F}$ ]fluoride is highly nucleophilic due to the weak ion-pairing between [ $^{18}\text{F}$ ]F $^-$  and counterion of the alkali metal cations (due to size/charge disproportionality of the two ions).

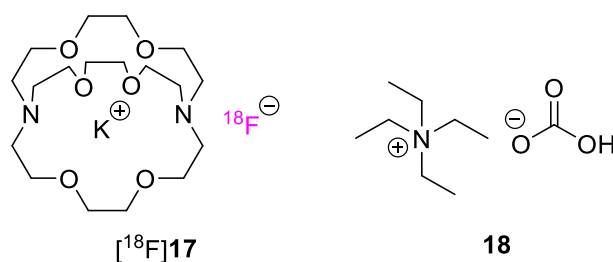


Figure 7. Kryptofix-222/ $\text{K}[^{18}\text{F}]\text{F}^-$  (**[ $^{18}\text{F}$ ]17**), and tetraethylammonium bicarbonate (**18**).

Despite nucleophilic radiofluorination being widely adopted for radiopharmaceutical production, there are two main disadvantages of this strategy: Firstly, the use of base can lead to unwanted side-product formation and may cause precursor degradation, and secondly, the azeotropic drying steps are very time-consuming. An overview of the  $^{18}\text{F}$ -preprocessing steps is displayed in Fig. 8.

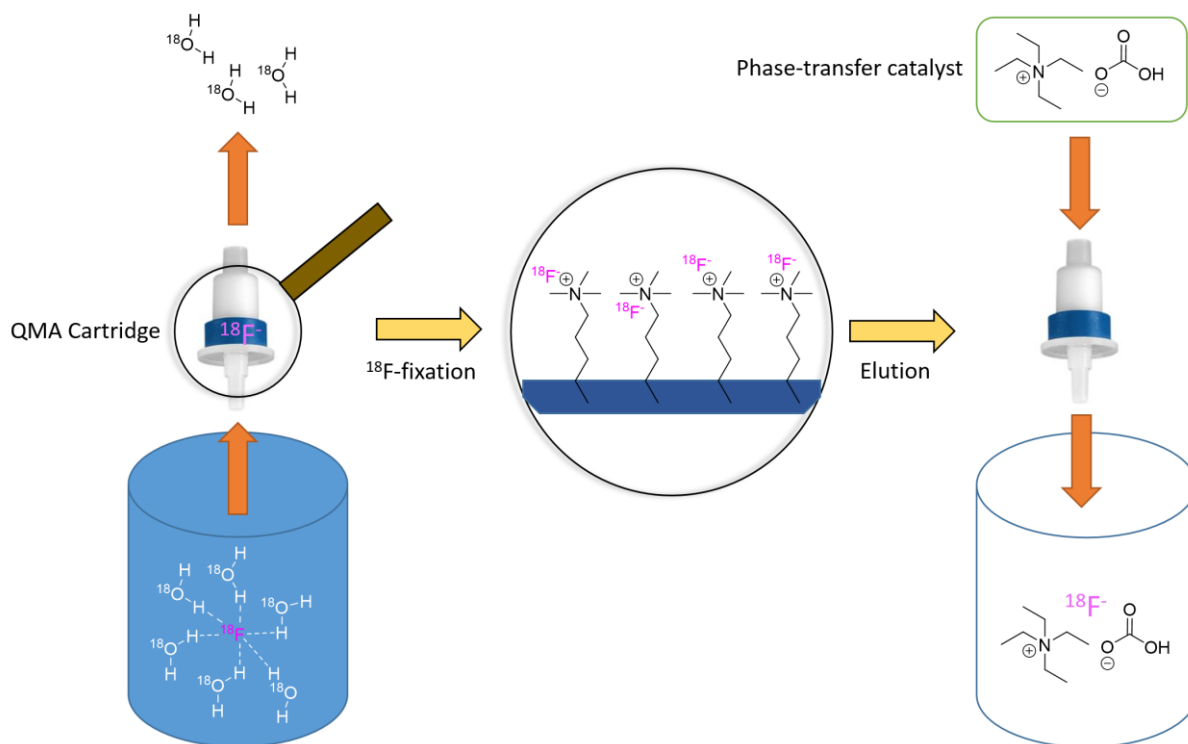
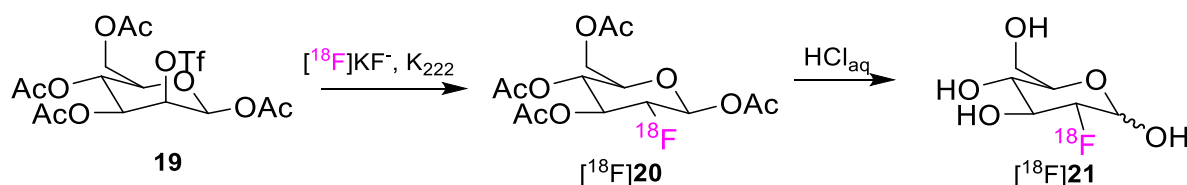


Figure 8. Diagram showing major  $^{18}\text{F}$ -preprocessing steps prior to nucleophilic radiofluorination.

### 1.2.3. Aliphatic $^{18}\text{F}$ -Substitution

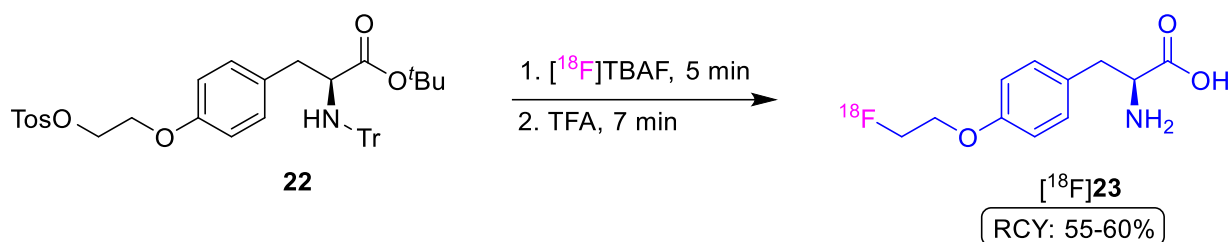
In practice, nucleophilic aliphatic  $^{18}\text{F}$ -substitution is the most widely applied method for the production of  $^{18}\text{F}$ -labeled radiopharmaceuticals. A good leaving group (LG), such as the halides Cl, Br, and I, or certain sulfonates (e.g. OTos, OTf), is required for aliphatic  $^{18}\text{F}$ -fluorination. Aliphatic  $^{18}\text{F}$ -fluorinations mainly proceed by an  $\text{S}_{\text{N}}2$  mechanism. Nucleophilic  $^{18}\text{F}$ -fluorination via  $\text{S}_{\text{N}}2$  mechanism can be advantageously employed to furnish a defined stereocenter in an  $^{18}\text{F}$ -labeled product. For example, Hamacher *et al.* successfully optimized the radiosynthesis of [ $^{18}\text{F}$ ]**21** via nucleophilic radiofluorination (Scheme 4).<sup>21</sup> The  $\text{S}_{\text{N}}2$  mechanism of the triflate with nucleophilic [ $^{18}\text{F}$ ] $\text{F}^-$  causes an inversion of the stereochemical center (Walden inversion), thereby furnishing [ $^{18}\text{F}$ ]FDG as the major product.



Scheme 4. Preparation of [ $^{18}\text{F}$ ]FDG ([ $^{18}\text{F}$ ]**21**) via nucleophilic radiofluorination.<sup>21</sup>

The preparation of *O*-(2-[ $^{18}\text{F}$ ]fluoroethyl)-L-tyrosine ([ $^{18}\text{F}$ ]FET, [ $^{18}\text{F}$ ]**23**), as reported by Hamacher *et al.*, is an important AAA tracer radiosynthesis relevant to this work (Scheme 5).<sup>22</sup>

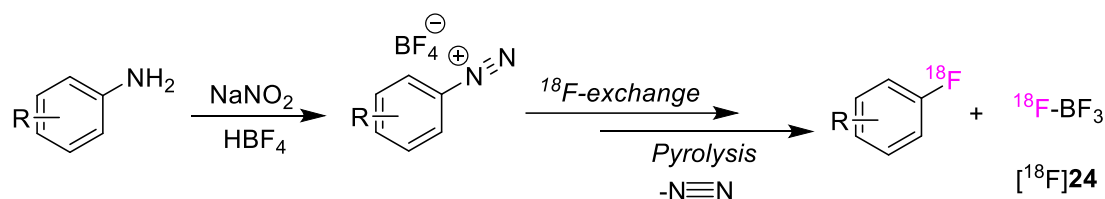
The nucleophilic radiofluorination proceeds with n.c.a. [ $^{18}\text{F}$ ]fluoride to access a radiofluorinated intermediate compound, which is subsequently deprotected using trifluoroacetic acid (TFA) to furnish [ $^{18}\text{F}$ ]**23**. The advantages of this procedure include the relatively short radiosynthesis time (75 min), the rapid purification by solid-phase extraction (SPE) and HPLC, high RCP,  $A_m$  ( $>18\text{ GBq}/\mu\text{mol}$ ) and RCYs. Moreover, the method was easy to implement into an automated radiosynthesis module and is currently the leading protocol for [ $^{18}\text{F}$ ]**23** production. [ $^{18}\text{F}$ ]**23** is currently applied for the routine clinical diagnosis of cerebral tumor detection using PET, and in the context of this project, we wish to use [ $^{18}\text{F}$ ]FET as a reference AAA tracer in comparison the newly developed  $^{18}\text{F}$ -labeled AAAs.



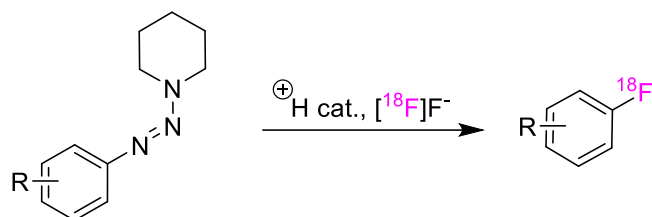
*Scheme 5. The preparation of [ $^{18}\text{F}$ ]**23** via nucleophilic radiofluorination.<sup>22</sup>*

### 1.2.4. Aromatic $^{18}\text{F}$ -Substitution

**A**



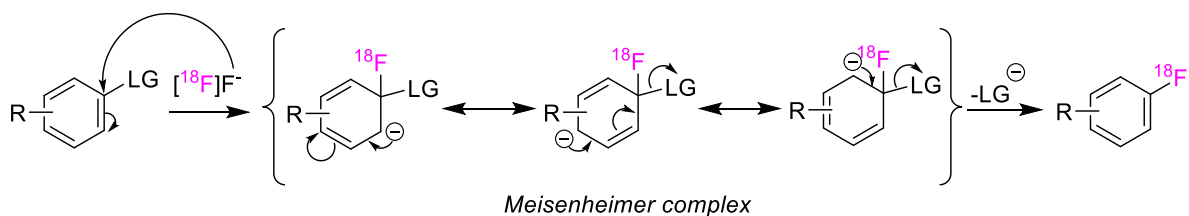
**B**



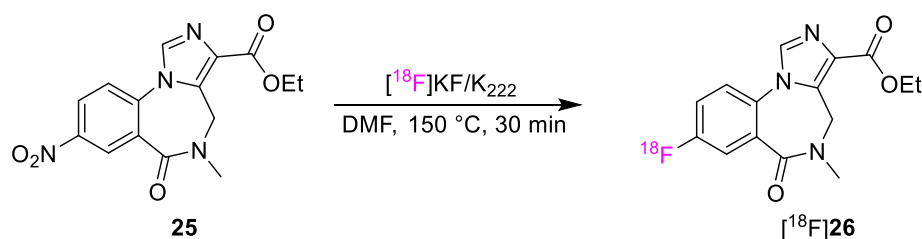
*Scheme 6. A) Balz-Schiemann reaction, and B) Wallach reaction.*<sup>23-26</sup>

Early examples of aromatic  $^{18}\text{F}$ -fluorination include the Balz-Schiemann and Wallach reactions (Schemes 6 A & B). Unfortunately, these protocols are cumbersome and furnish  $^{18}\text{F}$ -labeled arenes in low RCYs.<sup>24-26</sup>

**A**



**B**



*Scheme 7. A) The proposed mechanism of nucleophilic aromatic radiofluorination, and B) Preparation of [ $^{18}\text{F}$ ]**26**.*<sup>27</sup>

Nucleophilic aromatic  $^{18}\text{F}$ -substitution protocols typically proceed *via*  $\text{S}_{\text{N}}\text{Ar}$  mechanism (Scheme 7 A), whereby the presence of a good LG and an electron-withdrawing group (EWG) such as  $\text{NO}_2$  and  $\text{NMe}_3^+$  is typically required. The preparation of [ $^{18}\text{F}$ ]flumazenil ([ $^{18}\text{F}$ ]**26**) (a PET tracer for central benzodiazepine receptor imaging) is an example of radiofluorination *via*

$S_NAr$  mechanism (Scheme 7 B).<sup>27</sup> However, the high temperatures required for short reaction times using this strategy may not be compatible with sensitive precursors and functional groups. Moreover, the scope of this reaction is limited by the necessity of an EWG.

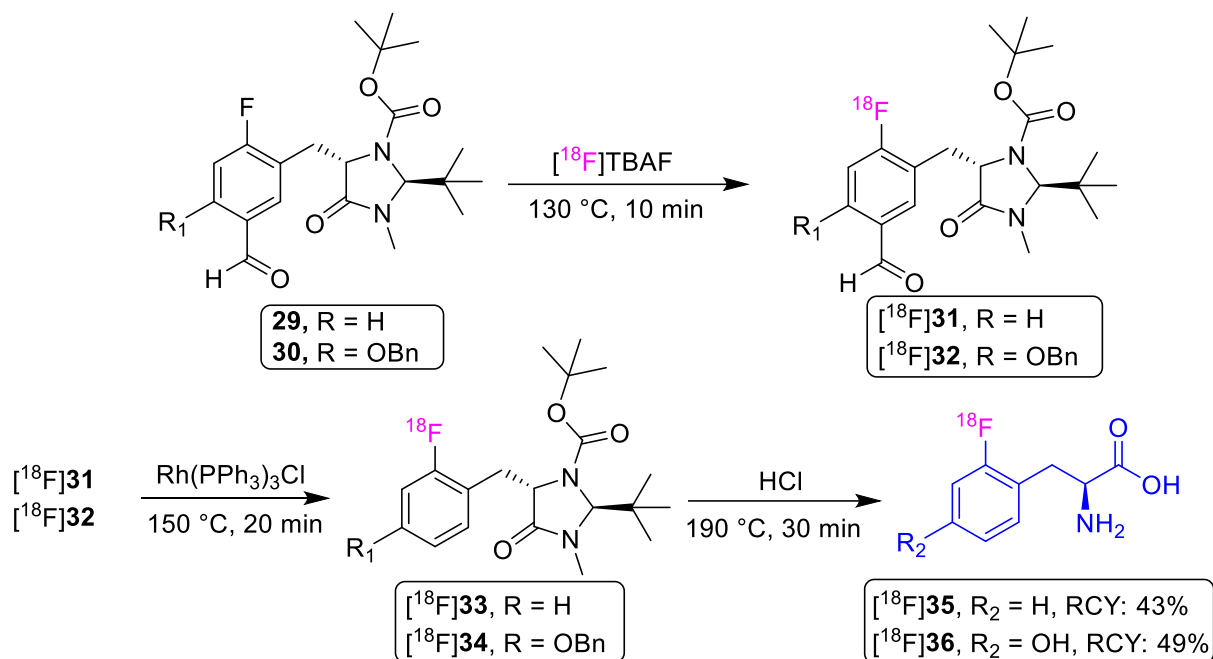


*Scheme 8. Preparation of [<sup>18</sup>F]28 using spirocyclic iodonium(III) ylide precursor.<sup>28</sup>*

In 2016, Liang *et al.* reported the preparation of 6-[<sup>18</sup>F]fluoro-*m*-tyrosine (6-[<sup>18</sup>F]FMT, [<sup>18</sup>F]28) utilizing spirocyclic iodonium(III) ylide precursors (Scheme 8).<sup>28</sup> [<sup>18</sup>F]28 was obtained in low RCY and the lengthy precursor synthesis (17% yield over five steps), this limited the practicality of this protocol. Additionally, the authors failed to account for the loss of [<sup>18</sup>F]fluoride on the reaction vessel walls when making their RCY determination.

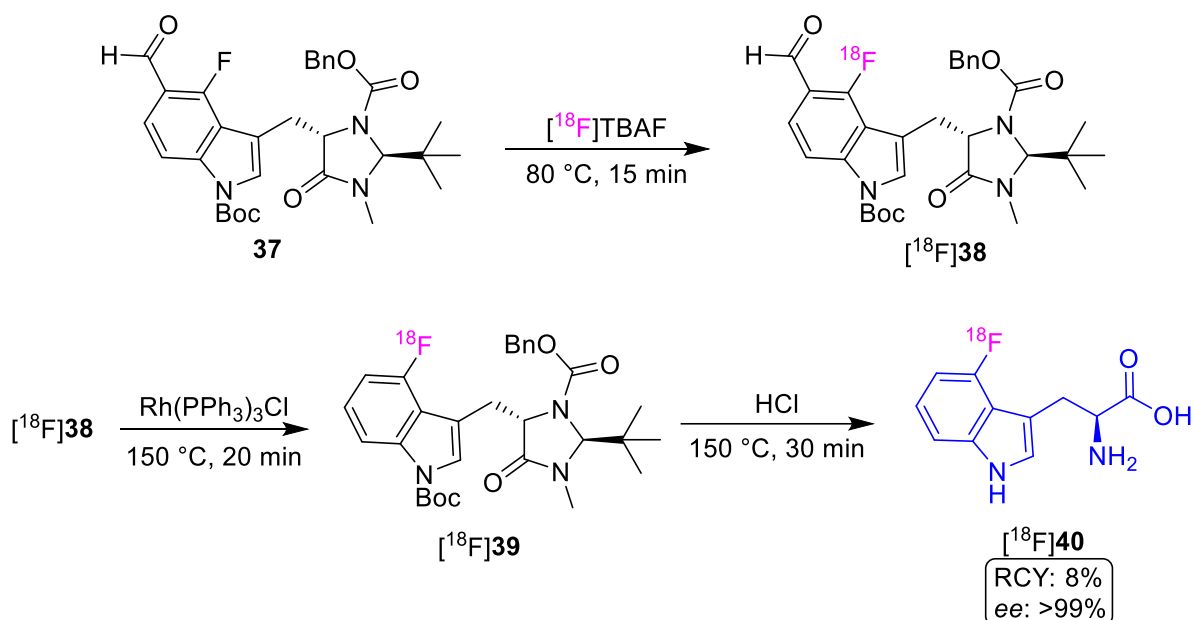
### 1.2.5. Radiofluorination via Isotopic Exchange

There are several accounts of isotopic <sup>18</sup>F-for-<sup>19</sup>F exchange being used as a radiofluorination approach towards <sup>18</sup>F-labeled AAA preparations.<sup>29-32</sup> Isotopic <sup>18</sup>F-for-<sup>19</sup>F exchange typically requires the presence of an activating group (e.g. aldehyde) on the aromatic ring. C. Melean *et al.* reported the use of Rh(PPh<sub>3</sub>)<sub>3</sub>Cl (Wilkinson's catalyst) towards 2-[<sup>18</sup>F]fluoro-L-phenylalanine (2-[<sup>18</sup>F]FPhe, [<sup>18</sup>F]35) and 2-[<sup>18</sup>F]fluoro-L-tyrosine (2-[<sup>18</sup>F]FTyr, [<sup>18</sup>F]36) preparations (Scheme 9) following <sup>18</sup>F-for-<sup>19</sup>F isotopic exchange *via* decarbonylation.<sup>30</sup> However, the very high reaction temperatures significantly limited the practicality of this protocol. A further drawback of this procedure is the relatively poor *ee* of the final products (>88%).



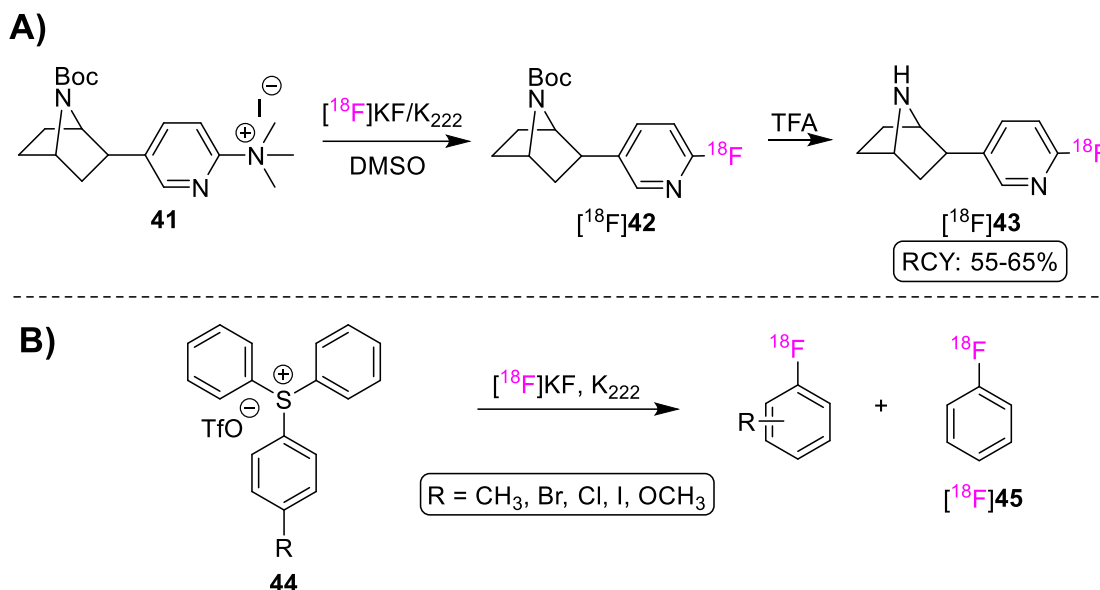
Scheme 9. Preparation of 2- $[\text{18F}]\text{35}$  and 2- $[\text{18F}]\text{36}$  using Wilkinson's catalyst.<sup>30</sup>

In a similar protocol to C. Melean *et al.*, a three-step radiosynthesis of 4- $[\text{18F}]\text{fluoro-L-tryptophan}$  (4- $[\text{18F}]\text{FTTrp}$ ,  $[\text{18F}]\text{40}$ ) was also reported (Scheme 10).<sup>31</sup> Although desirable *ee* values were obtained in the final product, the 11 step precursor synthesis, harsh reaction temperatures, inefficient hydrolysis, and low RCY limited the practicality of this procedure.



Scheme 10. Preparation of  $[\text{18F}]\text{40}$  using Wilkinson's catalyst.<sup>31</sup>

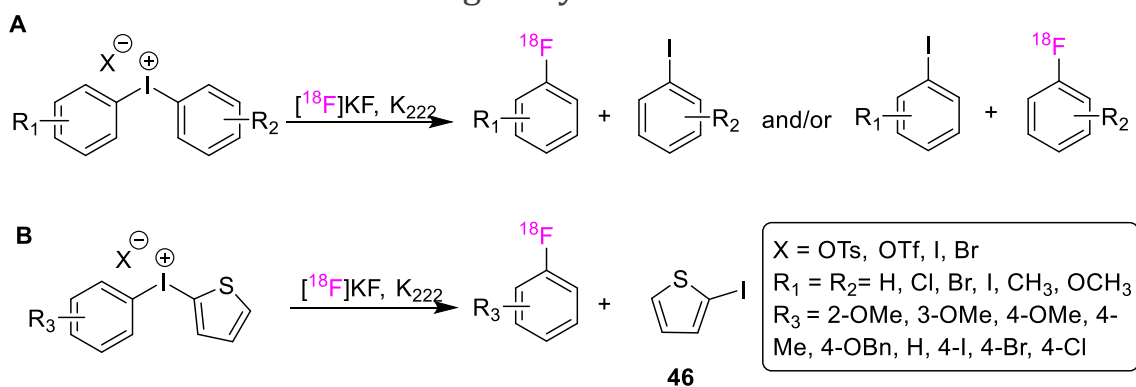
### 1.2.6. Radiofluorination via Quaternary Anilinium and Triarylsulfonium Salts



Scheme 11. A) Preparation of  $[^{18}\text{F}]\mathbf{43}$ , and B) Triarylsulfonium salts towards  $\text{S}_{\text{N}}\text{Ar}$  radiofluorination.<sup>33,34</sup>

In 1997, Carroll *et al.* reported a one-pot two-step preparation of norchloro $[^{18}\text{F}]$ fluoroepibatidine ( $[^{18}\text{F}]\mathbf{43}$ ) via  $\text{S}_{\text{N}}\text{Ar}$  radiofluorination of a trimethylammonium salt precursor (Scheme 11 A).<sup>33</sup> Mu *et al.* reported the use of triarylsulfonium salts towards the  $^{18}\text{F}$ -labeling of arenes based on the  $\text{S}_{\text{N}}\text{Ar}$  mechanism (Scheme 11 B).<sup>34</sup>

### 1.2.7. Radiofluorination Using Diaryliodonium Salts

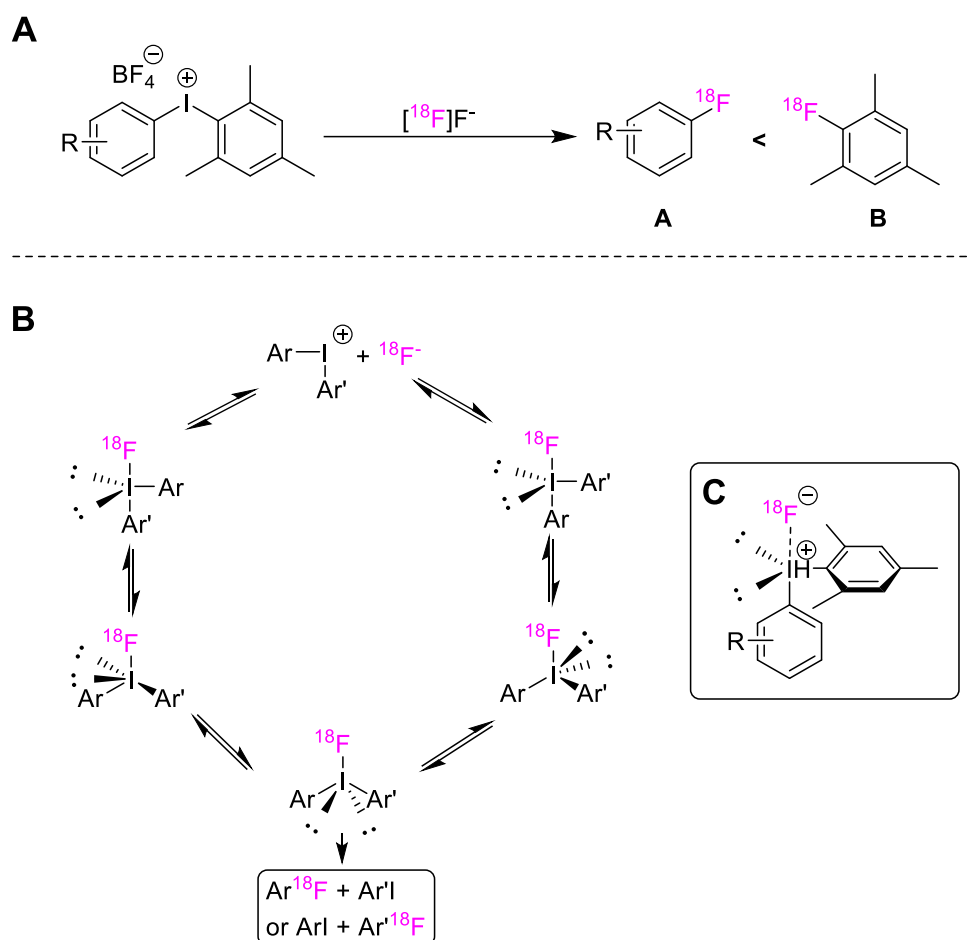


Scheme 12. Diaryliodonium salts towards aromatic  $^{18}\text{F}$ -labeling.<sup>38,39</sup>

It was found that diaryliodonium salts could be employed towards arene  $^{18}\text{F}$ -incorporation with a wide substrate scope; this proved advantageous compared to the aforementioned protocols (Scheme 12 A).<sup>35-37</sup> The regioselective radiofluorination of diaryliodonium salts is afforded due to the steric and electronic effects of the respective heteroarenes.<sup>38,39</sup> For asymmetrical

heteroarenes (Scheme 12 B),  $^{18}\text{F}$ -incorporation is found to proceed onto the more electron-deficient arene.

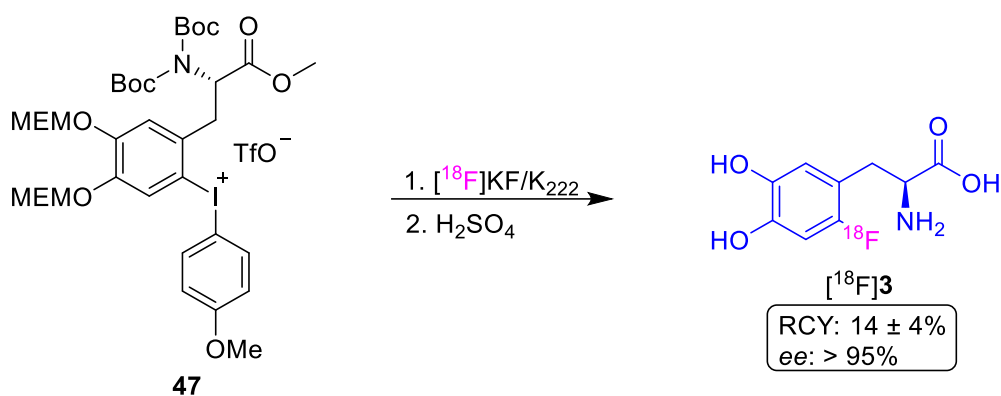
The aryl substituents were determined to have a substantial impact on the rate of radiofluorination of diaryliodonium salts. Gail *et al.* reported that *ortho*-substituents on the aromatic ring provide enhanced  $^{18}\text{F}$ -labeling rates.<sup>40</sup> The “ortho effect”, could be explained by an iodine-centered bipyramidal intermediated species, which preferentially directs the incoming  $[\text{}^{18}\text{F}]\text{F}^-$  nucleophile (Scheme 13). In this way, diaryliodonium salts with substituents in the *ortho*-position furnish elevated RCYs.<sup>41</sup>



Scheme 13. A) Radiofluorination of diaryliodonium salts B) Proposed “turnstile” mechanism for the radiofluorination of diaryliodonium salts. C)  $^{18}\text{F}$ -Diaryliodonium salt intermediate state.<sup>41</sup>

In 2015, DiMagno *et al.* succeeded to prepare  $[\text{}^{18}\text{F}]\mathbf{3}$  with n.c.a.  $[\text{}^{18}\text{F}]\text{fluoride}$  using a diaryliodonium salt precursor (Scheme 14).<sup>42</sup> The authors reported a high  $A_m$  of  $[\text{}^{18}\text{F}]\mathbf{3}$  (35 GBq/ $\mu\text{mol}$ ) using this method). Despite this protocol being implemented successfully into an automated module, lengthy precursor synthesis (28% over five steps) and low RCYs limited the feasibility of this approach. Although the use of diaryliodonium salts provides a

radiofluorination strategy that encompasses a wide substrate scope, their applications towards routine radiopharmaceutical preparations for clinical applications have been limited to date.



*Scheme 14. Nucleophilic radiofluorination towards  $^{18}\text{F}$ -labeled AAAs.<sup>42</sup>*

### 1.2.8. The Minimalist Approach

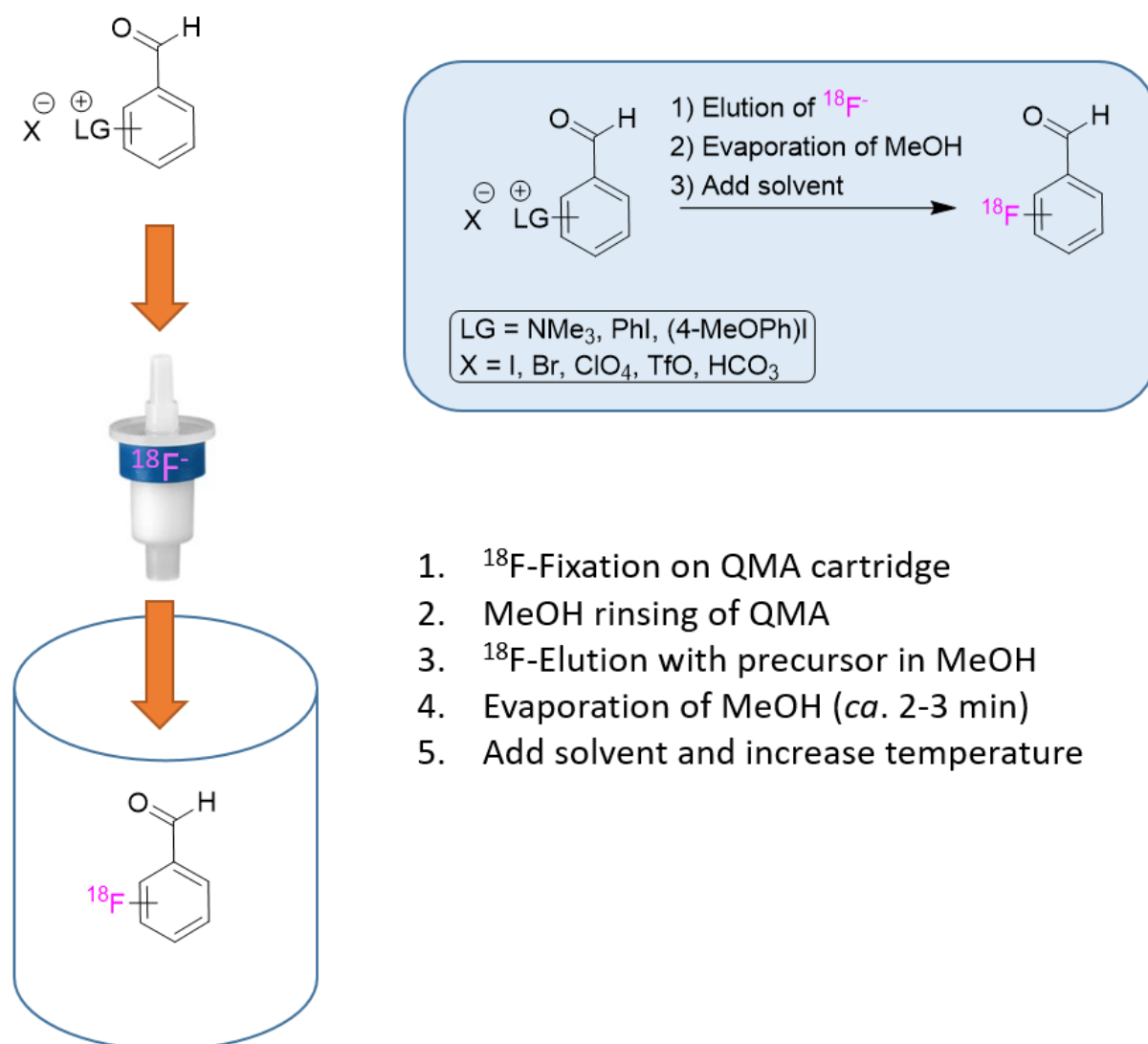
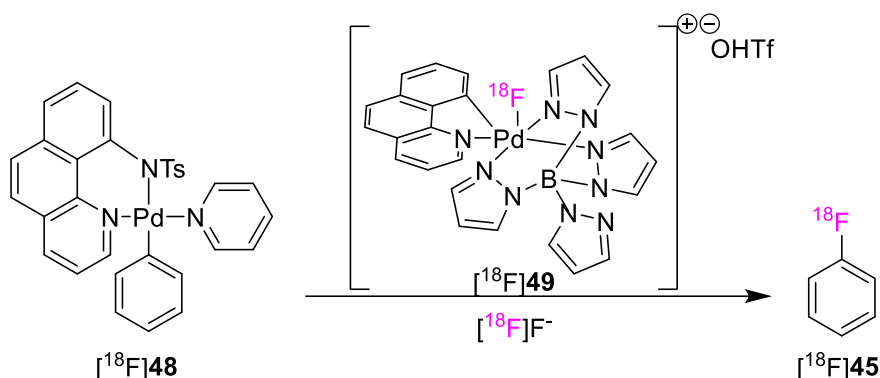


Figure 9. The minimalist approach.<sup>43</sup>

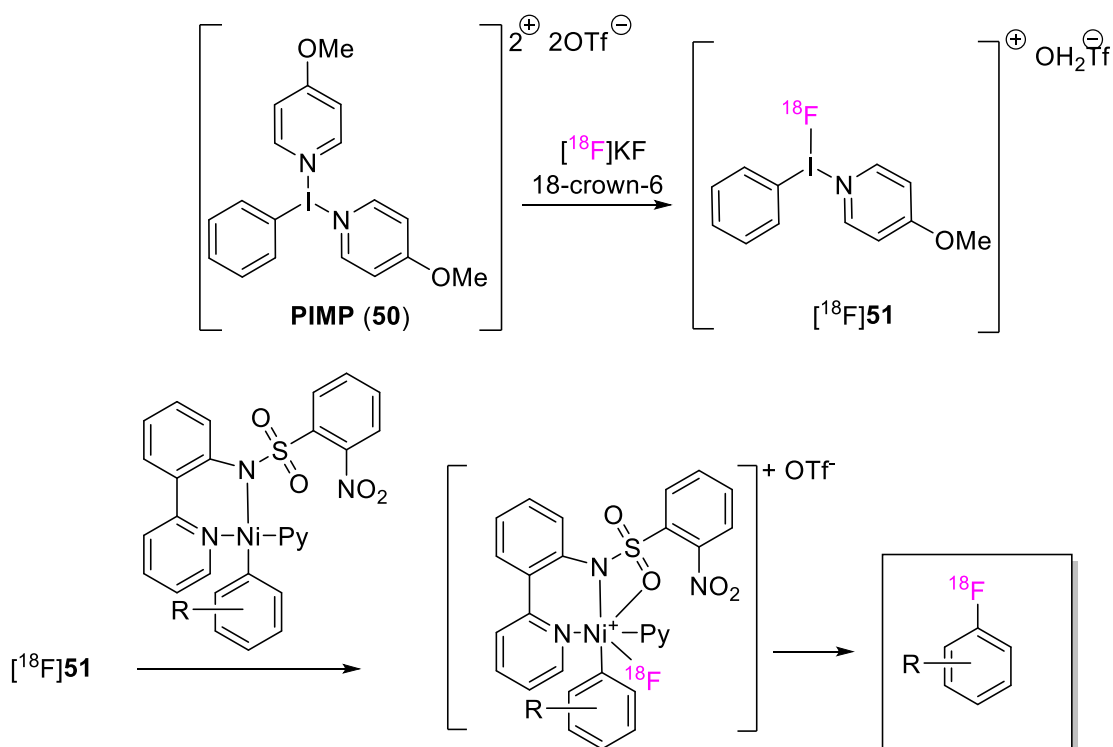
The minimalist approach, described by Richarz *et al.*, is a procedure devised to save time by omitting the routine azeotropic drying step, and negating the typically required base or alternative additives.<sup>43</sup> The method demonstrates that positively-charged precursors, such as a quaternary anilinium, diaryliodonium, or triarylsulfonium salts (onium salts), act as a counter-anions for [ $^{18}\text{F}$ ]F<sup>-</sup> displacement on the QMA cartridge, and elute the [ $^{18}\text{F}$ ]fluoride into the reaction vessel (Fig. 9). This technique has been demonstrated to have a broad substrate scope and accommodates for base-sensitive precursors and products.

### 1.2.9. Aromatic Transition Metal-Mediated Radiofluorination



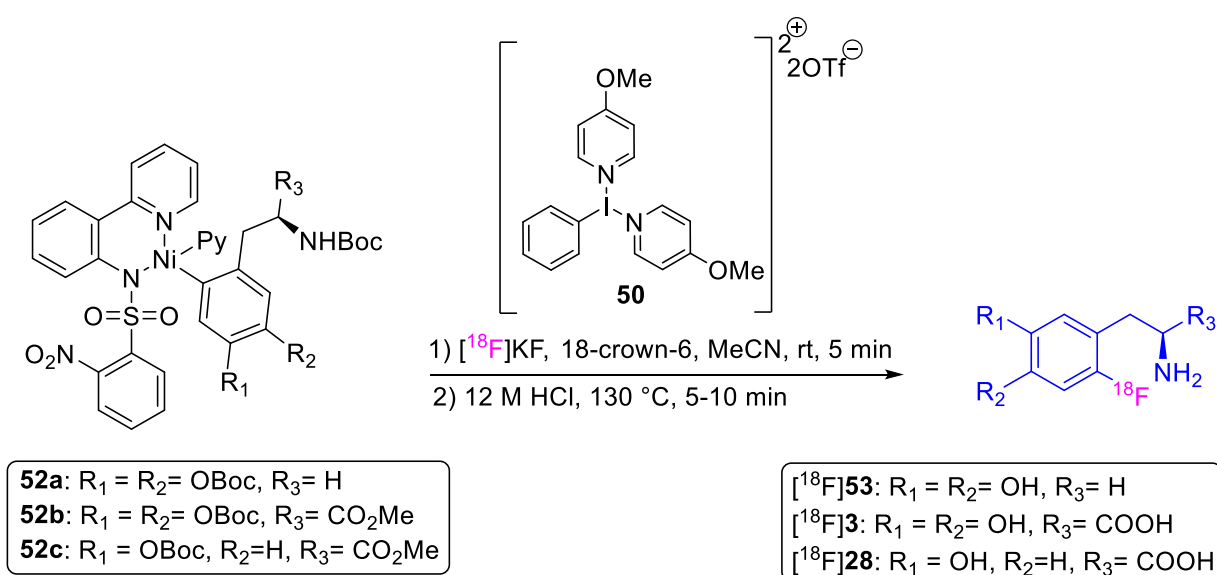
*Scheme 15. Umpolung of nucleophilic n.c.a. [ $^{18}\text{F}$ ]fluoride: oxidative addition into a Pd complex, proceeded by reductive elimination to furnish the desired  $^{18}\text{F}$ -labeled arene.<sup>44</sup>*

In 2011, Lee *et al.* reported a sophisticated two-step fluorination protocol for the late-stage  $^{18}\text{F}$ -incorporation of arenes using a radiofluorinated Pd(IV) complex (**[ $^{18}\text{F}$ ]49**) (Scheme 15).<sup>44</sup> This approach utilizes high  $A_m$  nucleophilic fluorine-18 for the preparation of an electrophilic radiofluorination Pd(IV) complex (**[ $^{18}\text{F}$ ]49**), which acts as an electron acceptor. The reaction mechanism permits the  $^{18}\text{F}$ -incorporation of electron-rich arenes, an otherwise significant challenge using conventional radiofluorination strategies. However, the two-step procedure increases the radiosynthesis time and requires azeotropic drying.



*Scheme 16. Overview of Ni-mediated radiofluorination.<sup>45</sup>*

Later, the same group developed a radiofluorination procedure employing hypervalent iodine oxidant [*bis*(onio)-substituted aryl iodine(III)] (**50**), which generates an *in situ* radiofluorination agent (Scheme 16).<sup>45</sup> The method builds on the previous findings and enables a one-step oxidative fluorination protocol for the late-stage <sup>18</sup>F-incorporation of arenes using aqueous solutions of [<sup>18</sup>F]fluoride. Despite the successes of Pd- and Ni-mediated radiofluorination protocols, major drawbacks such as the necessity to handle and prepare air- and moisture-sensitive transition metal complexes have hampered their adaptation for routine radiopharmaceutical production.<sup>46,47</sup> Moreover, any radiopharmaceuticals produced using these methods would require the determination of the Pd- or Ni-content as part of the quality control (QC) evaluation as outlined by the cGMP regulations.

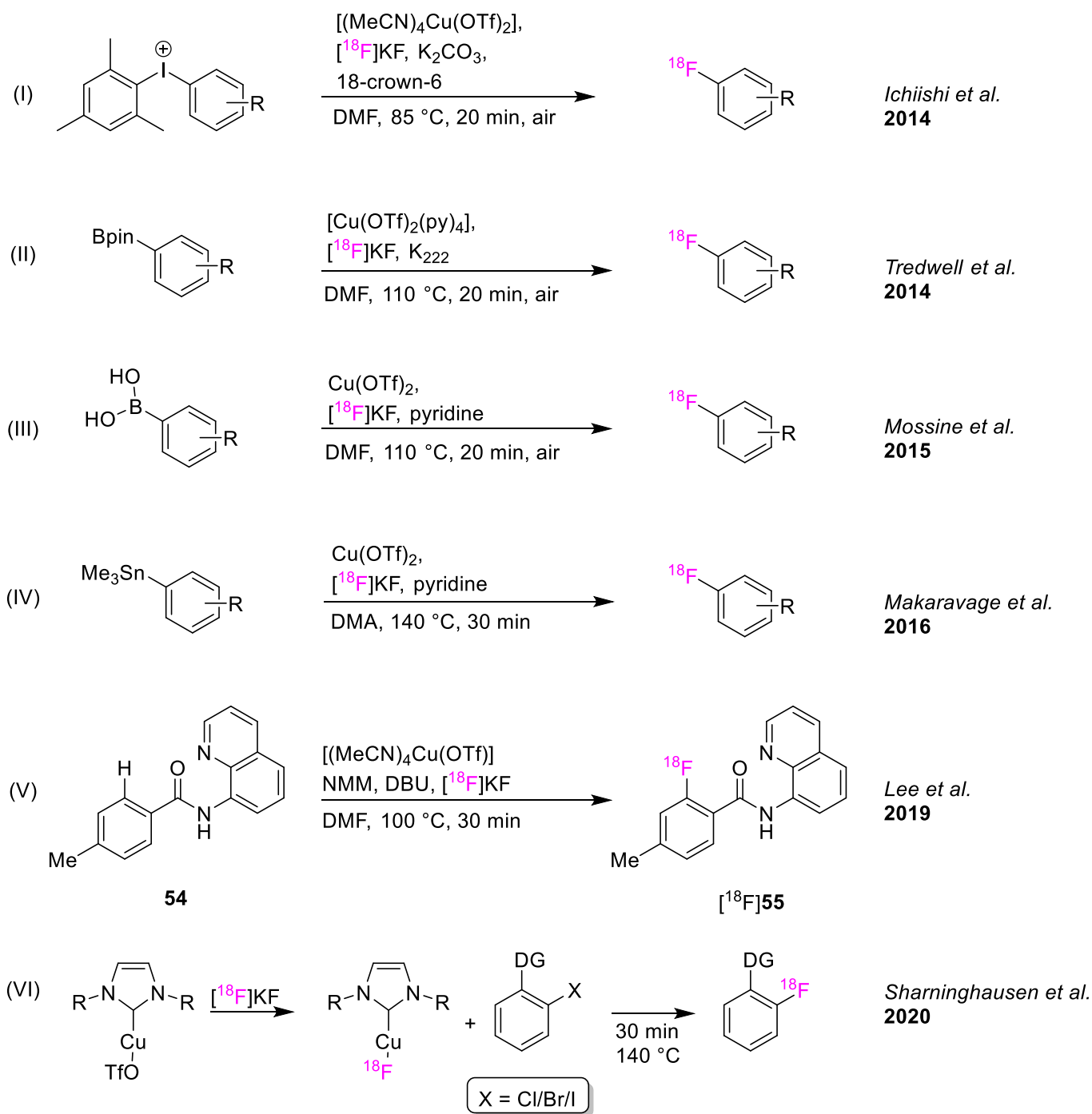


Scheme 17. Ni-Mediated radiofluorination towards <sup>18</sup>F-labeled AAAs.<sup>48</sup>

In 2015, Zlatopolskiy *et al.* applied the previously described Ni-mediated radiofluorination method towards the preparation of clinically relevant doses of [<sup>18</sup>F]**3** (RCY: 7 ± 1%), [<sup>18</sup>F]**28** (RCY: 5 ± 1%), and [<sup>18</sup>F]fluoro- L-dopamine ([<sup>18</sup>F]FDA, [<sup>18</sup>F]**53**, 12 ± 2%) (Scheme 17).<sup>48</sup> Despite the one-pot two-step procedure furnishing very high A<sub>m</sub> values for [<sup>18</sup>F]**3** (175 GBq/μmol) and [<sup>18</sup>F]**28** (60 GBq/μmol), the low RCYs of the <sup>18</sup>F-labeled AAAs and the moisture sensitivity of the **52a-c** were drawbacks of this approach. The latter aspect hampered the protocol from being implemented into an automated radiosynthesis module.

### 1.2.10. Cu-Mediated Radiofluorination

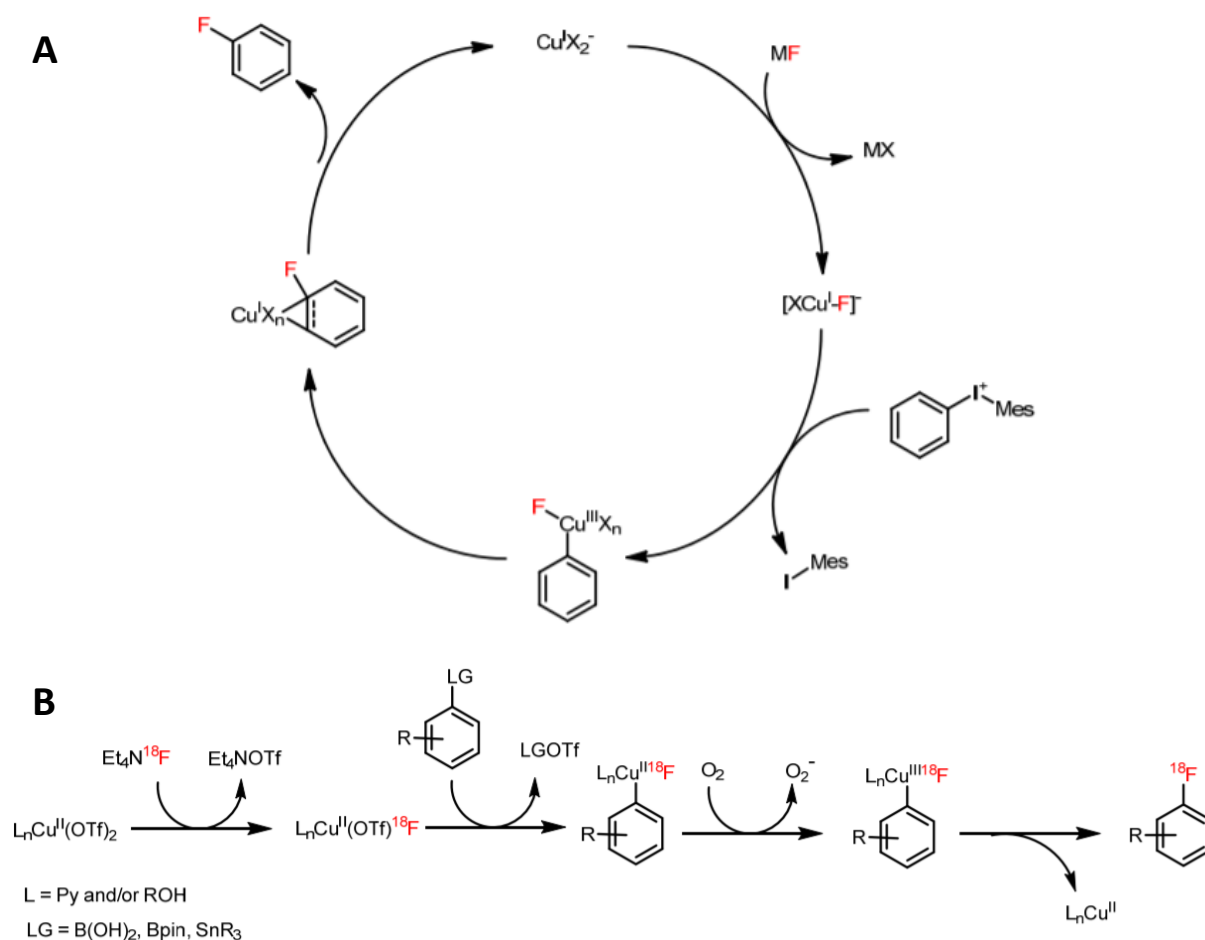
$^{18}\text{F}$ -Fluorinated arenes may also be accessed from their respective iodonium salt-, boron-, or stannane-containing precursors using the Cu(II)-mediated radiofluorination protocols pioneered by the groups of Scott and Gouverneur. Cu-Mediated radiofluorination enables the  $^{18}\text{F}$ -incorporation into electron-poor, electron-neutral and electron-rich arenes, and tolerates the presence of many functional groups.



Scheme 18. Timeline of Cu-mediated radiofluorination developments.<sup>49-54</sup>

Cu-Mediated radiofluorination reported by Ichishii *et al.* employed [(MeCN)<sub>4</sub>Cu(OTf)<sub>2</sub>] as a mediator and used (aryl)iodonium salts as substrates (Scheme 18 I).<sup>49</sup> Following these findings, Tredwell *et al.* developed a novel Cu-mediated fluorination procedure employing arylboropinacol esters (Ar-Bpin) as substrates (Scheme 18 II).<sup>50</sup> The proposed reaction mechanisms for Cu-mediated radiofluorination are described in Scheme 19. Ar-Bpin substrates in combination with [Cu(OTf)<sub>2</sub>(py)<sub>4</sub>], furnished <sup>18</sup>F-labeled arenes with impressive <sup>18</sup>F-incorporation rates (Scheme 18 II). Further developments by Mossine *et al.* and Makaravage *et al.* expanded the scope of Cu-mediated radiofluorinations to incorporate boronic acids and aryl stannanes, respectively (Scheme 18 III & IV).<sup>51,52</sup>

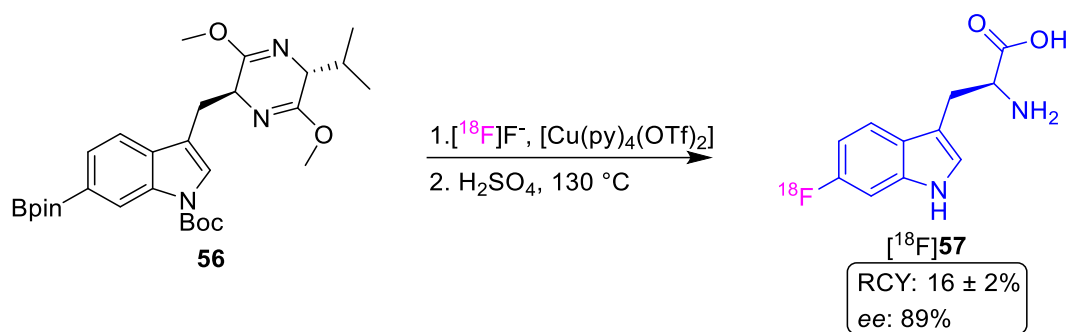
The group of Scott *et al.* recently reported the use of aminoquinolines as directing groups towards Cu-mediated aryl C-H bond radiofluorinations (Scheme 18 V).<sup>53</sup> One major advantage of this procedure is the omission of a LG (e.g. Bpin) commonly required for aryl <sup>18</sup>F-labeling. The final removal of the aminoquinoline moiety is achieved *via* base hydrolysis of the amide, furnishing the final product in moderate RCYs. Despite C-H <sup>18</sup>F-fluorination showing some promising results, the reaction has a limited substrate scope and requires strongly basic deprotection conditions. The same group later reported the Cu-mediated radiofluorination of aryl halides (Scheme 18 VI).<sup>54</sup> However, the presence of a suitable directing group is required for this reaction.



Scheme 19. A) Proposed mechanism for Cu-mediated radiofluorination using(mesityl)(aryl)iodonium salts, and B) Bpin-substituted arene.<sup>55</sup>

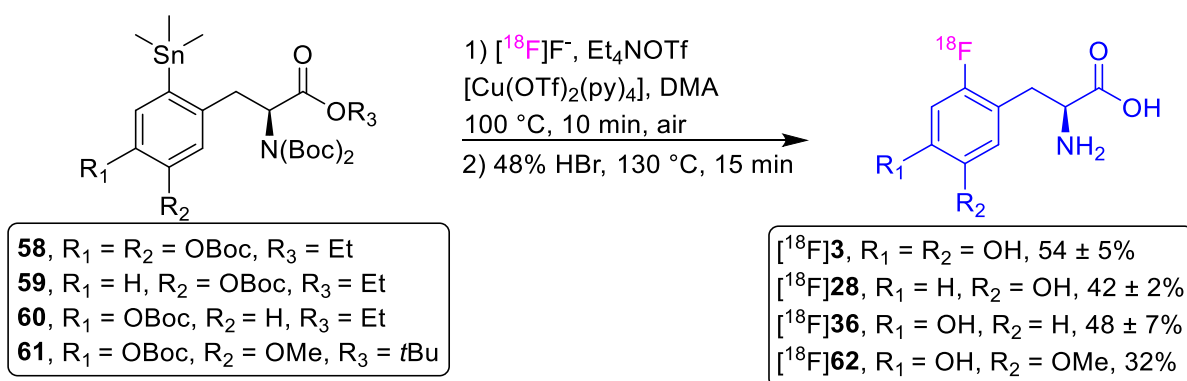
In contrast to the aforementioned Ni-/Pd-mediated radiofluorination approaches, Cu-mediated radiofluorination permitted aerobic conditions and advantageously employed bench-stable and easily-accessible/commercially available Cu-mediators. Despite the preliminary success of these Cu-mediated radiofluorinations, radiopharmaceutical applications on a preparative scale using these strategies remained a challenge. In 2015, Zlatopolskiy *et al.* described how Cu-mediated radiofluorinations using diaryliodonium salts and Bpin-substituted arenes could be achieved on a larger scale using a “low-base” approach. The method employed relatively less K<sub>2</sub>CO<sub>3</sub> for <sup>18</sup>F-elution, accounting for the base-sensitivity of the Cu-mediator.<sup>55</sup> The application of the “minimalist” approach (Section 1.2.8.), whereby [<sup>18</sup>F]fluoride is directly eluted from the anion-exchange resin by an alcoholic solution containing a suitable labeling precursor (e.g. diaryliodonium, triarylsulfonium or quaternary ammonium), was also applied towards Cu-mediated radiofluorination protocols. In these instances, the minimalist approach was found to enhance Cu-mediated radiofluorination due to the omission of time-consuming azeotropic drying and the absence of a base.<sup>55</sup>

### 1.2.10.1. Cu-Mediated Radiofluorination Towards $^{18}\text{F}$ -labeled AAA Preparations



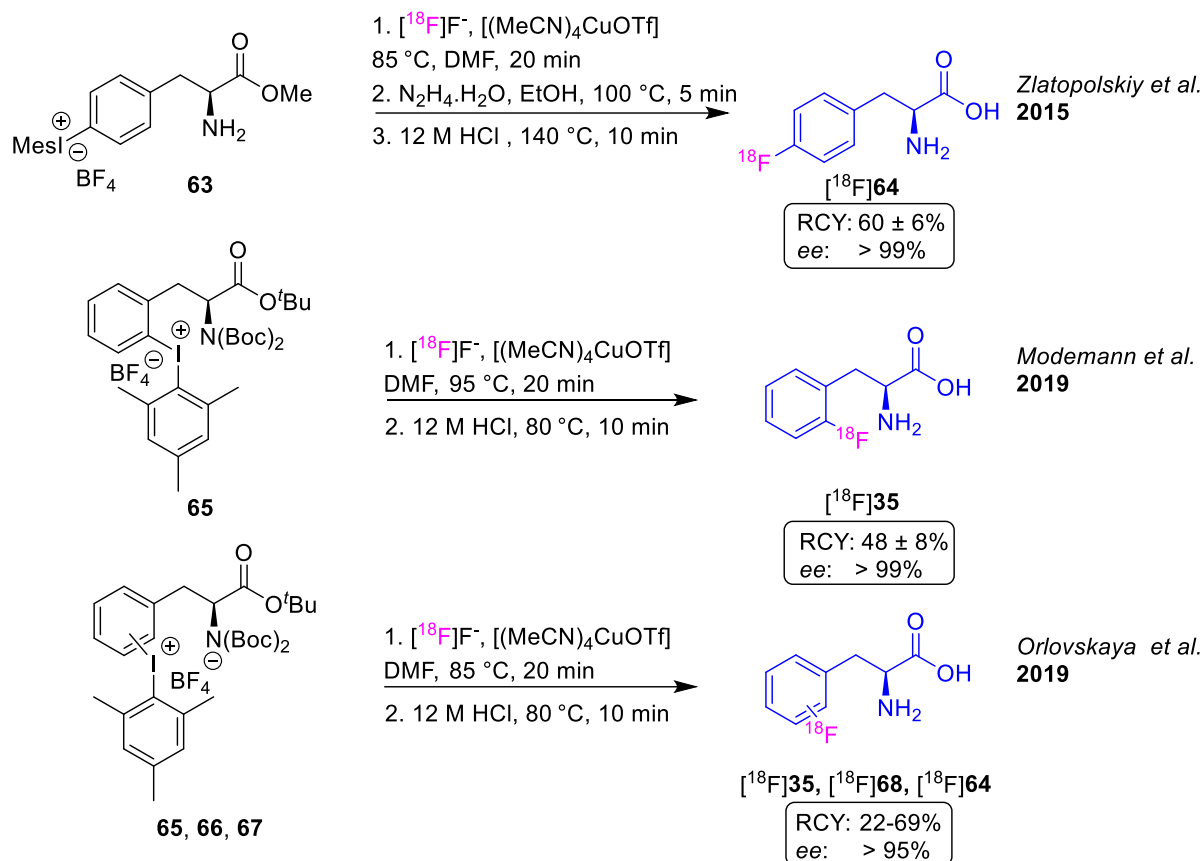
Scheme 20. Schöllkopf auxiliary towards  $^{18}\text{F}$ -labeled AAAs.<sup>56</sup>

Schäfer *et al.* employed Cu-mediated radiofluorination towards 6- $^{18}\text{F}$ FTrp using the Schöllkopf auxiliary (Scheme 20).<sup>56</sup> However, it was found that the *ee* of the final tracers was not always above 95% and that harsh reaction conditions ( $\text{H}_2\text{SO}_4$ , 130 °C) were required to ensure complete deprotection. Consequently, this made the synthesis more difficult to implement into automated modules. Additionally, the precursor synthesis route (37% over six steps) was lengthy. In 2017, Zarrad *et al.* reported the Cu-mediated radiofluorination using arylstannane precursors (Scheme 21). The protocol allowed AAA tracers including 6- $^{18}\text{F}$ FDOPA ( $^{18}\text{F}$ **3**), 6- $^{18}\text{F}$ FMT ( $^{18}\text{F}$ **28**), 2- $^{18}\text{F}$ FTyr ( $^{18}\text{F}$ **36**), and  $^{18}\text{F}$ OMFD ( $^{18}\text{F}$ **62**) to be accessed in high RCYs of 32–54% on a preparative scale.<sup>57</sup> Notably, this protocol described the highest RCY for 6- $^{18}\text{F}$ FDOPA ( $54 \pm 5\%$ ) to date.



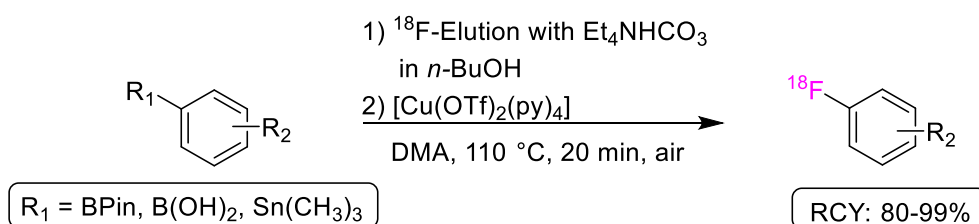
Scheme 21. Cu-Mediated radiofluorination of arylstannanes towards  $^{18}\text{F}$ -labeled AAAs.<sup>57</sup>

Cu-Mediated radiofluorination of diaryliodonium salts have also been used to furnish 2–4- $^{18}\text{F}$ FPhe ( $^{18}\text{F}$ **35**,  $^{18}\text{F}$ **68**,  $^{18}\text{F}$ **64**) (Scheme 22).<sup>55,58,59</sup> The “minimalist” approach has been employed for the preparation of  $^{18}\text{F}$ **64**.



Scheme 22. Cu-Mediated radiofluorination towards [ $^{18}\text{F}$ ]**35**, [ $^{18}\text{F}$ ]**68** and [ $^{18}\text{F}$ ]**64**.<sup>55,58,59</sup>

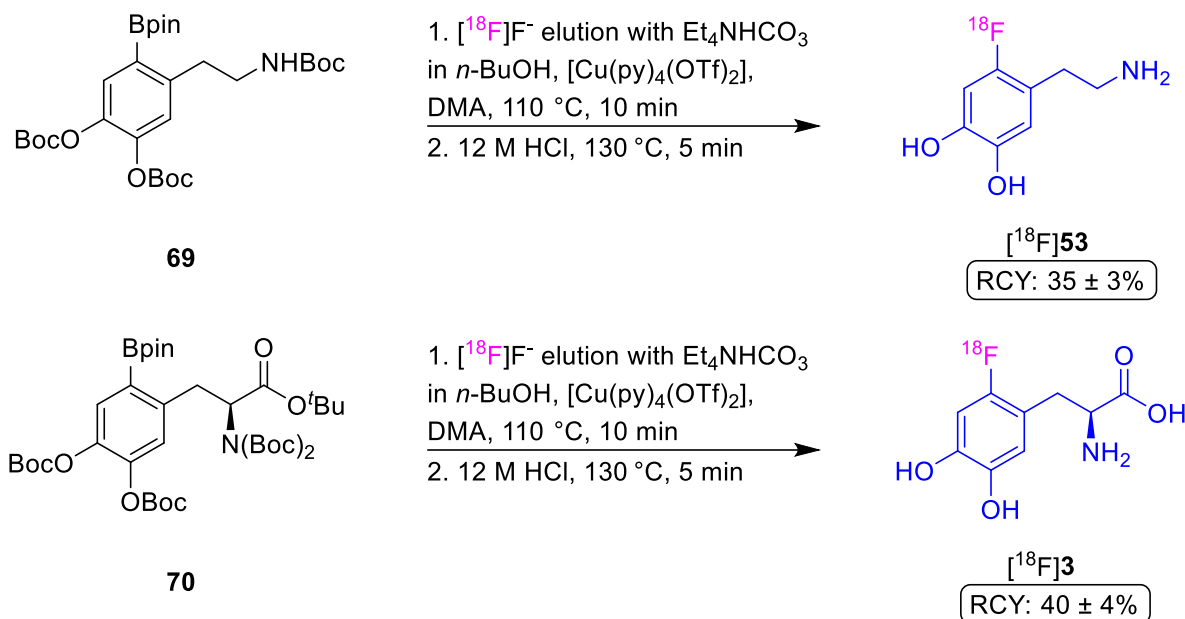
### 1.2.11. Alcohol-Enhanced Cu-Mediated Radiofluorination



Scheme 23. Alcohol-enhanced Cu-mediated radiofluorination.<sup>46</sup>

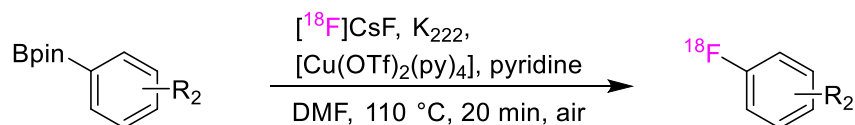
In 2016, Zischler *et al.* reported the beneficial effect of primary and secondary alcohols on the Cu-mediated radiofluorination of (Het)Aryl-Bpins, -B(OH)<sub>2</sub> and -SnR<sub>3</sub> (Scheme 23).<sup>46</sup> These findings contradict the previously held assumption that alcohols are unsuitable solvents for Cu-mediated radiofluorination.<sup>50</sup> The general procedure allows the efficient radiolabeling of a broad range of substrates, such as (het)aryltrialkylstannanes, (hetero)arylboronic acids, and pinacolyl boronate, with 80–99% RCY. Moreover, the approach describes  $^{18}\text{F}$ -elution using Et<sub>4</sub>NHCO<sub>3</sub> and alcoholic solutions; in this way, the time-consuming azeotropic drying step is circumvented. Compared to other alcohols, *n*-BuOH afforded the highest  $^{18}\text{F}$ -incorporation

rates for Bpin-substituted arenes (RCC:  $94 \pm 2\%$ ) and arylboronic acids (RCC:  $98 \pm 4\%$ ). Using the alcohol-enhanced Cu-mediated radiofluorination protocol [ $^{18}\text{F}$ ]**3** and [ $^{18}\text{F}$ ]**53** were accessed in high RCY and  $A_m$  values (39 and 37 GBq/ $\mu\text{mol}$  respectively) (Scheme 24).



Scheme 24. Preparation of [ $^{18}\text{F}$ ]**3** via alcohol-enhanced Cu-mediated radiofluorination.<sup>46</sup>

### 1.2.12. Cu-Mediated Radiofluorination Using Pyridine-Based Additives



Scheme 25. Pyridine-enhanced Cu-mediated radiofluorination.<sup>60</sup>

In 2017, Antuganov *et al.* first described the presence of pyridine to increase  $^{18}\text{F}$ -labeling efficiency *via* Cu-mediated radiofluorination (Scheme 25).<sup>60</sup> However, this protocol required time-consuming azeotropic drying. Two years later, the same group reported a more powerful method of  $^{18}\text{F}$ -labeling by combining aspects from the minimalist approach with the addition of DMAPOTf (**71**) as a PTC and base (Fig. 10).<sup>61</sup> The use of Oasis WAX cartridges (a weak lipophilic anion-exchange cartridge) was found to be advantageous compared to alternative QMA or Chromafix<sup>®</sup> cartridges for this method. The DMAPOTf in a solution of DMA serves to elute the fixed  $^{18}\text{F}^-$  (with elution efficiency of ca. 78%) and serves to increase the efficiency of the Cu-mediated radiofluorination substantially. Consequently, the ‘Antuganov approach’ requires only 0.25 M equivalents of  $[\text{Cu}(\text{OTf})_2(\text{py})_4](\text{Y})$  compared to the precursor (Fig. 10). This ultimately reduces the Cu-content present in the final reaction mixture, an important factor for cGMP radiopharmaceutical production.

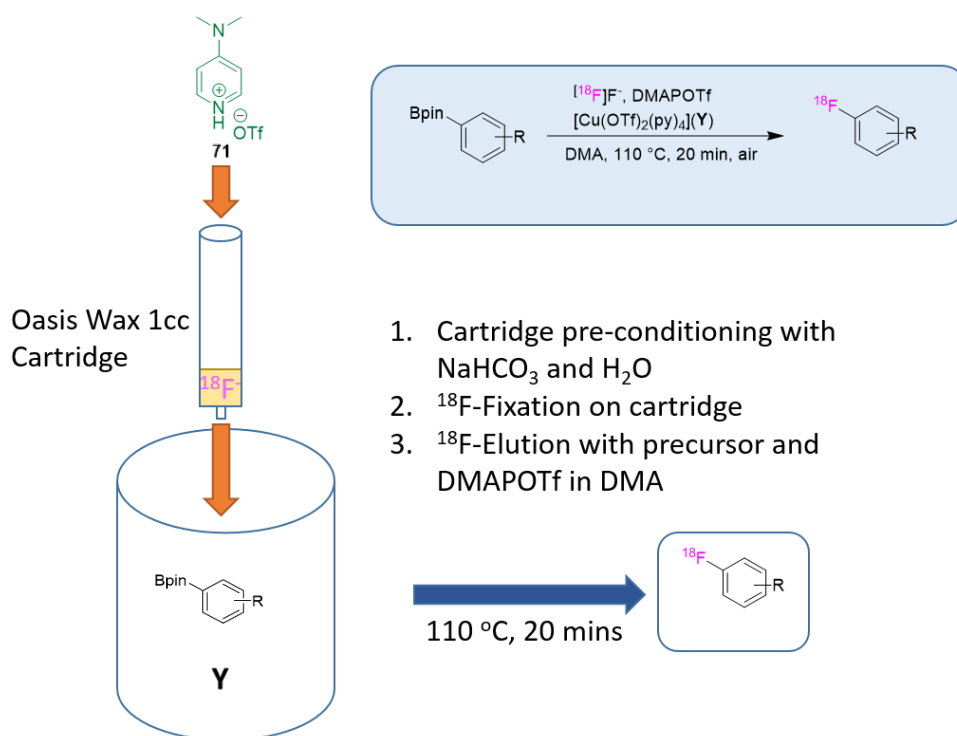
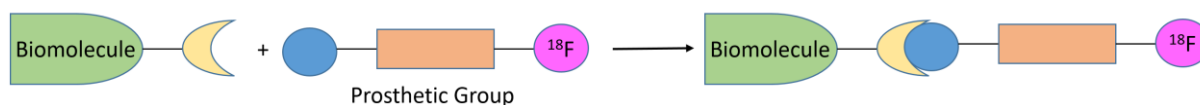


Figure 10. The Antuganov approach towards Cu-mediated radiofluorination.<sup>61</sup>

In the context of this project, alcohol-enhanced Cu-mediated radiofluorination has the following advantages:

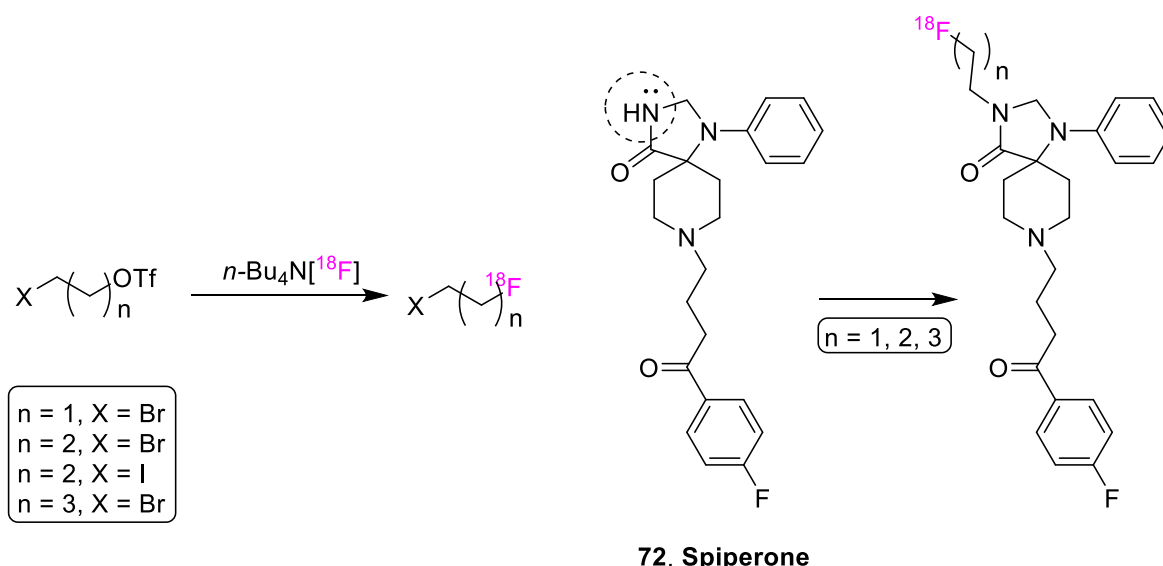
1. The rapid and high  $^{18}\text{F}$ -incorporation rates of electron-rich arene substrates, including those typically prevalent in AAAs.
2. The bench and moisture stability of the Cu-mediator complexes, therefore enabling their use for routine AAA tracer production in automated synthesis modules.
3. The facile one-step preparation/commercial availability of the Cu-mediators.
4. The commercial availability of Bpin-substituted reagents, thereby facilitating precursor synthesis.
5. The method permits the employment of arylstannane-based precursors as alternatives to Bpin- or boronic acid-substituted arenes.

### 1.2.13. Prosthetic Groups in Radiochemistry



Scheme 26. Indirect radiofluorination strategy using a prosthetic group.

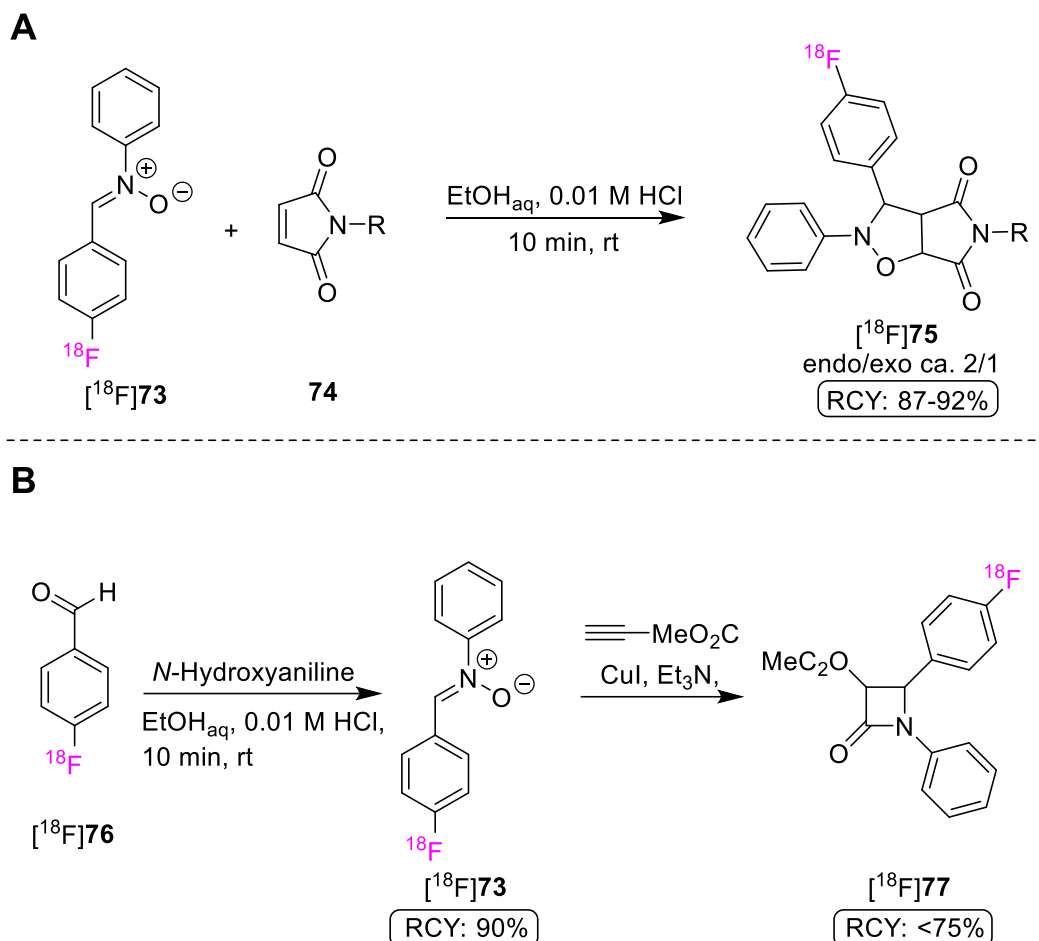
In many cases, the late-stage/direct radiofluorination of sensitive and complex molecules (e.g. peptides and proteins) is either very challenging or impossible. This is mainly due to the harsh reaction conditions, such as organic solvents, and high temperatures required for direct radiofluorination.<sup>62</sup> Instead, indirect radiofluorination methods using prosthetic groups can be a more practical alternative towards the production of  $^{18}\text{F}$ -labeled biomolecules (Scheme 26).



Scheme 27. Radiosynthesis of  $^{18}\text{F}$ -fluoroalkyl-spiperone ( $[^{18}\text{F}]\mathbf{72}$ ) via prosthetic group.<sup>63</sup>

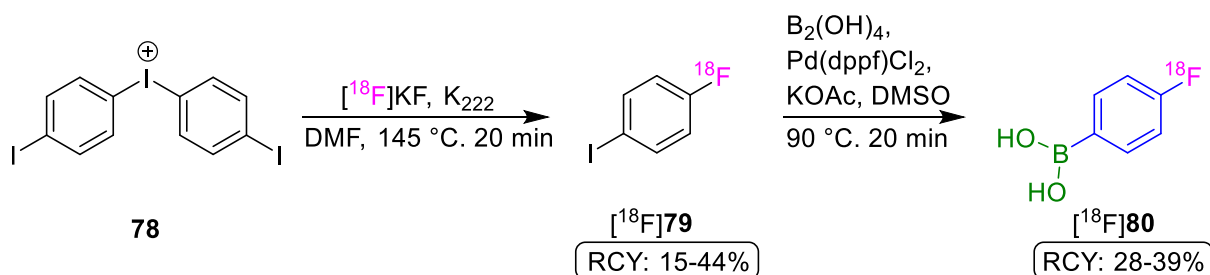
Radiochemists have developed a series of  $^{18}\text{F}$ -labeled auxiliary synthons (prosthetic groups), that selectively couple to the target biomolecule under mild reaction conditions (Scheme 27). Prosthetic groups typically contain a leaving group (LG) suitable for radiolabeling, and a separate LG used for the prosthetic groups coupling to a biomolecule.<sup>64</sup> For example, many research groups have succeeded to apply the (3 + 2) azide-alkyne Huisgen cycloaddition (Click reaction) towards radiosynthetic protocols.<sup>64–66</sup> Chemical and enzymatic stability of the 1,2,3-triazole moieties, as well as excellent radiolabeling regioselectivity, functional group tolerance, and mild reaction conditions are the main advantages of applying click chemistry towards biomolecule labeling. However, the presence of a Cu catalyst required for these protocols may cause peptide and protein degradation as well as other toxicity issues. To circumvent these limitations, Neumaier *et al.* reported the preparation of the prosthetic group C-(4-

[ $^{18}\text{F}$ ]fluorophenyl)-*N*-phenyl nitron ([ $^{18}\text{F}$ ]FPPN, [ $^{18}\text{F}$ ]73) towards 1,3-dipolar cycloaddition reactions with maleimides under a wide range of conditions (Scheme 28 A).<sup>67</sup> Unfortunately, it was found that the relatively high temperatures (80–110 °C) were inappropriate for the radiofluorination of peptides and proteins.



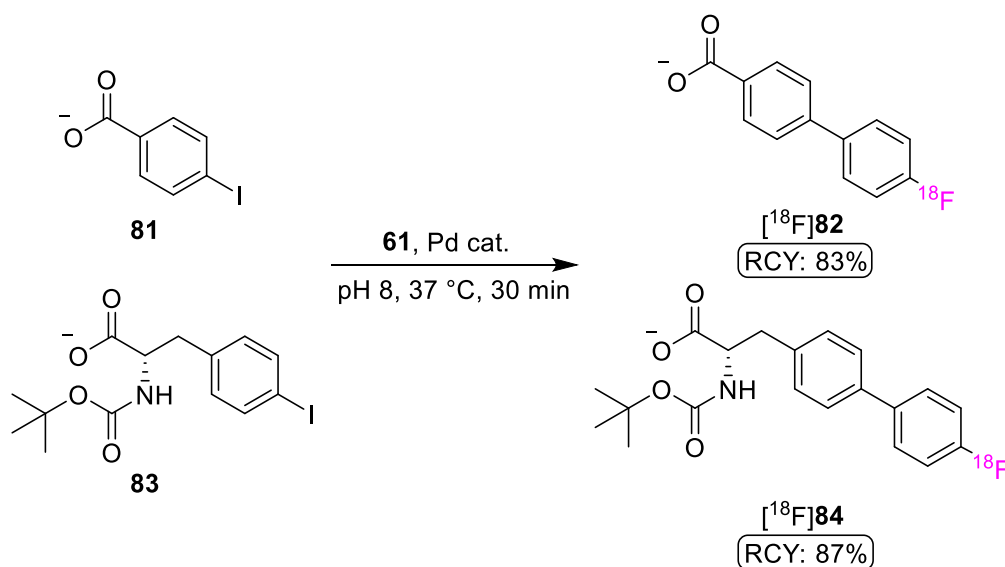
Scheme 28. [ $^{18}\text{F}$ ]83 as a versatile radiolabeled building block.<sup>67,68</sup>

In 2014, the same group reported the preparation of  $^{18}\text{F}$ -labeled  $\beta$ -lactams *via* the Kinugasa reaction (Scheme 28 B).<sup>68</sup> The mild click conditions and fast kinetics of the radio-Kinusaga reaction make the protocol an attractive indirect radiofluorination method for the radiolabeling of biopolymers, proteins, and peptides.



Scheme 29. PG [ $^{18}\text{F}$ ]80 radiosynthesis.<sup>69</sup>

In 2013, Gouverneur *et al.* applied the prosthetic group 4- $^{18}\text{F}$ fluorophenylboronic acid ( $^{18}\text{F}$ FBPA,  $^{18}\text{F}$ **80**) towards AA, protein and peptide radiolabeling (Schemes 29 & 30).<sup>69</sup> The radiosynthetic protocol employed diaryliodonium salts and Suzuki-Miyaura borylation to furnish the prosthetic group  $^{18}\text{F}$ **80**, which in turn is used for site-specific Suzuki-Miyaura coupling (SMC) with a suitable biomolecule. Despite the potential of  $^{18}\text{F}$ **80** for biomolecule radiolabeling, the main limitations of this protocol include the low RCYs (5–10%).



Scheme 30. SMC with aryl iodides **81** & **83**.<sup>69</sup>

Ferrieri *et al.* recently reported the application of  $^{18}\text{F}$ FPBA towards boron imaging in maize.<sup>70</sup> However, the procedure did not provide a RCY for the generation of  $^{18}\text{F}$ FPBA, used an excess of Cu-mediator, and involved a lengthy purification protocol.

### 1.3. Aromatic Amino Acids

The fundamental aromatic amino acid (AAA) molecular structure consists of an aromatic ring together with the amino acid core structure of a carboxylic acid and an amine group. All naturally occurring AAAs are chiral molecules. The stereochemical determination of amino acids is of particular importance as the *D* & *L* enantiomers give rise to vastly differing biological activity. The Nobel laureates Cahn, Ingold, and Prelog devised a systemic method for the unambiguous determination of chiral centers with either *S* (sinister = left) or *R* (rectus = right) annotation. However, the stereochemical determination of amino acids is usually represented in either *D* or *L* form: this can be derived from the glyceraldehyde the amino acid can theoretically be derived from (Fig. 11).

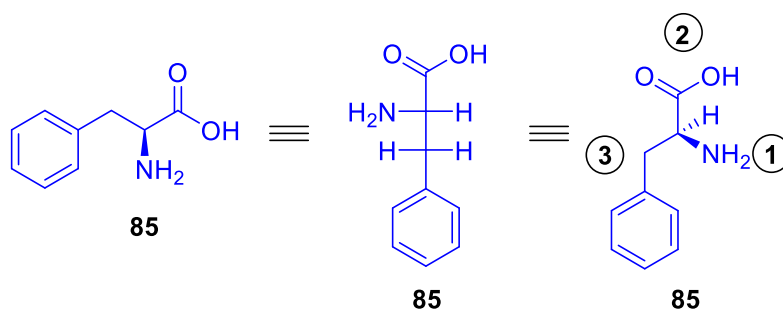
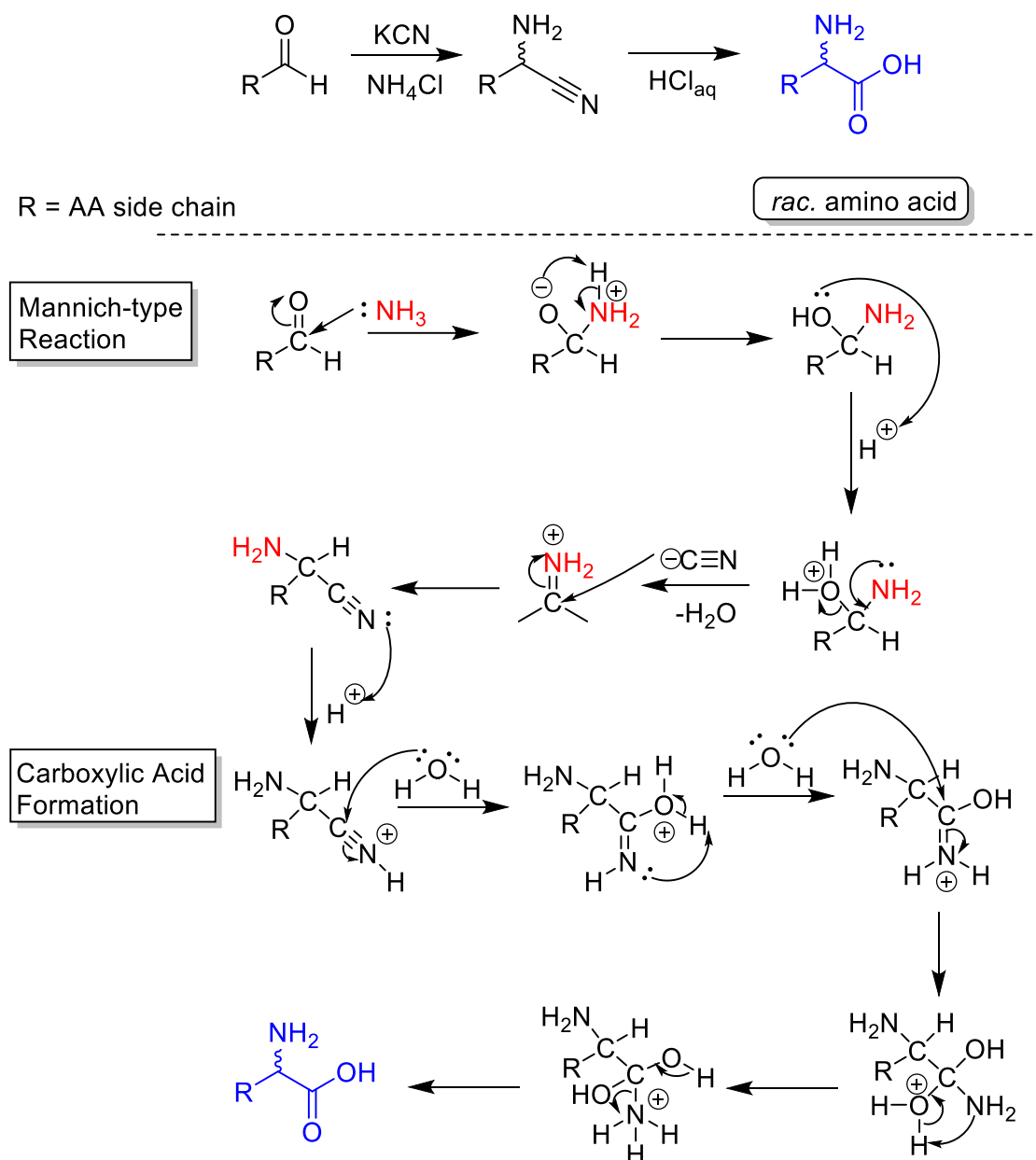


Figure 11. Stereochemistry of Phe: Fischer projection & Cahn-Ingold-Prelog configuration.

In the context of this project, it is crucial that the desired  $^{18}\text{F}$ -labeled AAA enantiomer is obtained. Therefore, the enantiomeric excess (*ee*) value of the AAA tracer must be over 95% following radiosynthesis.

### 1.3.1. Synthesis of Amino Acids



*Scheme 31. Mechanism of Strecker synthesis of racemic amino acids.<sup>71</sup>*

In 1850, Adolph Strecker succeeded in synthesizing racemic amino acids by reacting aldehydes with potassium cyanide, ammonia, and hydrochloric acid (Scheme 31).<sup>71</sup> The Mannich-type nucleophilic addition of ammonia to the carbonyl carbon atom and the subsequent condensation yields the racemic amine mixture. The Strecker reaction has been described as “excellent but tedious” in a more modern appraisal, and methods for more efficient were highly sought after.<sup>72</sup> Another example of amino acid preparation is the Hell-Volhard-Zelinsky (HVZ) reaction, frequently employed in combination with Gabriel’s synthesis.<sup>73-75</sup> Unfortunately, these synthetic routes cannot produce enantiomerically pure amino acids.

### 1.3.2. Ni- and Cu-BPB Complexes

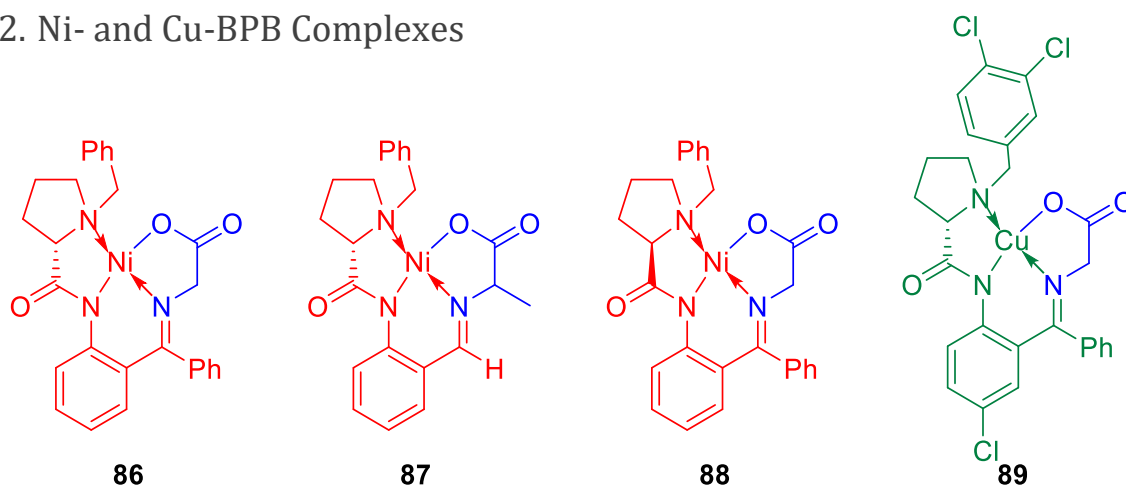
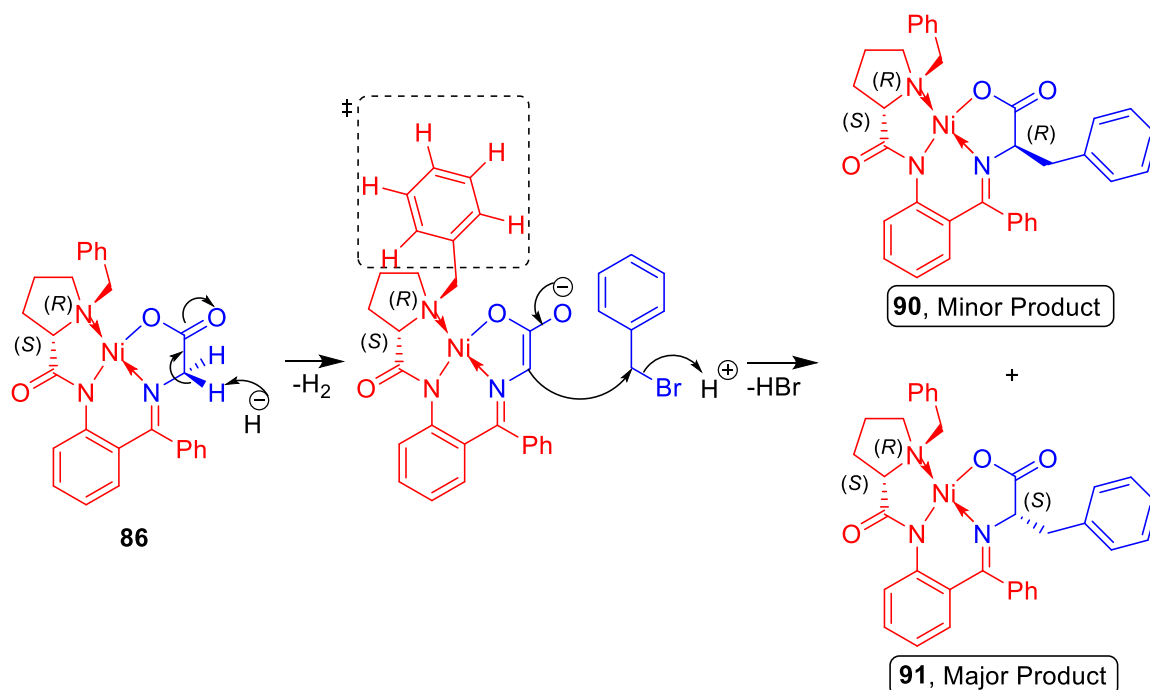
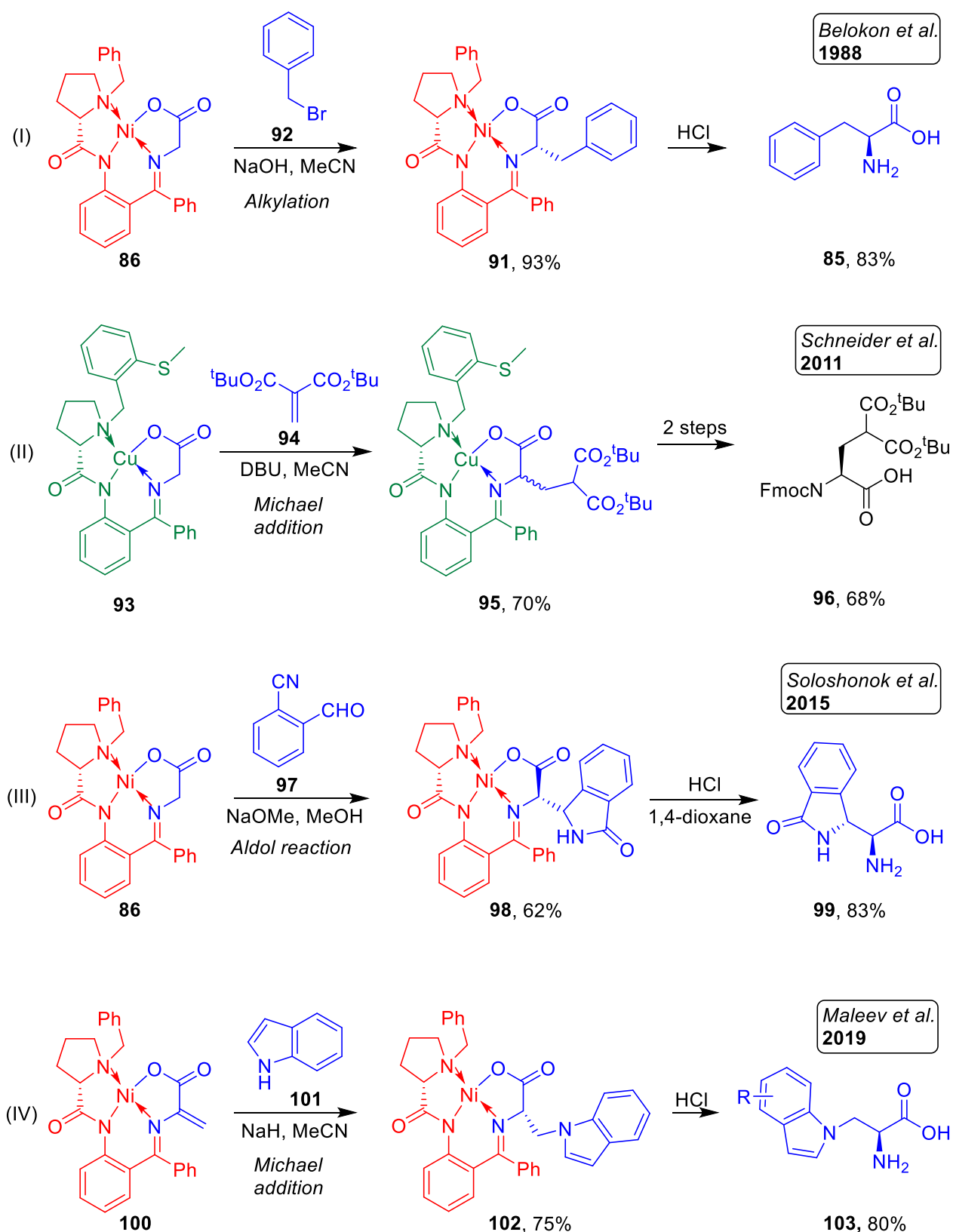


Figure 12. (*S/R*)-Ni/Cu-BPX “Belokon” complexes.

In 1988, Belokon *et al.* applied Ni(II) complexes of Schiff bases derived from (*S*)-*O*-(*N*-benzylpropyl)amino]-benzophenone (BPB) and Gly/Ala (BPX) towards the asymmetric synthesis of enantiomerically pure  $\alpha$ -amino acids (Fig. 12) (Scheme 32).<sup>76</sup> Belokon reported alkylation reactions of benzyl halides upon Ni-BPB complexes affording high diastereomeric excesses (*de* >80%). The Ni-BPB-AA complex diastereomers were found to be easily separable by column chromatography. Subsequent deprotection/decomplexation reaction using HCl was found to furnish the desired amino acids in excellent (70–90%) yields with >95% *ee* (Scheme 33 I). The protocol also enables the recovery of the chiral reagents of the Ni-BPB complexes following deprotection.



Scheme 32. A) Sterically bulky Ph-group, and B) Proposed alkylation mechanism upon Ni-BPB complex.<sup>76</sup>



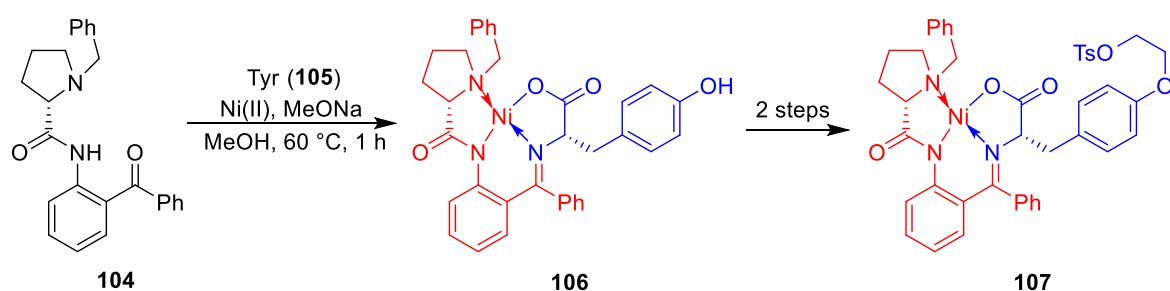
Scheme 33. Overview of notable AAA preparations using Ni/Cu-BPX complexes.<sup>76,78-80</sup>

Belokon also applied Cu-BPB chiral auxiliaries as alternatives to Ni-BPB complexes towards enantioselective AA synthesis.<sup>77</sup> However, Ni-BPB complexes were generally favored as the paramagnetic nature of Cu(II)-BPB was found to hamper NMR characterization. Nevertheless,

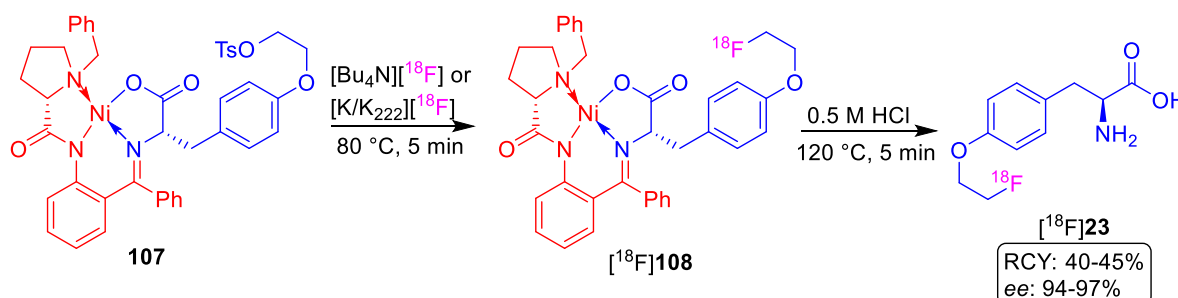
Schneider *et al.* described the use of the ligand (*S*)-2-(*N*-(2-methylthio)benzylpropyl)aminobenzophenone to prepare a five-coordinate Cu-BPB-Gly complex (**94**).<sup>78</sup> In this instance, the authors reported a higher yield (81%), although lower *de* (90%), for the corresponding Ni-BPB-AAA intermediate compared to the Cu-BPB-AAA (**103**) derivative. This is due to the poor coordination of the axial methylthio ligand to Ni(II). As the axial sulfur donor serves to further sterically shield the top face of the coordination plane towards incoming electrophiles, the Michael addition proceeds with greater diastereoselectivity. The protocol allowed the desired Fmoc-protected L- $\gamma$ -carboxyglutamic acid (**97**) to be prepared in good yield and excellent enantiomeric purity (*ee* > 99%) (Scheme 33 II).

In 2015, Soloshonok *et al.* described the preparation of (2*R*, 3*S*)- $\alpha$ -(1-oxoisindolin-3-yl)glycine (**98**) *via* aldol reaction of **97** upon **86**.<sup>79</sup> Following a cascade of transformations, the diastereomerically pure intermediate (**98**) was isolated by column chromatography. Thereafter, the diastereomerically pure AAA **99** was accessed in excellent yield (Scheme 33 III). The group of Maleev reported the preparation of enantiomerically pure (*ee* > 99%) **103** *via* aza-Michael addition (Scheme 33 IV).<sup>80</sup> The protocol provides selective intermolecular *N*-functionalization of indoles, which is otherwise challenging owing to the highly nucleophilic C-3 position of indoles.

#### Precursor Synthesis

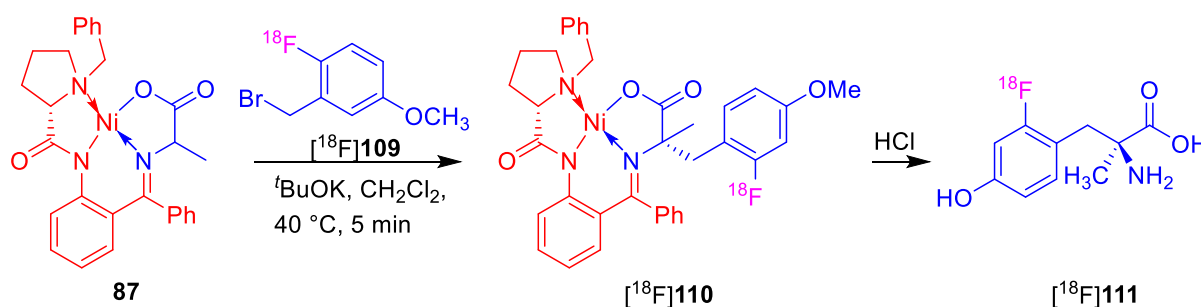


#### Radiochemistry



Scheme 34. Preparation  $[^{18}\text{F}]\text{23}$ , as reported by Krasikova *et al.*<sup>81</sup>

Krasikova *et al.* used Ni-BPB complexes to access [ $^{18}\text{F}$ ]FET ([ $^{18}\text{F}$ ]23) in high RCYs (Scheme 34).<sup>81</sup> Another approach by the same group using (*S*)-Ni-BPB-(*R/S*)-Ala was implemented towards the preparation of  $\alpha$ -methyl-2-[ $^{18}\text{F}$ ]FTyr ([ $^{18}\text{F}$ ]111) (Scheme 35).<sup>82,83</sup>



*Scheme 35. Asymmetrical approaches towards radiolabeled  $\alpha$ -methyl-AAAs.*

From a radiochemist's perspective, the preparation of enantiomerically pure  $^{18}\text{F}$ -labeled AAAs using Ni- or Cu-BPB complexes is an attractive method for the following reasons:

1. Precursor synthesis can theoretically be achieved on a multi-gram scale in a single step from commercially available Bpin-substituted benzyl halides.
2. The diastereomeric products are easily separable using column chromatography.
3. The facile UV detection ( $\lambda = 330\text{--}420\text{ nm}$ ) of the Ni/Cu-BPB and Ni/Cu-BPB-AAA precursor complexes aids chromatographic isolation.
4. The simple and high yielding three-step procedure towards Ni/Cu-BPB from commercially available reagents.
5. The possibility to substitute components of the Ni/Cu-BPX complexes in order to access the desired amino acid product (e.g. (*R*)-Ni-BPB).
6. The rapid and high-yielding deprotection reaction under acidic conditions.
7. The bench and moisture stability of the Ni/Cu-BPB-AA complexes.
8. The amine and carboxylic acid functionalities are protected, thereby permitting late-stage Cu-mediated radiofluorination.

## 1.4. Aromatic Amino Acids as PET Tracers

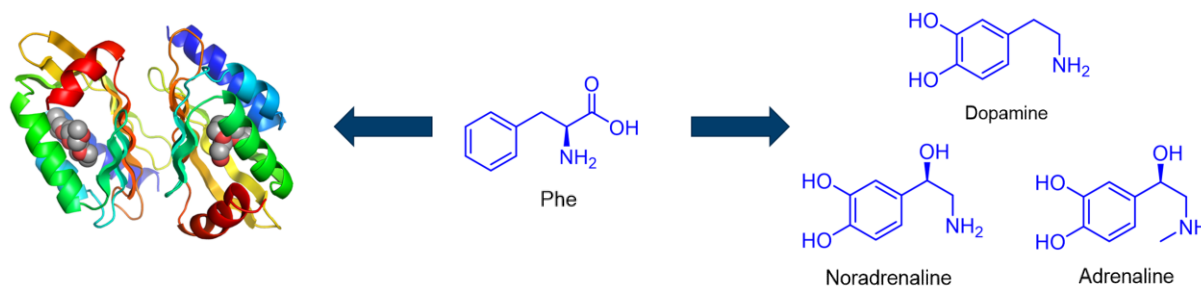


Figure 13. Phe as a building block for protein synthesis and neurotransmitter biosynthesis.<sup>84</sup>

AAAs are small molecular building blocks involved in a variety of biological functions, including protein synthesis and neurotransmitter biosynthesis (Fig. 13). Accordingly, amino acids may act as promising PET tracer candidates to visualize these biological processes. For example, the increased uptake of AAAs in tumor cells can be easily observed using PET using AAA tracers. In order to exploit the diagnostic potential of <sup>18</sup>F-labeled AAAs, it is essential to have an understanding of AAA metabolic pathways.

The vast potential of <sup>18</sup>F-labeled AAAs for PET imaging studies has led many research groups to investigate their respective preparations. Yet as previously outlined, the enantioselective preparation of AAAs and the necessity of PGs pose considerable synthetic obstacles. In addition, the <sup>18</sup>F-incorporation, deprotection, and purification may also present pertinent challenges.

In certain cases, preparative procedures report promising synthetic strategies and <sup>18</sup>F-incorporation rates, only for harsh deprotection conditions to limit their implementation towards automation or substantially reduce the overall RCY. Alternatively, optimal radiosynthesis can be achieved, but only following rigorous, and therefore impractical, precursor preparations. Essentially, for a protocol towards <sup>18</sup>F-labeled AAAs to be deemed practical, a compromise must be ascertained whereby both the precursor synthesis and radiosynthesis must be reasonably achievable.

### 1.4.1. Aromatic Amino Acid Metabolism

A general overview of AAA metabolism with respect to the blood-brain barrier (BBB) is displayed in Fig. 14.<sup>85,86</sup> The BBB is a semipermeable border that serves to protect the brain from potentially harmful molecules. In this way, the BBB is highly selective in the manner by which it allows or blocks the passage of specific molecules into the brain.<sup>87</sup> In principle, the AAA tracer will be metabolized in a similar manner to the unlabeled AAA (in accordance with the Tracer Principles). This concept may be exploited to visualize specific AAA metabolic pathways using PET, which may have associated abnormalities.

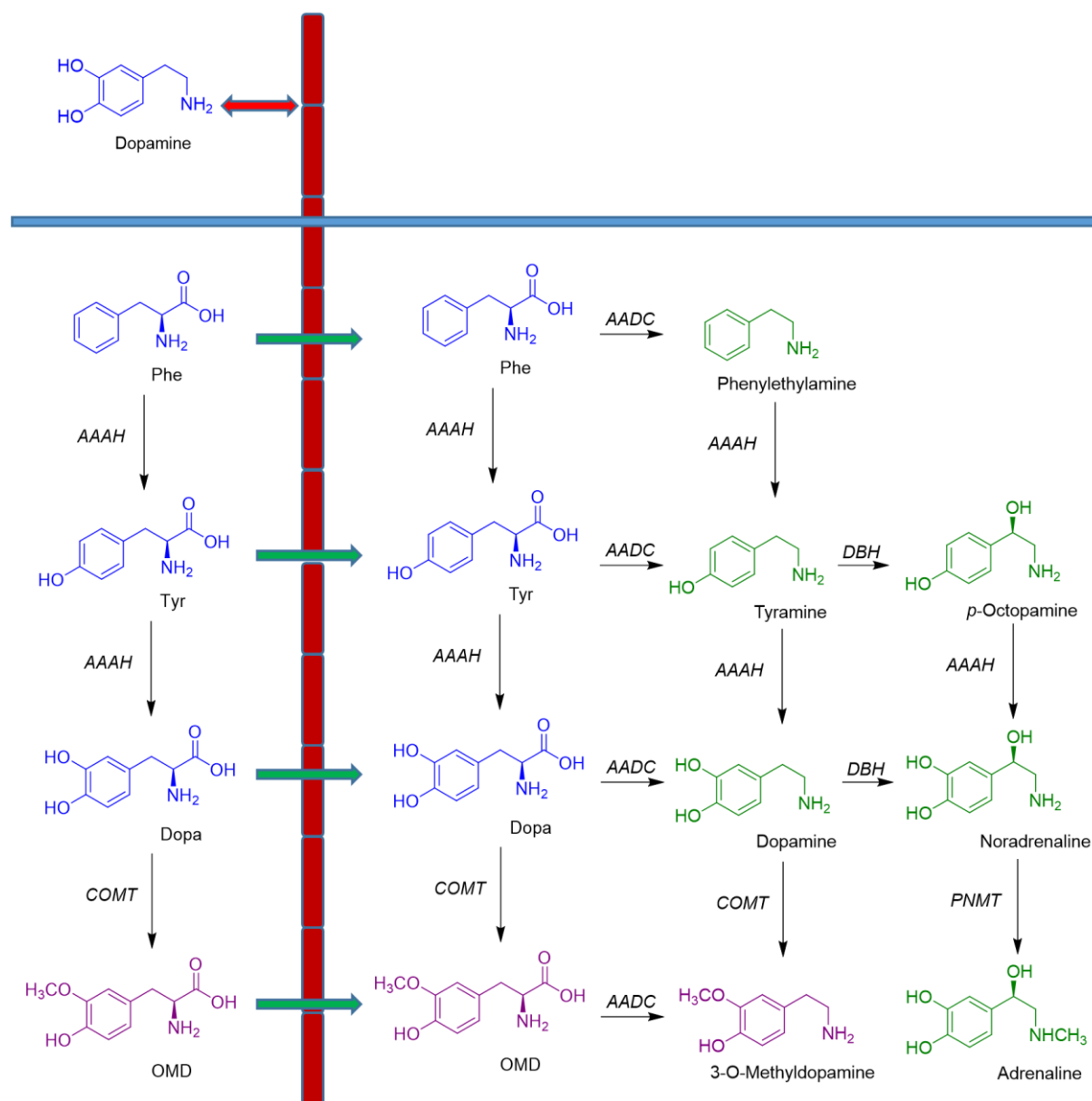


Figure 14. Overview of the BBB with AAA metabolism pathways.

The carboxylic acid group is required for an amino acid to pass the BBB. Hence, a monoamine molecule, such as dopamine, cannot pass the BBB; L-DOPA must first pass the BBB before

being metabolized to dopamine *via* amino acid decarboxylase (AADC) enzyme.<sup>88</sup> Thus, if we wish to observe the dopaminergic system using PET, an appropriate strategy is to administer [<sup>18</sup>F]**3**, which crosses the BBB and is subsequently metabolized to 6-[<sup>18</sup>F]Fdopamine (Fig. 14, 15). Despite enzymatic degradation being a mechanistic component of the [<sup>18</sup>F]**3**–PET tracer, premature decarboxylation of [<sup>18</sup>F]**3** prior to its transport across the BBB by AADC blocks the tracer’s passage into the brain. An overview of notable <sup>18</sup>F-labeled AAAs are shown in Fig. 15.

In order to address this issue, L-AAA tracers are often co-administered with peripheral AADC inhibitors such as benserazide.<sup>89</sup> Benserazide, which is unable to permeate through the BBB itself, has some structural similarities comparable with L-amino acids and serves to inhibit AADC. Enzymatic degradation of [<sup>18</sup>F]**3** also occurs *via* methylation by catechol-*O*-methyl transferase (COMT) enzyme.<sup>90-94</sup> COMT is one of several enzymes that is involved in the inactivation of various catecholamines, including [<sup>18</sup>F]**3**, dopamine, adrenaline, and noradrenaline. One strategy to minimize the degradative potential of COMT is the co-administration of Entacapone, which enables [<sup>18</sup>F]**3** to have a longer effect in the brain. However, a further strategy to minimize the role of COMT in [<sup>18</sup>F]**3** degradation is the complete removal of one of the catechol hydroxyl groups to form 6-[<sup>18</sup>F]FMT ([<sup>18</sup>F]**28**), thereby preventing COMT from recognizing and degrading the tracer. Additionally, monoamine oxidase (MAO) enzymes also further metabolize monoamines such as dopamine, noradrenaline, and adrenaline.

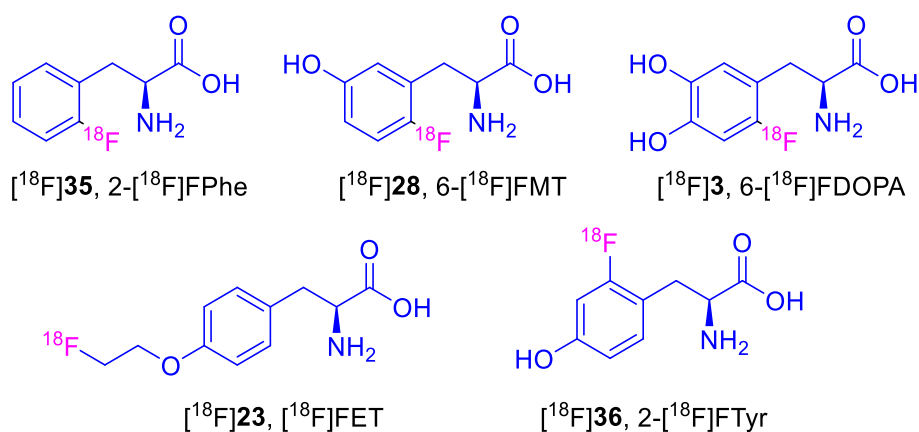


Figure 15. Notable <sup>18</sup>F-labeled AAA PET tracers.

### 1.4.2. The Noradrenergic System

Any part of the body that produces or is affected by the neurotransmitter noradrenaline (NA, **112**) is part of the noradrenergic system (Fig. 16). The primary function of the noradrenergic system is to prepare the body for action (e.g. fight or flight responses). Accordingly, NA release is found to be relatively low during sleep and relatively high during periods of stress. NA is produced in the *locus coeruleus* (LC), located in the pons region of the brain, and is found to enhance alertness and arousal. NA is additionally responsible for a variety of functions, including heart and blood rate regulation in the rest of the body. Irrespective of its location, NA exhibits the same mechanism: binding and activating adrenergic receptors on the cell surface. The noradrenergic system has also been linked with many psychiatric and neurodegenerative disorders. Specifically, in Alzheimer's disease (AD), a significant loss of neurons occurs in the LC.<sup>95,96</sup>

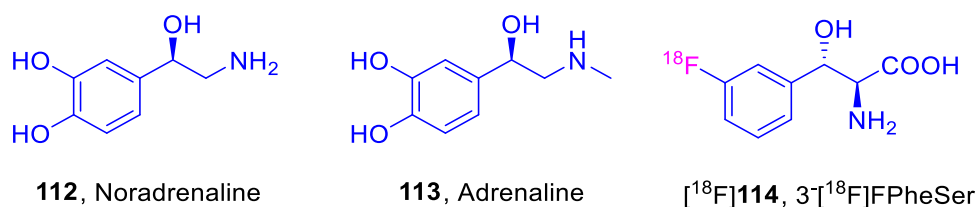
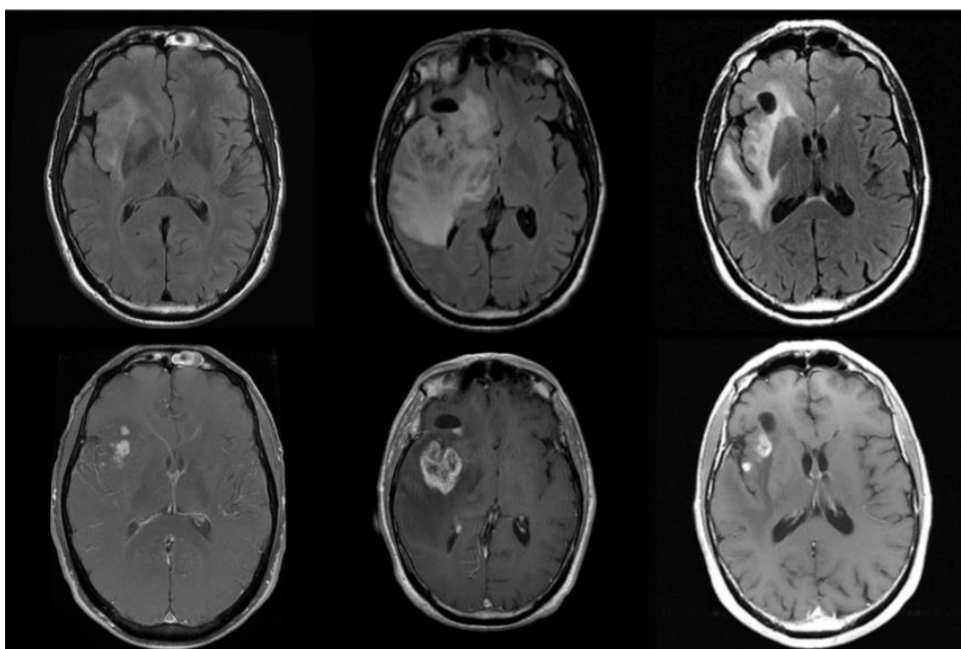


Figure 16. Noradrenaline (**112**, NA), adrenaline (**113**, A), and [<sup>18</sup>F]**114**.

In Parkinson's disease (PD), the loss of dopamine (DA) neurons in the *substantia nigra* is typically preceded by the degeneration of the LC-NA neurons.<sup>97</sup> Thus far, there have been numerous reports in the literature of noradrenergic system visualization *in vivo*.<sup>98-105</sup> However, these studies have usually concerned with the NA transporter density rather than the metabolic pathways of NA. The AAA tracer 3-[<sup>18</sup>F]fluoro- L-phenylserine ([<sup>18</sup>F]**114**), structurally similar to NA and adrenaline (**113**), could provide invaluable metabolic information concerning the noradrenergic system using PET (Fig. 16). Consequently, the novel tracer [<sup>18</sup>F]**114** could aid the diagnosis of patients suffering from AD, PD, and other neurodegenerative disorders.

### 1.4.3. $^{18}\text{F}$ -Labeled AAAs Towards Cerebral Tumor Imaging

Central nervous system (CNS) malignancies are the abnormal growth of cells in the spinal cord or brain tissue. In 2019, the American Cancer Society estimated that the number of deaths associated with CNS tumors to be approximately 17,500.<sup>106</sup> The diverse and complex nature of the CNS tumors often necessitates a combination of diagnostic and therapeutic techniques including radiation therapy, surgery, chemotherapy, and immunotherapy. Formerly, cerebral malignancy treatment consisted of solely radiotherapy and surgery. However, with recent developments in immunotherapy and chemotherapeutics, the need for rapid assessment of the therapies by response detection became of crucial importance. In this way, appropriate imaging is a fundamental component of CNS disease management.



*Figure 17. MRI images of a patient with glioblastoma (WHO IV). The images on the left indicate tumor presence. The middle images show apparent tumor growth following daily Temozolamide ( $75 \text{ mg/m}^2$ ) therapy. The images on the right show reduction of the tumor volume following Decadron administration (6 mg twice daily) one month later.<sup>107</sup>*

MRI serves to provide images that effectively delineate aqueous tissue structures with appreciable contrast and high spatial resolution (Fig. 17). Although MRI is well-established in clinical environments, effective cerebral malignancy identification, and management with solely MRI remains notoriously challenging. This is often due to anatomical distortions of healthy brain components in close proximity to the cerebral tumor, providing poor image contrast quality and structural ambiguity. This phenomenon is known as pseudoprogression: inflammatory response to therapy, which is near-impossible to distinguish compared to true

tumor progression.<sup>107</sup> In Fig. 17, it appears as though a patient has significantly increased tumor growth following Temozolamide therapy, followed by tumor reduction one month later.

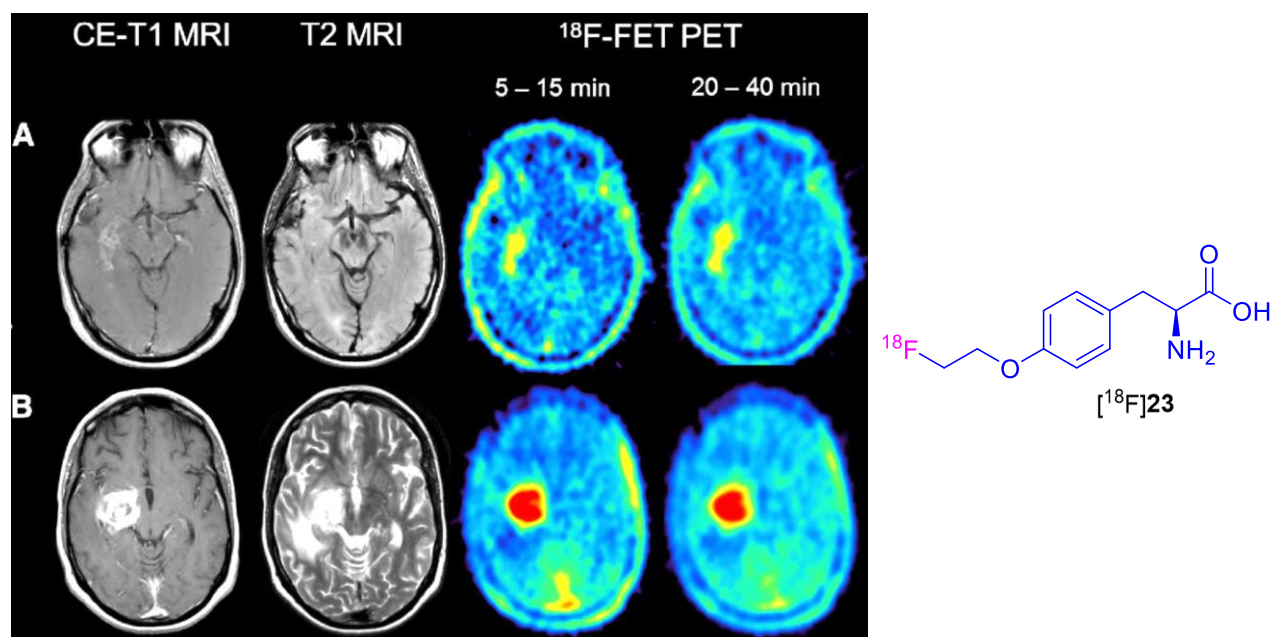


Figure 18. Contrast-enhanced (CE) MRI & [ $^{18}\text{F}$ ]FET-PET.<sup>108</sup>

This occurrence and similar phenomena represent a considerable limitation of MRI towards cerebral malignancy management. The AAA tracer [ $^{18}\text{F}$ ]23 emerged as an advantageous tracer alternative to [ $^{18}\text{F}$ ]FDG ([ $^{18}\text{F}$ ]3) towards tumor brain imaging using PET. [ $^{18}\text{F}$ ]23 is a tracer derivative of Tyr that exploits the overexpression of LAT1 amino acid transporter prevalent in tumor cells.<sup>108</sup> Healthy cell accumulation of [ $^{18}\text{F}$ ]23 is considerably lower than tumor accumulation, allowing the latter to be easily identified in PET images (Fig. 18).

#### 1.4.4. Amino Acids as PET Tracers for Parkinson's Disease

PD is a neurodegenerative disorder in the central nervous system (CNS) that primarily affects the motor system.<sup>109</sup> However, patients also experience more difficulties with non-motor symptoms such as behavioral and cognitive problems (e.g. Dementia) over longer periods.<sup>110</sup> Motor symptoms associated with PD arise as a result of cell death in the *substantia nigra* region of the brain. This causes the neurotransmitter dopamine to be less prevalent in the regions where dopamine is released (e.g. the striatum). Although the initial cause of cell death in the *substantia nigra* is not fully understood, the build-up of abnormal aggregates of proteins, Lewy bodies, in the neurons has been demonstrated to have a substantial effect.<sup>111</sup> A Lewy body comprises of the  $\alpha$ -synuclein protein as well ubiquitin,  $\alpha\text{B}$  crystalline, and neurofilament protein.

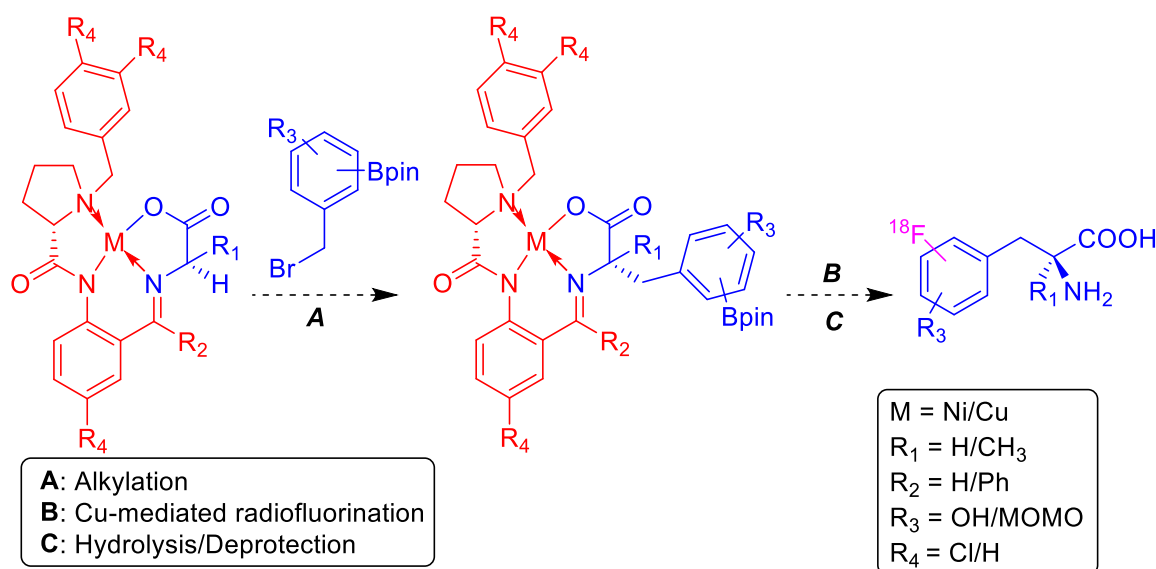
As of 2015, PD was reported to have affected approximately 6.2 million people, with 117,400 fatal cases.<sup>112,113</sup> The life expectancy upon PD diagnosis typically ranges from 7–15 years.<sup>114</sup>

As there is no cure for PD, the optimum way to prolong life expectancy in patients is by efficient diagnosis and subsequent treatment planning. As it is known that dopamine levels in the *substantia nigra* region in the brain are reduced in patients suffering from PD, an efficient method that has been developed involves the radiolabeling of L-DOPA (e.g. 6-[ $^{18}\text{F}$ ]FDOPA, [ $^{18}\text{F}$ ]**3**) which can provide diagnostic information using PET imaging. The primary reasoning behind administering [ $^{18}\text{F}$ ]**3** rather than [ $^{18}\text{F}$ ]**53**, is that the amino acid core structure is required for the molecule to pass through the BBB (Section 1.4.1.).

## 2. Aims & Objectives

Efficient radiosynthetic methods for the production of radiopharmaceuticals are urgently needed to satisfy the increasing demand for clinical diagnostics using PET. Many existing radiosynthetic protocols towards aromatic amino acid (AAA) PET tracers lack efficacy and are therefore deemed too impractical for routine clinical applications. As an unfortunate consequence, the vast potential of  $^{18}\text{F}$ -labeled AAAs remains to be fully explored. This work aims to establish a general procedure for accessing  $^{18}\text{F}$ -labeled AAAs (Scheme 36). In order to realize this goal, the following steps should be carried out:

1. The development of efficient synthetic protocols for radiolabeling precursors. Ideally, the precursors, such as Bpin-substituted Ni-BPX-AAA complexes, should be prepared in a few steps from commercially available reagents.
2. The optimization of the alcohol-enhanced Cu-mediated radiofluorination of Bpin-substituted Ni-BPX-AAA complexes.
3. The optimization of deprotection and isolation procedures for the  $^{18}\text{F}$ -labeled AAAs.
4. Feasibility studies of Cu-BPX complexes towards  $^{18}\text{F}$ -labeled AAA preparations.
5. The investigation of the applicability of Ni-BPX complexes for the preparation of [ $^{18}\text{F}$ ]FPhSer, a potential imaging agent for the noradrenergic system.
6. Implementation of the established protocol for the preparation of  $^{18}\text{F}$ -labeled AAAs into an automated radiosynthesis module.

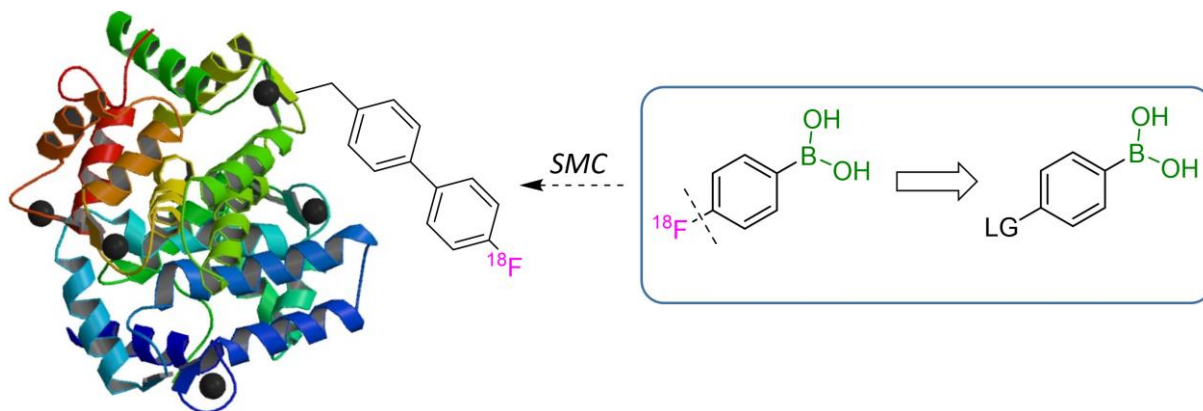


*Scheme 36. Overview of precursor synthesis and radiosynthesis steps.*

For coherency, the respective objectives and strategies discussed herein are divided into organic preparative (Section 3. 1.) and radiochemical (Section 3. 08.) sections. In order to facilitate the successful adaption of the  $^{18}\text{F}$ -labeled AAAs production method for routine clinical application, emphasis will be placed on optimization concerning the following criteria:

- Starting material costs and commercial availability of the reagents
- Radiochemical yields (RCYs), molar activities ( $A_m$ ), enantiomeric excess ( $ee$ )
- Current good manufacturing practice (cGMP) compliance
- Preparation times
- Reproducibility
- Implementation of the procedure towards automated modules

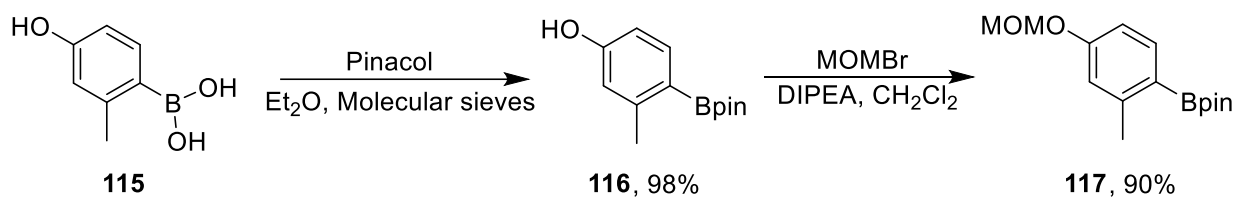
Following successful preparation, the  $^{18}\text{F}$ -labeled AAAs should be subjected to preclinical evaluation. An additional focus of the thesis concerns the development of the promising prosthetic group 4- $^{18}\text{F}$ fluorophenylboronic acid *via* Cu-mediated radiofluorination. The latter  $^{18}\text{F}$ -synthon has been recently reported to enable site-specific peptide/protein labeling *via* Suzuki-Miyaura coupling (SMC) (Scheme 37).<sup>69</sup> However, limitations of the literary preparation of [ $^{18}\text{F}$ ]**80**, include arduous multi-step precursor preparation and low RCYs.



*Scheme 37. Site-specific labeling of biomolecules using prosthetic group [ $^{18}\text{F}$ ]**80**.<sup>115</sup>*

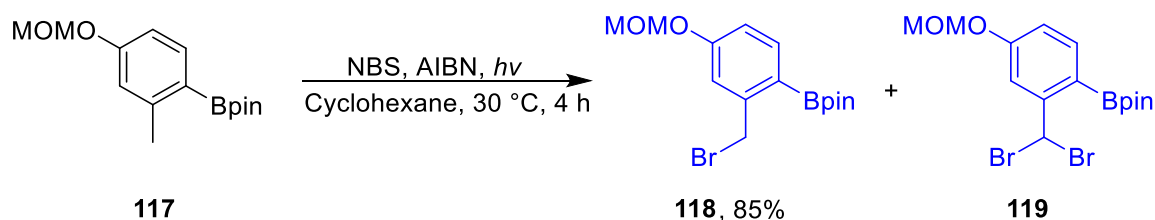
### 3. Results & Discussion

#### 3.1. Preparation of Alkylating Agents



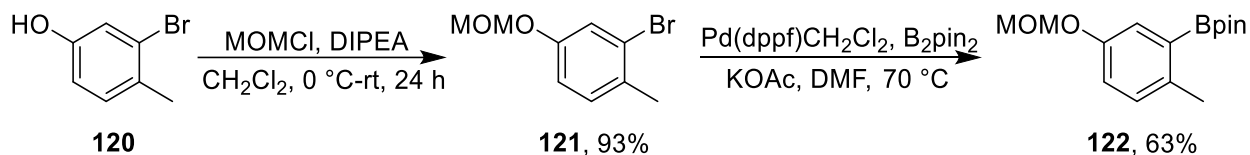
*Scheme 38. The preparation 117.*

The synthesis towards alkylating agent **119** commenced with the pinacol protection of the commercially available (4-hydroxy-2-methyl)phenylboronic acid (**115**) using 4 Å molecular sieves in Et<sub>2</sub>O, the reaction proceeded with near quantitative yields (Scheme 38). The methoxy-*O*-methyl-protection (MOM) of **116** was achieved using bromomethyl methyl ether (MOMBr) and *N,N*-diisopropylethylamine (DIPEA) in CH<sub>2</sub>Cl<sub>2</sub>. The MOM-PG was chosen to facilitate the global acidic deprotection of the radiofluorinated Ni-BPX-AAA during the radiosynthesis.



*Scheme 39. Preparation of alkylating agent 118.*

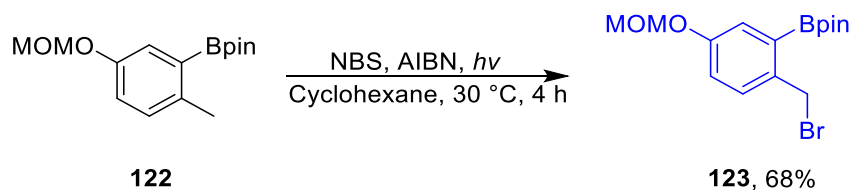
The radical bromination of **117** in a quartz reaction vessel using *N*-bromosuccinimide (NBS), azobisisobutyronitrile (AIBN), and an irradiating light source (550 W) afforded the alkylating agent **118** in high yield (Scheme 39) and trace amounts of side product **119**. MOM-protection of the commercially available 3-bromo-4-methylphenol (**120**) was achieved using a prepared 2.1 M MOMCl solution in toluene and DIPEA (Scheme 40).<sup>116</sup> Thereafter, the Suzuki-Miyaura borylation of **121** under inert conditions allowed the compound **122** to be accessed in 63% yield.



*Scheme 40. The preparation of 122.*

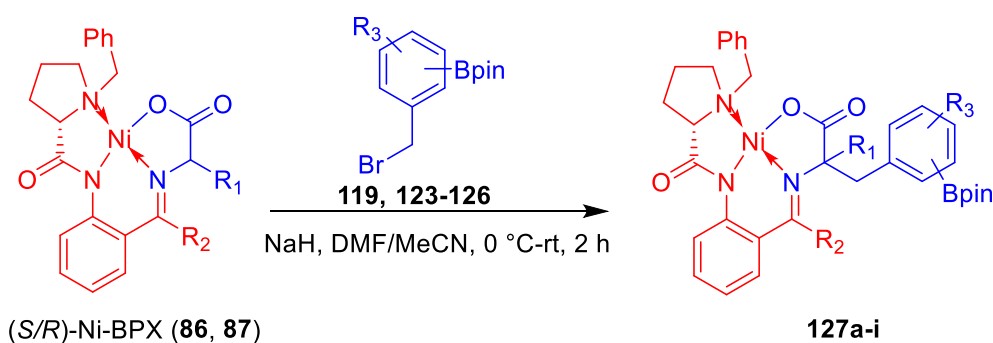
The radical bromination of **122** was carried out similarly to the previously described protocol to furnish the alkylating agent **123** with moderate yield (Scheme 41). Moreover, the *para*-position of the MOM-PG proved to have a profound negative influence on the stability of the

product (**123**). A possible explanation could be that partial MOM-deprotection occurs during the radical bromination, giving rise to side-products and associated impurities.



*Scheme 41. Preparation of the alkylating agent **123**.*

Alkylation of the commercially available **124-126** upon **86** and **87** afforded the desired diastereomer (*S,S*)-Ni-BPX-AAA complexes (**127a-c**) in good yields. Despite both diastereomeric NiBPX-AAA complexes being formed upon alkylation, the isolation of the desired (*S,S*)-Ni-BPB-AAA diastereomers **127a-j** was easily achieved by column chromatography and recrystallization (Scheme 42).



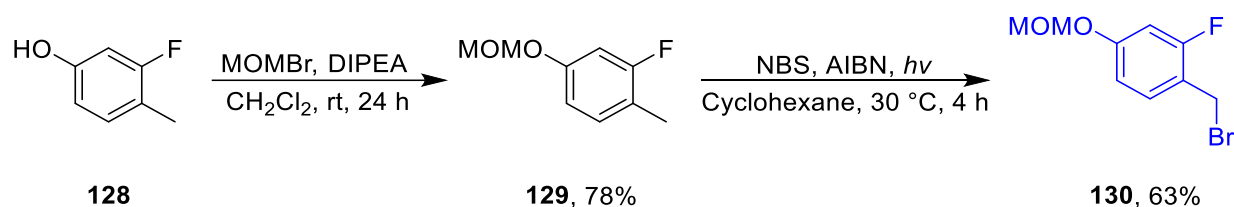
*Scheme 42. Alkylation of upon (*S/R*)-Ni-BPX complexes.*

Entry	Alkylating agent	Ni-BPX complex	Product	Yield (%)
1	<b>124</b> , R <sub>3</sub> = H, <i>o</i> -Bpin	<b>86</b> , R <sub>1</sub> = H, R <sub>2</sub> = Ph	<b>127a</b>	78
2	<b>125</b> , R <sub>3</sub> = H, <i>m</i> -Bpin	<b>86</b> , R <sub>1</sub> = H, R <sub>2</sub> = Ph	<b>127b</b>	81
3	<b>126</b> , R <sub>3</sub> = H, <i>p</i> -Bpin	<b>86</b> , R <sub>1</sub> = H, R <sub>2</sub> = Ph	<b>127c</b>	85
4	<b>119</b> , R <sub>3</sub> = 5-OMOM, 2-Bpin	<b>86</b> , R <sub>1</sub> = H, R <sub>2</sub> = Ph	<b>127d</b>	78
5	<b>123</b> , R <sub>3</sub> = 4-OMOM, 2-Bpin	<b>86</b> , R <sub>1</sub> = H, R <sub>2</sub> = Ph	<b>127e</b>	40
6	<b>124</b> , R <sub>3</sub> = H, <i>o</i> -Bpin	<b>87</b> , R <sub>1</sub> = CH <sub>3</sub> , R <sub>2</sub> = H	<b>127f</b>	72
7	<b>125</b> , R <sub>3</sub> = H, <i>m</i> -Bpin	<b>87</b> , R <sub>1</sub> = CH <sub>3</sub> , R <sub>2</sub> = H	<b>127g</b>	76
8	<b>126</b> , R <sub>3</sub> = H, <i>p</i> -Bpin	<b>87</b> , R <sub>1</sub> = CH <sub>3</sub> , R <sub>2</sub> = H	<b>127h</b>	79
9	<b>119</b> , R <sub>3</sub> = 5-OMOM, 2-Bpin	<b>87</b> , R <sub>1</sub> = CH <sub>3</sub> , R <sub>2</sub> = H	<b>127i</b>	46

*Table 3. Preparation of Bpin-substituted Ni-BPX complexes **127a-i** via alkylation.*

### 3.2. Preparation of Reference Compounds

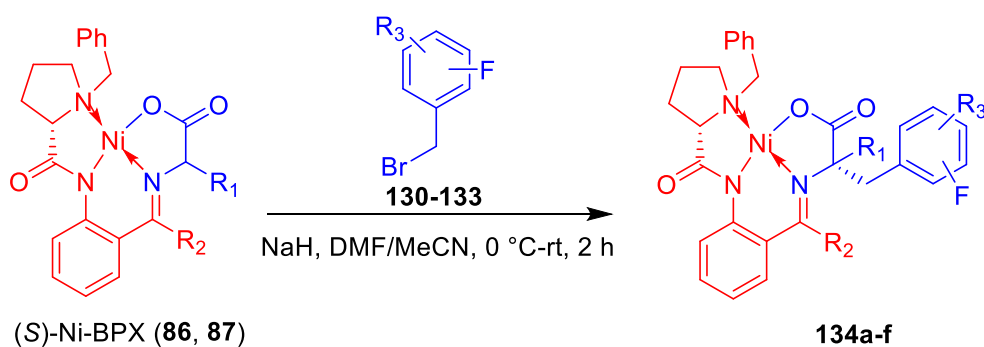
Reference compounds are the non-radioactive fluorinated ( $^{19}\text{F}$ ) compounds used for product confirmation by chromatographic analysis. Moreover, reference compounds are required to construct the calibration curves needed for the carrier amount or  $A_s$  determination of an  $^{18}\text{F}$ -labeled product. Most of the AAA reference compounds, including 2–4-FPhe, 6-FMT, and 2-FTyr, were commercially available in either L-AAA or racemic (L & D) enantiomeric forms.



*Scheme 43. Preparation of the alkylating agent 130.*

However, some of the Ni-BPX-AAA and  $\alpha$ -Me-AAAs reference compounds required preparation. MOM-protection of the commercially available 3-fluoro-4-methylphenol (**128**) allowed **129** to be accessed in good yield (Scheme 43). Thereafter, radical bromination of **129** was carried out using NBS and AIBN to furnish 2-(2-(bromomethyl)-4-(methoxymethoxy)phenyl)-4,4,5,5-tetramethyl-1,3,2-dioxaborolane (**130**), which was purified by column chromatography and quickly used in the following alkylation reaction due to stability concerns.

Ni-BPX-AAA reference compounds were prepared in a similar manner as previously described to furnish the diastereomeric Ni-BPX-AAAs (**127a-c**), whereby the commercially available **131–133** were employed as alkylating agents. Mrs. Elizaveta Urusova prepared **134b**. The synthetic route towards the  $\alpha$ -Me-AAA reference compounds proceeded with the alkylation reaction upon (S)-Ni-BPB-(RS)-Ala (**87**) with excellent yields (Scheme 44).<sup>117</sup>

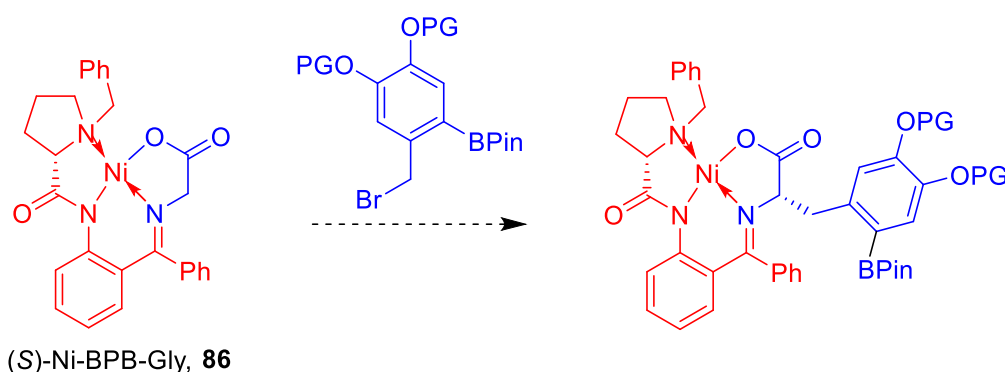


*Scheme 44. Alkylation of 130-133 upon 86 and 87.<sup>117</sup>*

Entry	Alkylating agent	Ni-BPX complex	Product	Yield (%)
1	<b>131</b> , R <sub>3</sub> = H, <i>o</i> -F	<b>86</b> , R <sub>1</sub> = H, R <sub>2</sub> = Ph	<b>134a</b>	72
2	<b>132</b> , R <sub>3</sub> = H, <i>m</i> -F	<b>86</b> , R <sub>1</sub> = H, R <sub>2</sub> = Ph	<b>134b</b>	78
3	<b>130</b> , R <sub>3</sub> = 4-OMOM, 2-F	<b>86</b> , R <sub>1</sub> = H, R <sub>2</sub> = Ph	<b>134c</b>	64
4	<b>131</b> , R <sub>3</sub> = H, <i>o</i> -F	<b>87</b> , R <sub>1</sub> = CH <sub>3</sub> , R <sub>2</sub> = H	<b>134d</b>	74
5	<b>132</b> , R <sub>3</sub> = H, <i>m</i> -F	<b>87</b> , R <sub>1</sub> = CH <sub>3</sub> , R <sub>2</sub> = H	<b>134e</b>	77
6	<b>133</b> , R <sub>3</sub> = H, <i>p</i> -F	<b>87</b> , R <sub>1</sub> = CH <sub>3</sub> , R <sub>2</sub> = H	<b>134f</b>	82

Table 4. Preparation of reference compounds **134a-f** via alkylation.

### 3.3. Preparative Strategies Towards 6-[<sup>18</sup>F]FDOPA Precursor

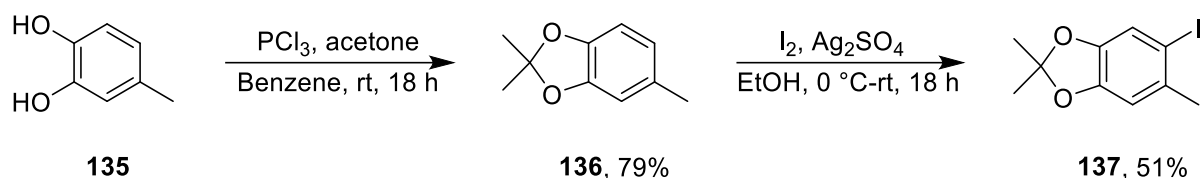


Scheme 45. Overview of the proposed synthetic route towards a 6-[<sup>18</sup>F]FDOPA precursor.

A couple of synthetic strategies towards a 6-[<sup>18</sup>F]FDOPA precursor were attempted (Scheme 45).

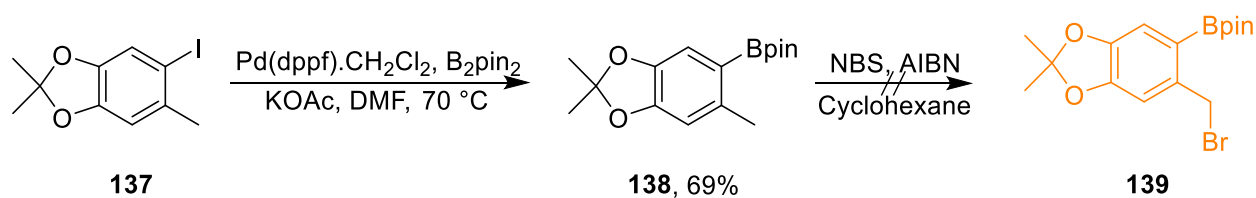
#### 3.4.1. Synthetic Route A

The initial synthetic route commenced with the acetal protection of the 4-methylcatechol (**135**) using acetone, phosphorous trichloride in benzene (Scheme 46). Acidic deprotection of the acetal PG was found to be achieved under similar conditions as the MOM-PG. Therefore, the global acidic deprotection of the Ni-BPB-AAA complex and the catechol moiety could be achieved during radiosynthesis. Following protecting group incorporation, aryl iodination of **136** using iodine and silver sulfate in EtOH was successfully carried out in 51% yield. For this step, the dropwise addition of the iodine in EtOH into the reaction mixture was necessary to maintain a low reaction temperature. In this way, the formation of a diiodinated product was minimized.



*Scheme 46. Synthesis of aryl iodide 137.*

The Suzuki-Miyaura borylation (SMB) of **137** afforded **138** in good yield. The subsequent radical bromination step using NBS and AIBN was carried out in cyclohexane to prepare the appropriate alkylating agent **139**. Although **139** was successfully formed (Fig. 19), the radical bromination reaction was found to generate many degradative products, and we failed to isolate **139** successfully (Scheme 57).



*Scheme 47. Attempted preparation of alkylating agent 139.*

It was thought that varying the temperature, radical initiator (AIBN) concentration or reaction solvent would provide product stability. However, without success, we turned our attention to alternative catechol protecting groups.

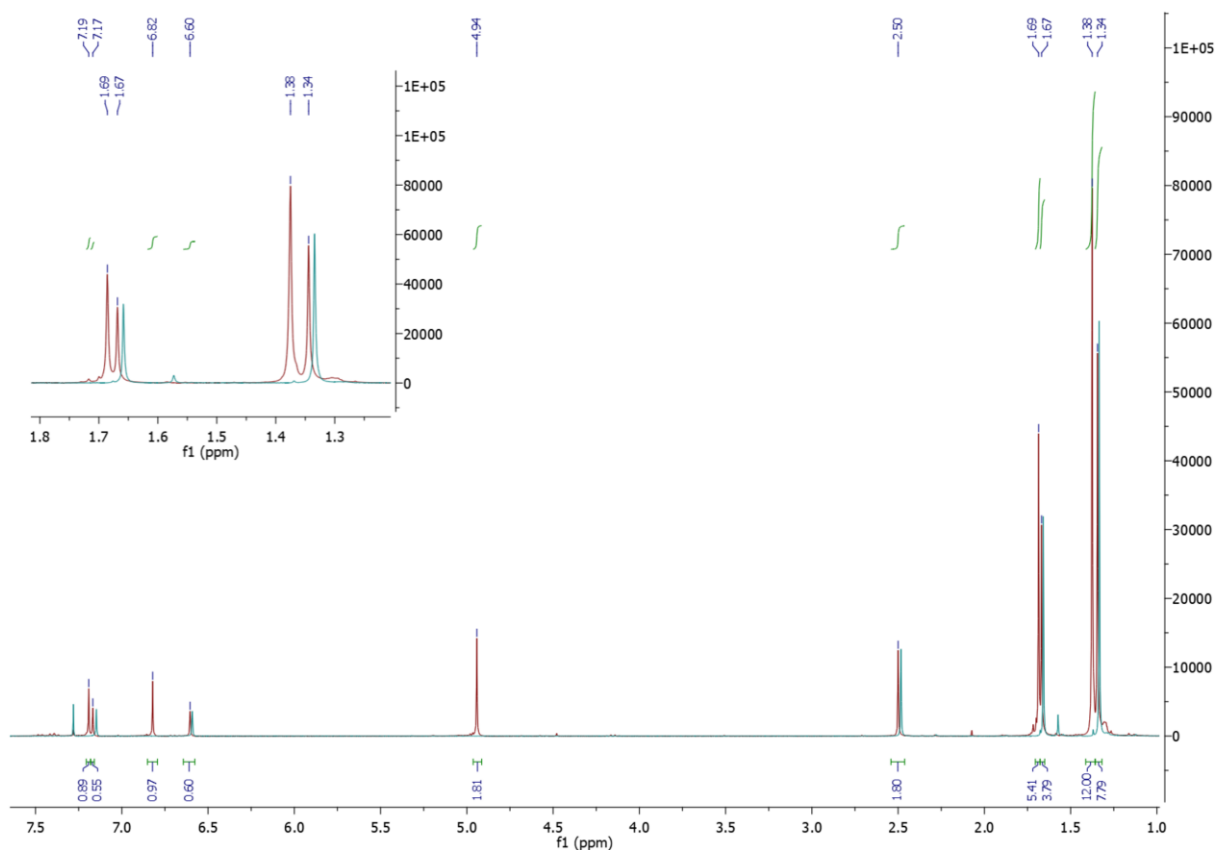


Figure 19. Superimposed NMR spectra of starting material **138** (green) and **139** (red). Product formation is evident due to the appearance of the benzylic bromide peak at 4.94 ppm.

As discussed previously, labile PGs in the *para* position to the benzyl position presented a considerable stability issue upon radical bromination. In order to circumvent this problem, we succeeded in substituting the acetal-PG for both Boc- and MOM-PGs (Scheme 47).

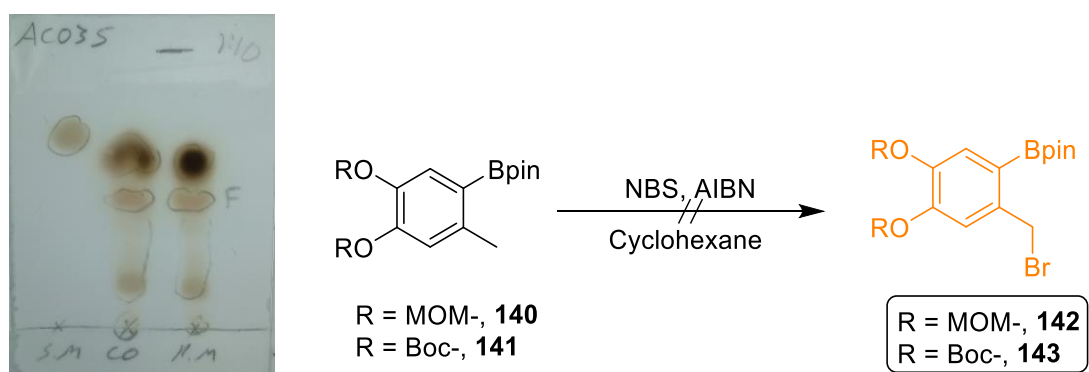


Figure 20 & Scheme 47. TLC indicating product decomposition following attempted radical bromination.

Despite the alternative PGs being employed, radical bromination was still not achievable under the revised conditions (Fig. 21). After several further attempts had failed, the synthetic route was abandoned.

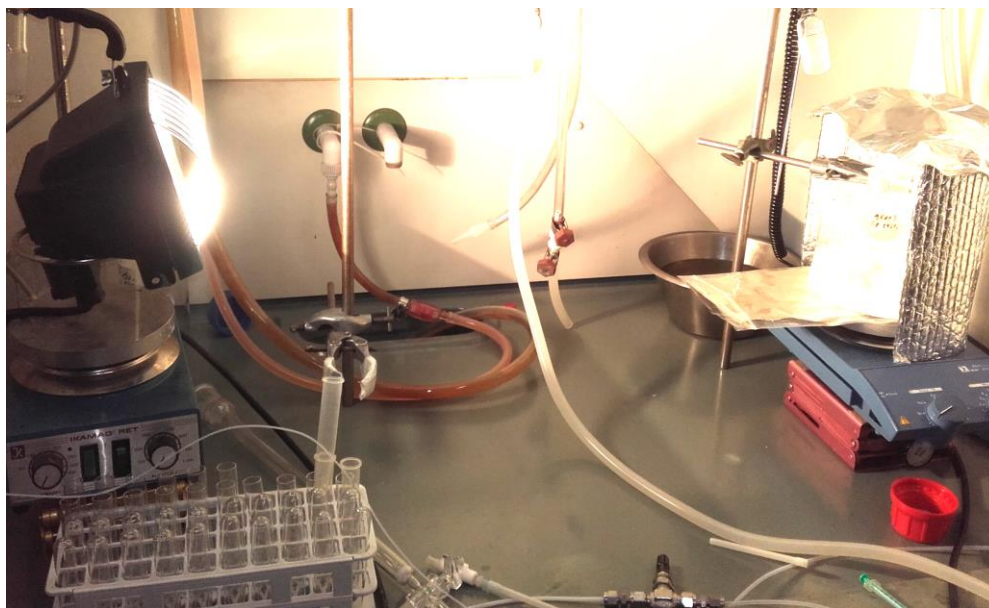
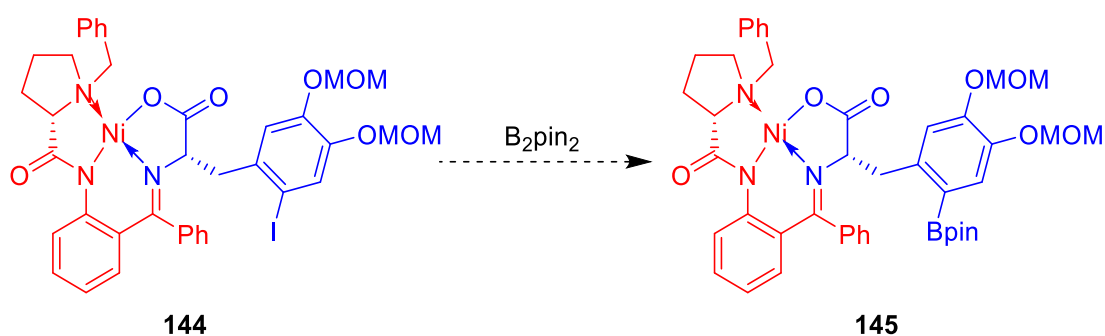


Figure 21. Radical bromination reaction apparatus.

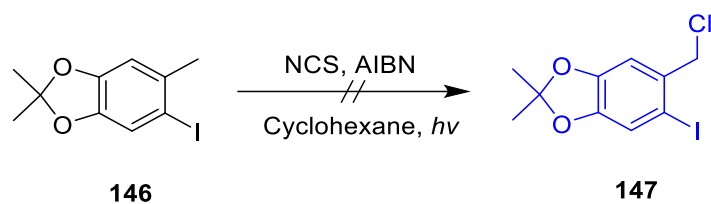
Although MOM-PGs provide rapid deprotection under acidic conditions and are ideal for radiosynthetic purposes, we experienced several instability issues with some of the MOM-protected compounds despite keeping them stored at  $-8\text{ }^{\circ}\text{C}$  and under Ar. Accordingly, Wuts *et al.* reported the sensitivity of MOM-PGs towards  $\text{I}_2$ ,  $\text{Br}_2$ , and  $\text{Cl}_2$ .<sup>118</sup> As quite a number of the reactions in this work are brominations, iodinations or generate HBr (alkylation), in some cases we were forced to apply the MOM-protected compound to the subsequent reaction in order to avoid product losses.

### 3.4.2. Synthetic Route B



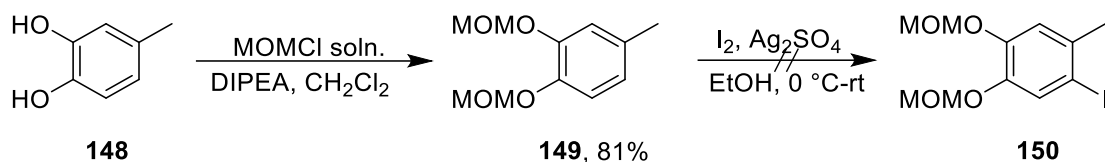
Scheme 48. Intended synthetic route towards target **145** via late-stage borylation.

A second synthetic route towards a  $[\text{}^{18}\text{F}]\textbf{3}$  precursor (**145**) focused on the late-stage introduction of the Bpin LG *via* SMB (Scheme 48). Initially, the radical chlorination of **146** was carried out (Scheme 49) towards the benzylic chloride **147**. Unfortunately, no evidence of product formation was obtained despite multiple attempts. Radical bromination of **146** resulted in the deiodination of the compound.



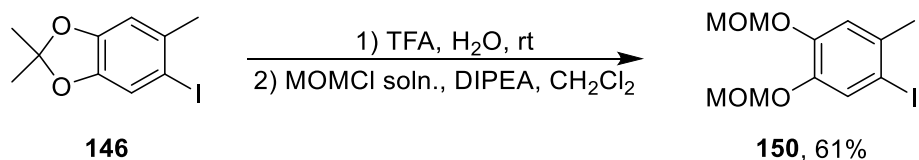
*Scheme 49. Attempted radical chlorination of 146*

MOM-protection of 4-methylcatechol (**148**) using MOMCl and DIPEA in cyclohexane afforded **149** in good yields (Scheme 50). Iodination of **149** was found to give rise to selective deprotection, as described by the group of Keith *et al.*<sup>119</sup> Owing to the impractical nature of this occurrence and the relatively expensive Ag<sub>2</sub>SO<sub>4</sub>, pursuit of the aryl iodide **150** via this synthetic pathway was abandoned.

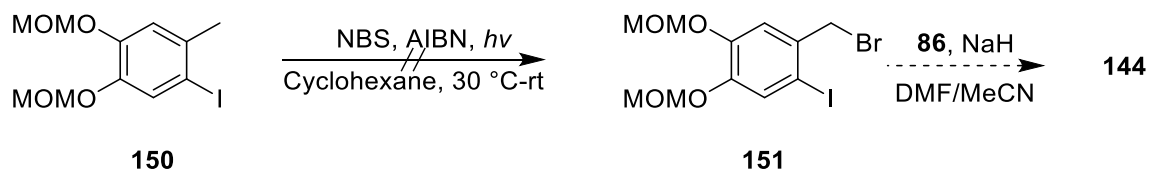


*Scheme 50. Preparation of 150.*

With the exchange of the PGs, the aryl iodide **146** was converted to **150** via deprotection using TFA, followed by MOM-protection using MOMCl (Scheme 51). However, the radical bromination of **150** gave rise to multiple unstable products (Scheme 52). Therefore, with the successful preparation of a suitable alkylating agent, synthetic route B was also discontinued.



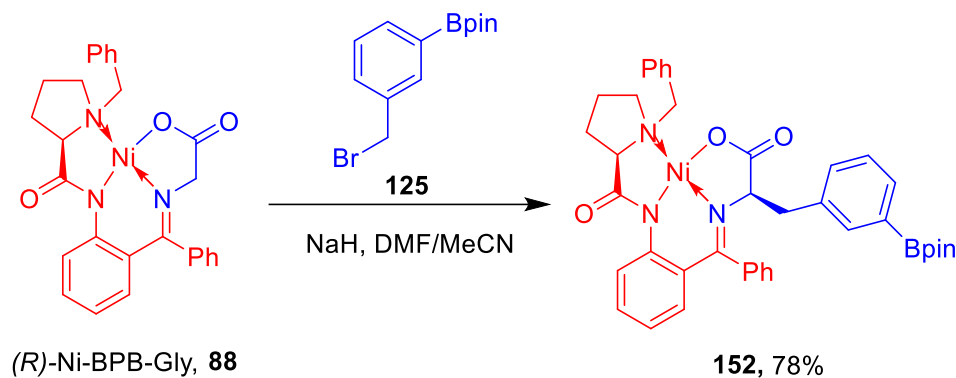
*Scheme 51. PG-Substitution to afford 150.*



*Scheme 52. Attempted radical bromination towards 151.*

### 3.5. Preparation of (*R*)-AAA Tracer Precursor

The use of (*R*)-Ni-BPB complexes allows the (*R*)-AAA enantiomer to be accessed. The role of non-natural D-amino acids is not fully understood to date; there have been conflicting reports in the literature surrounding their function and metabolism. The development of an  $^{18}\text{F}$ -labeled D-AAA may reveal new metabolic pathways to be exploited for tumor detection using PET.<sup>120</sup>

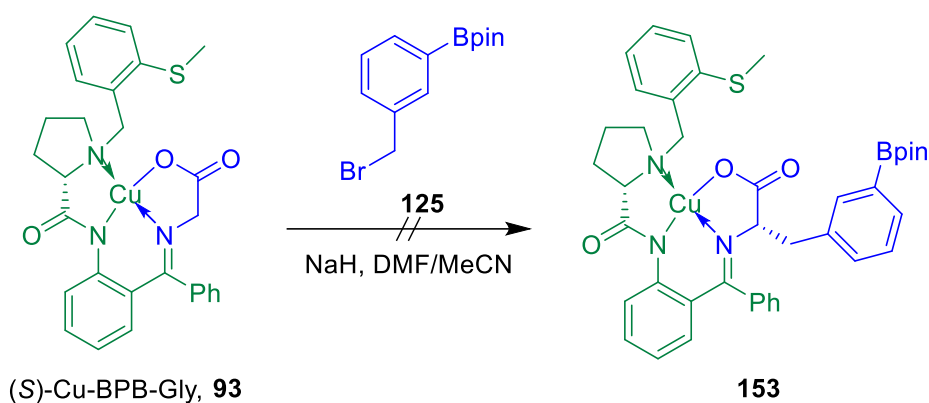


*Scheme 53. Preparation of 3-(*R*)-[ $^{18}\text{F}$ ]FPhe precursor **152**.*

Alkylation of **125** upon the **88** was achieved in 78% yield (Scheme 53). The commercially available alkylating agent **125** was purposefully selected, as the initial PET measurements in healthy rat models indicated that the 3-position for  $^{18}\text{F}$ -labeled AAAs provided the highest brain uptake values (see Appendix).

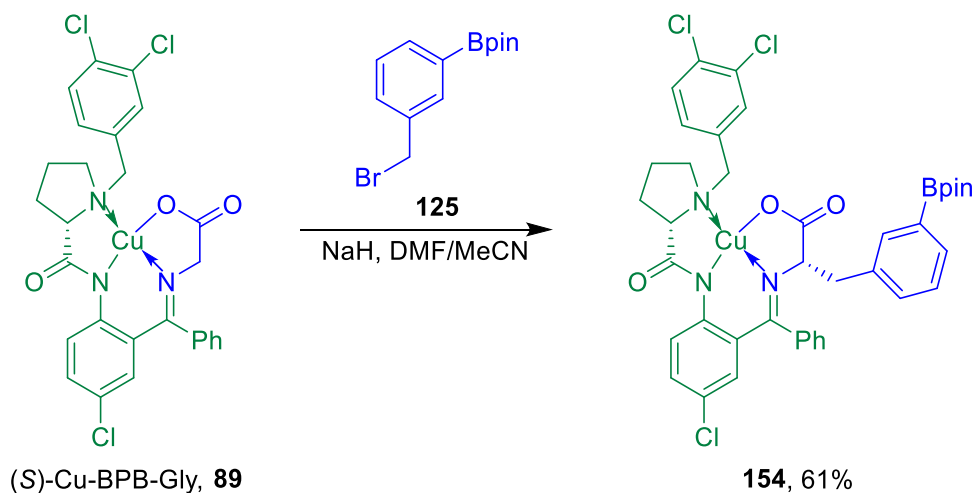
### 3.6. Preparation of (*S*)-AAA Tracer Precursor Using Cu-BPB-Gly Complexes

Cu-BPB complexes have been demonstrated to be suitable alternatives to Ni-BPB complexes.<sup>78</sup> Schneider *et al.* described the use of the ligand (*S*)-2-(*N*-(2-methylthio)benzylprolyl)aminobenzophenone to prepare a five-coordinate Cu-BPB-Gly complex (**93**). As Cu would be used for Cu-mediated radiofluorination, and now, as a Cu-BPB auxiliary, a single trace metal would be used for the entirety of the AAA tracer preparation.



Scheme 54. (*S*)-Cu-BPB-Gly complexes towards radiolabeling precursor **153**.

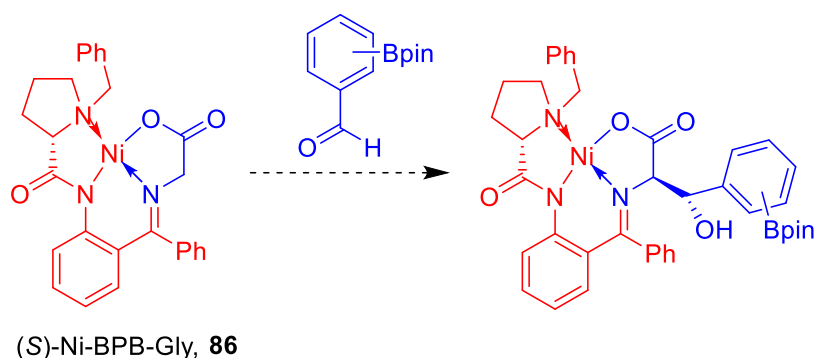
From a *c*GMP perspective, the advantageous omission of Ni would negate the required testing for an additional trace metal. The synthesis of suitable Cu-BPB complexes for the precursor synthesis was investigated. Initially, alkylation of **125** upon **93** did not proceed, and we searched for alternative Cu-BPB complexes (Scheme 54). Saghiyan *et al.* reported the use of (*S*)-*N*-(2-benzoylphenyl)-1-(3,4-dichlorobenzyl)pyrrolidine-2-carboxamide (3,4-DCBPB) towards enhanced asymmetric synthesis of  $\alpha$ -amino acids.<sup>121</sup> The chlorinated benzyl substituents afforded the desired (*S,S*)-diastereomer upon alkylation. Accordingly, the alkylation of **125** upon **87** afforded the precursor **154** in moderate yield (Scheme 55).



Scheme 55. (*S*)-Cu-BPB-Gly complexes towards <sup>18</sup>F-labeled AAAs.

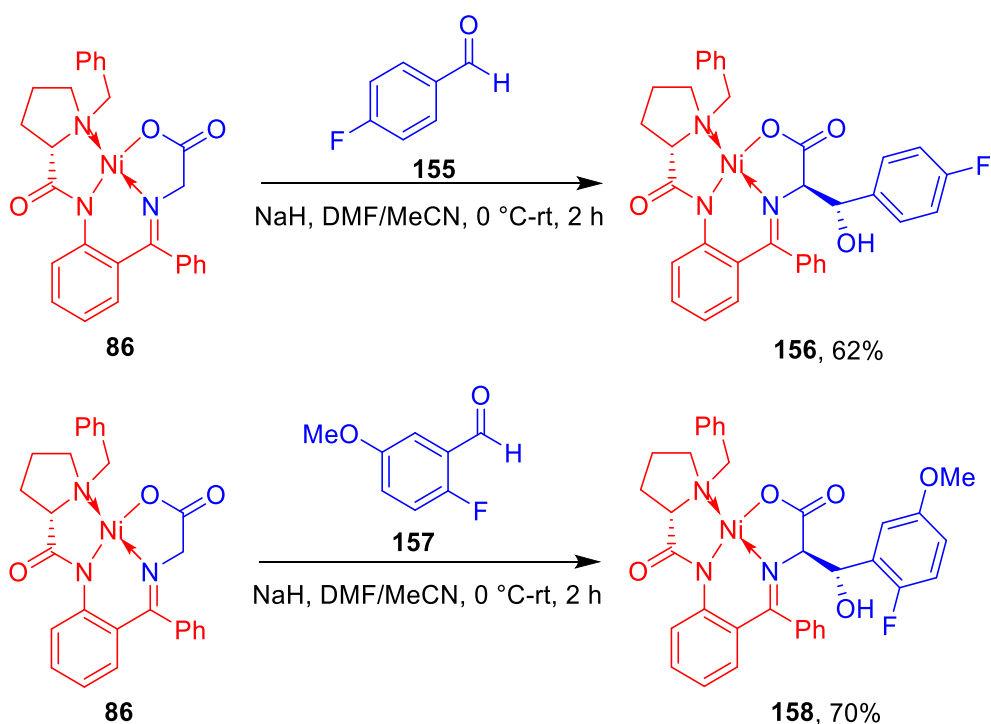
One drawback of this approach is the paramagnetism of Cu-BPB complexes, therefore making them unsuitable for NMR analysis.

### 3.7. Preparations Towards [ $^{18}\text{F}$ ]FPheSer



*Scheme 56. Prospective preparation of [ $^{18}\text{F}$ ]FPheSer precursors.*

The facile preparation of the previous Ni-BPB-AAA precursor compounds prompted the investigation of potential noradrenergic tracers based on their analogous structure to noradrenaline (**123**) (Fig. 16). Moreover, aldol reactions upon Ni-BPB complexes had been previously reported in the literature.<sup>79</sup> Using an (*R*)-Ni-BPB complex (e.g. **88**), one can selectively access the desired (2*S*,3*R*)-stereoconfiguration in the final  $^{18}\text{F}$ -labeled AAA *via* aldol reaction, and deprotection. Although using an (*S*)-Ni-BPB-Gly would generate the alternative PheSers containing the “non-natural” (2*R*,3*S*)-stereoconfiguration, these initial reactions were carried out as a proof-of-principle synthesis in order to ensure the aldol reaction proceeded under the desired reaction conditions. Accordingly, PheSer-based AAA tracer precursors were perceived to be accessed upon aldol reaction of suitably-substituted benzaldehydes upon (*S*)-Ni-BPB-Gly complexes (**86**) (Scheme 56). Initially, the preparation of the corresponding reference compounds **156** and **158** were carried out prior to the precursor (Scheme 57).



Scheme 57. Aldol reactions upon Ni-BPB complexes.

### 3.7.1. Synthetic Route A

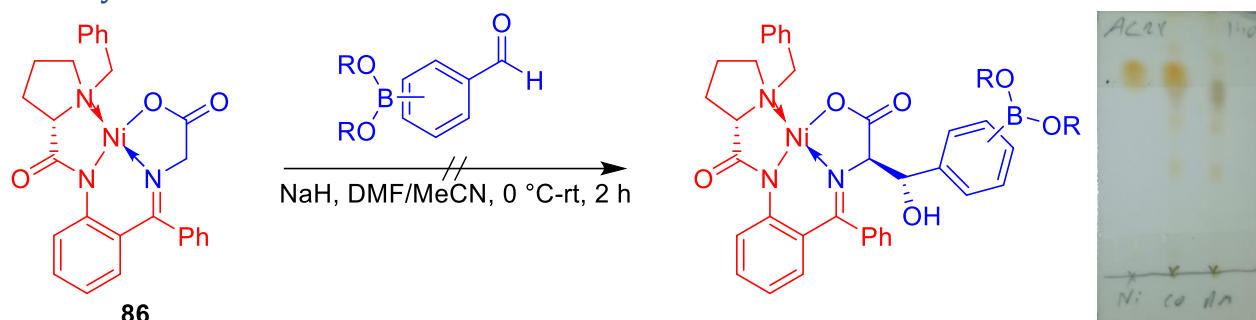
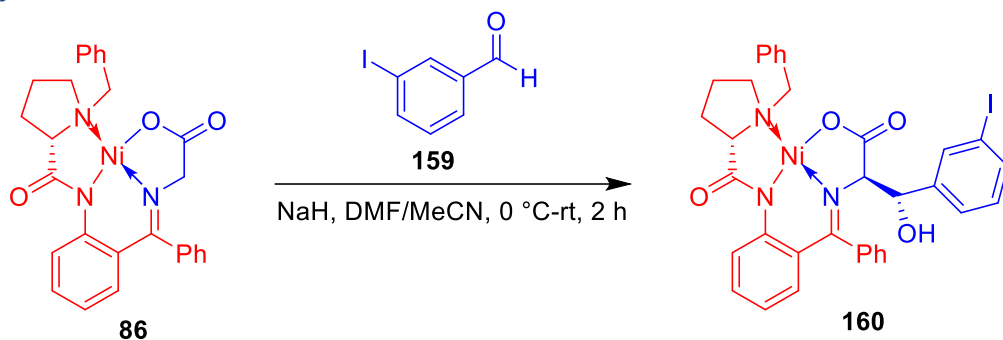


Figure 22 & scheme 58. Attempted aldol reactions upon **86**, and corresponding TLC.

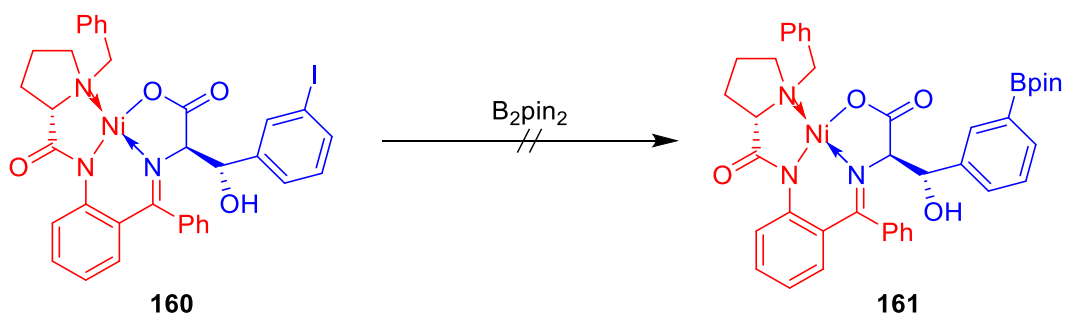
Despite the successful preparation of **156** and **158** via aldol reaction upon **86**, the aldol reactions using boronic acid and Bpin-substituted benzaldehydes proved far more challenging (Scheme 58). Although there was evidence of product formation, rapid degradation was observed despite altering the base concentration, employing several additives (e.g. DABCO), and augmenting the reaction temperature (Fig. 22).

### 3.7.2. Synthetic Route B



*Scheme 59. Aldol reaction of **159** upon **86**.*

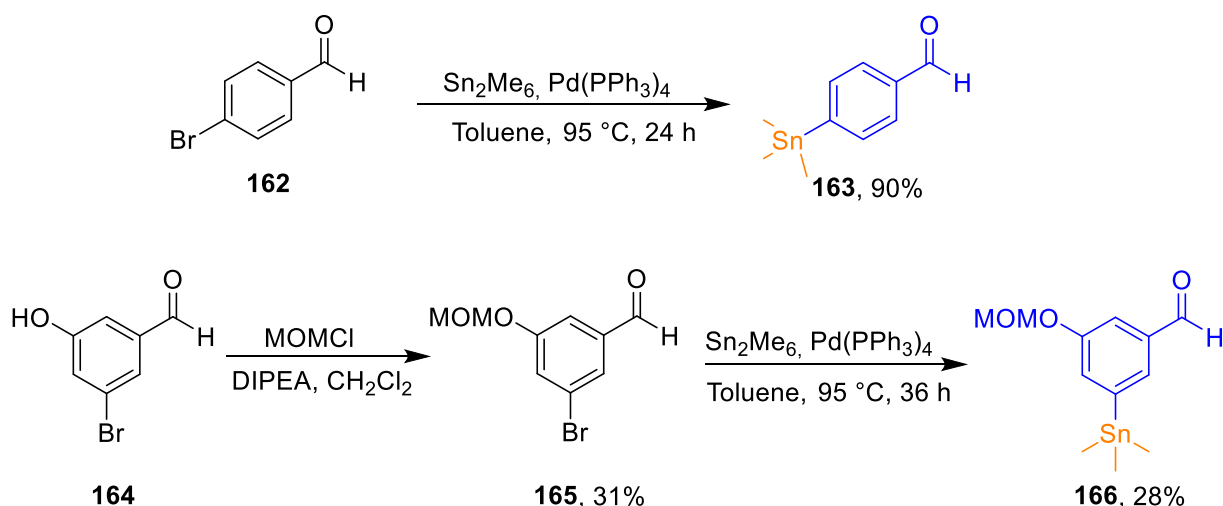
A secondary approach towards a suitable [ $^{18}\text{F}$ ]FPheSer precursor involved the aldol reaction of 3-iodobenzaldehyde (**159**) upon **86** (Scheme 59). Unfortunately, the Suzuki-Miyaura borylation of **160** failed to access the desired precursor **161** (Scheme 60).



*Scheme 60. Attempted aryl borylation towards **161**.*

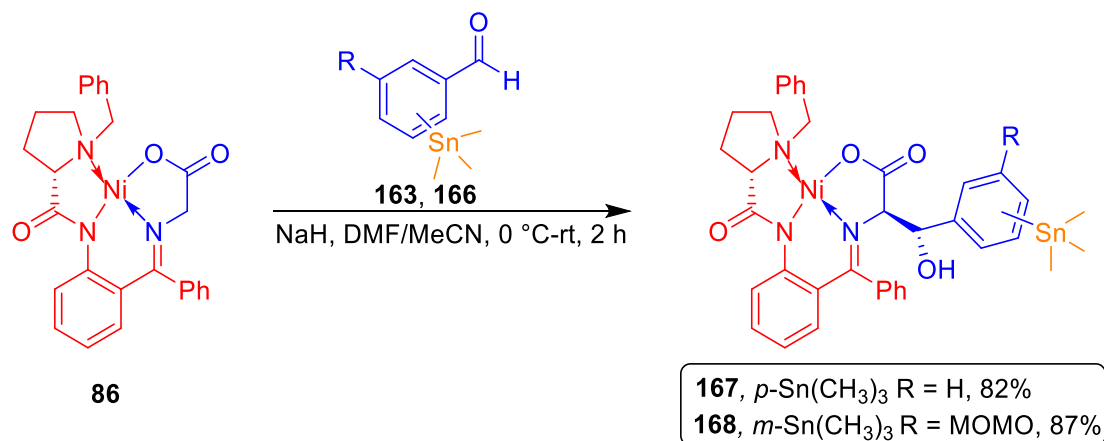
### 3.7.3. Synthetic Route C

Due to the unsuccessful aldol reactions of boron-containing benzaldehyde, a number of arylstannanes derivatives (**163**) and (**166**) were synthesized. As previously described, arylstannanes are also substrates of Cu-mediated radiofluorination and act as viable alternatives to aryl-boronic acids and Bpin-substituted arenes.



Scheme 61. Preparative procedures towards stannylated benzaldehydes **163** and **166**.<sup>122</sup>

The stannylation of **162** afforded the desired **163** in excellent yield.<sup>122</sup> The MOM-protection of the commercially available **164** furnished **165** in 31% yield. Thereafter, the stannylation of **165** allowed **166** to be accessed in 28% yield (Scheme 61). The aldol reactions of **163** and **166** upon **86** were found to proceed well, allowing the desired Ni-BPB-AAA precursors to be accessed in good yields (Scheme 62). Unfortunately, it was found that these stannylated Ni-complexes showed signs of instability, irrespective of being kept under argon and being stored in a refrigerator ( $-8\text{ }^\circ\text{C}$ ). This was mirrored from the inconsistent high-resolution mass spectrum (HRMS) results, which indicated complex degradation.



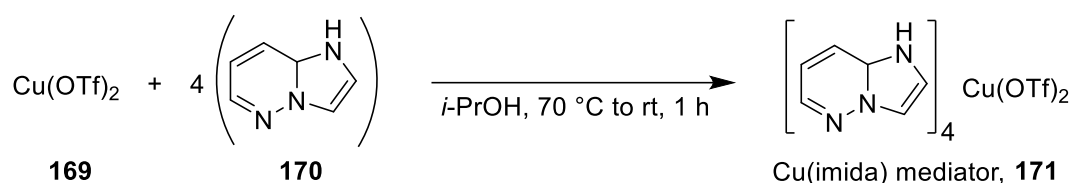
Scheme 62. Preparation of stannylated precursors **167** and **168**.

## 3.08. Radiochemistry

### 3.08.1. Cu-Mediated Radiofluorination

Following precursor synthesis, the radiolabeling of the corresponding precursors was carried out according to the alcohol-enhanced Cu-mediated radiofluorination protocol. The Cu-mediator employed for radiofluorination was commercially available  $[\text{Cu}(\text{OTf})_2(\text{py})_4]$ . The optimized alcohol-enhanced Cu-mediated radiofluorination conditions allowed the  $^{18}\text{F}$ -labeled Ni-BPB-AAAs to be furnished with high radiofluorination rates (Table 4). The radiolabeling was optimized with respect to temperature, time, and precursor/Cu quantity (Figure 28 & 29).

At a later stage in the project, we began to explore the use of alternative Cu-mediators for radiofluorination. After some initial screening radiofluorination experiments on model compounds, we discovered that tetrakis(imidazo(1,2-b)pyridazine) copper(II) triflate ( $\text{Cu}(\text{imida})$  mediator **171**) was found to furnish slightly higher  $^{18}\text{F}$ -incorporation rates than  $[\text{Cu}(\text{OTf})_2(\text{py})_4]$  in some instances. Although the  $[\text{Cu}(\text{imida})(\text{OTf})]$  complex is not commercially available, it was easily prepared from  $\text{Cu}(\text{OTf})_2$  (**169**) and **170** according to the method described by Antuganov *et al.* The preparation of **171** was carried out by Niklas Kolks (Scheme 63).<sup>123</sup>



Scheme 63. Preparation of tetrakis(imidazo(1,2-b)pyridazine) copper(II) triflate.

### 3.08.2. Optimization of $^{18}\text{F}$ -Labeling Conditions

Optimization with respect to reaction temperature was carried out with precursor **127b** at 100 °C, 110 °C, and 120 °C. It was found that 110 °C for 15 minutes afforded the highest  $^{18}\text{F}$ -incorporation of the three temperatures (Fig. 23).

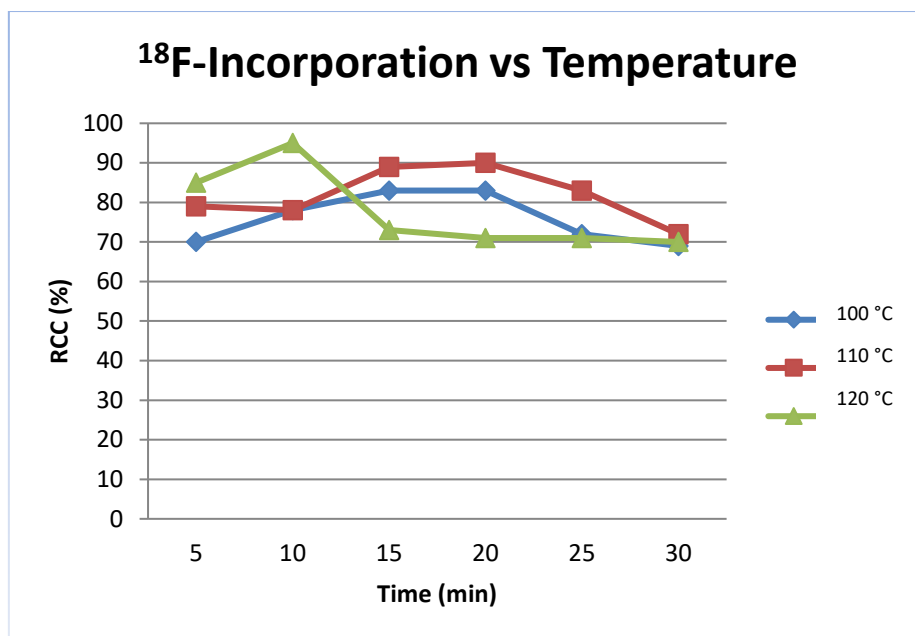


Figure 23. The dependency of  $^{18}\text{F}$ -incorporation on temperature. Conditions: [ $^{18}\text{F}$ ]Fluoride ( $\sim 50$  MBq) was loaded onto a QMA- $\text{CO}_3^-$  cartridge from the male side. The cartridge was washed with water (1 mL) in the same direction and flushed with air (5 mL). Thereafter,  $^{18}\text{F}^-$  was eluted from the female side with a solution of  $\text{Et}_4\text{NHCO}_3$  (3 mg) in MeOH (0.7 mL). The MeOH was evaporated under a flow of air within 5 min. A solution of **127b** (10  $\mu\text{mol}$ ) and  $\text{Cu}(\text{OTf})_2(\text{py})_4$  (13.6 mg, 20  $\mu\text{mol}$ ) in  $n\text{-BuOH/DMA}$  (1:3, 750  $\mu\text{L}$ ) was added, the reaction mixture was heated at the corresponding temperature for 15 min under air, diluted with water (1 mL) and analyzed by HPLC. All experiments were carried out in triplicate.

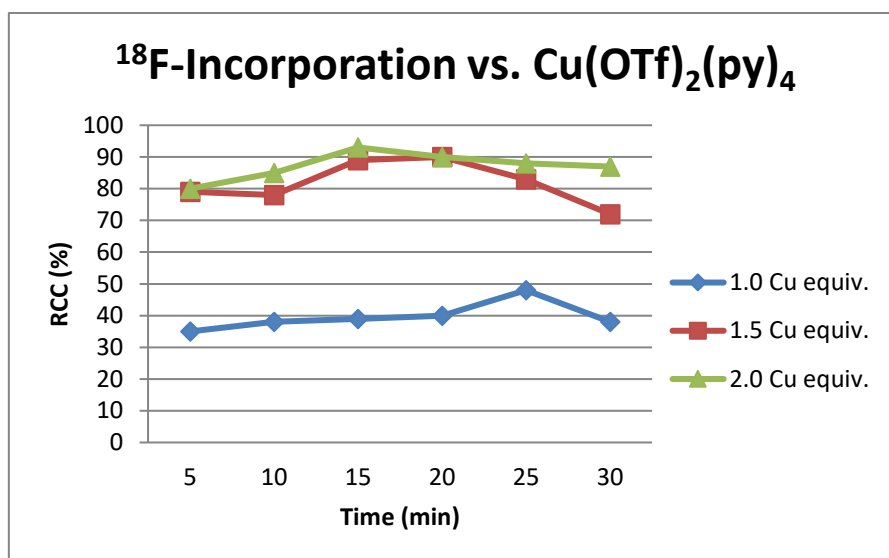
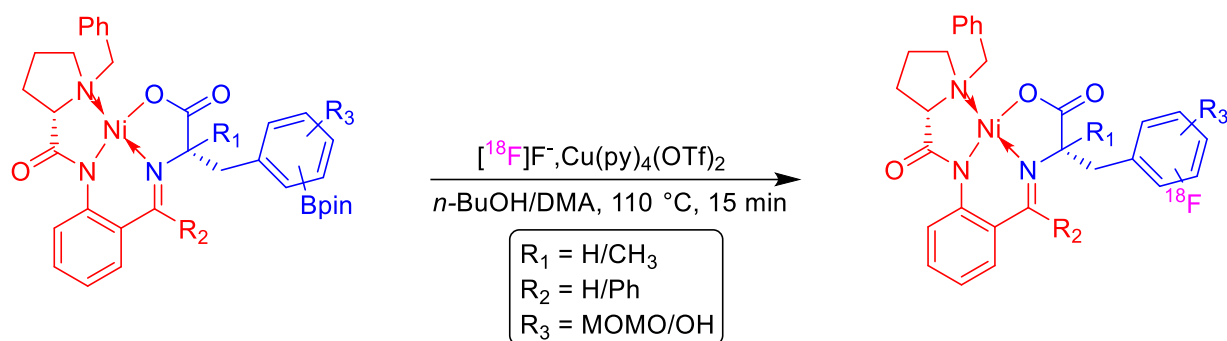


Figure 24. The dependency of  $^{18}\text{F}$ -incorporation on Cu mediator concentration. Conditions:  $[\text{}^{18}\text{F}]\text{Fluoride}$  ( $\sim 50$  MBq) was loaded onto a  $\text{QMA-CO}_3^-$  cartridge from the male side. The cartridge was washed with water (1 mL) in the same direction and flushed with air (5 mL). Thereafter,  $^{18}\text{F}^-$  was eluted from the female side with a solution of  $\text{Et}_4\text{NHCO}_3$  (3 mg) in MeOH (0.7 mL). The MeOH was evaporated under a flow of air within 5 min. A solution of **127b** (10  $\mu\text{mol}$ ) and the corresponding  $\text{Cu}(\text{OTf})_2(\text{py})_4$  amount in  $n\text{-BuOH/DMA}$  (1:3, 750  $\mu\text{L}$ ) was added, the reaction mixture was heated at the 110  $^\circ\text{C}$  for 15 min under air, diluted with water (1 mL) and analyzed by HPLC. All experiments were carried out in triplicate.

The relative concentration of the Ni-BPB-AAA precursor with respect to the concentration of the Cu-mediator was found to have a profound impact on the rate of  $^{18}\text{F}$ -incorporation. The optimization of the Cu-mediator concentration was carried out whilst bearing in mind that the Cu-content in the  $^{18}\text{F}$ -labeled AAA solution should be as low as possible. Optimization with respect to the equivalents of  $[\text{Cu}(\text{OTf})_2(\text{py})_4]$  was carried out with precursor **127b** at 110  $^\circ\text{C}$ . It was found that the application of 2 molar equivalents of  $[\text{Cu}(\text{OTf})_2(\text{py})_4]$  at 110  $^\circ\text{C}$  for 15 minutes afforded the highest  $^{18}\text{F}$ -incorporation among the tested conditions (Fig. 24). The data obtained correlated with the  $n\text{-BuOH/DMA}$  solvent ratio of (1:3) as outlined in the alcohol-enhanced manuscript by Zischler *et al.*<sup>46</sup>

### 3.08.3. Cu-Mediated Radiofluorination of Ni-BPX-AAA Complexes



Scheme 64.  $^{18}\text{F}$ -Incorporation rates via Cu-mediated radiofluorination.

Entry	Ni-BPX-AAA Precursor	RCC (%) (n = 4)
1	<b>127a</b> , $\text{R}_1, \text{R}_3 = \text{H}$ , $\text{R}_2 = \text{Ph}$ , <i>o</i> -Bpin	$[^{18}\text{F}]\textbf{134a}$ ( $92 \pm 5$ )
2	<b>127b</b> , $\text{R}_1, \text{R}_3 = \text{H}$ , $\text{R}_2 = \text{Ph}$ , <i>m</i> -Bpin	$[^{18}\text{F}]\textbf{134b}$ ( $90 \pm 2$ )
3	<b>127c</b> , $\text{R}_1, \text{R}_3 = \text{H}$ , $\text{R}_2 = \text{Ph}$ , <i>p</i> -Bpin	$[^{18}\text{F}]\textbf{172}$ ( $86 \pm 4$ )
4	<b>127d</b> , $\text{R}_1 = \text{H}$ , $\text{R}_2 = \text{Ph}$ , $\text{R}_3 = 5\text{-OMOM}$ , <i>o</i> -Bpin	$[^{18}\text{F}]\textbf{173}$ ( $90 \pm 3$ )
5	<b>127e</b> , $\text{R}_1 = \text{H}$ , $\text{R}_2 = \text{Ph}$ , $\text{R}_3 = 4\text{-OMOM}$ , <i>o</i> -Bpin	$[^{18}\text{F}]\textbf{134c}$ ( $90 \pm 6$ )
6	<b>127f</b> , $\text{R}_1 = \text{CH}_3$ , $\text{R}_2 = \text{H}$ , $\text{R}_3 = \text{H}$ , <i>o</i> -Bpin	$[^{18}\text{F}]\textbf{134d}$ ( $84 \pm 6$ )
7	<b>127g</b> , $\text{R}_1 = \text{CH}_3$ , $\text{R}_2 = \text{H}$ , $\text{R}_3 = \text{H}$ , <i>m</i> -Bpin	$[^{18}\text{F}]\textbf{134e}$ ( $89 \pm 7$ )
8	<b>127h</b> , $\text{R}_1 = \text{CH}_3$ , $\text{R}_2 = \text{H}$ , $\text{R}_3 = \text{H}$ , <i>p</i> -Bpin	$[^{18}\text{F}]\textbf{134f}$ ( $92 \pm 4$ )
9	<b>127i</b> , $\text{R}_1 = \text{CH}_3$ , $\text{R}_2 = \text{H}$ , $\text{R}_3 = 5\text{-OMOM}$ , <i>o</i> -Bpin	$[^{18}\text{F}]\textbf{174}$ ( $84 \pm 3$ )

Table 5.  $^{18}\text{F}$ -Labeling: Ni-BPX-AAA (**127a–i**, 10  $\mu\text{mol}$ ),  $\text{Cu}(\text{OTf})_2(\text{py})_4$  (20  $\mu\text{mol}$ ),  $[^{18}\text{F}]\text{F}^-/\text{Et}_4\text{NHCO}_3$  (50–1500 MBq), 250  $\mu\text{L}$  *n*-BuOH/750  $\mu\text{L}$  DMA, air, 110  $^\circ\text{C}$ , 15 min. All experiments were carried out at least in triplicate. Radio-HPLC was used to determine the RCYs, given in the form of mean  $\pm$  standard deviation.

The radiofluorination of the Ni-BPB-AAA complexes was carried out according to the aforementioned alcohol-enhanced Cu-mediated radiofluorination protocol (Scheme 64). The  $^{18}\text{F}$ -incorporation was found to be very high in all cases (Table 5).

### 3.08.4. Optimization of Deprotection Conditions

The final step of the AAA tracer radiosynthesis was the deprotection of the radiofluorinated Ni/Cu-BPB-AAA intermediates ( $[^{18}\text{F}]\mathbf{134a-f}$ ,  $[^{18}\text{F}]\mathbf{172-174}$ ). We found this step to be more challenging than anticipated, as the deprotection was not proceeding with low concentrations of HCl, contrary to the literature.<sup>76</sup> Moreover, we also required the deprotection reaction to cleave the MOM-protecting groups present in several precursors.

Initially, we attempted to use C18 cartridges to isolate the  $^{18}\text{F}$ -labeled Ni-BPB-AAA intermediates prior to deprotection. However, it was found that large volumes of MeCN or MeOH were required to elute the  $^{18}\text{F}$ -labeled products from the cartridges effectively. As larger reaction mixture volumes are typically undesirable, due to lengthy evaporation times and potential automated radiosynthesis complications, we chose to evaporate the *n*-BuOH/DMA prior to deprotection.

We found that the removal of *n*-BuOH/DMA from the reaction vial prior to the addition of HCl became a crucial aspect for successful Ni-BPB-AAA decomplexation to occur. The removal of *n*-BuOH/DMA under reduced pressure was achieved in 12 min at 110 °C. Thereafter, 1 mL 12 M HCl was added to the reaction vial, and the reaction mixture was stirred at 110 °C for 15 min.

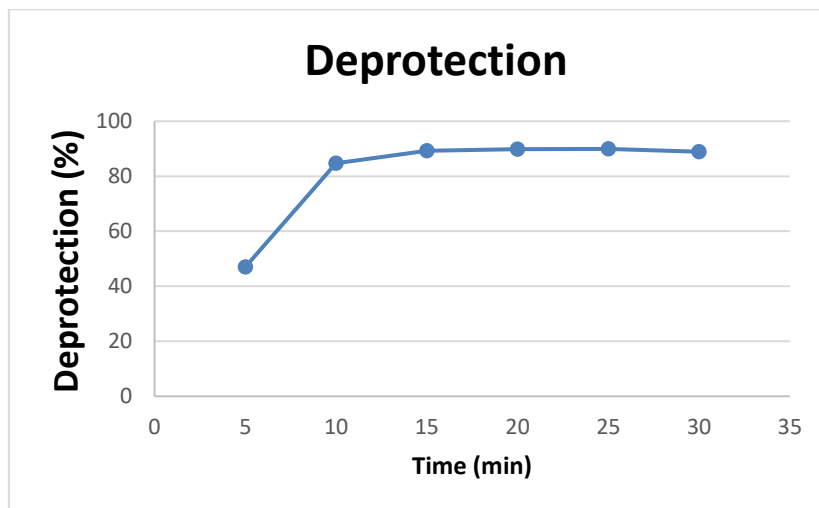
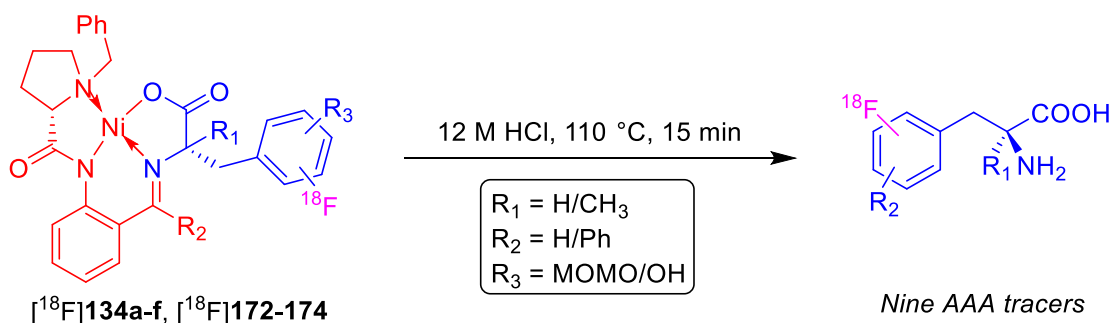


Figure 25. Deprotection of  $^{18}\text{F}$ -labeled Ni-BPX-AAA intermediates at 110 °C.

The deprotection step was optimized with respect to time, temperature, and HCl concentration. It was found that 12 M HCl (1 mL) at 110 °C for 15 min provided the highest deprotection yield (Fig. 25) (Scheme 65). Exceeding any of these parameters usually resulted in lower RCYs or the infeasibility of the method towards automated module implementation.



*Scheme 65. Optimized deprotection of radiofluorinated intermediate complexes.*

Successful deprotection was typically observable by the color change from deep red to pale yellow. The color change indicates the decomplexation of the radiolabeled Ni(II)-complex intermediates, which appear deep red. Following successful deprotection, the stirred HCl solution was removed from the reaction vial under reduced pressure at 110 °C for 15 min. The introduction of a base-trap (containing 2 M NaOH), placed after the cold-trap, was required to remove  $[\text{F}]\text{HF}$  formed from the reaction of HCl and unreacted  $[\text{F}]\text{fluoride}$ .

One obstacle that we encountered was the formation of a radiofluorinated side-product during 2- $[\text{F}]\text{FTyr}$  ( $[\text{F}]\text{36}$ ), 6- $[\text{F}]\text{FMT}$  ( $[\text{F}]\text{28}$ ), and  $\alpha\text{-Me-6-}[\text{F}]\text{FMT}$  ( $[\text{F}]\text{175}$ ) preparations (Fig. 26). This observation may have been due to a side-reaction initiated by the cleaved MOM-PGs. Accordingly, the collection of  $[\text{F}]\text{36}$ ,  $[\text{F}]\text{28}$ , and  $[\text{F}]\text{175}$  product peaks had to be very precise. Therefore, in these instances, RCY had to be forfeited to obtain RCP >95% in the products.

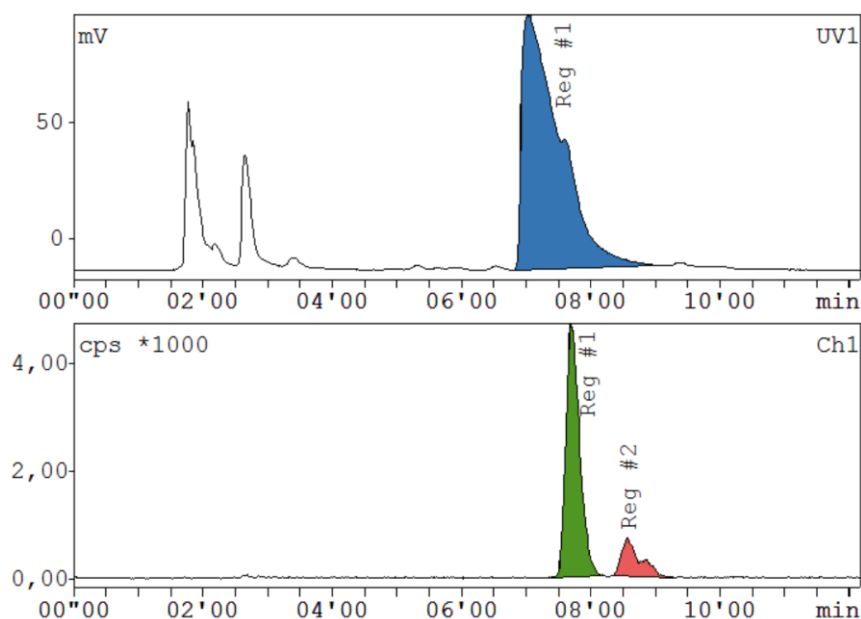


*Figure 26. Chromatogram showing side product formation during  $[\text{F}]\text{36}$  synthesis.*

### 3.08.5. $^{18}\text{F}$ -labeled AAA Isolation & Purification

The crude  $^{18}\text{F}$ -labeled AAA residue following HCl evaporation was dissolved with 1 mL 6% EtOH solution, and isolated by semi-preparative HPLC. The products were confirmed by the co-injection of the  $^{18}\text{F}$ -labeled AAA and the suitable AAA reference compound.

## 3.09. General Overview of Radiosynthesis

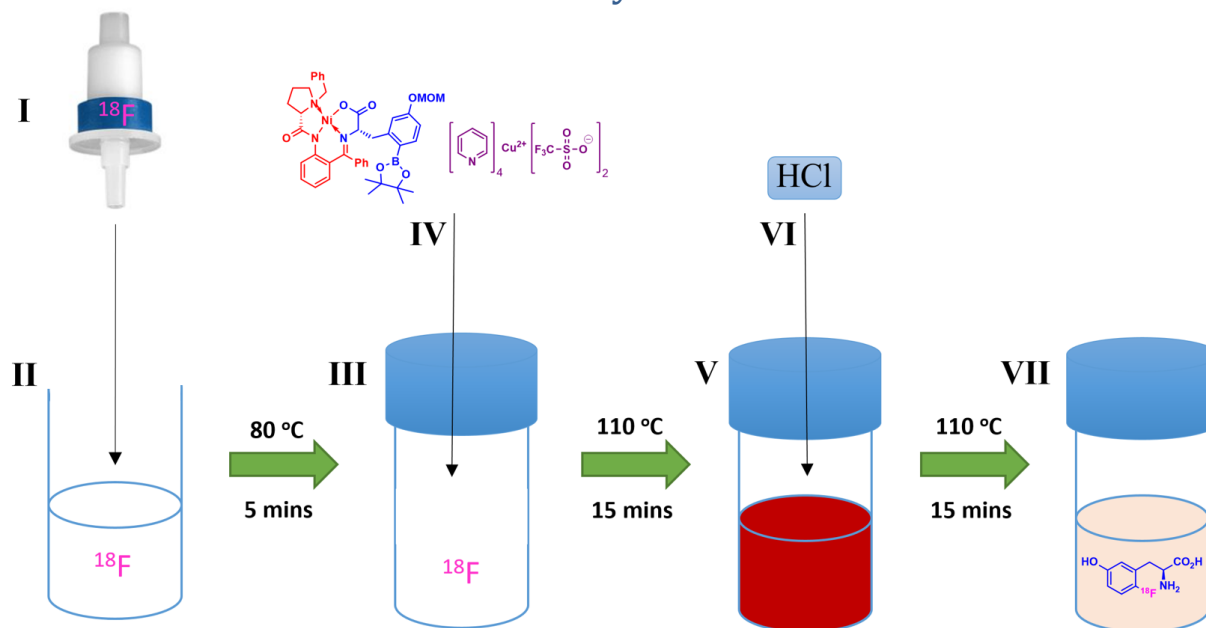
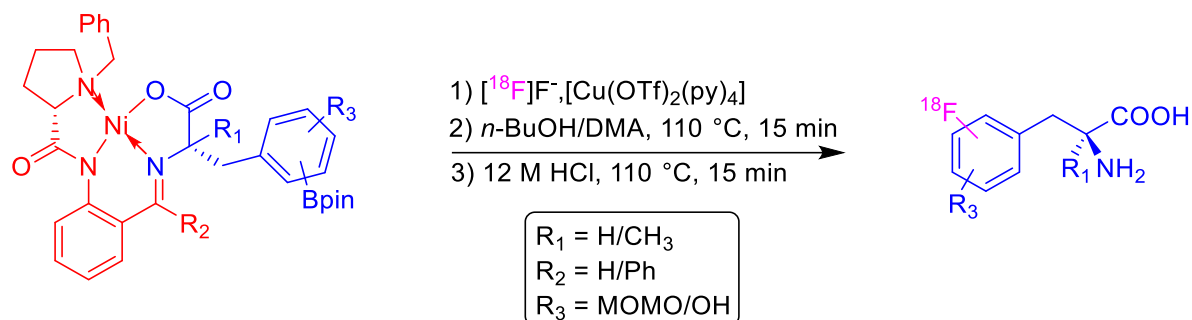


Figure 27. A general overview of the major radiosynthesis steps.

The radiosynthetic protocol towards  $^{18}\text{F}$ -labeled AAA is illustrated in Fig. 27. The outlined steps include:

- I.  $^{18}\text{F}$ -Fixation onto a QMA light carbonate cartridge
- II. Elution of  $[\text{}^{18}\text{F}]\text{F}^-$  into the reaction vessel using a methanolic solution of  $\text{Et}_4\text{NCO}_3$
- III. Evaporation of methanol
- IV. Addition of Ni-BPX-Gly and Cu-mediator in *n*-BuOH/DMA into the reaction vessel
- V. Evaporation of *n*-BuOH/DMA reaction solvents
- VI. Addition of 1 mL 12 M HCl
- VII. Evaporation of acidic solution and HPLC purification

### 3.10. Preparation of $^{18}\text{F}$ -Labeled AAAs Using (*S* or *R*)-Ni-BPX-AAA Complexes

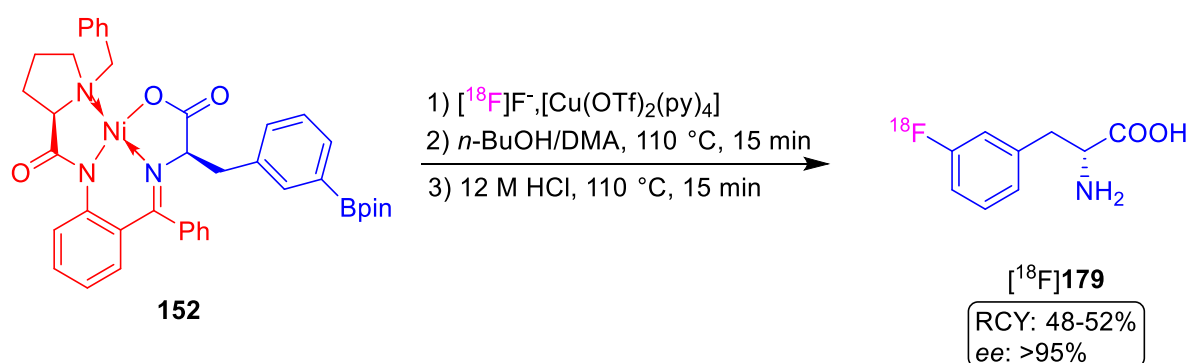


Scheme 66. Preparation of  $^{18}\text{F}$ -labeled AAAs using (*S*)-Ni-BPX-AAA complexes.

Entry	Ni-BPX-AAA Precursor	RCY (%) (n = 6)
1	<b>127a</b> , $\text{R}_1, \text{R}_3 = \text{H}$ , $\text{R}_2 = \text{Ph}$ , <i>o</i> -Bpin	$[^{18}\text{F}]\textbf{35}$ ( $52 \pm 6$ )
2	<b>127b</b> , $\text{R}_1, \text{R}_3 = \text{H}$ , $\text{R}_2 = \text{Ph}$ , <i>m</i> -Bpin	$[^{18}\text{F}]\textbf{68}$ ( $58 \pm 2$ )
3	<b>127c</b> , $\text{R}_1, \text{R}_3 = \text{H}$ , $\text{R}_2 = \text{Ph}$ , <i>p</i> -Bpin	$[^{18}\text{F}]\textbf{74}$ ( $56 \pm 4$ )
4	<b>127d</b> , $\text{R}_1 = \text{H}$ , $\text{R}_2 = \text{Ph}$ , $\text{R}_3 = 5\text{-OMOM}$ , <i>o</i> -Bpin	$[^{18}\text{F}]\textbf{28}$ ( $26 \pm 5$ )
5	<b>127e</b> , $\text{R}_1 = \text{H}$ , $\text{R}_2 = \text{Ph}$ , $\text{R}_3 = 4\text{-OMOM}$ , <i>o</i> -Bpin	$[^{18}\text{F}]\textbf{36}$ ( $25 \pm 5$ )
6	<b>127f</b> , $\text{R}_1 = \text{CH}_3$ , $\text{R}_2 = \text{H}$ , $\text{R}_3 = \text{H}$ , <i>o</i> -Bpin	$[^{18}\text{F}]\textbf{176}$ ( $50 \pm 3$ )
7	<b>127g</b> , $\text{R}_1 = \text{CH}_3$ , $\text{R}_2 = \text{H}$ , $\text{R}_3 = \text{H}$ , <i>m</i> -Bpin	$[^{18}\text{F}]\textbf{177}$ ( $56 \pm 4$ )
8	<b>127h</b> , $\text{R}_1 = \text{CH}_3$ , $\text{R}_2 = \text{H}$ , $\text{R}_3 = \text{H}$ , <i>p</i> -Bpin	$[^{18}\text{F}]\textbf{178}$ ( $53 \pm 4$ )
9	<b>127i</b> , $\text{R}_1 = \text{CH}_3$ , $\text{R}_2 = \text{H}$ , $\text{R}_3 = 5\text{-OMOM}$ , <i>o</i> -Bpin	$[^{18}\text{F}]\textbf{175}$ ( $42 \pm 7$ )

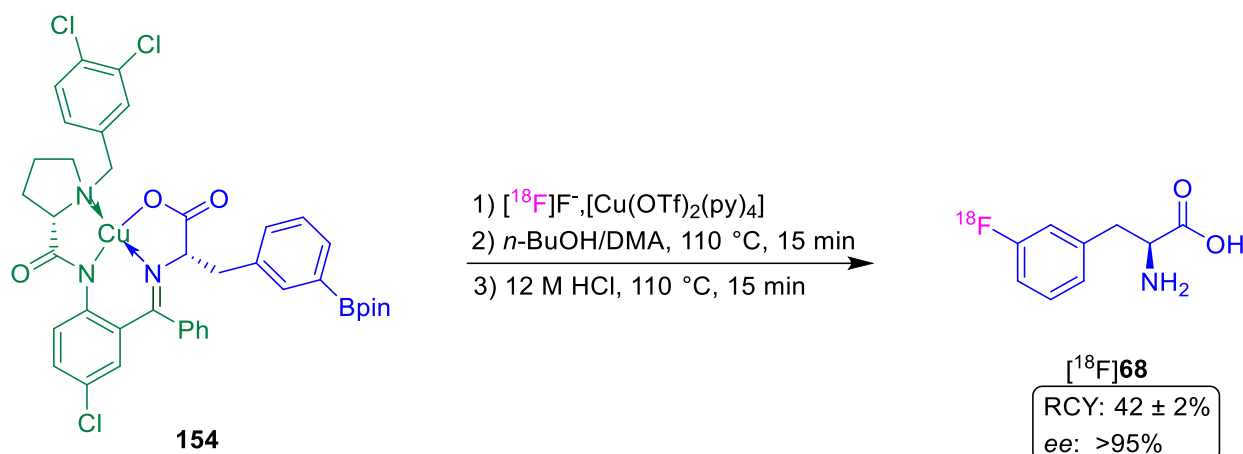
Table 6.  $^{18}\text{F}$ -labeled AAA products.

The application of the optimized radiosynthesis conditions furnished the  $^{18}\text{F}$ -labeled AAAs in 20–60% RCY, with *ee* > 95%, and RCP >95% (Scheme 66). Similarly, the applied protocol using a Bpin-substituted (*R*)-Ni-BPB-AAA precursor yielded  $[^{18}\text{F}]\textbf{179}$  (Scheme 67).



Scheme 67. Preparation of 3-(*R*)- $[^{18}\text{F}]\text{FPhe}$  ( $[^{18}\text{F}]\textbf{179}$ ).

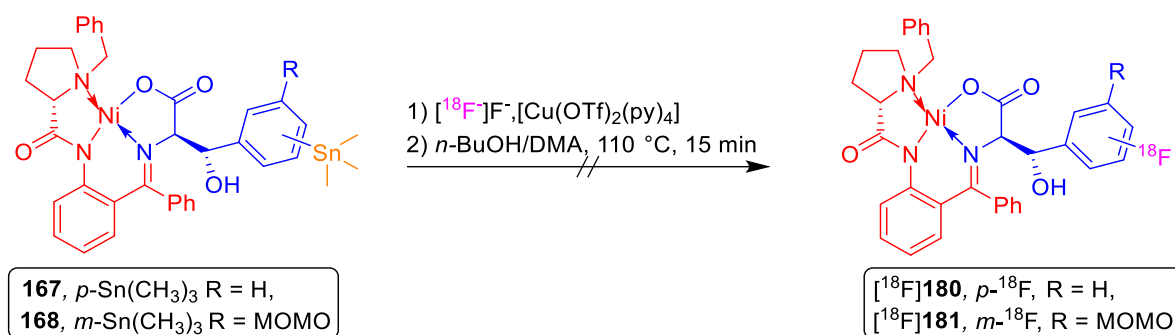
### 3.11. Preparation of $^{18}\text{F}$ -AAA Tracers Using a Cu-BPX-AAA Complex



*Scheme 68. Preparation of [ $^{18}\text{F}$ ]68 using Cu-BPB complexes.*

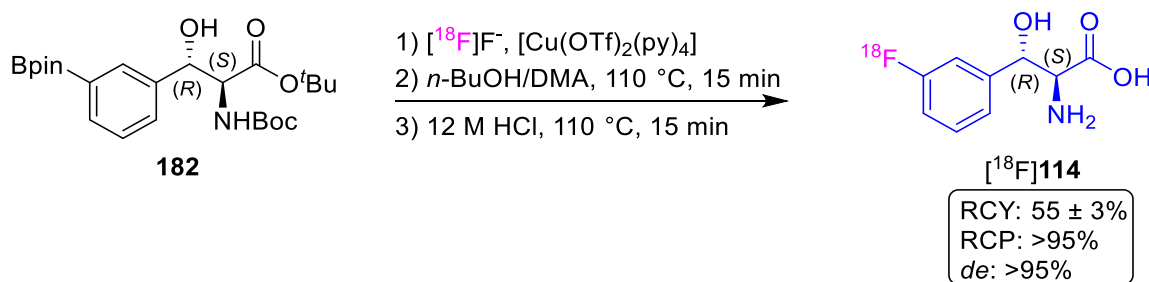
The established radiosynthetic protocol using a Bpin-substituted Cu-BPB-AAA precursor also afforded [ $^{18}\text{F}$ ]68 in good RCY and excellent purity (Scheme 68). However, the deprotection step appeared to be more challenging in this instance. Thus, [ $^{18}\text{F}$ ]68 was obtained in a lower RCY than from the Bpin-substituted Ni-BPB-AAA precursor (**127b**) derivative. Nevertheless, the employment of Cu- instead of Ni-containing precursors has the advantage of requiring only a single trace metal determination as part of radiopharmaceutical QC analysis.

### 3.12. Preparation of 3- $^{18}\text{F}$ FPheSer



Scheme 69. Attempted radiofluorination of **167** and **168**.

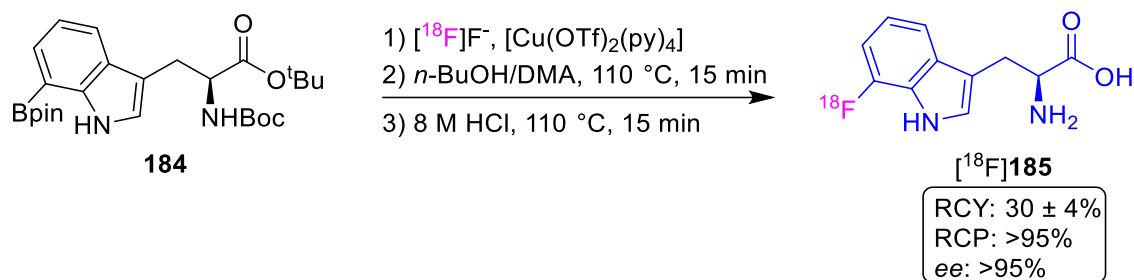
Despite the successful preparation of precursors **167** and **168** via aldol reaction of trimethyltin-substituted benzaldehydes upon **86**, the instability of the compounds proved to be a significant limitation. This was reflected by the precursor degradation that was observed during MS characterization. Unfortunately, Cu-mediated radiofluorination of the trimethyltin-substituted Ni-BPB-AAA precursors provided no evidence of a radiolabeled product (Scheme 69). Similarly, the radiofluorination protocol reported by Zarrad *et al.* failed to produce the desired  $^{18}\text{F}$ -labeled Ni-BPB-AAA intermediates.<sup>57</sup> One possible explanation for this failure may be that the acidic proton from the  $\beta$ -hydroxyl group interfered with the Cu-mediated radiofluorination mechanism. However, it is more likely that the  $\text{Sn}(\text{CH}_3)_3$  group sensitivity or complex instability was responsible.



Scheme 70. Preparation of  $^{18}\text{F}$ **114**.

A final attempt towards  $^{18}\text{F}$ **114** was carried out using a Boc-protected precursor **182** (prepared by Mrs. Elizaveta Urusova). Using the established alcohol-enhanced Cu-mediated radiofluorination protocol,  $^{18}\text{F}$ **114** was obtained upon the deprotection of the radiolabeled intermediate ( $^{18}\text{F}$ **183**) in very high RCY with excellent RCP and *de* (Scheme 70).

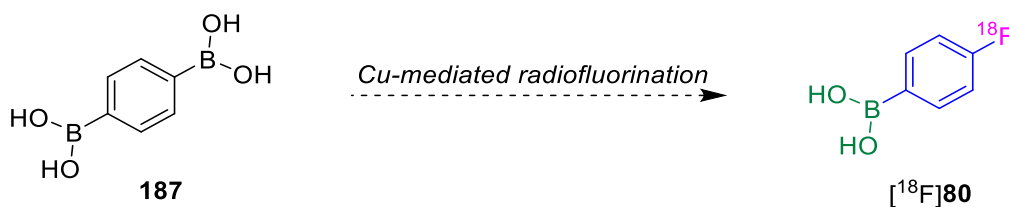
### 3.13. Preparation of 7- $^{18}\text{F}$ Trp



Scheme 71. Preparation of [ $^{18}\text{F}$ ]185.

The established radiosynthetic method was additionally applied towards the preparation of 7- $^{18}\text{F}$ Trp ([ $^{18}\text{F}$ ]185) from the precursor **184** (provided by Niklas Kolks) (Scheme 71). Schäfer *et al.* described how [ $^{18}\text{F}$ ]185 can be applied for the visualization of Trp-accumulating tumors using PET.<sup>56</sup> However, the application of the established protocol furnished [ $^{18}\text{F}$ ]185 upon deprotection of the radiolabeled intermediate ([ $^{18}\text{F}$ ]186) in a lower RCY than the reported value in the literature.

### 3.14. Preparation of Prosthetic Group [ $^{18}\text{F}$ ]FPBA



Scheme 72. Proposed reaction scheme towards the prosthetic group [ $^{18}\text{F}$ ]80.

Finally, this work sought to optimize the preparation of the promising prosthetic group 4- $^{18}\text{F}$ fluorophenylboronic acid ([ $^{18}\text{F}$ ]FPBA, [ $^{18}\text{F}$ ]80), a powerful  $^{18}\text{F}$ -synthon for site-specific Suzuki-Miyaura coupling (Scheme 72). Initially, the established Cu-mediated radiofluorination protocol was applied towards the preparation of [ $^{18}\text{F}$ ]80. Despite unexpectedly rapid radiofluorination (ca. 50% RCY in 0.5 min), product degradation and the generation of side-products limited this protocol (Fig. 28). The presence of  $n\text{-BuOH}$  was found to be one source responsible for rapid side-product formation. Possibly, this may be due to the reactive nature of a bisboronic acid substrate, and a Cu(II) complex in the presence of a tertiary alcohol.

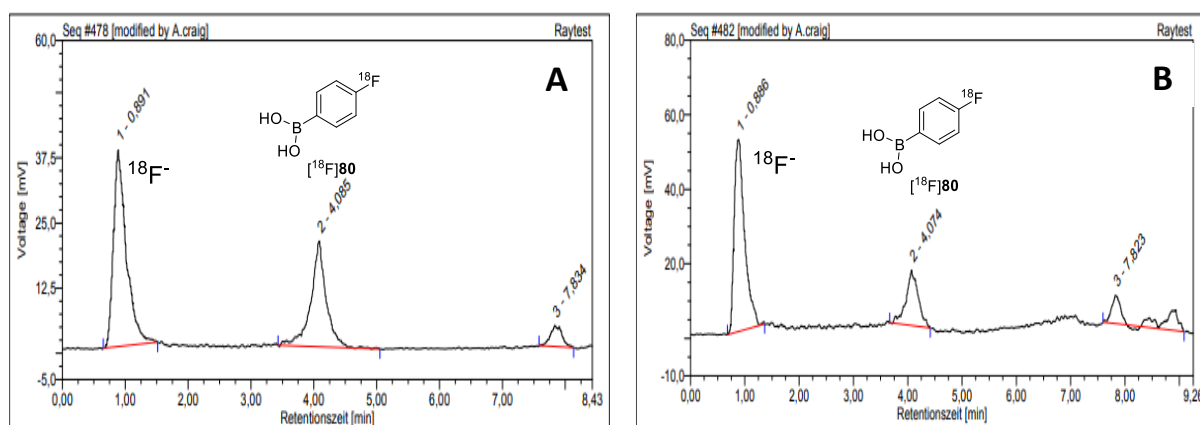


Figure 28. Radio-HPLC traces showing unreacted  $[^{18}\text{F}]\text{F}^-$ ,  $[^{18}\text{F}]\mathbf{80}$ , and an unknown radiolabeled impurity: A) After 0.5 min, B) after 30 min. Gradient A1 (see Experimental section).

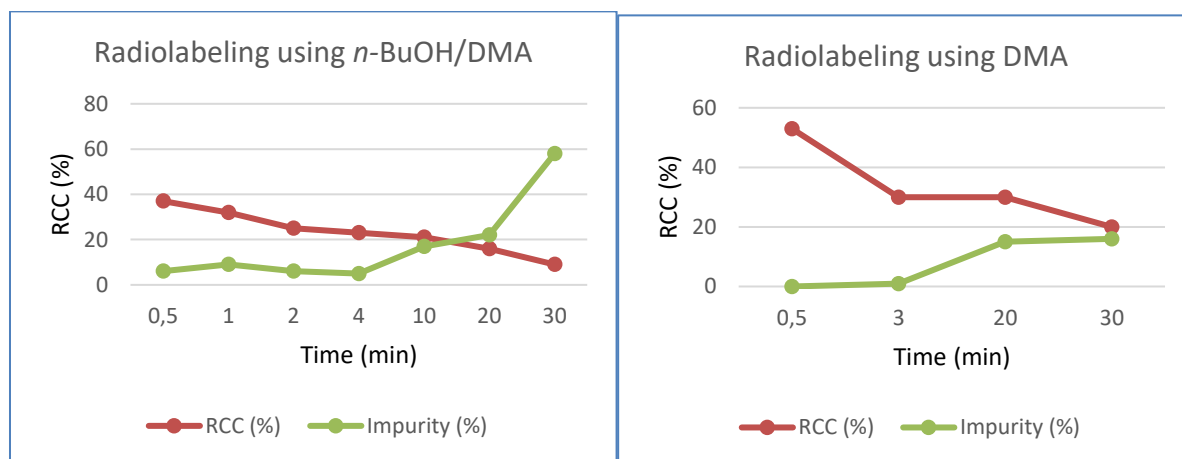


Figure 29.  $^{18}\text{F}$ -Incorporation with and without  $n\text{-BuOH}$ .

Although the use of pure DMA afforded more product stability, it was clear that degradation also occurred from some other source (Fig. 29). The degradation was identified to be related to the Cu-mediator concentration in the reaction mixture. The standard Cu-mediated radiofluorination procedure towards  $^{18}\text{F}$ -labeled AAAs uses two molar equivalents of the Cu-mediator to furnish the AAA tracer in high RCYs. However, it became evident that a secondary reaction concerning the boronic acid motif of  $[^{18}\text{F}]\mathbf{80}$  occurs, due to a subsequent Cu-mediated pathway. In this way, we encountered a synthetic dilemma whereby the Cu-mediator is required for successful radiofluorination, yet is simultaneously responsible for product degradation. In any case, we attempted to establish a radiofluorination procedure with lower concentrations of  $[\text{Cu}(\text{OTf})_2(\text{py})_4]$  to minimize product degradation. Unfortunately, this approach was found to substantially reduce the RCY, and ultimately rendered the procedure redundant.

In order to overcome this limitation, we turned our attention to the Antuganov approach towards the  $^{18}\text{F}$ -labeling of arenes (Fig. 10).<sup>61</sup> As this protocol employs DMAPOTf and only 0.25 molar equivalents of Cu-mediator, it was found that side-product formation was largely suppressed, and the applied method successfully furnished [ $^{18}\text{F}$ ]**80** in high RCYs (as determined by HPLC) within 15 minutes.

The radiosynthetic procedure towards [ $^{18}\text{F}$ ]**80** was further optimized with respect to Cu equivalent amount, Cu-mediator type, and temperature (Figs. 30–32) (Scheme 73). Interestingly, the use of the Cu(imida) (**171**) instead of  $[\text{Cu}(\text{OTf})_2(\text{py})_4]$  provided significantly reduced RCCs.

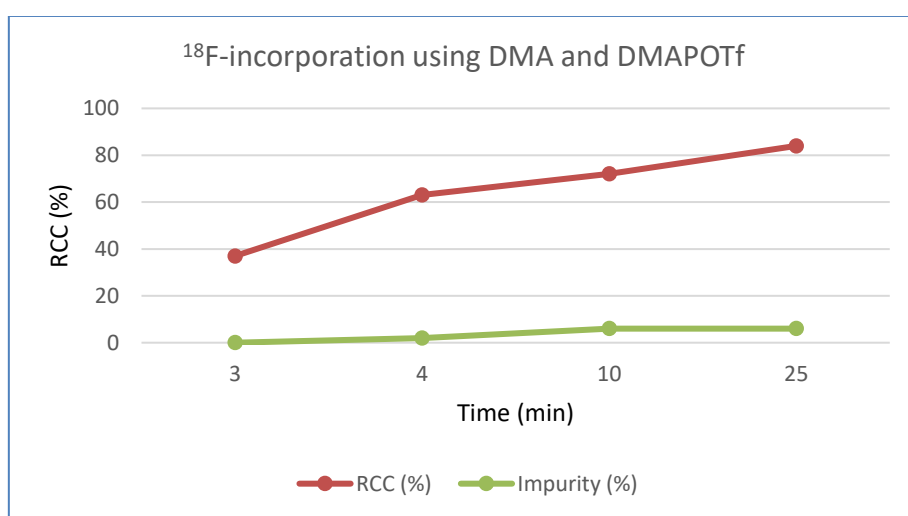


Figure 30.  $^{18}\text{F}$ -Incorporation using the Antuganov approach.

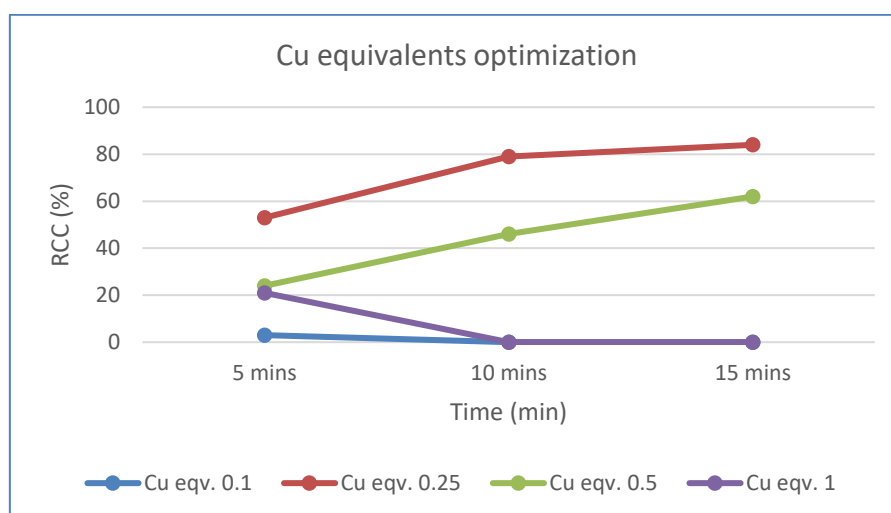


Figure 31. The dependency of  $^{18}\text{F}$ -incorporation on Cu mediator concentration.

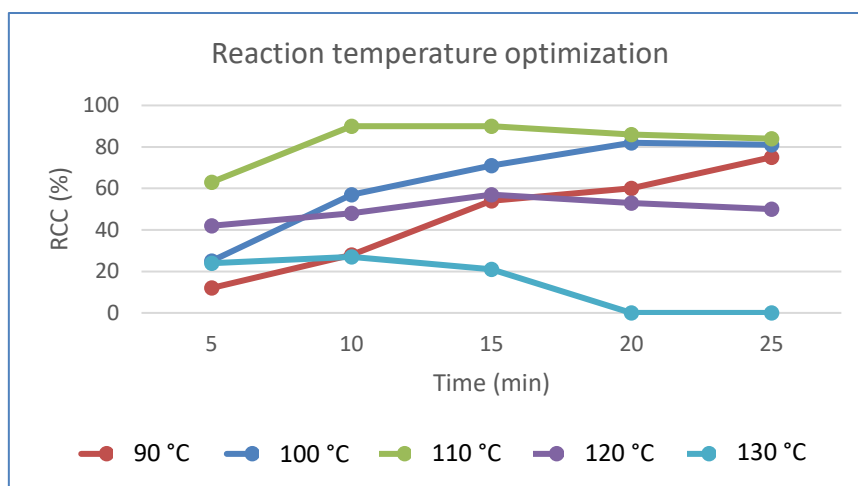
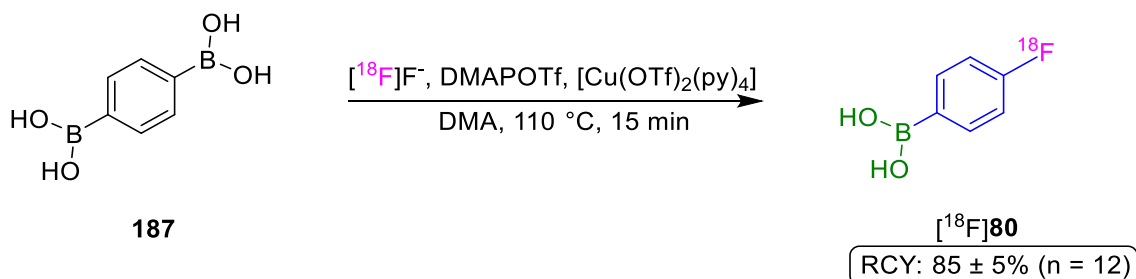
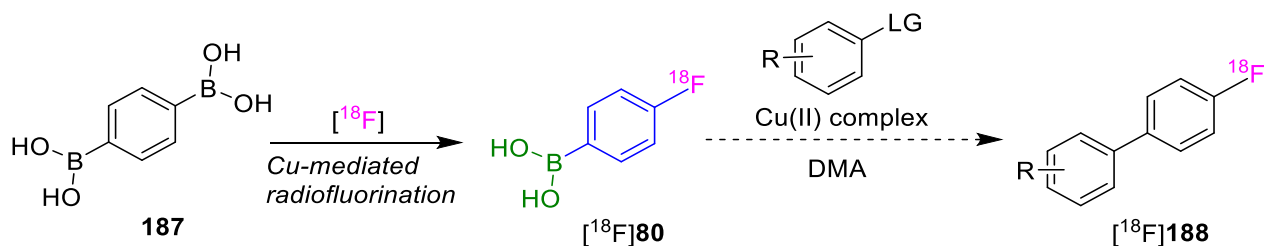


Figure 32. The dependency of  $^{18}\text{F}$ -incorporation on temperature.



Scheme 73. The preparation of  $[^{18}\text{F}]\text{80}$ .

Retrospectively, we revisited our previous synthetic dilemma concerning the highly reactive nature of  $[^{18}\text{F}]\text{80}$  in the presence of a Cu(II) complex and sought to harness the reactivity of  $[^{18}\text{F}]\text{80}$  to our advantage. Accordingly, we were attracted by the possibility of developing a one-pot radiolabeling and cross-coupling reaction, and now looked to classical Cu-catalyzed synthesis procedures (e.g. Chan-Lam coupling) for suitable reactions (Scheme 74).



Scheme 74. Proposed one-pot two-step preparation.

Despite several initial attempts to instigate the secondary cross-coupling reaction, our efforts were met with failure. Irrespective of these early setbacks, we intend to explore this promising pathway further in the future.

### 3.15. Automated Synthesis

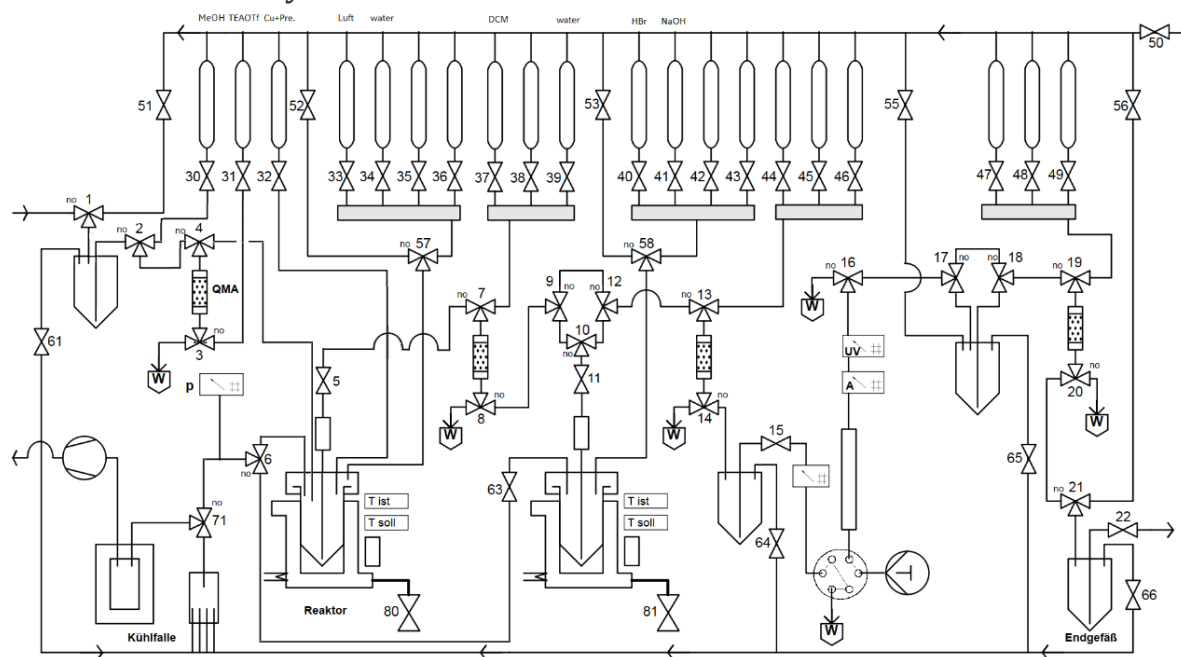


Figure 33. Automated synthesis schematic used to produce AAA tracers.

The preparation of [ $^{18}\text{F}$ ]**68** was exemplarily carried out using an automated module to furnish the  $^{18}\text{F}$ -labeled product (Fig. 33). However, a robust radiosynthetic protocol was not established due to limitations concerning the evaporation of the acidic reaction solvent at 130 °C. In certain modules, the reactor pressure may be too high to accommodate these temperatures and pressures. Therefore, longer deprotection at lower temperatures may be a more suitable option in these cases.

### 3.16. $^{18}\text{F}$ -Labeled Product Analysis

The radiochemical and chemical purities of the final products were determined using HPLC. The retention times ( $k$ ) of the reference compounds were compared with retention times of the final products to confirm the successful radiosynthesis of the tracer (see experimental section).

### 3.17. Carrier Amount & Specific Activity Determination

Following a literary procedure,<sup>58</sup> the carrier amounts in the final AAA preparations were determined as an alternative to the  $A_s$  or  $A_m$  of the products, which both dependent on radioactivity amount. The batch of ( $^{18}\text{F}$ )**68**) obtained after HPLC purification was left to stay for 24 h and thereafter concentrated under reduced pressure. The residue was redissolved in 0.2%  $\text{H}_3\text{PO}_4$  in 6% EtOH (1 mL), and 10  $\mu\text{L}$  was injected into the HPLC system. The peak area was determined, and the carrier amount was calculated according to the calibration curve ( $\lambda = 210 \text{ nm}$ ) (Fig. 34).

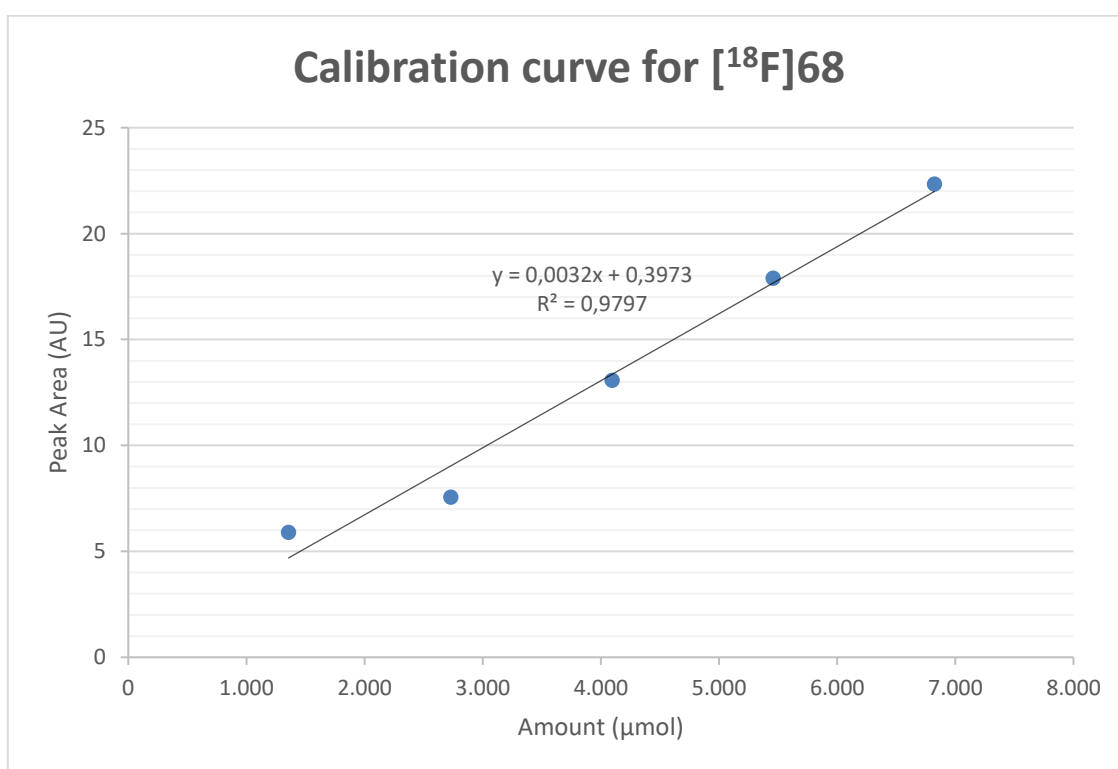


Figure 34. Carrier amount determination of [ $^{18}\text{F}$ ]68 using HPLC

Peak Area of injected (10  $\mu\text{L}$ ) 3-FPhe = 6.96 mAU.

Mass of 3-FPhe per batch: 39.8  $\mu\text{g}$ . Amount of 3-FPhe per batch: 0.22  $\mu\text{mol}$ .

### 3.18. Cu- and Ni-Content Determination

Sample	Ni		Cu	
	Mean [mg/L]	Amount per product batch (mg)	Mean [mg/L]	Amount per product batch (mg)
2-[ <sup>18</sup> F]FPhe	0.125	0.004	0.703	0.021
3-[ <sup>18</sup> F]FPhe	0.215	0.006	1.803	0.054
4-[ <sup>18</sup> F]FPhe	0.041	0.001	0.82	0.024
2-[ <sup>18</sup> F]FTyr	2.016	0.060	4.413	0.013
6-[ <sup>18</sup> F]FMT	27.4	0.082	84.6	0.2538
α-Me-2-[ <sup>18</sup> F]FPhe	0.845	0.025	1.213	0.036
α Me-3-[ <sup>18</sup> F]FPhe	9.42	0.028	15	0.045
α-Me-4-[ <sup>18</sup> F]FPhe	58.3	0.1749	124	0.372
3-[ <sup>18</sup> F]FPhe*	-	-	0.248	0.007

*Table 7. ICP-MS-Determined Cu & Ni-content of final products.*

The presence of Ni and Cu traces in the final product were determined using inductively coupled plasma mass spectrometry (ICP-MS). This analysis was carried out at the central analytical department (ZEA-3) in the Jülich research center (FZJ). The table above displays the Cu- & Ni-content in the final products (Tab. 7).

The trace metal concentrations obtained from these analyses were found to be within the acceptable range of cGMP guidelines. Therefore, the established radiosynthetic protocol furnishes <sup>18</sup>F-labeled AAAs in ready-to-use solutions, which can be directly applied for preclinical evaluation.

\*Obtained using the Bpin-substituted Cu-BPB complex **154**.

## 4. Conclusion

This work describes a general protocol for the preparation of a number of structurally diverse  $^{18}\text{F}$ -labeled AAAs by applying a combination of late-stage alcohol-enhanced Cu-mediated radiofluorination with chiral Ni or Cu complexes as precursors (Fig. 35). This protocol provides significant improvements compared to previously described AAA tracer preparations. The following objectives were realized:

1. The Bpin-substituted Ni-BPB complexes are easily accessible on a multi-gram scale from commercially available starting materials in a few synthetic steps.
2. Late-stage  $^{18}\text{F}$ -incorporation *via* alcohol-enhanced Cu-mediated radiofluorination enabled the efficient radiolabeling of Bpin-substituted Ni/Cu-BPX complexes.
3. The rapid decomposition of the intermediate radiofluorinated Ni/Cu-BPX complexes was easily achieved under acidic conditions.
4. The developed HPLC conditions employed aqueous EtOH as the mobile phase enabled the rapid isolation of the  $^{18}\text{F}$ -labeled AAAs in ready-to-use solutions in high RCYs, with very high enantiomeric and radiochemical purities.
5. Bpin-Substituted  $^{18}\text{F}$ FPheSer precursors could not be obtained *via a* simple aldol reaction of a Bpin-substituted aldehyde upon Ni-BPB complexes, owing to product instability.
6. The alcohol-enhanced Cu-mediated radiofluorination of precursor **182**, prepared *via* multi-step synthesis, enables the preparation of 3- $^{18}\text{F}$ FPheSer, as a novel tracer for the potential imaging of the noradrenergic system.
7. Bpin-Substituted Cu-BPX precursors can also be used for the preparation of  $^{18}\text{F}$ -labeled AAAs. This approach has the advantage of using a single trace metal for AAA tracer preparation.
8. The established radiochemical protocol is well-suited for implementation into an automated radiosynthesis module, thus facilitating the routine *c*GMP production of the  $^{18}\text{F}$ -labeled AAAs. Despite the successful preparation of  $^{18}\text{F}$ **68** using an automated module, a robust fully-automated protocol has yet to be established.
9. Cu-Mediated radiofluorination enables the one-step preparation of  $^{18}\text{F}$ FPBA, a prosthetic group for subsequent conjugation to biopolymers.

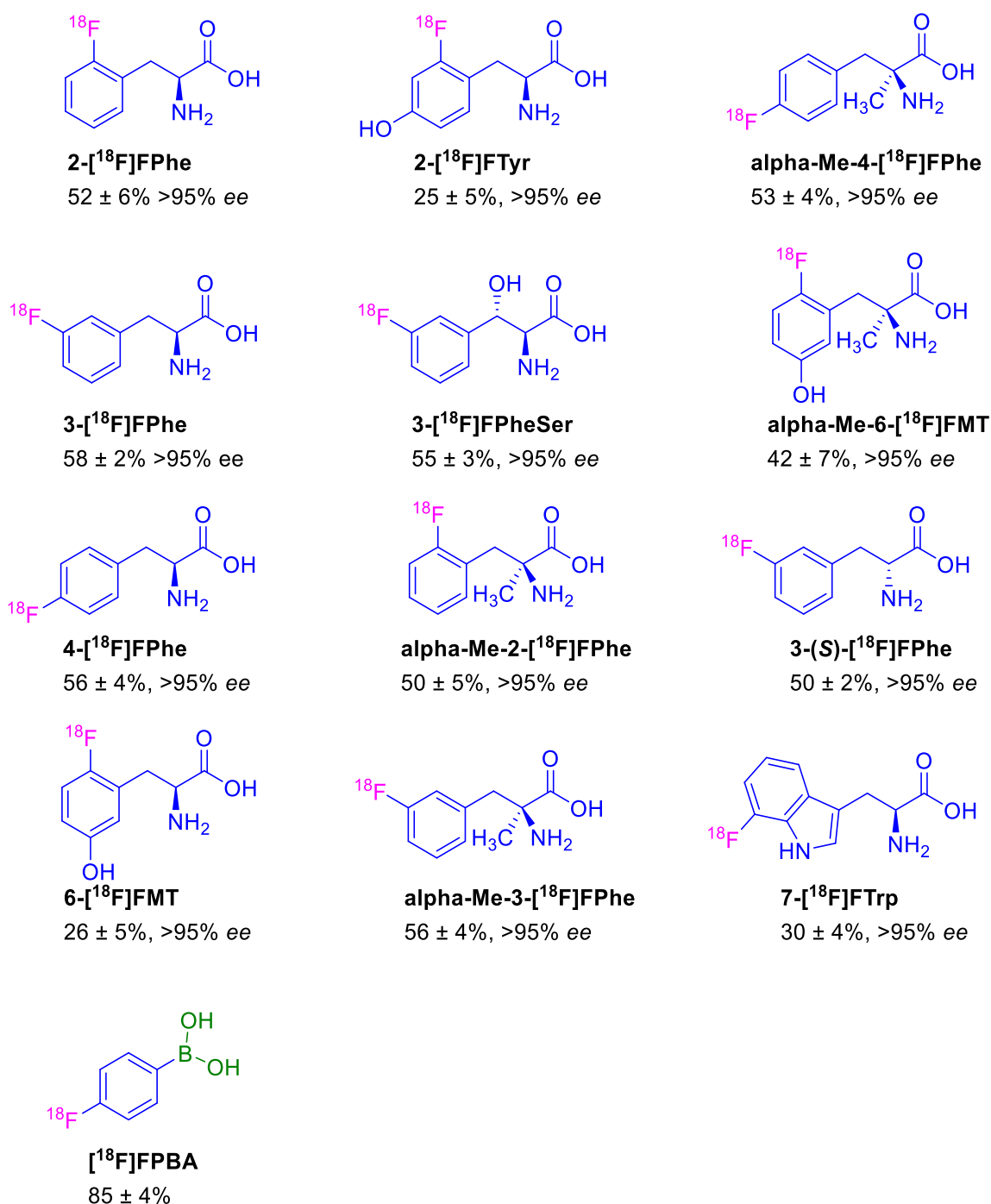


Figure 35. Overview of tracer products and prosthetic groups with their associated RCYs.

To conclude, alcohol-enhanced Cu-mediated radiofluorination of BPin-substituted Ni/Cu-BPX-AAA complexes is a powerful and practical procedure for the rapid production of structurally diverse <sup>18</sup>F-labeled AAAs. The attractiveness of the method is highlighted by the accessibility of the radiolabeling precursors in a few synthetic steps and high RCYs. The single-step preparation of the prosthetic group [<sup>18</sup>F]FPBA from a commercially available compound is a further achievement of this work.

## 5. Experimental

### 5.1. Organic Synthesis

If not otherwise stated, all chemical compounds, including reference compounds and solvents were obtained from Merck (Sigma-Aldrich, Germany), Thermo-Fisher Scientific (Alfa Aesar and Acros, Germany), Fluorochem (United Kingdom). They were used directly without prior purification. Thin-layer chromatography (TLC) experiments were carried out using pre-coated plates of silica gel 60 F254 (Merck, Darmstadt, Germany), and were analyzed under a UV lamp at 254 nm. Moisture sensitive reactions were carried out in pre-heated glassware (2 h at 140 °C) and proceeded under an argon atmosphere. All reactions were stirred magnetically, and the organic layers were dried over anhydrous  $\text{MgSO}_4$ .  $^1\text{H}$  NMR spectra were collected applying a Bruker Avance II 300 (Bruker Corporation, MA, USA) (300 MHz), Bruker Avance (600 MHz), Bruker Avance 200 (200 MHz), or Varian Inova (400 MHz) spectrometer using  $\text{CDCl}_3$  or  $(\text{CD}_3)_2\text{SO}$  as a solvent.  $^1\text{H}$  and  $^{13}\text{C}$  chemical shifts are reported in ppm relative to residual peaks of deuterated solvents. Higher-order NMR spectra were approximately interpreted as first-order spectra, if possible. The observed signal multiplicities are characterized as follows: s = singlet, d = doublet, t = triplet, q = quartet, quin = quintet, m = multiplet, and br = broad. Coupling constants ( $J$ ) were reported in hertz (Hz).  $^{13}\text{C}$  NMR spectra [additional APT (Attached Proton Test)] were collected via Bruker Avance II 300 (75.5 MHz), Varian Inova (101 MHz), Bruker Avance 200 (50.3 MHz), and Bruker Avance II 600 (125.9 MHz).  $^{19}\text{F}$  spectra were collected applying a Bruker Avance II 300 and Bruker Avance II 600 (376 MHz). All chemical shifts ( $\delta$ , ppm) are provided with respect to the residual deuterated solvent peaks. Low-resolution electron spray ionization mass spectrometry [LRMS (ESI)] analyses of compounds were obtained using a LTQ Orbitrap XL (Thermo Fisher Scientific, Bremen, Germany). High-resolution electron spray ionization mass spectrometry [HRMS (ESI)] analyses of compounds were obtained using a Fourier-transform ion-cyclotron resonance LTQ FT Ultra (Thermo Fisher Scientific, Bremen, Germany). Low resolution electron impact ionization mass spectrometry gas chromatography (LRMS/GC) analyses were carried out using a ISQ GCMS system (Thermo Fisher Scientific, Bremen, Germany) equipped with ISQ (single quadrupole massspectrometer) and Trace 1310 (GC-chromatograph) under following conditions: ionization potential: 70 eV; detecting ion polarity: positive; scan:  $m/z$  50–500; GC column: Optima 5 Accent 30  $m \times 0.25$  mm ID  $\times 0.25$   $\mu\text{m}$  FD (Macherey-Nagel, Düren, Germany), temperature gradient (°C): 0–5 min: 70; 5–10 min: 70→270; 10–15 min: 270; GC injector + transfer line: isotherm 300 °C; flow rate (carrier gas): 1.2 mL/min (He, splitting: 1:10). High resolution

electron impact ionization mass spectrometry gas chromatography (HRMS/GC) analyses were carried out using a Exactive GC system (Thermo Fisher Scientific, Bremen, Germany) equipped with Orbitrap mass analyzer, Trace 1310 (GC-chromatograph) and TriPlus (RSH autoinjector) under following conditions: ionization potential: 70 eV; detecting ion polarity: positive; ion source temperature: 250 °C; resolution: 60000; scan:  $m/z$  50–500; GC column: TraceGold-5 SIL MS 30 m×0.25 mm ID×0.25  $\mu$ m FD (Thermo Fisher Scientific, Bremen, Germany), temperature gradient (°C): 0–1 min: 40; 1–17 min: 40→280; 17–22 min: 280; GC injector + transfer line: isotherm 300 °C; flow rate (carrier gas): 1 mL/min (He, split: 1:20). Elemental analysis (C, H): Vario MICRO Cube (Elementar Analysensysteme GmbH, Langenselbold, Germany). Elemental analysis (C, H, O): Vario EL Cube (Elementar Analysensysteme GmbH, Langenselbold, Germany); analyses were carried out in triplicate.

The C-Bpin signal was unobservable in the  $^{13}\text{C}$  NMR spectra.

The preparation of the MOMCl solution (2.1 M, 18% w/w, 0.91 g/mL) in toluene was carried out according to the protocol described by Berliner *et al.*<sup>116</sup>

The compounds relevant to this work prepared by either Niklas Kolks or Elizaveta Urusova are shown in Fig 36.

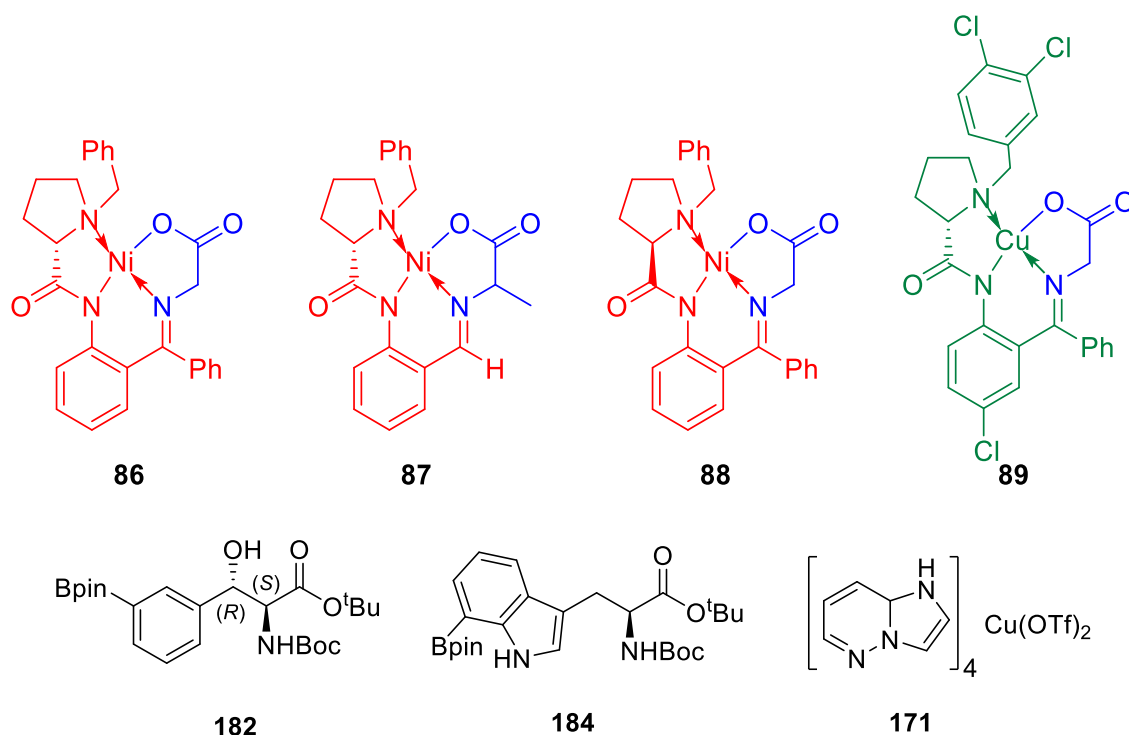


Fig 36. Compounds prepared by Niklas Kolks or Elizaveta Urusova.

#### 5.1.1. General Procedure for Alkylation Upon Ni/Cu-BPA-Gly or Ala (GP1)

NaH (60% suspension in mineral oil) (1.6 equiv) was added in small portions to a solution of Cu/Ni-(*S*)-BPA-Gly or -Ala (1 equiv) and the *corresponding alkylating agent* (1.6 equiv) in DMF/MeCN (1:2) at 0 °C and the reaction mixture was stirred at 0 °C for 20 min and thereafter, stirred at room temperature for an additional 2 hours. The reaction mixture was poured into an ice-cold 0.5 M pH 5.5 sodium phosphate buffer (10 mL), the resulting emulsion was extracted thrice with EtOAc, and washed thrice with brine. The organic fraction was dried and concentrated under reduced pressure to give a red residue, which was purified by column chromatography on silica gel using a gradient elution of acetone/CHCl<sub>3</sub> to afford the crude product which was further purified by chromatography on C18 silica gel using gradient elution with aqueous MeCN and, finally, triturated with EtOAc/hexane to yield green Cu-BPB-AA or red Ni-BPA-AA solid, respectively.

#### 5.1.2. General Procedure for Aldol Upon (*S*)-Ni-BPB-Gly (GP2)

NaH (60% suspension in mineral oil) (1.6 equiv) was added in small portions to a solution of Ni-(*S*)-BPA-Gly (1 equiv) and the *corresponding aldehyde* (1.6 equiv) in DMF/MeCN (1:2) at 0 °C and the reaction mixture was stirred at 0 °C for 20 min and thereafter, stirred at room temperature for an additional 2 hours. The reaction mixture was poured into an ice-cold 0.5 M pH 5.5 sodium phosphate buffer (10 mL), the resulting emulsion was extracted thrice with EtOAc, and washed thrice with brine. The organic fraction was dried and concentrated under reduced pressure to give a red residue, which was purified by column chromatography on silica gel using a gradient elution of acetone/CHCl<sub>3</sub> to afford the crude product which was further purified by chromatography on C18 silica gel using gradient elution with aqueous MeCN and, finally, triturated with EtOAc/hexane to yield red Ni-BPA-AAA solid.

#### 5.1.3. General Procedure for Radical Bromination (GP3)

A solution of the *corresponding toluene* (1 equiv), NBS (1.1 equiv), and AIBN (0.1 equiv) in cyclohexane (40 mL) was stirred under Ar under irradiation with a light source (550 W) in a quartz reaction vessel for 3 hours. The reaction mixture was filtered, and the filter cake was washed with hexane. The organic extract was dried and concentrated under reduced pressure to give a yellow oil, which was purified by column chromatography on silica gel using a gradient elution of EtOAc/hexane to give the desired product.

#### 5.1.4. General Procedure for Suzuki-Miyaura Borylation (GP4)

A suspension of KOAc (3 equiv), the *corresponding aryl halide* (1 equiv), B<sub>2</sub>pin<sub>2</sub> (1.5 equiv), and Pd(dppf)Cl<sub>2</sub>·CH<sub>2</sub>Cl<sub>2</sub> (0.1 equiv) in anhydrous DMF (30–40 mL) was stirred at 70 °C under Ar for 6 h. The resulting emulsion was cooled to ambient temperature and added to H<sub>2</sub>O (40 mL) before being extracted with EtOAc (4 × 30 mL). The combined organic fractions were washed with H<sub>2</sub>O (4 × 30 mL), brine (4 × 30 mL), dried, and concentrated under reduced pressure to give the crude product which was further purified by column chromatography to yield the desired product.

#### 5.1.5. General Procedure for MOM-Protection (GP5)

A solution of 2.1 M MOMCl solution in toluene (10 mL) prepared according to a literary procedure<sup>116</sup> was slowly added to a stirred ice-cold solution of the *corresponding phenol* (68.4 mmol) and DIPEA (10 mL, 7.42 g, 57.4 mmol) in anhydrous CH<sub>2</sub>Cl<sub>2</sub> (40 mL) under Ar. Thereafter, the cooling bath was removed, and the reaction mixture was stirred for 24 hours. The reaction mixture was washed with H<sub>2</sub>O (3 × 30 mL), brine (3 × 30 mL), dried, and concentrated under reduced pressure. The crude orange residue was purified by column chromatography (EtOAc/hexane, gradient elution 10–40%), affording the desired product.

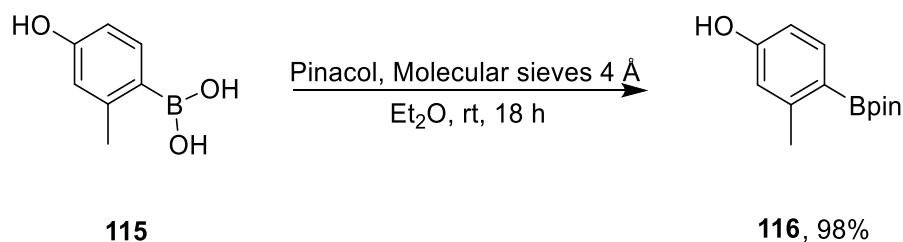
#### 5.1.6. General Procedure for Stannylation (GP6)

Hexamethyldistannane (2 equiv) and the *corresponding arene* (1 equiv) were stirred under Ar for 20 minutes. Di(chlorobis(diphenyl phosphine butane) palladium (II) (0.1 equiv) was added, and the mixture was stirred at reflux until the starting material was completely consumed in the reaction (ca. 24 h). The reaction mixture was cooled to room temperature, filtered through Celite<sup>®</sup>, and concentrated under reduced pressure. The crude product residue was redissolved in EtOAc and purified by column chromatography (CH<sub>2</sub>Cl<sub>2</sub>/cyclohexane, gradient elution 80–50% and 0.5% acetic acid) to afford the desired product.

#### 5.1.7. General Procedure for Iodination (GP7)

A solution of iodine (1 equiv) in ethanol (50 mL) was added dropwise to a stirred solution of the *corresponding arene* (1 equiv) and Ag<sub>2</sub>SO<sub>4</sub> (1 equiv) in ethanol (80 mL) at 0 °C. The black reaction mixture was allowed to come to room temperature before being stirred for 18 hours. The resulting green reaction mixture was filtered through Celite<sup>®</sup>, washed with ethanol (3 × 20 mL), and the combined fractions were poured slowly into a saturated sodium bicarbonate solution (40 mL). The organic fractions were washed with water (3 × 30 mL), brine (2 × 30 mL), and dried over anhydrous MgSO<sub>4</sub>. The dried solution was concentrated under vacuum and purified by silica gel column chromatography to afford the desired product.

**4,4,5,5-Tetramethyl-2-(2-methyl-4-hydroxyphenyl)-1,3,2-dioxaborolane (116)**



Following a literature procedure,<sup>46</sup> a suspension of molecular sieves (4 Å) (7 g) in a solution of (2-methyl-4-hydroxyphenyl)boronic acid (**115**, 5.00 g, 33.0 mmol), and pinacol (4.14 g, 35.0 mmol) in anhydrous Et<sub>2</sub>O (100 mL) was stirred under Ar at ambient temperature for 18 hours. The reaction mixture was filtered, and the filter cake was washed with Et<sub>2</sub>O. The filtrate was dried and concentrated under reduced pressure to give an oily residue, which was purified by column chromatography using gradient elution with EtOAc/hexane affording the *title compound* in 98% yield (7.61 g, 32.5 mmol) as a colorless oil.

R<sub>f</sub> 0.62, (1:10 EtOAc/hexane).

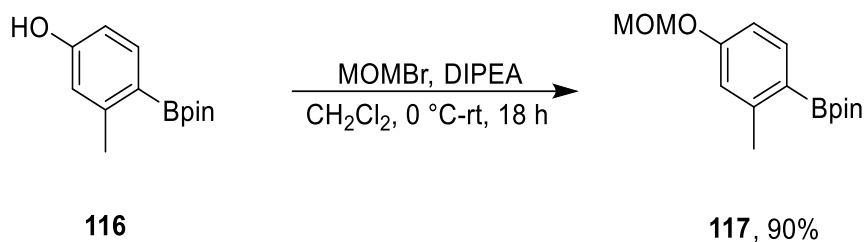
<sup>1</sup>H NMR (400 MHz, CDCl<sub>3</sub>) δ 7.68 (t, *J* = 9.9 Hz, 1H), 6.66 – 6.58 (m, 2H), 5.24 (s, 1H), 2.49 (s, 3H), 1.33 (s, 12H).

<sup>13</sup>C NMR (101 MHz, CDCl<sub>3</sub>) δ 157.80, 147.57, 138.02, 116.78, 111.83, 83.25, 24.82, 22.17. C-Bpin was not observed.

HRMS/GC: *R*<sub>t</sub> 12.90 min, C<sub>13</sub>H<sub>19</sub>O<sub>3</sub>B<sup>+</sup>, [M]<sup>+</sup> calcd. 234.1422, observed 234.1421; correct isotopic pattern.

Elemental analysis calcd (%) for C<sub>13</sub>H<sub>19</sub>O<sub>3</sub>B (234.4): C 66.70, H 8.18; found C 66.69, H 8.17.

**2-(4-(Methoxymethoxy)-2-methylphenyl)-4,4,5,5-tetramethyl-1,3,2-dioxaborolane (117)**



MOMBr (0.7 mL, 1.07 g, 8.56 mmol) was slowly added to a stirred ice-cold solution of 4,4,5,5-tetramethyl-2-(2-methyl-4-hydroxyphenyl)-1,3,2-dioxaborolane (**116**) (1.00 g, 4.27 mmol) and DIPEA (1.49 mL, 1.11 g, 8.55 mmol) in anhydrous CH<sub>2</sub>Cl<sub>2</sub> (40 mL) under Ar. Thereafter, the cooling bath was removed, and the reaction mixture was stirred for 18 hours. The reaction mixture was washed with H<sub>2</sub>O (2 × 30 mL) and washed with brine (2 × 30 mL). The organic fraction was and concentrated under reduced pressure to give an oily brown residue, which was purified by column chromatography using gradient elution with EtOAc/hexane (0–20%) affording the *title compound* in 90% yield (1.07 g, 3.85 mmol) as a yellow oil.

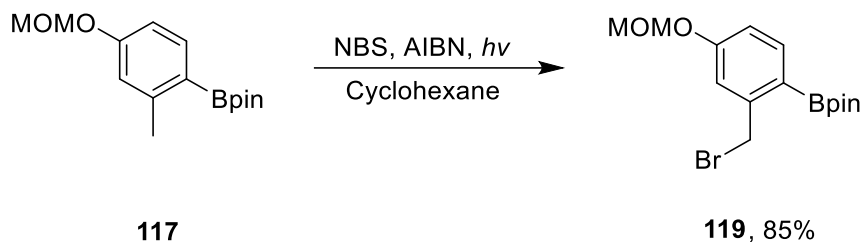
R<sub>f</sub> 0.31, (1:20 EtOAc/hexane).

<sup>1</sup>H NMR (300 MHz, CDCl<sub>3</sub>) δ 7.75 (d, *J* = 9.0 Hz, 1H), 6.90 – 6.82 (m, 2H), 5.21 (s, 2H), 3.49 (s, 3H), 2.56 (s, 3H), 1.36 (s, 12H).

<sup>13</sup>C NMR (101 MHz, CDCl<sub>3</sub>) δ 159.27, 147.27, 137.75, 117.41, 112.32, 93.96, 83.18, 55.98, 24.88, 22.38.

HRMS (ESI) *m/z* (M + Na)<sup>+</sup>, C<sub>13</sub>H<sub>19</sub>BO<sub>3</sub>Na<sup>+</sup> calcd. 301.1582, observed 301.1584; correct isotopic pattern.

**2-(4-(Methoxymethoxy)-2-bromomethylphenyl)-4,4,5,5-tetramethyl-1,3,2-dioxaborolane (118)**



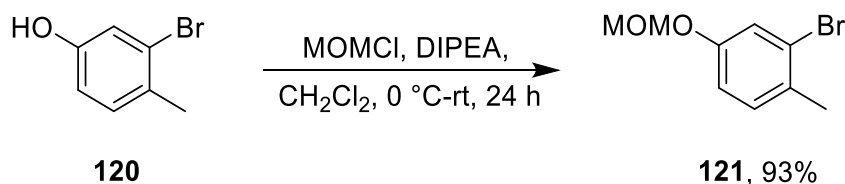
The above compound (**118**) was prepared according to GP3 whereby, **117** (4.00 g, 14.3 mmol), NBS (2.55 g, 14.3 mmol), AIBN (0.40 g, 2.44 mmol) and cyclohexane (40 mL) were utilized. Yield: 85% (4.36 g, 1.70 mmol). **118** was directly introduced to the next step owing to its instability.

$R_f$  0.14, (1:10 EtOAc/hexane).

$^1\text{H}$  NMR (200 MHz,  $\text{CDCl}_3$ )  $\delta$  7.77 (d,  $J$  = 8.3 Hz, 1H), 7.07 (d,  $J$  = 2.4 Hz, 1H), 6.96 (dd,  $J$  = 8.3, 2.4 Hz, 1H), 5.20 (s, 2H), 4.89 (s, 2H), 3.47 (s, 3H), 1.36 (s, 12H).

$^{13}\text{C}$  NMR (50 MHz,  $\text{CDCl}_3$ )  $\delta$  159.56, 146.36, 138.31, 117.81, 115.16, 94.12, 83.68, 56.15, 56.03, 33.75, 24.89. C-Bpin was not observed.

**2-Bromo-4-(methoxymethoxy)-1-methylbenzene (121)**



The above compound (**121**) was prepared according to GP5 whereby **120** (4.6 g, 24.6 mmol), DIPEA (10 mL), MOMCl solution (10 mL, 7.42 g, 57.4 mmol), and  $\text{CH}_2\text{Cl}_2$  (40 mL) were utilized. Yield: 93% (5.30 g, 23 mmol).

$R_f$ : 0.75, (1:2 EtOAc/hexane).

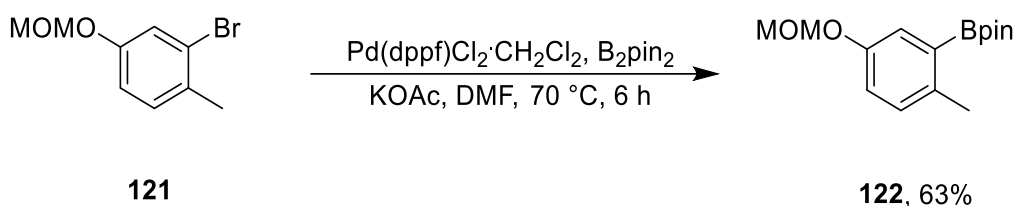
$^1\text{H}$  NMR (400 MHz,  $\text{CDCl}_3$ )  $\delta$  7.28 (d,  $J$  = 2.5 Hz, 1H), 7.15 (dd,  $J$  = 8.4, 0.5 Hz, 1H), 6.92 (dd,  $J$  = 8.4, 2.5 Hz, 1H), 5.15 (s, 1H), 3.49 (s, 1H), 2.35 (s, 1H).

$^{13}\text{C}$  NMR (101 MHz,  $\text{CDCl}_3$ )  $\delta$  155.76, 131.06, 130.97, 124.76, 120.24, 115.42, 94.65, 55.99, 21.89.

HRMS/GC:  $R_t$  12.90 min,  $C_9H_{11}BrO_2^+$ ,  $[M]^+$  calcd. 229.9937, observed 229.9935; correct isotopic pattern.

Elemental analysis calcd (%) for  $C_9H_{10}BrO_2$  (231.09): C 46.78, H 4.80, O 13.85; found C 46.7  $\pm$  < 0.1, H 4.79  $\pm$  0.17, O 14.2  $\pm$  < 0.1.

**2-(5-(Methoxymethoxy)-2-methylphenyl)-4,4,5,5-tetramethyl-1,3,2-dioxaborolane (122)**



The above compound (**122**) was prepared according to GPX whereby, **121** (0.5 g, 2.16 mmol),  $B_2pin_2$  (0.66 g, 2.6 mmol),  $Pd(dppf)Cl_2 \cdot CH_2Cl_2$  (0.1 g, 0.15 mmol), and KOAc (0.44 g, 4.54 mmol) and DMF (10 mL) were utilized. Yield: 72% (0.43 g, 1.55 mmol).

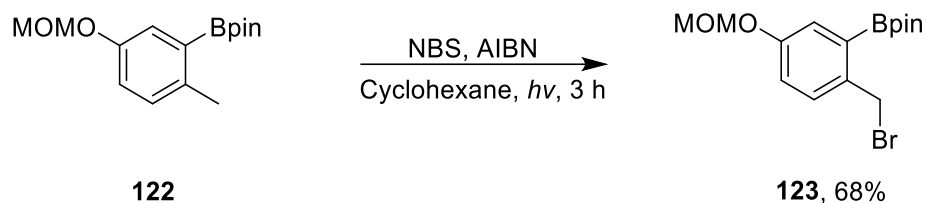
$R_f$ : 0.45, (1:10 EtOAc/hexane).

$^1H$  NMR (300 MHz,  $CDCl_3$ )  $\delta$  7.41 (d,  $J$  = 2.8 Hz, 1H), 7.09 (d,  $J$  = 8.3 Hz, 1H), 7.01 (dd,  $J$  = 8.3, 2.8 Hz, 1H), 5.17 (s, 2H), 3.48 (s, 3H), 2.48 (s, 3H), 1.34 (s, 12H).

$^{13}C$  NMR (101 MHz,  $CDCl_3$ )  $\delta$  154.38, 138.18, 130.85, 123.27, 118.84, 94.58, 83.47, 77.00, 55.87, 24.86, 21.23.

HRMS (ESI)  $m/z$  ( $M + Na$ ) $^+$ ,  $C_{15}H_{23}O_4BNa^+$  calcd. 301.1582, observed 301.1584; correct isotopic pattern.

**2-(2-(Bromomethyl)-5-(methoxymethoxy)phenyl)-4,4,5,5-tetramethyl-1,3,2-dioxaborolane (**123**)**

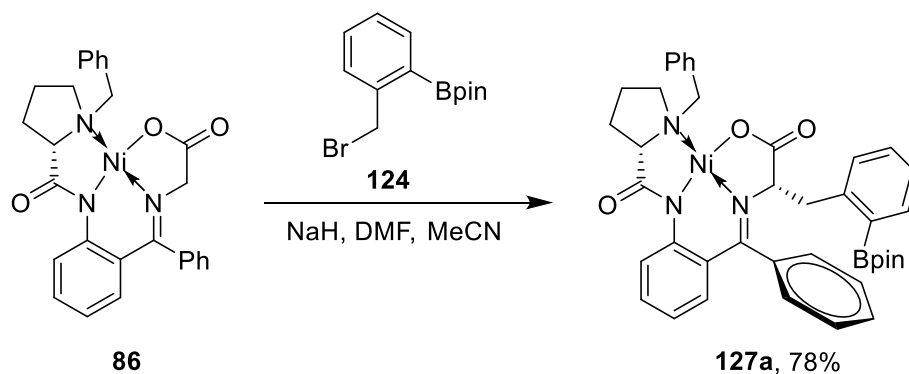


The above compound (**123**) was prepared according to GP3 whereby, **122** (0.62 g, 2.25 mmol), NBS (0.40 g, 2.45 mmol), AIBN (44 mg, 0.245 mmol) and cyclohexane (40 mL) were utilized. Yield: 68% (0.55 g, 1.54 mmol). **123** was directly introduced to the next step owing to its instability.

R<sub>f</sub>: 0.60, (1:3 EtOAc/hexane).

<sup>1</sup>H NMR (300 MHz, CDCl<sub>3</sub>)  $\delta$  7.49 (dd,  $J$  = 9.9, 2.6 Hz, 1H), 7.17 – 7.02 (m, 2H), 5.20 (d,  $J$  = 6.0 Hz, 2H), 3.50 (s, 3H), 2.53 (s, 2H), 1.37, 1.39 (2 $\times$ s, 12H).

**(*S,S*)-Ni-BPB-2-BpinPhe (127a)**



The above compound (**127a**) was prepared according to GP1 whereby, **86** (0.52 g, 1.05 mmol), **124** (0.5 g, 16.8 mmol), NaH (60% suspension in mineral oil) (70 mg, 16.8 mmol) and DMF/MeCN 1:2 (30 mL) were utilized. Yield: 78% (0.59 g, 0.82 mmol).

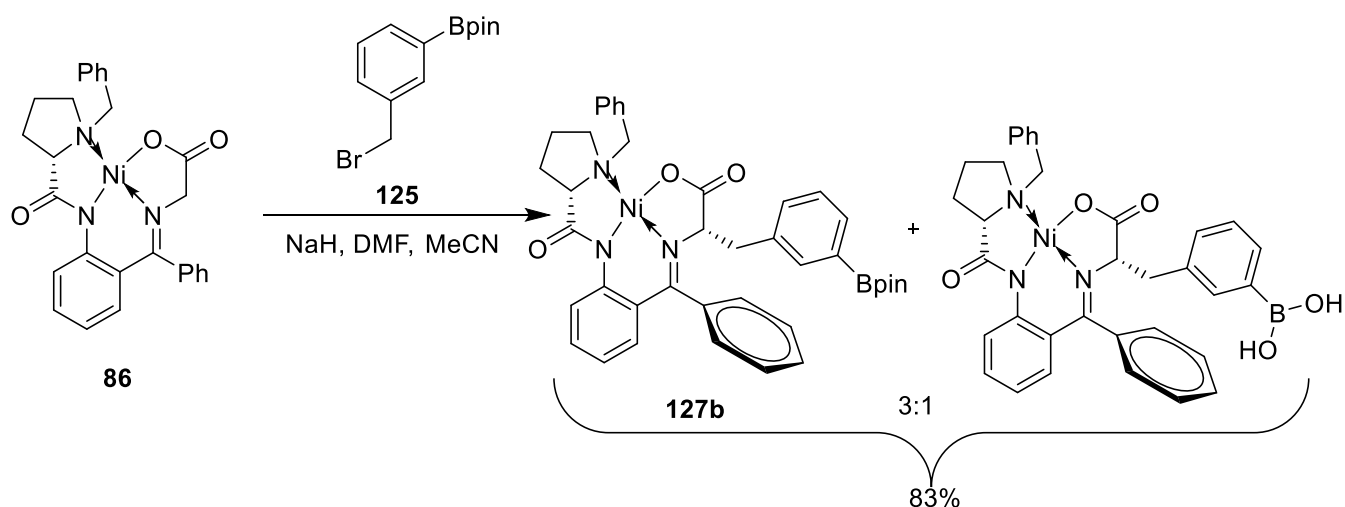
R<sub>f</sub> 0.42, (1:20 acetone/CHCl<sub>3</sub>).

<sup>1</sup>H NMR (300 MHz, CDCl<sub>3</sub>) δ 8.32 (d, *J* = 13.2 Hz, 1H), 8.05 (d, *J* = 7.3 Hz, 2H), 7.89 – 7.76 (m, 1H), 7.55 – 7.21 (m, 8H), 7.19 – 7.00 (m, 3H), 6.60 (t, *J* = 7.6 Hz, 1H), 6.54 – 6.47 (m, 1H), 5.95 (d, *J* = 7.6 Hz, 1H), 4.36 (d, *J* = 12.6 Hz, 1H), 4.27 (t, *J* = 5.9 Hz, 1H), 3.87 (d, *J* = 5.9 Hz, 2H), 3.55 – 3.35 (m, 2H), 3.32 – 3.04 (m, 2H), 2.84 – 2.66 (m, 1H), 2.62 – 2.44 (m, 1H), 2.15 – 1.86 (m, 2H), 1.19 (s, 6H), 1.11 (s, 6H).

<sup>13</sup>C NMR (75 MHz, CDCl<sub>3</sub>) δ 180.34, 178.47, 170.73, 142.74, 142.50, 136.92, 134.00, 133.72, 133.34, 132.05, 131.47, 131.36, 131.09, 129.01, 128.76, 128.70, 128.56, 128.35, 127.90, 127.32, 126.44, 126.18, 123.05, 120.38, 83.64, 72.96, 70.80, 62.99, 57.13, 42.35, 31.06, 24.94, 24.34, 23.80. C-Bpin was not observed. Pairs of methyl groups of the Bpin residue were inequivalent. *o*- and *m*-Carbons of the phenyl group of the [(2-amido)phenyl]phenylmethanimine fragment were inequivalent.

HRMS (ESI) *m/z* (M + H)<sup>+</sup>, C<sub>40</sub>H<sub>43</sub>N<sub>3</sub>O<sub>5</sub>NiB<sup>+</sup> calcd. 714.2644, observed 714.2642; correct isotopic pattern.

**(*S,S*)-Ni-BPB-3-BpinPhe (127b)**



The above compound (**127b**) was prepared according to GP1 whereby, **86** (0.78 g, 1.56 mmol), **125** (0.65 g, 2.20 mmol), NaH (60% suspension in mineral oil) (100 mg, 2.50 mmol) and DMF/MeCN 1:2 (10 mL) were utilized. Yield: 83% (0.90 g; total yield of **159b** and the corresponding boronic acid). In this instance partial hydrolysis of the pinacol moiety proceeding reversed-phase purification was observable in the  $^1\text{H}$  NMR spectrum. As boronic acids are typically even better substrates for the alcohol-enhanced Cu-mediated radiofluorination than the corresponding Bpin esters, no attempt to separate it (or to convert it back into the Bpin ester) was made and the mixture was directly used for the radiolabeling step. Omission of the RP purification step could lead to lower  $^{18}\text{F}$ -incorporation rates.

$R_f$  0.42, (1:20 acetone/ $\text{CHCl}_3$ ).

$^1\text{H}$  NMR (400 MHz,  $\text{CDCl}_3$ ; before RP purification)  $\delta$  8.33 (d,  $J = 8.7$  Hz, 1H), 8.02 (d,  $J = 7.4$  Hz, 2H), 7.82 (d,  $J = 7.4$  Hz, 1H), 7.61 (s, 1H), 7.59 – 7.47 (m, 2H), 7.45 – 7.37 (m, 2H), 7.35 – 7.22 (m, 4H), 7.20 – 7.12 (m, 2H), 6.81 (d,  $J = 7.4$  Hz, 1H), 6.68 (d,  $J = 3.9$  Hz, 2H), 4.32 (d,  $J = 13.5$  Hz, 1H), 4.26 (dt,  $J = 13.5, 7.2$  Hz, 1H), 3.48 (d,  $J = 12.7$  Hz, 1H), 3.30 (dd,  $J = 9.6, 7.6$  Hz, 1H), 3.20 (dd,  $J = 13.7, 4.6$  Hz, 1H), 3.16 – 3.09 (m, 1H), 2.95 (dd,  $J = 13.7, 6.0$  Hz, 1H), 2.60 – 2.42 (m, 1H), 2.40 – 2.26 (m, 2H), 2.02 – 1.90 (m, 1H), 1.83 – 1.71 (m, 1H), 1.31 (s, 6H), 1.29 (s, 6H).

$^{13}\text{C}$  NMR (101 MHz,  $\text{CDCl}_3$ ; before RP purification)  $\delta$  180.30, 178.60, 171.11, 143.02, 136.82, 135.08, 134.14, 133.71, 133.50, 133.29, 133.18, 132.24, 131.54, 129.67, 128.98, 128.86, 128.76, 128.73, 128.15, 127.91, 127.17, 126.00, 123.40, 120.40, 83.82, 71.51, 70.33, 63.13, 57.15, 40.15, 30.74, 24.86, 24.77, 23.28. C-Bpin was not observed. Pairs of methyl groups of

HRMS (ESI)  $m/z$  ( $M + H$ )<sup>+</sup>, C<sub>40</sub>H<sub>42</sub>N<sub>3</sub>O<sub>5</sub>NiB<sup>+</sup> calcd. 714.2644, observed 714.2643; correct isotopic pattern.

Reaction scheme showing the synthesis of **127c** from **86** and **126**.

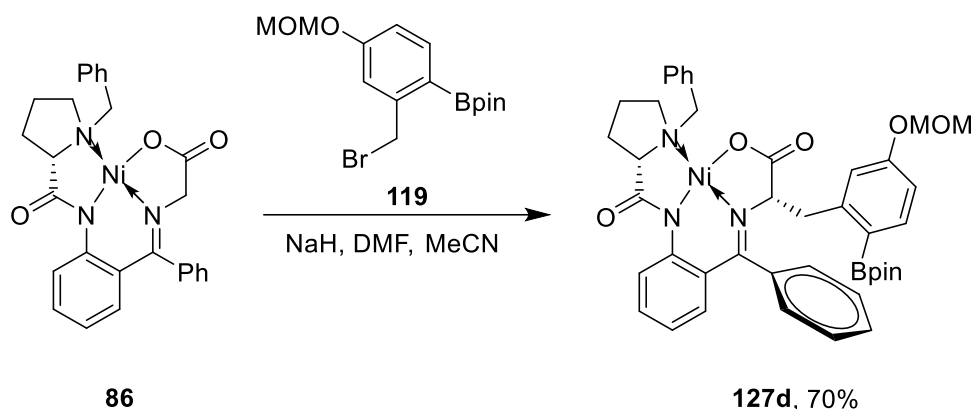
Reactant **86** (a nickel complex) reacts with **126** (4-(bromomethyl)phenylboronic pinacol ester) in the presence of  $\text{NaH}$ ,  $\text{DMF}$ , and  $\text{MeCN}$  to form **127c** (85% yield).

R<sub>f</sub> 0.42, (1:20 acetone/CHCl<sub>3</sub>).

<sup>13</sup>C NMR (101 MHz, CDCl<sub>3</sub>) δ 180.42, 178.65, 171.23, 142.94, 138.91, 135.32, 134.19, 133.50, 133.14, 132.37, 131.54, 130.00, 129.80, 129.12, 128.95, 128.77, 128.72, 127.83, 127.12, 126.03, 123.41, 120.57, 83.78, 71.28, 70.34, 63.34, 57.41, 39.54, 30.66, 24.90, 24.67, 23.19. *C*-Bpin was not observed. Pairs of methyl groups of the Bpin residue were inequivalent. *o*- and *m*-Carbons of the phenyl group of the [(2-amido)phenyl]phenylmethanimine residue were inequivalent.

91

**(*S,S*)-Ni-BPB-2-Bpin-5-MOMO-Phe (127d)**



The above compound (**127d**) was prepared according to GP1 whereby, **86** (1.76 g, 3.53 mmol), **119** (1.89 g, 5.29 mmol), NaH (60% suspension in mineral oil) (142 mg, 3.54 mmol) and DMF/MeCN 1:2 (30 mL) were utilized. Yield: 70% (1.90 g, 2.46 mmol).

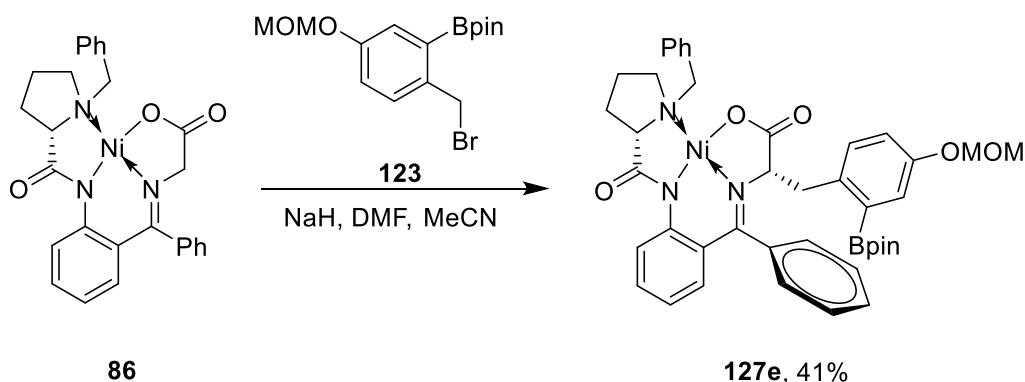
R<sub>f</sub> 0.34, (1:8 acetone/CHCl<sub>3</sub>).

<sup>1</sup>H NMR (400 MHz, CDCl<sub>3</sub>) δ 8.39 (dd, *J* = 8.7, 1.0 Hz, 1H), 8.06 (d, *J* = 7.0 Hz, 2H), 7.74 (t, *J* = 10.1 Hz, 1H), 7.51 – 7.29 (m, 4H), 7.21 (d, *J* = 2.0 Hz, 1H), 7.19 – 7.04 (m, 4H), 6.92 (dd, *J* = 8.3, 2.4 Hz, 1H), 6.59 (ddd, *J* = 8.2, 7.0, 1.0 Hz, 1H), 6.51 (dd, *J* = 8.2, 2.0 Hz, 1H), 5.93 (d, *J* = 7.7 Hz, 1H), 4.93 (dd, *J* = 34.0, 6.8 Hz, 2H), 4.38 (d, *J* = 12.6 Hz, 1H), 4.25 (dd, *J* = 7.6, 4.8 Hz, 1H), 4.01 – 3.82 (m, 2H), 3.51 (d, *J* = 12.7 Hz, 1H), 3.41 (dd, *J* = 10.5, 6.8 Hz, 1H), 3.37 – 3.23 (m, 2H), 3.21 (s, 3H), 2.93 – 2.73 (m, 1H), 2.62 – 2.45 (m, 1H), 2.18 – 1.92 (m, 2H), 1.18 (s, 6H), 1.10 (s, 6H).

<sup>13</sup>C NMR (101 MHz, CDCl<sub>3</sub>) δ 180.22, 178.49, 170.62, 159.22, 144.59, 142.92, 138.38, 133.96, 133.74, 133.36, 132.03, 131.51, 129.09, 128.78, 128.69, 128.54, 128.27, 128.16, 126.12, 123.14, 120.25, 118.62, 114.73, 93.88, 83.41, 72.74, 70.83, 62.92, 57.13, 55.87, 42.60, 30.81, 24.89, 24.42, 23.88. C-Bpin was not observed. Pairs of methyl groups of the Bpin residue were inequivalent. *o*- and *m*-Carbons of the phenyl group of the [(2-amido)phenyl]phenylmethanimine residue were inequivalent.

HRMS (ESI) *m/z* (*M* + *H*)<sup>+</sup>, C<sub>42</sub>H<sub>47</sub>N<sub>3</sub>O<sub>7</sub>NiB<sup>+</sup> calcd. 774.2856, observed 774.2853; correct isotopic pattern.

**(*S,S*)-Ni-BPB-2-Bpin-4-MOMO-Phe (127e)**



The above compound (**127e**) was prepared according to GP1 whereby, **86** (0.58 g, 1.16 mmol), **123** (0.5 g, 1.40 mmol), NaH (60% suspension in mineral oil) (56 mg, 1.40 mmol) and DMF/MeCN 1:2 (15 mL) were utilized. Yield: 41% (0.37 g, 0.51 mmol).

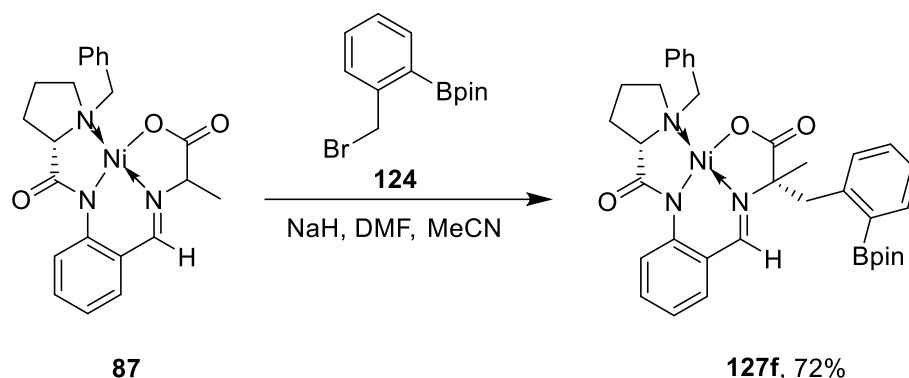
R<sub>f</sub> 0.71, (1:10 acetone/ CHCl<sub>3</sub>).

<sup>1</sup>H NMR (400 MHz, CDCl<sub>3</sub>) δ 8.36 (d, *J* = 8.5 Hz, 1H), 8.03 (d, *J* = 7.2 Hz, 2H), 7.72 (d, *J* = 8.2 Hz, 1H), 7.47 – 7.27 (m, 4H), 7.23 – 6.99 (m, 5H), 6.90 (d, *J* = 7.0 Hz, 1H), 6.57 (t, *J* = 7.2 Hz, 1H), 6.48 (d, *J* = 7.8 Hz, 1H), 5.90 (d, *J* = 6.9 Hz, 1H), 4.91 (dd, *J* = 32.9, 6.6 Hz, 2H), 4.35 (d, *J* = 12.6 Hz, 1H), 4.28 – 4.19 (m, 1H), 3.96 – 3.78 (m, *J* = 20.8 Hz, 2H), 3.48 (d, *J* = 12.7 Hz, 1H), 3.44 – 3.36 (m, 1H), 3.34 – 3.23 (m, 2H), 3.18 (s, 3H), 2.89 – 2.71 (m, 1H), 2.59 – 2.41 (m, 1H), 2.14 – 1.92 (m, 2H), 1.15 (s, 6H), 1.08 (s, 6H).

<sup>13</sup>C NMR (101 MHz, CDCl<sub>3</sub>) δ 180.19, 178.49, 170.61, 159.21, 144.55, 142.84, 138.36, 133.91, 133.72, 133.34, 132.00, 131.48, 129.07, 128.75, 128.67, 128.52, 128.25, 128.13, 127.33, 126.10, 123.12, 120.27, 118.59, 114.71, 93.85, 83.38, 72.71, 70.80, 62.90, 57.12, 55.84, 42.56, 30.79, 24.86, 24.39, 23.85. *C*-Bpin was not observed. Pairs of methyl groups of the Bpin residue were inequivalent. *o*- and *m*-Carbons of the phenyl group of the [(2-amido)phenyl]phenylmethanimine fragment were inequivalent.

HRMS (ESI) *m/z* (*M* + *H*)<sup>+</sup>, C<sub>42</sub>H<sub>46</sub>N<sub>3</sub>O<sub>7</sub>NiB<sup>+</sup> calcd. 774.2856, observed 774.2853; correct isotopic pattern.

**(*S,S*)-Ni-BPA-2-BpinPhe (127f)**



The above compound (**127f**) was prepared according to GP1 whereby, **87** (0.40, 0.92 mmol), **124** (0.44 g, 1.48 mmol), NaH (60% suspension in mineral oil) (70 mg, 1.75 mmol) and DMF/MeCN 1:2 (10 mL) were utilized. Yield: 72% (0.50 g, 0.77 mmol).

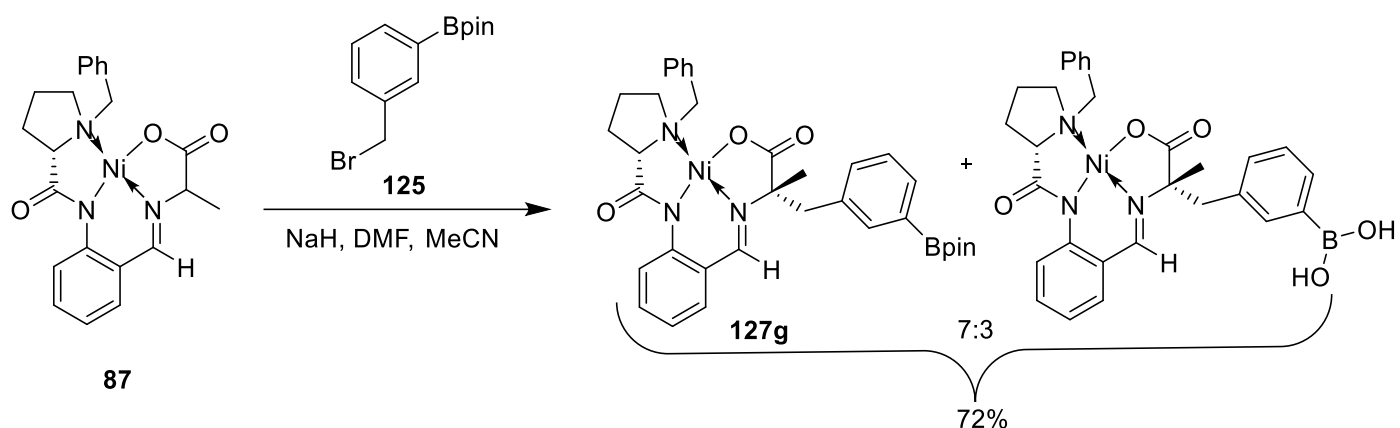
R<sub>f</sub>: 0.42, (1:10 acetone/CHCl<sub>3</sub>).

<sup>1</sup>H NMR (400 MHz, CDCl<sub>3</sub>) δ 8.49 (d, *J* = 8.7 Hz, 1H), 7.97 (d, *J* = 7.2 Hz, 2H), 7.89 (d, *J* = 7.2 Hz, 1H), 7.47 – 7.39 (m, 2H), 7.37 – 7.30 (m, 4H), 7.28 – 7.20 (m, 2H), 7.13 (dd, *J* = 7.9, 1.6 Hz, 1H), 6.92 – 6.86 (m, *J* = 7.9 Hz, 1H), 4.36 (d, *J* = 12.6 Hz, 1H), 3.73 (d, *J* = 13.4 Hz, 1H), 3.55 (dd, *J* = 13.4, 3.5 Hz, 2H), 3.43 (ddt, *J* = 14.8, 7.5, 3.5 Hz, 1H), 3.30 (t, *J* = 8.3 Hz, 1H), 2.83 – 2.67 (m, 1H), 2.36 – 2.24 (m, 2H), 2.12 – 2.00 (m, 1H), 1.91 – 1.77 (m, 1H), 1.60 (s, 3H), 1.26 (s, 6H), 1.20 (s, 6H).

<sup>13</sup>C NMR (101 MHz, CDCl<sub>3</sub>) δ 182.00, 181.45, 161.94, 142.57, 141.88, 136.84, 133.68, 133.33, 133.24, 131.65, 130.95, 130.93, 128.88, 128.68, 126.52, 123.53, 123.34, 120.88, 83.69, 74.69, 70.17, 62.92, 57.29, 44.70, 30.85, 25.65, 25.25, 24.24, 23.36. C-Bpin was not observed. Pairs of methyl groups of the Bpin residue were inequivalent.

HRMS (ESI) *m/z* (*M* + *H*)<sup>+</sup>, C<sub>35</sub>H<sub>40</sub>N<sub>3</sub>O<sub>5</sub>NiB<sup>+</sup> calcd. 652.2488, observed 652.2484; correct isotopic pattern.

**(*S,S*)-Ni-BPA-3-BpinPhe (159g)**



The above compound (**127g**) was prepared according to GP1 whereby, **87** (0.55 g, 1.26 mmol), **125** (0.50 g, 1.68 mmol), NaH (60% suspension in mineral oil) (74 mg, 1.85 mmol) and DMF/MeCN 1:2 (10 mL) were utilized. Yield: 72% (0.57 g, 0.91 mmol). RP Chromatography using aqueous MeCN and consequent evaporation of the eluent at 40 °C caused hydrolysis of Bpin ester to give the corresponding boronic acid as side product. As boronic acids are typically even better substrates for the alcohol-enhanced Cu-mediated radiofluorination than Bpin esters, no attempt to separate it (or to convert it back into the Bpin ester) was made and the mixture was directly used for the radiolabeling step. Omission of the RP purification step could lead to lower  $^{18}\text{F}$ -incorporation rates.

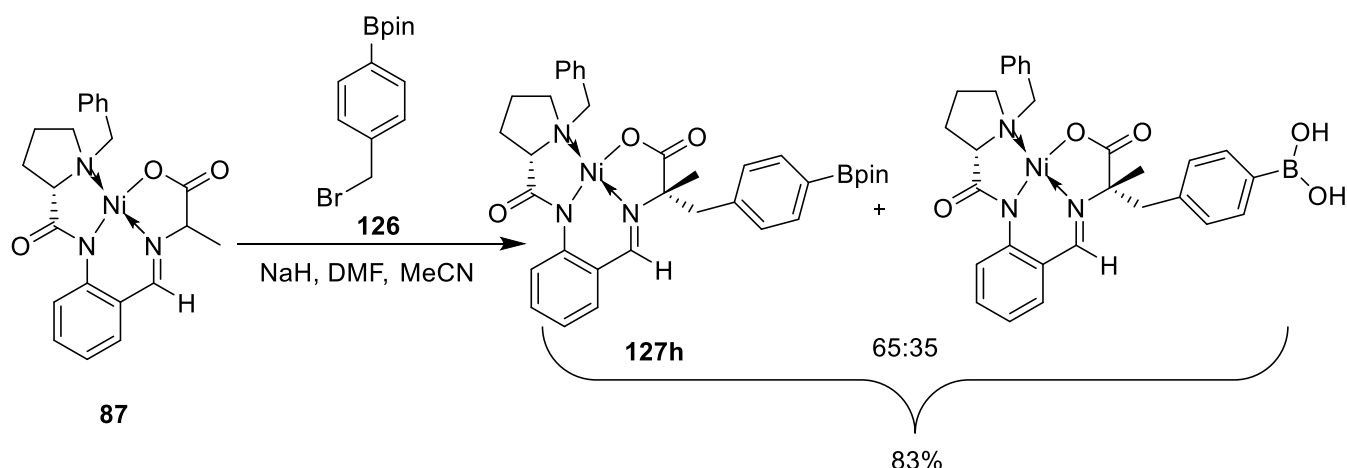
R<sub>f</sub>: 0.45, (1:10 acetone/CHCl<sub>3</sub>).

$^1\text{H}$  NMR (400 MHz, CDCl<sub>3</sub>; before RP purification)  $\delta$  8.60 (d,  $J$  = 8.7 Hz, 1H), 7.94 (d,  $J$  = 7.6 Hz, 2H), 7.80 (d,  $J$  = 6.5 Hz, 1H), 7.50 (s, 1H), 7.40 – 7.22 (m, 8H), 6.93 (t,  $J$  = 7.3 Hz, 1H), 4.33 (d,  $J$  = 12.6 Hz, 1H), 3.55 (d,  $J$  = 12.6 Hz, 1H), 3.39 (d,  $J$  = 13.3 Hz, 1H), 3.31 – 3.18 (m, 2H), 2.94 – 2.86 (m, 1H), 2.51 – 2.36 (m, 1H), 2.30 – 2.16 (m, 2H), 2.00 – 1.89 (m, 1H), 1.76 – 1.66 (m, 1H), 1.62 (s, 3H), 1.22 (s, 6H), 1.18 (s, 6H).

$^{13}\text{C}$  NMR (101 MHz, CDCl<sub>3</sub>; before RP purification)  $\delta$  181.51, 181.12, 161.19, 143.08, 137.32, 134.53, 133.88, 133.61, 133.55, 133.43, 133.08, 131.66, 128.90, 128.67, 128.09, 123.65, 123.00, 120.96, 83.75, 74.23, 70.00, 62.70, 57.11, 47.53, 30.77, 24.84, 24.80, 24.61, 23.04. C-Bpin was not observed. Pairs of methyl groups of the Bpin residue were inequivalent.

HRMS (ESI)  $m/z$  ( $\text{M} + \text{H}^+$ ), C<sub>35</sub>H<sub>40</sub>N<sub>3</sub>O<sub>5</sub>NiB<sup>+</sup> calcd. 652.2488, observed 652.2484; correct isotopic pattern.

**(*S,S*)-Ni-BPA-4-BpinPhe (**127h**)**



The above compound (**127h**) was prepared according to GP1 whereby, **87** (0.50 g, 1.15 mmol), **126** (0.55 g, 1.85 mmol), NaH (60% suspension in mineral oil) (74 mg, 1.85 mmol) and DMF/MeCN 1:2 (10 mL) were utilized. Yield: 83% (0.59 g, 0.95 mmol, total yield of **127h** and the corresponding boronic acid). RP Chromatography using aqueous MeCN and consequent evaporation of MeCN at 40 °C under reduced pressure caused partial hydrolysis of Bpin ester to give the corresponding boronic acid as side product. As boronic acids are typically even better substrates for the alcohol-enhanced Cu-mediated radiofluorination than Bpin esters, no attempt to separate it (or to convert it back into the Bpin ester) was made and the mixture was directly used for the radiolabeling step. Omission of the RP purification step could lead to substantially lower  $^{18}\text{F}$ -incorporation rates.

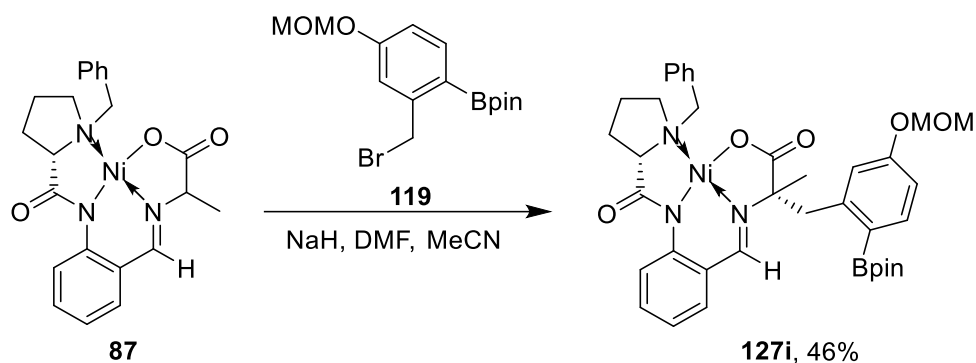
R<sub>f</sub>: 0.49, (1:10 acetone/CHCl<sub>3</sub>).

$^1\text{H}$  NMR (400 MHz, CDCl<sub>3</sub>; before RP purification)  $\delta$  8.54 (d,  $J$  = 8.6 Hz, 1H), 7.97 – 7.91 (m, 2H), 7.83 (d,  $J$  = 8.0 Hz, 2H), 7.56 (s, 1H), 7.37 – 7.26 (m, 5H), 7.16 (d,  $J$  = 8.0 Hz, 2H), 6.96 (t,  $J$  = 7.0 Hz, 1H), 4.30 (d,  $J$  = 12.7 Hz, 1H), 3.51 (d,  $J$  = 12.7 Hz, 1H), 3.39 (d,  $J$  = 13.3 Hz, 1H), 3.27 – 3.14 (m, 2H), 2.83 (d,  $J$  = 13.3 Hz, 1H), 2.27 – 2.10 (m, 3H), 2.01 – 1.89 (m, 1H), 1.64 (s, 3H), 1.62 – 1.54 (m, 1H), 1.33 (s, 12H).

$^{13}\text{C}$  NMR (101 MHz, CDCl<sub>3</sub>; before RP purification)  $\delta$  181.55, 180.88, 161.00, 142.97, 138.55, 135.08, 133.82, 133.72, 133.10, 131.63, 130.02, 128.90, 128.67, 123.70, 123.13, 121.18, 83.72, 74.52, 70.04, 62.87, 57.30, 48.05, 30.73, 25.43, 24.79, 24.72, 22.94.

HRMS (ESI)  $m/z$  ( $\text{M} + \text{H}^+$ ), C<sub>35</sub>H<sub>40</sub>N<sub>3</sub>O<sub>5</sub>NiB<sup>+</sup> calcd. 652.2488, observed 652.2485; correct isotopic pattern.

**(*S,S*)-Ni-BPA-2-Bpin-5-MOMO-Phe (127i)**



The above compound (**127i**) was prepared according to GP1 whereby, **87** (765 mg, 1.76 mmol), **119** (1.00 g, 2.81 mmol), NaH (60% suspension in mineral oil) (0.32 g, 8.0 mmol) and DMF/MeCN 1:2 (30 mL) were utilized. Yield: 46% (0.57 g, 0.80 mmol).

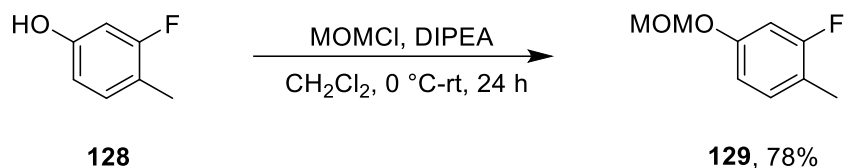
R<sub>f</sub>: 0.54, (1:8 acetone/CHCl<sub>3</sub>).

<sup>1</sup>H NMR (400 MHz, CDCl<sub>3</sub>) δ 8.52 (d, *J* = 8.6 Hz, 1H), 8.02 – 7.97 (m, 2H), 7.84 (d, *J* = 8.4 Hz, 1H), 7.35 (t, *J* = 7.5 Hz, 2H), 7.31 – 7.20 (m, 4H), 7.12 – 7.05 (m, 2H), 6.99 (dd, *J* = 8.4, 2.4 Hz, 1H), 6.91 – 6.84 (m, 1H), 5.04 (d, *J* = 0.5 Hz, 1H), 4.39 (d, *J* = 12.6 Hz, 1H), 3.75 (d, *J* = 13.6 Hz, 1H), 3.60 – 3.48 (m, 4H), 3.35 (d, *J* = 5.6 Hz, 3H), 2.98 – 2.82 (m, 1H), 2.78 (s, 2H), 2.35 (ddd, *J* = 18.8, 12.0, 6.8 Hz, 2H), 2.15 – 2.05 (m, 1H), 1.95 – 1.83 (m, 1H), 1.73 (s, 2H), 1.59 (s, 3H), 1.23 (t, *J* = 14.8 Hz, 12H).

<sup>13</sup>C NMR (101 MHz, CDCl<sub>3</sub>) δ 181.59, 161.88, 159.35, 143.99, 142.66, 138.61, 133.71, 133.36, 133.33, 131.72, 128.92, 128.74, 123.60, 123.35, 120.90, 118.93, 114.29, 94.03, 83.52, 74.55, 70.22, 62.91, 57.45, 56.10, 44.63, 30.91, 29.59, 25.34, 25.22, 24.33, 23.41. C-Bpin was not observed. Pairs of methyl groups of the Bpin residue were inequivalent.

HRMS (ESI) *m/z* (M + H)<sup>+</sup>, C<sub>37</sub>H<sub>44</sub>N<sub>3</sub>O<sub>7</sub>NiB<sup>+</sup> calcd. 712.27040, observed 712.26955; correct isotopic pattern.

### 2-Fluoro-4-(methoxymethoxy)-1-methylbenzene (**129**)



The above compound (**129**) was prepared according to GP5 whereby **128** (8.63 g, 68.4 mmol), DIPEA (10 mL), MOMCl solution (10 mL), and CH<sub>2</sub>Cl<sub>2</sub> (40 mL) were utilized. Yield: 78% (9.07 g, 53.3 mmol).

R<sub>f</sub>: 0.32, (1:10 EtOAc/hexane).

<sup>1</sup>H NMR (400 MHz, CDCl<sub>3</sub>) δ 7.14 – 7.04 (m, 1H), 6.81 – 6.72 (m, 2H), 5.15 (s, 2H), 3.49 (s, 3H), 2.23 (d, *J* = 1.9 Hz, 3H).

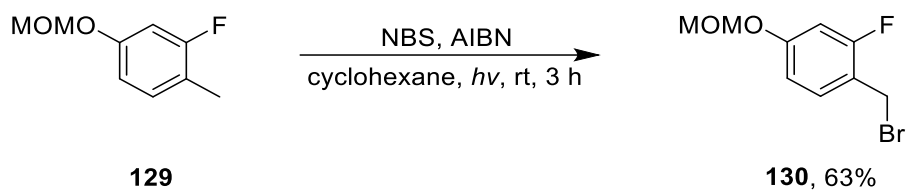
<sup>13</sup>C NMR (101 MHz, CDCl<sub>3</sub>) δ 161.44 (d, *J* = 244.3 Hz), 156.33 (d, *J* = 10.8 Hz), 131.42 (d, *J* = 6.8 Hz), 117.85 (d, *J* = 17.4 Hz), 111.64 (d, *J* = 3.2 Hz), 103.86 (d, *J* = 25.5 Hz), 94.63, 55.95, 13.76 (d, *J* = 3.1 Hz).

<sup>19</sup>F NMR (376 MHz, CDCl<sub>3</sub>) δ -115.14.

HRMS/GC: R<sub>t</sub> 7.91 min, C<sub>9</sub>H<sub>11</sub>FO<sub>2</sub><sup>+</sup>, [M]<sup>+</sup> calcd. 170.0738, observed 170.0737.

Elemental analysis calcd (%) for C<sub>9</sub>H<sub>10</sub>FO<sub>2</sub> (170.18): C 63.52, H 6.52, O 18.80; found C 63.7 ± 0.22, H 6.84 ± 0.01, O 21.4 ± 0.22.

**1-(Bromomethyl)-2-fluoro-4-(methoxymethoxy)benzene (130)**



The above compound (**130**) was prepared according to GP3 whereby, **129** (1 g, 5.90 mmol), NBS (1.15 g, 6.50 mmol), AIBN (100 mg, 0.61 mmol) and cyclohexane (40 mL) were utilized. Yield: 63% (0.93 g, 3.7 mmol).

R<sub>f</sub>: 0.63, (1:3 EtOAc/hexane).

<sup>1</sup>H NMR (400 MHz, CDCl<sub>3</sub>) δ 7.32 – 7.24 (m, 1H), 6.83 – 6.76 (m, 2H), 5.16 (s, 2H), 4.50 (d, *J* = 0.7 Hz, 2H), 3.47 (s, 3H).

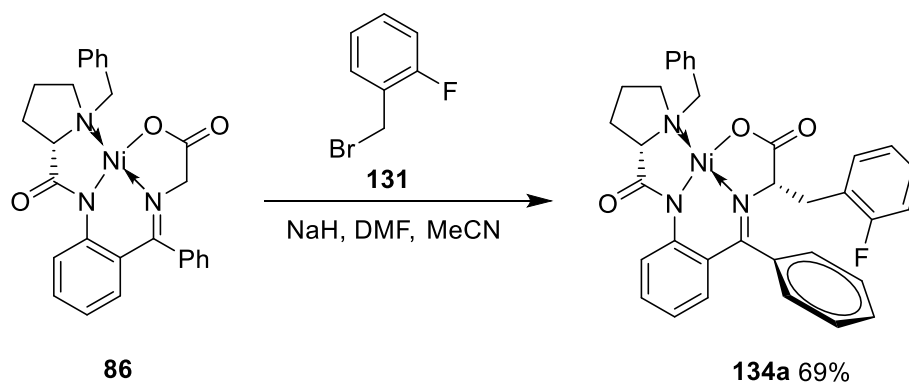
<sup>13</sup>C NMR (101 MHz, CDCl<sub>3</sub>) δ 161.20 (d, *J* = 250.1 Hz), 158.89 (d, *J* = 10.9 Hz), 131.67 (d, *J* = 5.0 Hz), 118.28 (d, *J* = 14.6 Hz), 112.33 (d, *J* = 3.1 Hz), 104.19 (d, *J* = 24.8 Hz), 94.42, 56.15, 26.09 (d, *J* = 3.9 Hz).

<sup>19</sup>F NMR (376 MHz, CDCl<sub>3</sub>) δ –114.27.

LRMS/GC: *R*<sub>t</sub> 10.59 min, C<sub>9</sub>H<sub>10</sub>BrFO<sub>2</sub><sup>+</sup>, [M]<sup>+</sup> calcd. 247.98, observed 248.00.

HRMS/GC: *R*<sub>t</sub> 10.97 min, C<sub>9</sub>H<sub>11</sub>FO<sub>2</sub><sup>+</sup>, [M]<sup>+</sup> calcd. 247.9843, observed 247.9840; correct isotopic pattern.

**(*S,S*)-Ni-BPB-2-FPhe (134a)**



The above compound (**134a**) was prepared according to GP1 whereby, **86** (0.94 g, 1.89 mmol), **131** (0.5 g, 2.65 mmol), NaH (60% suspension in mineral oil) (120 mg, 3.0 mmol) and DMF/MeCN 1:2 (20 mL) were utilized. Yield: 69% (0.83 g, 1.29 mmol; according to the  $^1\text{H}$ -NMR solvate with 0.5 mol.  $\text{Et}_2\text{O}$ ).

$R_f$  0.35, (1:8 acetone/ $\text{CHCl}_3$ ).

$^1\text{H}$  NMR (400 MHz,  $\text{CDCl}_3$ )  $\delta$  8.28 (d,  $J = 8.7$  Hz, 1H), 7.99 (d,  $J = 7.2$  Hz, 2H), 7.61 – 7.47 (m, 2H), 7.46 – 7.40 (m, 1H), 7.40 – 7.09 (m, 9H), 6.98 (d,  $J = 7.5$  Hz, 1H), 6.65 (d,  $J = 4.1$  Hz, 2H), 4.29 (dd,  $J = 9.1, 3.5$  Hz, 2H), 3.56 – 3.43 (m, 1H), 3.31 (t,  $J = 8.3$  Hz, 1H), 3.22 – 3.06 (m, 2H), 3.02 – 2.89 (m, 1H), 2.47 – 2.23 (m, 3H), 2.01–1.87 (m, 1H), 1.78 – 1.58 (m, 1H).

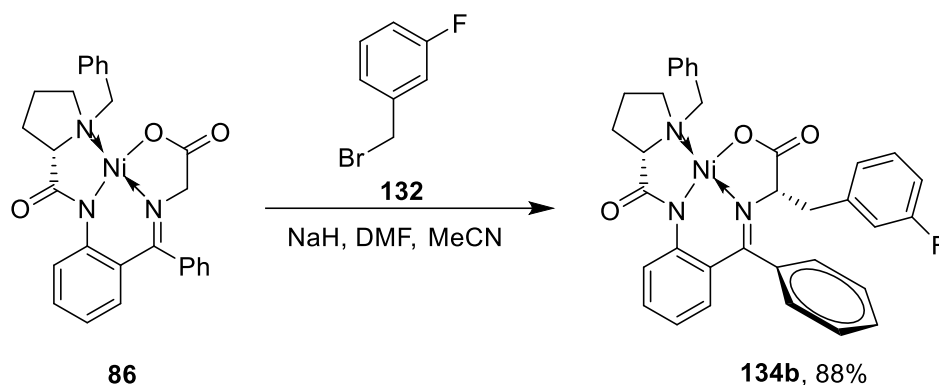
$^{13}\text{C}$  NMR (101 MHz,  $\text{CDCl}_3$ )  $\delta$  180.25, 178.41, 171.98, 162.03 (d,  $J = 246.6$  Hz), 142.90, 134.07, 133.56, 133.18, 132.89 (d,  $J = 4.4$  Hz), 132.32, 131.53, 129.70, 129.34 (d,  $J = 8.1$  Hz), 128.95, 128.91, 128.76, 128.19 (d,  $J = 3.1$  Hz), 127.14, 126.21, 124.73 (d,  $J = 3.2$  Hz), 123.25, 123.09 (d,  $J = 15.8$  Hz), 120.49, 115.74, 115.52, 70.79, 70.34, 63.23, 57.03, 33.28, 30.76, 23.11. *o*- and *m*-Carbons of the phenyl group of the [(2-amido)phenyl]phenylmethanimine residue were inequivalent.

$^{19}\text{F}$  NMR (376 MHz,  $\text{CDCl}_3$ )  $\delta$  -115.29.

HRMS (ESI)  $m/z$  ( $M + H$ ) $^+$ ,  $\text{C}_{34}\text{H}_{30}\text{N}_3\text{O}_3\text{NiF}^+$  calcd. 606.1698, observed 606.1698; correct isotopic pattern.

The analytical data were in accordance with the literature.<sup>117</sup>

**(*S,S*)-Ni-BPB-3-FPhe (134b)**



The above compound (**134b**) was prepared according to GP1 whereby, **86** (0.52, 10.5 mmol), 1-(bromomethyl)-3-fluorobenzene (**132**, 0.5 g, 16.8 mmol), NaH (60% suspension in mineral oil) (70 mg, 16.8 mmol) and DMF/MeCN 1:2 (30 mL) were utilized. Yield: 88% (0.59 g, 0.82 mmol; according to the  $^1\text{H}$ -NMR solvate with 0.5 mol.  $\text{Et}_2\text{O}$ ).

$R_f$  0.42, (1:20 acetone/ $\text{CHCl}_3$ ).

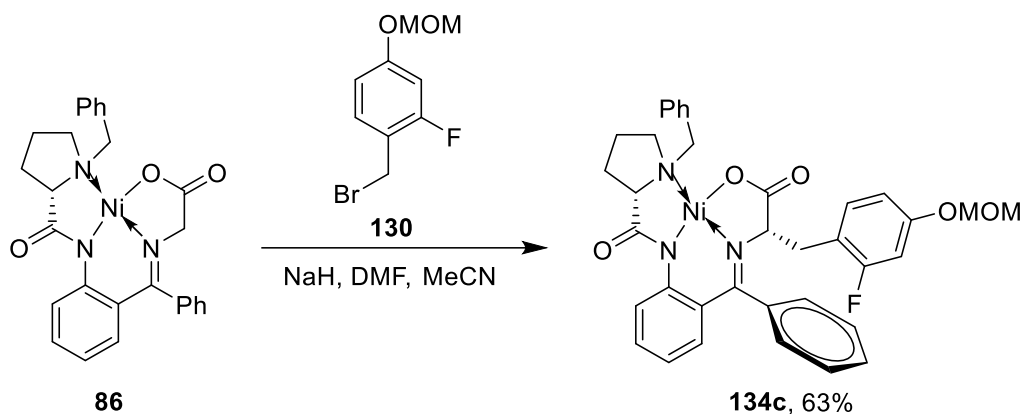
$^1\text{H}$  NMR (400 MHz,  $\text{CDCl}_3$ )  $\delta$  8.23 (d,  $J = 8.3$  Hz, 1H), 8.01 (d,  $J = 6.7$  Hz, 2H), 7.65 – 7.49 (m, 2H), 7.48 – 7.38 (m, 1H), 7.39 – 7.22 (m, 4H), 7.21 – 7.00 (m, 3H), 6.98 – 6.78 (m, 3H), 6.73 – 6.59 (m, 2H), 4.38 – 4.12 (m, 2H), 3.58 – 3.40 (m, 2H), 3.32 (t,  $J = 7.9$  Hz, 1H), 3.23 – 3.11 (m, 1H), 3.06 (d,  $J = 12.1$  Hz, 1H), 2.87 (dd,  $J = 12.1, 4.9$  Hz, 1H), 2.62 – 2.43 (m, 1H), 2.43 – 2.28 (m, 2H), 2.08 – 1.89 (m, 1H), 1.86 – 1.69 (m, 1H).

$^{13}\text{C}$  NMR (101 MHz,  $\text{CDCl}_3$ )  $\delta$  180.37, 178.22, 171.36, 163.07 (d,  $J = 246.6$  Hz), 142.91, 138.32 (d,  $J = 7.4$  Hz), 134.07, 133.53, 133.25, 132.49, 131.51, 130.15 (d,  $J = 8.2$  Hz), 129.90, 129.08 (d,  $J = 22.6$  Hz), 128.83, 128.80, 127.76, 127.17, 126.23, 126.20, 126.06, 123.44, 120.63, 117.34 (d,  $J = 21.0$  Hz), 114.37 (d,  $J = 20.9$  Hz), 71.13, 65.83, 63.32, 57.23, 39.53, 30.73, 23.20. *o*- and *m*-Carbons of the phenyl group of the [(2-amido)phenyl]phenylmethanimine residue were inequivalent.

$^{19}\text{F}$  NMR (376 MHz,  $\text{CDCl}_3$ )  $\delta$  -112.49.

HRMS (ESI)  $m/z$  ( $\text{M} + \text{H}$ ) $^+$ ,  $\text{C}_{34}\text{H}_{30}\text{N}_3\text{O}_3\text{NiF}^+$  calcd. 606.1698, observed 606.1698; correct isotopic pattern.

**(*S,S*)-Ni-BPB-2-F-4-MOMO-Phe (134c)**



The above compound (**134c**) was prepared according to GP1 whereby, **86** (1.06 g, 2.13 mmol), **130** (0.85 g, 3.41 mmol), NaH (60% suspension in mineral oil) (136 mg, 3.40 mmol) DMF/MeCN 1:2 (30 mL) were utilized. Yield: 63% (0.89 g, 1.34 mmol).

R<sub>f</sub>: 0.57, (1:8 acetone/CHCl<sub>3</sub>).

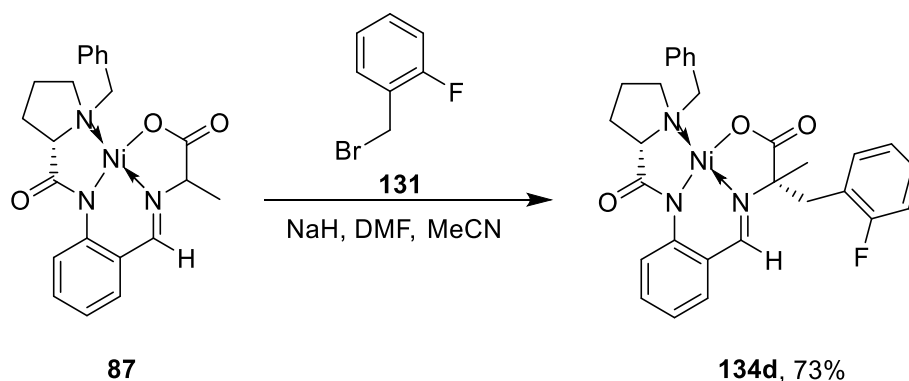
<sup>1</sup>H NMR (400 MHz, CDCl<sub>3</sub>) δ 8.26 (d, *J* = 8.7 Hz, 1H), 8.00 (d, *J* = 7.3 Hz, 2H), 7.59 – 7.47 (m, 2H), 7.42 (t, *J* = 6.8 Hz, 1H), 7.31 (t, *J* = 7.4 Hz, 2H), 7.27 – 7.22 (m, 2H), 7.20 – 7.10 (m, 2H), 7.08 – 6.98 (m, 2H), 6.94 (d, *J* = 7.4 Hz, 1H), 6.91 – 6.85 (m, *J* = 3.1 Hz, 1H), 6.71 – 6.56 (m, 2H), 5.06 (dd, *J* = 23.4, 6.7 Hz, 2H), 4.30 (d, *J* = 12.7 Hz, 1H), 4.25 (t, *J* = 5.1 Hz, 1H), 3.51 (d, *J* = 12.7 Hz, 1H), 3.42 (s, 3H), 3.37 – 3.29 (m, 1H), 3.16 (d, *J* = 7.5 Hz, 1H), 3.11 (d, *J* = 5.1 Hz, 1H), 3.03 – 2.90 (m, 1H), 2.65 – 2.46 (m, *J* = 9.6 Hz, 1H), 2.46 – 2.27 (m, 2H).

<sup>13</sup>C NMR (101 MHz, CDCl<sub>3</sub>) δ 180.21, 178.36, 171.91, 157.13 (d, *J* = 240.9 Hz), 153.68 (d, *J* = 1.8 Hz), 142.83, 133.97, 133.55, 133.13, 132.31, 131.51, 129.68, 128.88, 128.81, 128.77, 128.20, 128.17, 127.15, 126.20, 123.76 (d, *J* = 17.8 Hz), 123.28, 120.52, 120.25 (d, *J* = 4.1 Hz), 116.95 (d, *J* = 8.0 Hz), 116.06 (d, *J* = 24.3 Hz), 95.00, 70.72, 70.36, 63.18, 57.06, 56.02, 33.55, 30.78, 23.10. *o*- and *m*-Carbons of the phenyl group of the [(2-amido)phenyl]phenylmethanimine residue were inequivalent.

<sup>19</sup>F NMR (376 MHz, CDCl<sub>3</sub>) δ -124.36.

HRMS (ESI) *m/z* (*M* + *H*)<sup>+</sup>, C<sub>36</sub>H<sub>5</sub>N<sub>3</sub>O<sub>5</sub>NiF<sup>+</sup> calcd. 666.1909, observed 666.1910; correct isotopic pattern.

**(*S,S*)-Ni-BPA-2-FPhe (134d)**



The above compound (**134d**) was prepared according to GP1 whereby, **87** (0.29 g, 0.66 mmol), **131** (0.17 g, 0.90 mmol), NaH (60% suspension in mineral oil) (36 mg, 0.90 mmol) and DMF/MeCN 1:2 (10 mL) were utilized. Yield: 73% (263 mg, 0.48 mmol).

R<sub>f</sub>: 0.61, (1:10 acetone/CHCl<sub>3</sub>).

<sup>1</sup>H NMR (400 MHz, CDCl<sub>3</sub>) δ 8.49 (d, *J* = 8.5 Hz, 1H), 7.93 (d, *J* = 8.5 Hz, 2H), 7.54 (d, *J* = 2.4 Hz, 1H), 7.45 – 7.29 (m, 5H), 7.26 – 7.23 (m, 2H), 7.19 (td, *J* = 7.5, 1.1 Hz, 1H), 7.06 – 6.99 (m, 1H), 6.96 – 6.90 (m, 1H), 4.30 (d, *J* = 12.7 Hz, 1H), 3.56 (d, *J* = 12.7 Hz, 1H), 3.34 – 3.16 (m, 4H), 2.53 – 2.35 (m, 1H), 2.30 – 2.13 (m, 2H), 1.92 (td, *J* = 10.8, 6.4 Hz, 1H), 1.76 – 1.68 (m, 1H), 1.63 (s, 3H).

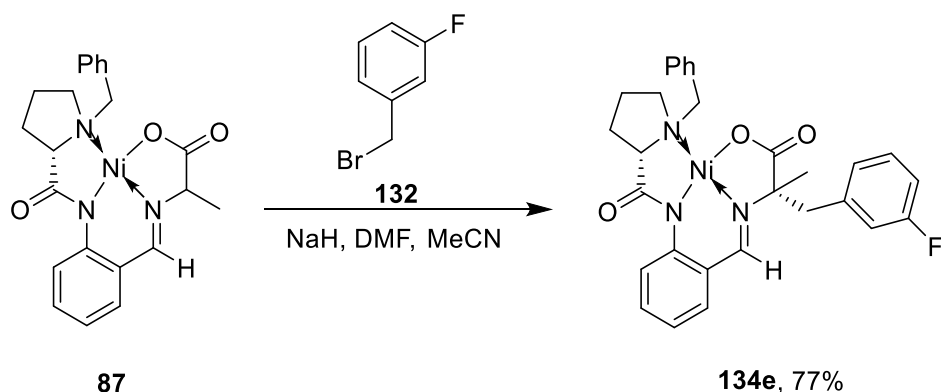
<sup>13</sup>C NMR (101 MHz, CDCl<sub>3</sub>) δ 181.47, 181.16, 161.99 (d, *J*<sub>F, C=NH</sub> = 2.6 Hz), 161.13 (d, *J* = 248.5 Hz), 142.81, 133.84, 133.62, 133.07, 132.46 (d, *J* = 4.1 Hz), 131.64, 129.31 (d, *J* = 8.3 Hz), 128.98, 128.74, 124.54 (d, *J* = 3.4 Hz), 123.60, 123.42, 122.68 (d, *J* = 15.2 Hz), 121.21, 115.53 (d, *J* = 22.7 Hz), 74.13, 70.04, 62.81, 57.02, 39.60, 30.73, 25.61, 22.93.

<sup>19</sup>F NMR (376 MHz, CDCl<sub>3</sub>) δ -116.72.

HRMS (ESI) *m/z* (M + H)<sup>+</sup>, C<sub>29</sub>H<sub>28</sub>N<sub>3</sub>O<sub>3</sub>NiF<sup>+</sup> calcd. 544.1541, observed 544.1542; correct isotopic pattern.

The analytical data were in accordance with the literature.<sup>117</sup>

**(*S,S*)-Ni-BPA-3-FPhe (134e)**



The above compound (**134e**) was prepared according to GP1 whereby, **87** (0.20 g, 0.46 mmol), **132** (0.15 g, 0.79 mmol), NaH (60% suspension in mineral oil) (33 mg, 0.83 mmol) and DMF/MeCN 1:2 (30 mL) were utilized. Yield: 77% (0.194 g, 0.35 mmol).

R<sub>f</sub>: 0.55, (1:10 acetone/CHCl<sub>3</sub>).

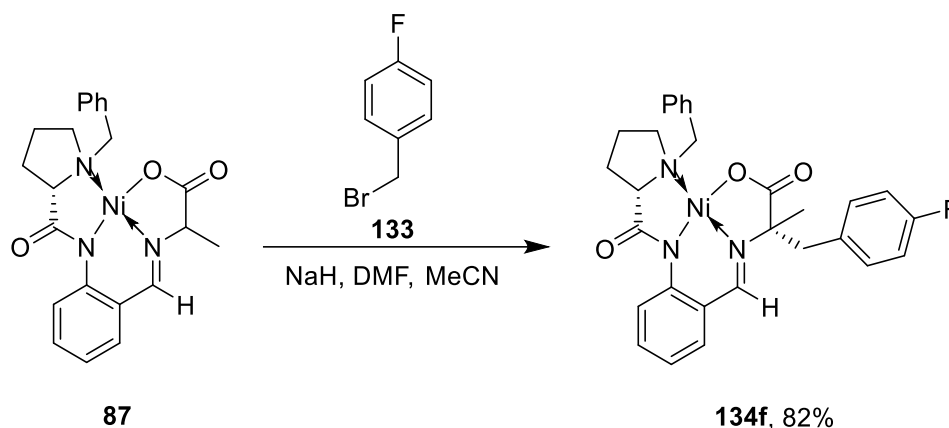
<sup>1</sup>H NMR (400 MHz, CDCl<sub>3</sub>) δ 8.52 (d, *J* = 8.7 Hz, 1H), 7.93 (d, *J* = 7.2 Hz, 2H), 7.51 (s, 1H), 7.40 – 7.29 (m, 4H), 7.26 – 7.20 (m, 2H), 7.07 (td, *J* = 8.4, 1.8 Hz, 1H), 7.01 – 6.91 (m, *J* = 7.2 Hz, 2H), 6.86 (d, *J* = 7.6 Hz, 1H), 4.29 (d, *J* = 12.7 Hz, 1H), 3.54 (d, *J* = 12.7 Hz, 1H), 3.34 (d, *J* = 13.5 Hz, 1H), 3.29 – 3.19 (m, 2H), 2.82 (d, *J* = 13.5 Hz, 1H), 2.52 – 2.33 (m, 1H), 2.33 – 2.13 (m, 2H), 2.00 – 1.87 (m, 1H), 1.80 – 1.69 (m, 1H), 1.62 (s, 3H).

<sup>13</sup>C NMR (101 MHz, CDCl<sub>3</sub>) δ 181.61, 180.81, 162.93 (d, *J* = 246.8 Hz), 161.13, 143.01, 137.89 (d, *J* = 7.3 Hz), 133.92, 133.82, 133.11, 131.63, 130.01 (d, *J* = 8.1 Hz), 129.00, 128.75, 126.45 (d, *J* = 2.7 Hz), 123.76, 123.06, 121.29, 117.38 (d, *J* = 21.2 Hz), 114.38 (d, *J* = 21.0 Hz), 74.28, 70.06, 62.91, 57.20, 47.21, 30.78, 25.64, 22.91.

<sup>19</sup>F NMR (376 MHz, CDCl<sub>3</sub>) δ –112.42.

HRMS (ESI) *m/z* (M + H)<sup>+</sup>, C<sub>29</sub>H<sub>28</sub>N<sub>3</sub>O<sub>3</sub>NiF<sup>+</sup> calcd. 544.1541, observed 544.1541; correct isotopic pattern.

**(*S,S*)-Ni-BPA-4-FPhe (134f)**



The above compound (**134f**) was prepared according to GP1 whereby, **87** (0.24 g, 0.54 mmol), **133** (0.16 g, 0.87 mmol), NaH (60% suspension in mineral oil) (34 mg, 0.87 mmol) and DMF/MeCN 1:2 (30 mL) were utilized. Yield: 82% (0.26 g, 0.48 mmol).

R<sub>f</sub>: 0.53, (1:10 acetone/CHCl<sub>3</sub>).

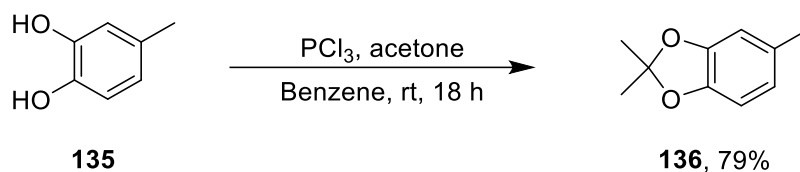
<sup>1</sup>H NMR (400 MHz, CDCl<sub>3</sub>) 8.53 (d, *J* = 8.5 Hz, 1H), 7.95 (d, *J* = 8.5 Hz, 2H), 7.52 (s, 1H), 7.42 – 7.21 (m, 5H), 7.16 – 7.04 (m, 4H), 6.97 (t, *J* = 7.9 Hz, 1H), 4.30 (d, *J* = 12.7 Hz, 1H), 3.54 (d, *J* = 12.7 Hz, 1H), 3.33 (d, *J* = 13.6 Hz, 1H), 3.29 – 3.20 (m, 2H), 2.81 (d, *J* = 13.6 Hz, 1H), 2.48 – 2.32 (m, 1H), 2.32 – 2.15 (m, 2H), 1.95 (td, *J* = 10.7, 6.4 Hz, 1H), 1.76 (dtd, *J* = 8.8, 6.4, 3.2 Hz, 1H), 1.63 (s, 3H).

<sup>13</sup>C NMR (101 MHz, CDCl<sub>3</sub>) δ 181.64, 180.89, 162.53 (d, *J* = 246.2 Hz), 161.07, 143.00, 133.91, 133.89 (d, *J* = 4.8 Hz), 132.24, 132.16, 131.65, 131.21 (d, *J* = 3.4 Hz), 129.03, 128.78, 123.79, 123.12, 121.33, 115.49 (d, *J* = 21.2 Hz), 74.58, 70.03, 62.97, 57.26, 46.93, 30.83, 25.36, 22.87.

<sup>19</sup>F NMR (376 MHz, CDCl<sub>3</sub>) δ -115.23.

HRMS (ESI) *m/z* (M + H)<sup>+</sup>, C<sub>29</sub>H<sub>28</sub>N<sub>3</sub>O<sub>3</sub>NiF<sup>+</sup> calcd. 544.1541, observed 544.1541; correct isotopic pattern.

### 2,2,5-Trimethylbenzo[*d*][1,3]dioxole (**136**)



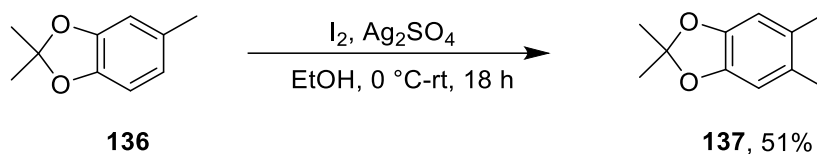
Following a literature procedure,<sup>145</sup> a solution of phosphorous trichloride (6.59 g, 48 mmol) in benzene (10 mL) was slowly added to a stirred solution of **135** (15.0 g, 120.8 mmol) and acetone (10.6 mL, 72 mmol) in benzene (150 mL) under Ar. The reaction mixture was allowed to stir for 18 h at room temperature, before being slowly added to a saturated solution of  $\text{K}_2\text{CO}_3$  (100 mL). The organic phase was washed with 10% w/v NaOH solution (100 mL), brine ( $3 \times 40$  mL), dried over anhydrous  $\text{MgSO}_4$ , and concentrated under vacuum to give the title compound in (15.66 g, 95.4 mmol) 79% yield as a colorless oil.

$R_f$ : 0.68, (1:10 EtOAc/hexane).

$^1\text{H}$  NMR (300 MHz,  $\text{CDCl}_3$ )  $\delta$  7.15 (s, 1H), 6.74 – 6.66 (m, 2H), 2.53 (s, 3H), 1.72 (s, 6H).

The analytical data were in accordance with the literature.<sup>124</sup>

### 5-Iodo-2,2,6-trimethylbenzo[d][1,3]dioxole (**137**)

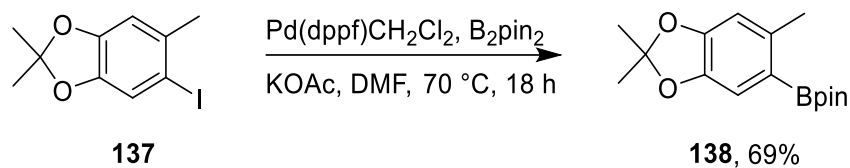


A solution of iodine (11.1 g, 35.6 mmol) in ethanol (50 mL) was added dropwise to a stirred solution of **136** (5.84 g, 35.6 mmol) and Ag<sub>2</sub>SO<sub>4</sub> (9.0 g, 35.6 mmol) in ethanol (80 mL) at 0 °C. The black reaction mixture was allowed to come to room temperature before being stirred for 18 hours. The resulting green reaction mixture was filtered through Celite<sup>®</sup>, washed with ethanol (3 × 20 mL), and the combined fractions were poured slowly into a saturated sodium bicarbonate solution (40 mL). The organic fractions were washed with water (3 × 30 mL), brine (2 × 30 mL), and dried over anhydrous MgSO<sub>4</sub>. The dried solution was concentrated under vacuum and purified by silica gel column chromatography to afford the *title compound* in 51% yield (**137**, 5.24 g, 18.0 mmol) as pale yellow oil. **137** was directly introduced to the next step owing to its instability.

R<sub>f</sub>: 0.33, (hexane).

<sup>1</sup>H NMR (300 MHz, CDCl<sub>3</sub>) δ 7.15 (s, 1H), 6.74 – 6.66 (m, 1H), 2.35 (s, 3H), 1.67 (s, 6H).

**4,4,5,5-Tetramethyl-2-(2,2,6-trimethylbenzo[d][1,3]dioxol-5-yl)-1,3,2-dioxaborolane  
(138)**



The above compound (**138**) was prepared according to GP4 whereby, **137** (2 g, 6.25 mmol), B<sub>2</sub>pin<sub>2</sub> (3.2 g, 12.5 mmol), Pd(dppf)CH<sub>2</sub>Cl<sub>2</sub> (0.51 g, 0.6 mmol), KOAc (1.84 g, 18.7 mmol) and DMF (40 mL) were utilized. Yield: 69% (**138**, 1.25 g, 4.32 mmol) as colorless crystals.

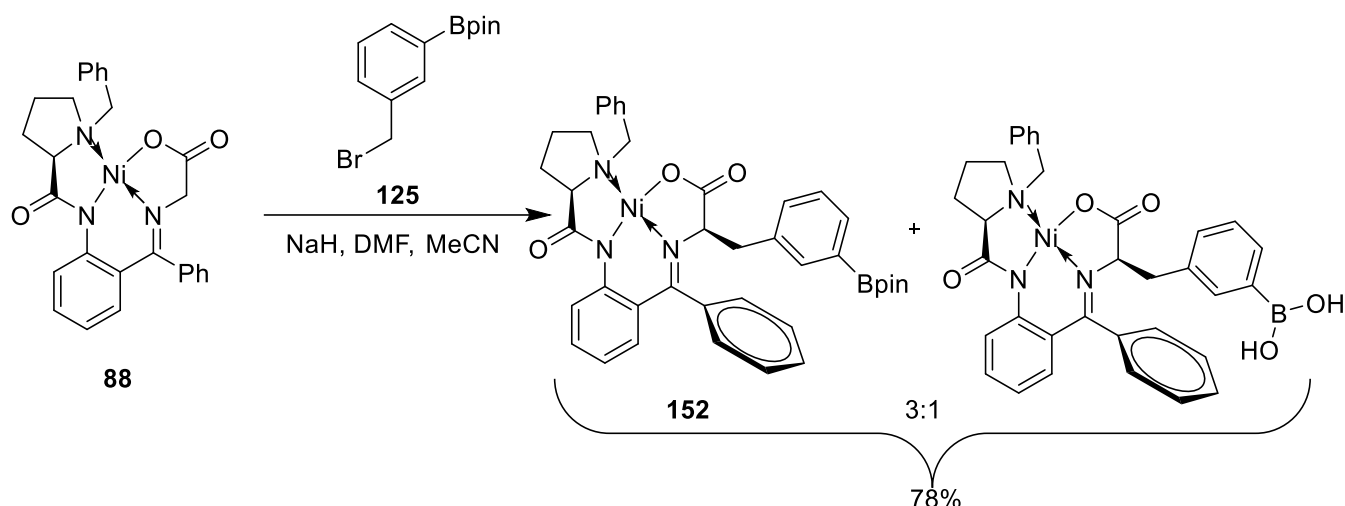
R<sub>f</sub>: 0.24, (1:10 EtOAc/hexane).

<sup>1</sup>H NMR (300 MHz, CDCl<sub>3</sub>) δ 7.15 (s, 1H), 6.59 (s, 1H), 2.48 (s, 3H), 1.66 (s, 6H), 1.33 (s, 12H).

<sup>13</sup>C NMR (75 MHz, CDCl<sub>3</sub>) δ 149.61, 144.92, 139.78, 117.44, 114.57, 110.41, 83.18, 25.78, 24.85, 21.88. C-Bpin was not observed. Pairs of methyl groups of the Bpin residue were inequivalent.

HRMS (ESI) *m/z* (M + H)<sup>+</sup>, C<sub>16</sub>H<sub>23</sub>O<sub>4</sub>B<sup>+</sup> calcd. 291.17677, observed 291.17652; correct isotopic pattern.

**(*R,R*)-Ni-BPB-3-Bpin-Phe (152)**



The above compound (**152**) was prepared according to GP1 whereby, **88** (713 mg, 1.43 mmol), **125** (0.51 g, 1.7 mmol), NaH (60% suspension in mineral oil) (91 mg, 2.28 mmol) and DMF/MeCN 1:2 (30 mL) were utilized. This product mixture is confirmed in the MS. Yield: 78% (795 mg). In this instance partial hydrolysis of the pinacol moiety proceeding reversed-phase purification was observable in the  $^1\text{H}$  NMR spectrum. As boronic acids are typically even better substrates for the alcohol-enhanced Cu-mediated radiofluorination than the corresponding Bpin esters, no attempt to separate it (or to convert it back into the Bpin ester) was made and the mixture was directly used for the radiolabeling step. Omission of the RP purification step could lead to lower  $^{18}\text{F}$ -incorporation rates.

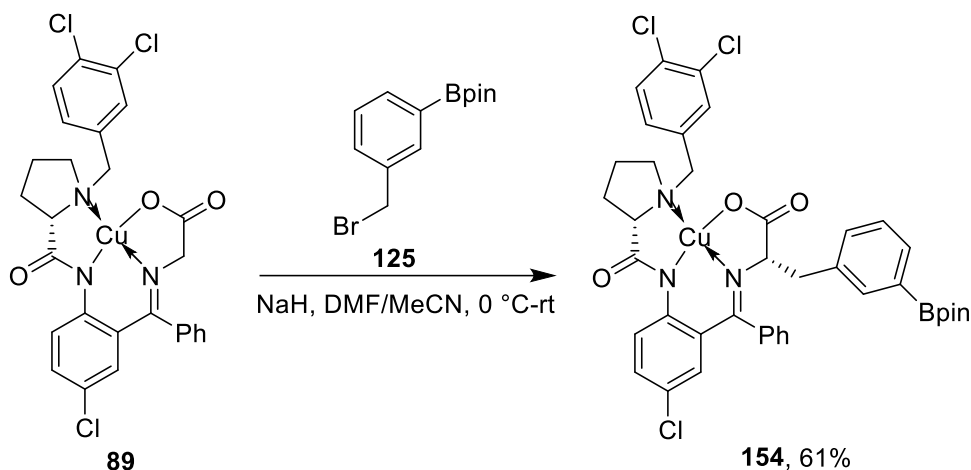
$R_f$  0.43, (1:20 acetone/chloroform).

$^1\text{H}$  NMR (400 MHz,  $\text{CDCl}_3$ )  $\delta$  8.31 (d,  $J = 8.7$  Hz, 1H), 8.22 (d,  $J = 8.7$  Hz, 2H), 8.03 (t,  $J = 7.9$  Hz, 5H), 7.94 (d,  $J = 7.3$  Hz, 2H), 7.82 (d,  $J = 7.3$  Hz, 1H), 7.76 (s, 2H), 7.64 – 7.10 (m, 20H), 7.03 (d,  $J = 7.6$  Hz, 2H), 6.83 – 6.62 (m, 9H), 4.38 – 4.12 (m, 5H), 3.48 – 3.38 (m, 2H), 3.37 – 3.26 (m, 2H), 3.21 (dd,  $J = 13.8, 4.7$  Hz, 1H), 3.16 – 3.08 (m, 1H), 3.05 (dd,  $J = 13.8, 3.9$  Hz, 2H), 2.96 (dd,  $J = 13.8, 6.1$  Hz, 1H), 2.89 – 2.76 (m, 3H), 2.56 – 2.41 (m, 1H), 2.34 (dt,  $J = 9.6, 6.1$  Hz, 1H), 2.26 (dd,  $J = 15.1, 7.5$  Hz, 3H), 2.11 – 1.93 (m, 5H), 1.88 (s, 6H), 1.79 – 1.67 (m, 1H), 1.36 (dd,  $J = 13.0, 6.1$  Hz, 1H), 1.34 – 1.24 (m, 12H).

$^{13}\text{C}$  NMR (101 MHz,  $\text{CDCl}_3$ )  $\delta$  180.46, 179.84, 171.47, 142.77, 136.40, 134.50, 134.09, 133.56, 133.41, 133.09, 132.45, 131.62, 131.55, 129.96, 129.25, 129.07, 128.92, 128.82, 128.12, 127.87, 127.07, 123.64, 83.87, 71.31, 70.52, 70.43, 63.57, 57.47, 39.48, 30.69, 24.88, 24.80, 23.50. C-Bpin was not observed. Pairs of methyl groups of the Bpin residue were inequivalent.

HRMS (ESI)  $m/z$  ( $M + H$ )<sup>+</sup>, **152**: C<sub>40</sub>H<sub>42</sub>N<sub>3</sub>O<sub>5</sub>NiB<sup>+</sup> calcd. 714.26492, observed 714.26443; correct isotopic pattern.

**(*S,S*)-Cu-BPB-3-BpinPhe (**154**)**



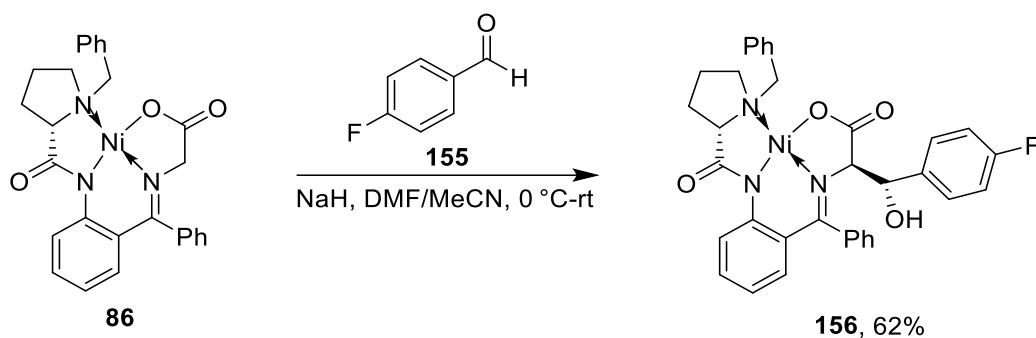
The above compound (**154**) was prepared according to GP1 whereby, **89** (0.40 g, 0.66 mmol), **125** (0.314 g, 1.06 mmol), NaH (60% suspension in mineral oil) (42 mg, 1.06 mmol) and DMF/MeCN 1:2 (30 mL) were utilized. Yield: 61% (0.33 g, 0.40 mmol).

The paramagnetic nature of Cu(II) rendered characterization by NMR spectroscopy inapplicable.

R<sub>f</sub> 0.42, (1:20 acetone/CHCl<sub>3</sub>).

HRMS (ESI)  $m/z$  ( $M + H$ )<sup>+</sup>, C<sub>40</sub>H<sub>39</sub>N<sub>3</sub>O<sub>5</sub>CuCl<sub>3</sub>B<sup>+</sup> calcd. 823.1405, observed 823.1386; correct isotopic pattern.

**(S,S)-Ni-BPB-4-F-PheSer (156)**



The above compound (**156**) was prepared according to GP2 whereby, **86** (0.80 g, 1.61 mmol), **155** (0.30 g, 2.42 mmol), NaH (60% suspension in mineral oil) (0.1 g, 2.5 mmol) and DMF/MeCN 1:2 (30 mL) were utilized. Yield: 62% (0.62 g, 1.00 mmol) as red crystalline solid.

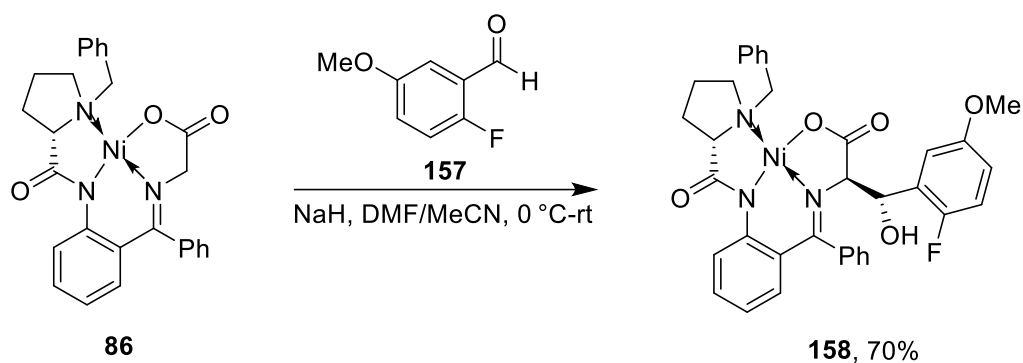
R<sub>f</sub>: 0.41 (1:8 acetone/CHCl<sub>3</sub>).

<sup>1</sup>H NMR (400 MHz, CDCl<sub>3</sub>) δ 8.48 (dd, *J* = 8.7, 1.2 Hz, 1H), 7.61 (m, 3H), 7.51 – 7.44 (m, 2H), 7.42 – 7.27 (m, 7H), 7.27 – 7.22 (m, 2H), 7.18 (d, *J* = 7.2 Hz, 1H), 6.87 (dd, *J* = 8.3, 1.8 Hz, 1H), 6.81 (ddd, *J* = 8.3, 6.9, 1.2 Hz, 1H), 4.96 (d, *J* = 9.6 Hz, 1H), 4.71 (dd, *J* = 9.6, 5.4 Hz, 1H), 4.42 (d, *J* = 5.5 Hz, 1H), 3.78 (d, *J* = 13.9 Hz, 2H), 3.55 (d, *J* = 13.9 Hz, 1H), 3.38 (dd, *J* = 9.6, 3.6 Hz, 1H), 2.53 (m, 1H), 2.22 (dd, *J* = 12.9, 10.2 Hz, 1H), 1.90 (ddd, *J* = 13.9, 7.7, 3.6 Hz, 1H), 1.49 (m, 1H), 1.43 – 1.31 (m, 1H).

<sup>13</sup>C NMR (101 MHz, CDCl<sub>3</sub>) δ 181.85, 178.04, 173.03, 163.24 (d, *J* = 248.5 Hz), 143.37, 135.82, 135.79, 133.79, 133.62 (d, *J* = 81.9 Hz), 131.97, 131.15, 130.41, 129.57 (d, *J* = 7.9 Hz), 129.53, 129.21, 128.97, 127.43, 125.94, 123.84, 121.01, 115.65 (d, *J* = 21.2 Hz), 73.62, 72.74, 68.32, 60.01, 55.41, 31.39, 23.78.

<sup>19</sup>F NMR (376 MHz, CDCl<sub>3</sub>) δ –113.30.

**(*S,S*)-Ni-BPB-2-F-5-MeO-PheSer (158)**



The above compound (**158**) was prepared according to GP2 whereby, **86** (673 mg, 1.35 mmol), **157** (0.25 g, 1.62 mmol), NaH (60% suspension in mineral oil) (87 mg, 2.18 mmol) and DMF/MeCN 1:2 (30 mL) were utilized. Yield: 70% (0.62 g, 0.95 mmol) as red solid.

R<sub>f</sub>: 0.35, (1:8 acetone/CHCl<sub>3</sub>).

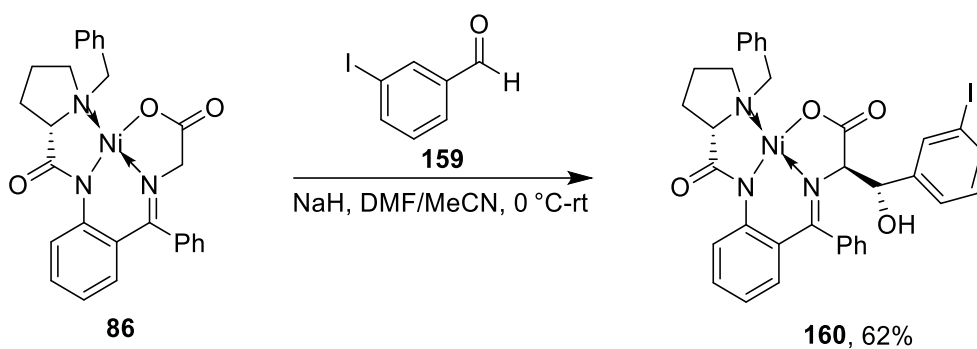
<sup>1</sup>H NMR (300 MHz, CDCl<sub>3</sub>) δ 8.51 (d, *J* = 8.6 Hz, 1H), 7.64 – 7.55 (m, 3H), 7.41 – 7.26 (m, 7H), 7.25 – 7.16 (m, 3H), 7.02 (m, 1H), 6.84 (dd, *J* = 8.3, 1.7 Hz, 1H), 6.78 (m, 1H), 4.44 (d, *J* = 4.3 Hz, 1H), 3.95 (d, *J* = 13.8 Hz, 1H), 3.71 – 3.60 (m, 2H), 3.57 (s, 3H), 3.32 (dd, *J* = 9.4, 3.7 Hz, 1H), 2.47 – 2.35 (m, 1H), 2.35 – 2.21 (m, 1H), 1.98 – 1.85 (m, 1H), 1.65 (s, 1H), 1.43 (m, 2H). Spectrum contains dichloromethane and acetone impurity peaks.

<sup>13</sup>C NMR (101 MHz, CDCl<sub>3</sub>) δ 181.76, 178.41, 174.26, 155.17 (d, *J* = 42.4), 143.34, 133.80, 133.51 (d, *J* = 106.6 Hz), 131.94, 131.11, 130.23, 129.26 (*J* = 15.4 Hz), 128.93 (d, *J* = 21.0 Hz), 126.73, 126.13, 123.49, 120.77, 116.12 (d, *J* = 24.7 Hz), 115.27 (d, *J* = 8.4 Hz), 113.44, 73.12, 68.17, 66.73, 59.58, 55.56, 54.85, 31.27, 23.71.

<sup>19</sup>F NMR (376 MHz, CDCl<sub>3</sub>) δ –126.48.

HRMS (ESI) *m/z* (M + H)<sup>+</sup>, C<sub>35</sub>H<sub>32</sub>N<sub>3</sub>O<sub>5</sub>NiF<sup>+</sup> calcd. 652.17522, observed 652.17529, correct isotopic pattern.

**(*S,S*)-Ni-BPB-5-I-PheSer (160)**

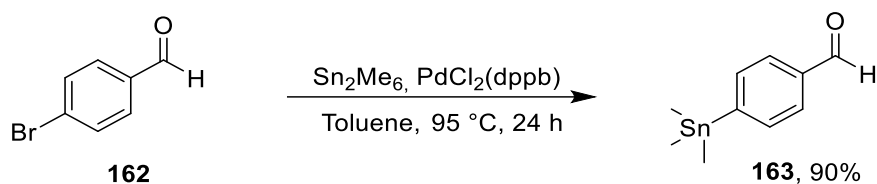


The above compound (**160**) was prepared according to GP2 whereby, **86** (358 mg, 0.72 mmol), **159** (200 mg, 0.86 mmol), NaH (60% suspension in mineral oil) (46 mg, 1.15 mmol) and DMF/MeCN 1:2 (30 mL) were utilized. Yield: 62% (324 mg, 0.44 mmol).

R<sub>f</sub>: 0.36 (1:8 acetone/CHCl<sub>3</sub>).

<sup>1</sup>H NMR (300 MHz, CDCl<sub>3</sub>) δ 8.65 (d, *J* = 8.7 Hz, 1H), 7.84 (d, *J* = 7.0 Hz, 2H), 7.61 (s, 3H), 7.48 – 7.11 (m, 10H), 6.95 – 6.74 (m, 2H), 4.94 (s, 1H), 4.65 (s, 1H), 4.37 (d, *J* = 5.3 Hz, 1H), 3.99 (d, *J* = 13.8 Hz, 1H), 3.58 (d, *J* = 13.8 Hz, 2H), 3.39 (dd, *J* = 9.5, 4.0 Hz, 1H), 2.45 – 2.24 (m, 2H), 1.95 (dd, *J* = 13.8, 6.7 Hz, 1H), 1.45 (dd, *J* = 10.3, 6.7 Hz, 2H).

#### 4-Trimethylstannylbenzaldehyde (**211**)



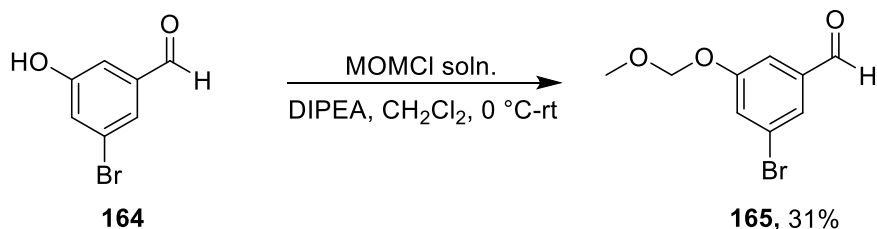
The above compound (**163**) was prepared according to GP6 whereby, **162** (0.2 g, 10.8 mmol), hexamethyldistannane (0.46 mL, 0.73 g, 22.2 mmol), di(chlorobis(diphenyl phosphine butane) palladium (II) (7.58 mg, 0.108 mmol) and toluene (40 mL) were utilized. Yield: 90% (0.26 g, 0.967 mmol).

R<sub>f</sub>: 0.71 (1:10 EtOAc/Hex).

<sup>1</sup>H NMR (300 MHz, CDCl<sub>3</sub>) δ 10.00 (s, 1H), 7.82 (d, *J* = 7.9 Hz, 2H), 7.69 (d, *J* = 7.9 Hz, 2H), 0.36 (s, 9H).

The analytical data were in accordance with the literature.<sup>122</sup>

#### 3-Bromo-5-(methoxymethoxy)benzaldehyde (**165**)



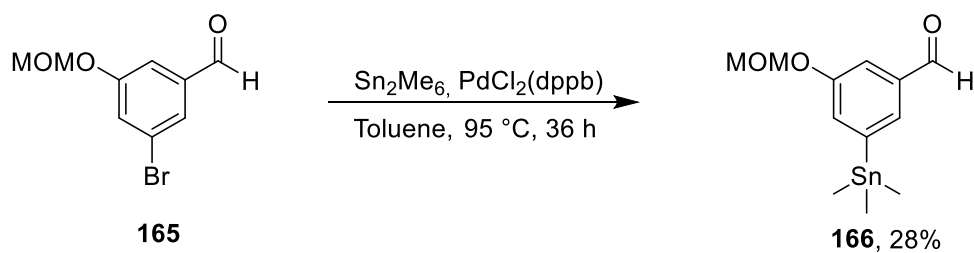
The above compound (**165**) was prepared according to GP5 whereby, **164** (1 g, 4.97 mmol), and CH<sub>2</sub>Cl<sub>2</sub> (40 mL) were utilized. Yield: 31% (0.378 g, 1.54 mmol).

R<sub>f</sub>: 0.75 (1:2 EtOAc/hexane).

<sup>1</sup>H NMR (400 MHz, CDCl<sub>3</sub>) δ 9.92 (s, 1H), 7.67 – 7.66 (m, 1H), 7.50 – 7.46 (m, 2H), 5.24 (s, 2H), 3.51 (s, 3H).

<sup>13</sup>C NMR (101 MHz, CDCl<sub>3</sub>) δ 190.41, 158.46, 138.74, 126.21, 125.51, 123.52, 115.39, 94.54, 56.34.

### 3-(Methoxymethoxy)-5-(trimethylstannyl)benzaldehyde (**166**)



The above compound (**166**) was prepared according to GP6 whereby, **165** (0.4 g, 1.63 mmol), hexamethyldistannane (0.70 mL, 3.36 mmol), 1,1'-Bis(diphenylphosphino)ferrocene]dichloropalladium (II) (11 mg, 0.108 mmol) and toluene (40 mL) were utilized. Yield: 28% (0.148 g, 0.016 mmol).

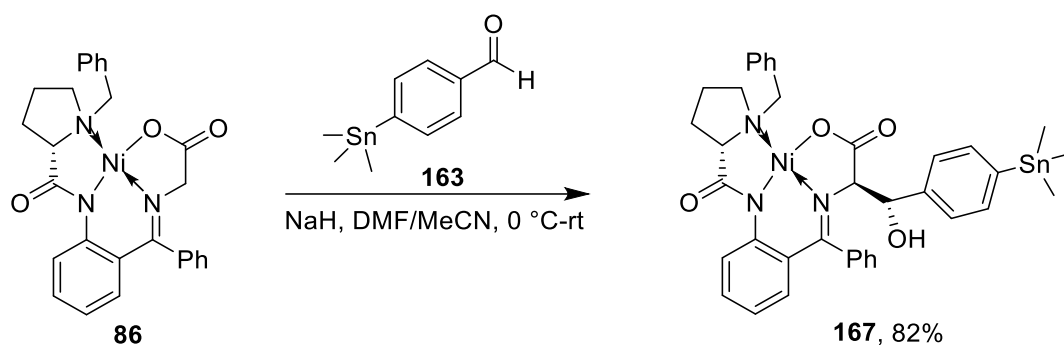
R<sub>f</sub>: 0.83 (1:10 EtOAc/hexane).

$^1\text{H}$  NMR (300 MHz,  $\text{CDCl}_3$ )  $\delta$  10.01 (s, 1H), 7.64 (s, 1H), 7.52 – 7.37 (m, 2H), 5.25 (s, 2H), 3.52 (s, 3H), 0.48 – 0.22 (m, 9H).

$^{13}\text{C}$  NMR (75 MHz,  $\text{CDCl}_3$ )  $\delta$  192.62, 157.27, 145.34, 137.02, 131.09, 130.29, 115.39, 94.45, 56.18, -9.40.

Compound **166** degraded during MS analysis.

**(*S,S*)-Ni-BPB-4-trimethylstannyl-PheSer (**167**)**



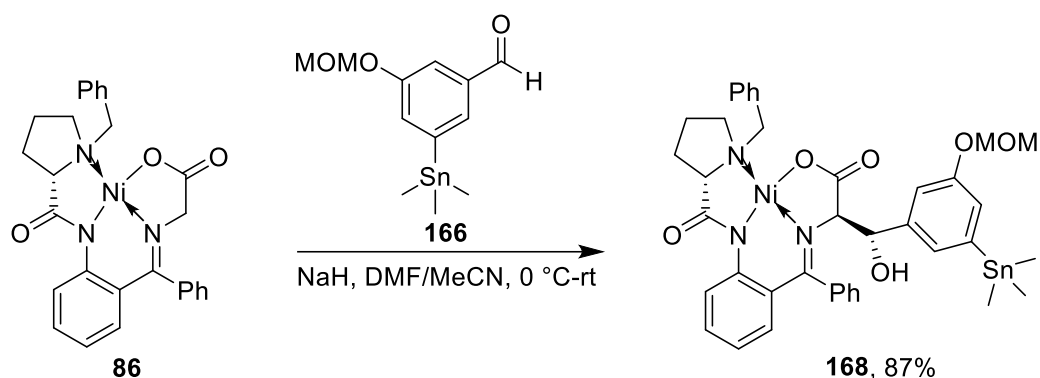
The above compound (**167**) was prepared according to GP2 whereby, **86** (0.3 g, 0.6 mmol), **163** (0.26 g, 0.967 mmol), NaH (60% suspension in mineral oil) (39 mg, 0.967 mmol) and DMF/MeCN 1:2 (30 mL) were utilized. Yield: 82% (0.378 g, 0.49 mmol).

R<sub>f</sub>: 0.38 (1:10 acetone/CHCl<sub>3</sub>).

<sup>1</sup>H NMR (300 MHz, CDCl<sub>3</sub>) δ 8.61 (d, *J* = 8.7 Hz, 1H), 7.63 (m, 5H), 7.34 (m, 7H), 7.15 (m, 3H), 6.88 (dd, *J* = 8.2, 1.4 Hz, 1H), 6.78 (t, *J* = 7.6 Hz, 1H), 4.91 (d, *J* = 9.8 Hz, 1H), 4.70 (dd, *J* = 9.8, 5.4 Hz, 1H), 4.41 (d, *J* = 5.4 Hz, 1H), 4.02 (d, *J* = 13.9 Hz, 1H), 3.54 (d, *J* = 13.9 Hz, 1H), 3.46 – 3.34 (m, 1H), 3.21 (dd, *J* = 9.8, 4.0 Hz, 1H), 2.47 (dd, *J* = 18.7, 9.8 Hz, 1H), 2.15 (td, *J* = 10.6, 6.2 Hz, 1H), 2.03 – 1.89 (m, 1H), 1.68 – 1.39 (m, 2H), 0.23 – 0.01 (m, 9H).

HRMS (ESI) *m/z* (M + H)<sup>+</sup>, C<sub>37</sub>H<sub>39</sub>N<sub>3</sub>O<sub>4</sub>NiSn<sup>+</sup> calcd. 768.13943, observed 768.13957; correct isotopic pattern.

**(*S,S*)-Ni-BPB-3-trimethylstannyl-5-MOMO-PheSer (168)**



The above compound (**168**) was prepared according to GP1 whereby, **86** (0.14 g, 0.28 mmol), **166** (148 mg, 0.45 mmol), NaH (60% suspension in mineral oil) (18 mg, 0.45 mmol) and DMF/MeCN 1:2 (30 mL) were utilized. Yield: 87% (201.6 mg, 0.24 mmol).

R<sub>f</sub>: 0.58 (1:10 acetone/CHCl<sub>3</sub>).

<sup>1</sup>H NMR (300 MHz, CDCl<sub>3</sub>) δ 8.57 (d, *J* = 8.6 Hz, 1H), 7.50 (m, 3H), 7.34 – 7.17 (m, 6H), 7.17 – 7.04 (m, 4H), 6.99 (s, 1H), 6.80 (dd, *J* = 8.2, 1.4 Hz, 1H), 6.75 – 6.66 (m, 1H), 4.98 – 4.85 (m, 2H), 4.62 (s, 1H), 4.33 (d, *J* = 5.5 Hz, 1H), 3.89 (d, *J* = 13.9 Hz, 1H), 3.55 – 3.38 (m, 2H), 3.27 – 3.14 (m, 4H), 2.36 – 2.18 (m, 3H), 1.85 (t, *J* = 9.2 Hz, 1H), 1.48 – 1.32 (m, 2H), 0.12 – -0.12 (m, 9H).

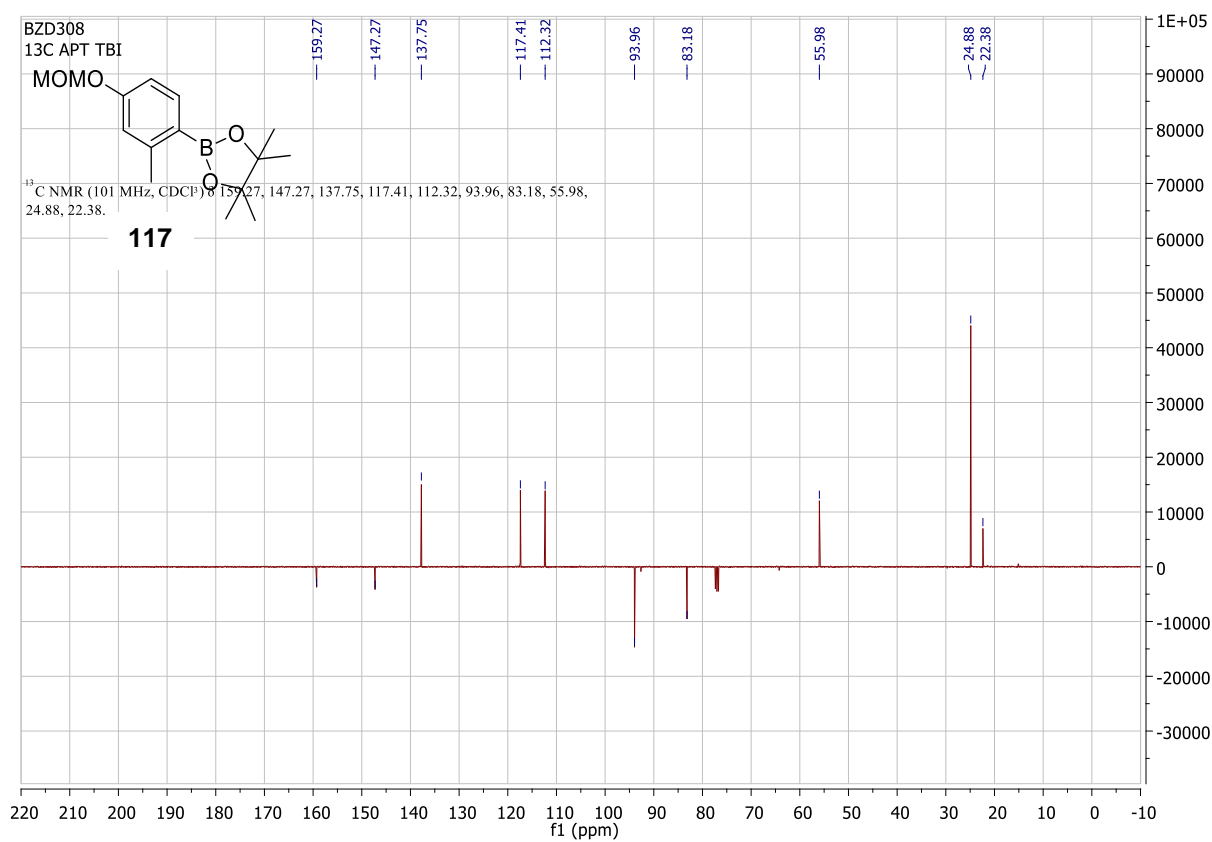
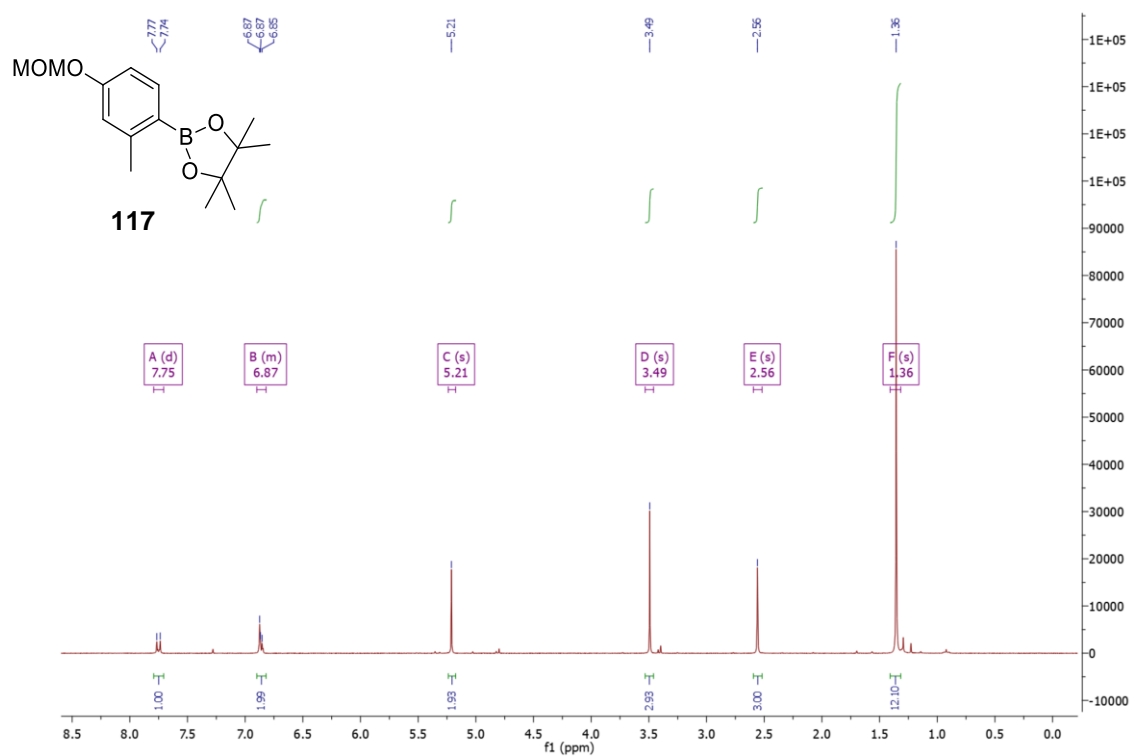
<sup>13</sup>C NMR (75 MHz, CDCl<sub>3</sub>) δ 181.19, 178.17, 172.77, 157.37, 144.53, 143.55, 140.82, 133.99, 133.97, 133.00, 132.19, 130.91, 130.23, 129.38, 128.75, 128.26, 127.97, 126.80, 125.58, 123.84, 123.47, 120.79, 115.67, 94.60, 73.81, 73.17, 67.50, 59.19, 55.96, 54.65, 31.28, 23.69, -9.67.

Compound **168** degraded during MS analysis.

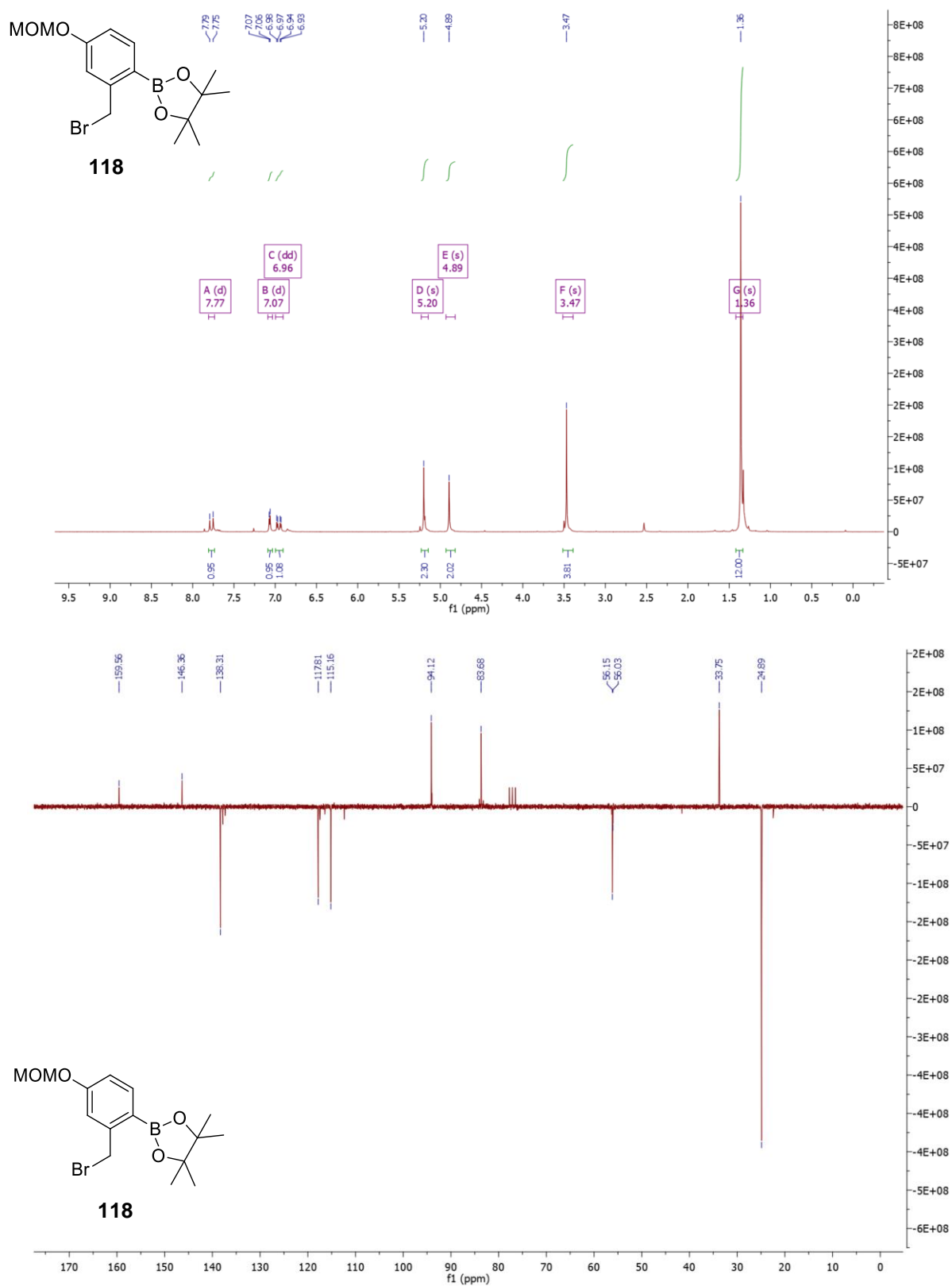
## 6. NMR Spectra

2-(4-(Methoxymethoxy)-2-methylphenyl)-4,4,5,5-tetramethyl-1,3,2-dioxaborolane (**117**)  $^1\text{H}$  NMR ( $\text{CDCl}_3$ )

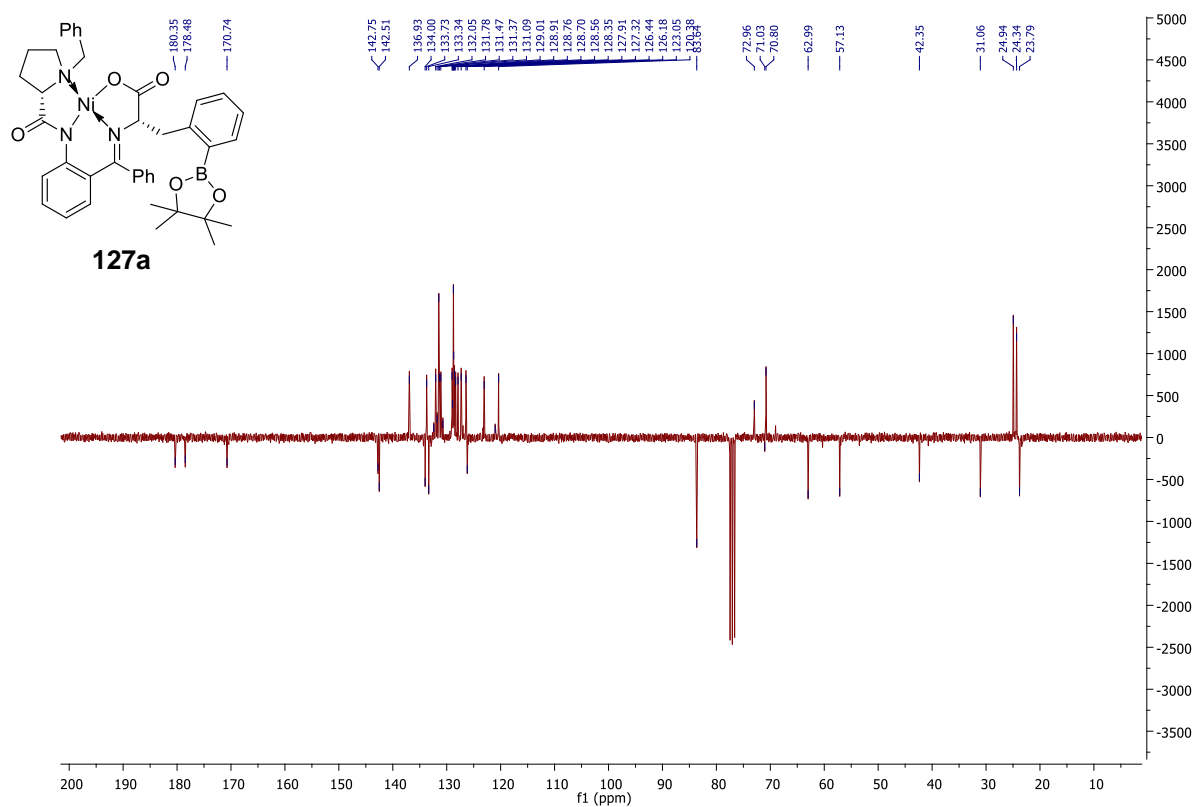
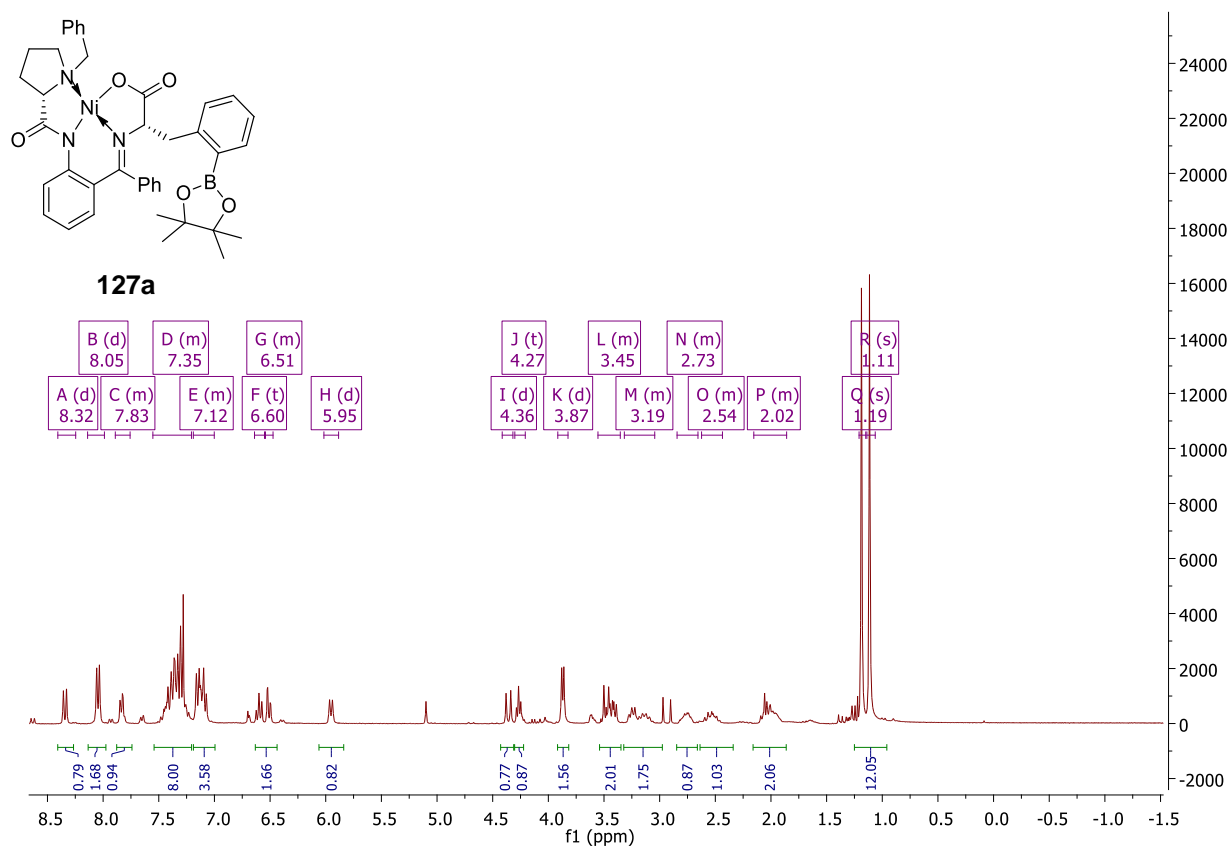
$^1\text{H}$  NMR (400 MHz)



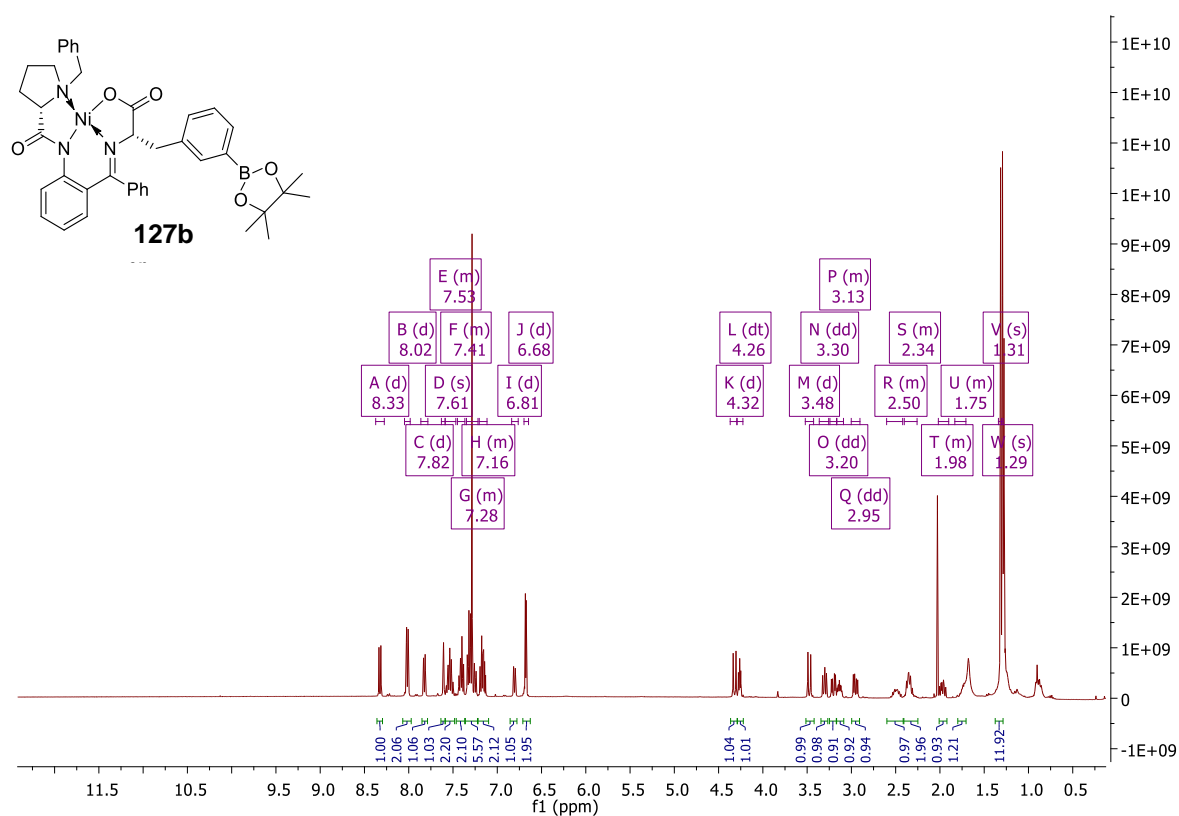
**2-(2-(Bromomethyl)-4-(methoxymethoxy)phenyl)-4,4,5,5-tetramethyl-1,3,2-dioxaborolane (118)** (CDCl<sub>3</sub>) <sup>1</sup>H NMR (400 MHz) <sup>13</sup>C NMR (101 MHz)



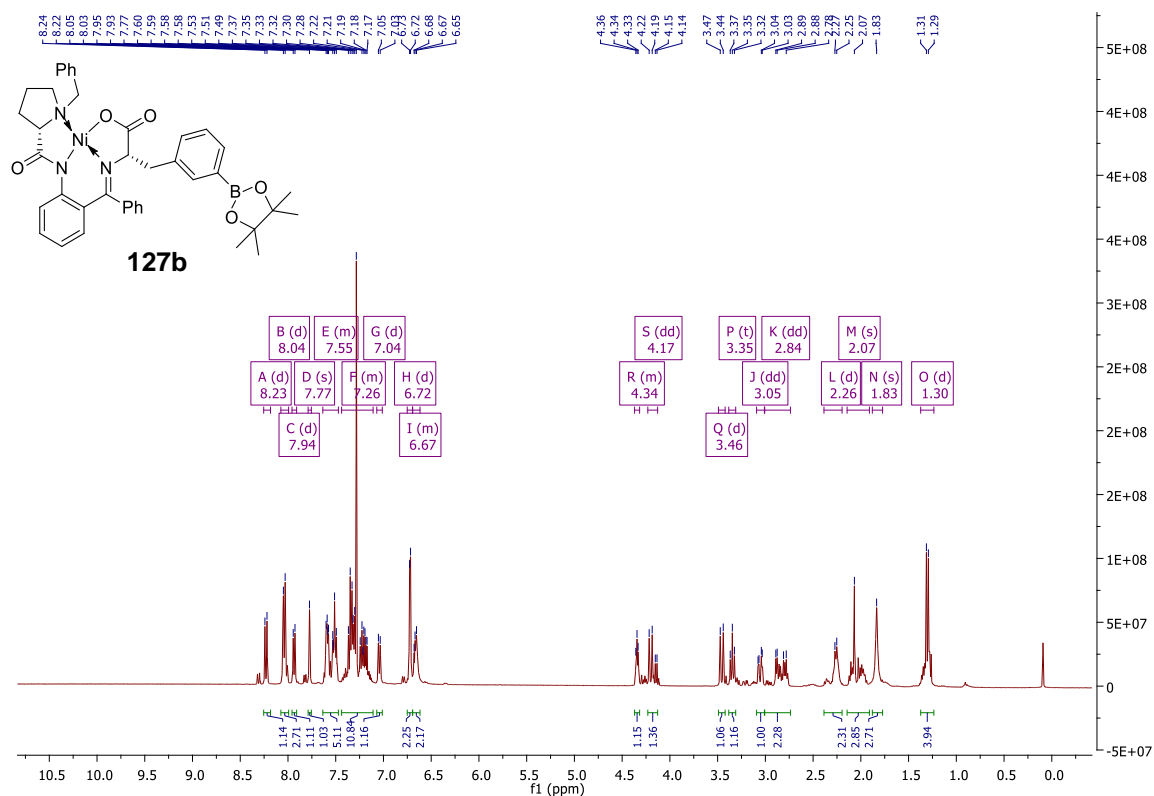
**(*S,S*)-Ni-BPB-2-BpinPhe (127a)** (CDCl<sub>3</sub>) <sup>1</sup>H NMR (300 MHz, CDCl<sub>3</sub>) and <sup>13</sup>C NMR (75 MHz)

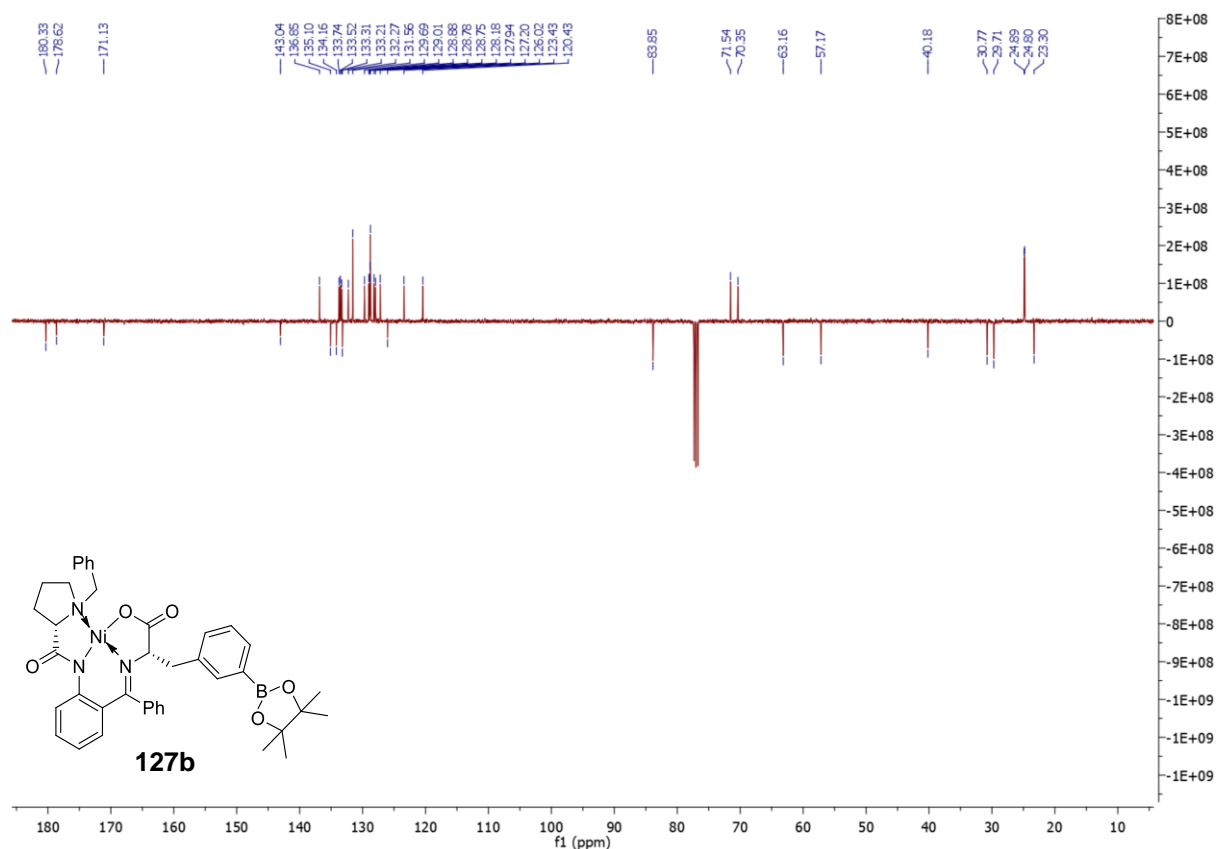


**(*S,S*)-Ni-BPB-3-BpinPhe (127b) (CDCl<sub>3</sub>) <sup>1</sup>H NMR (400 MHz)**

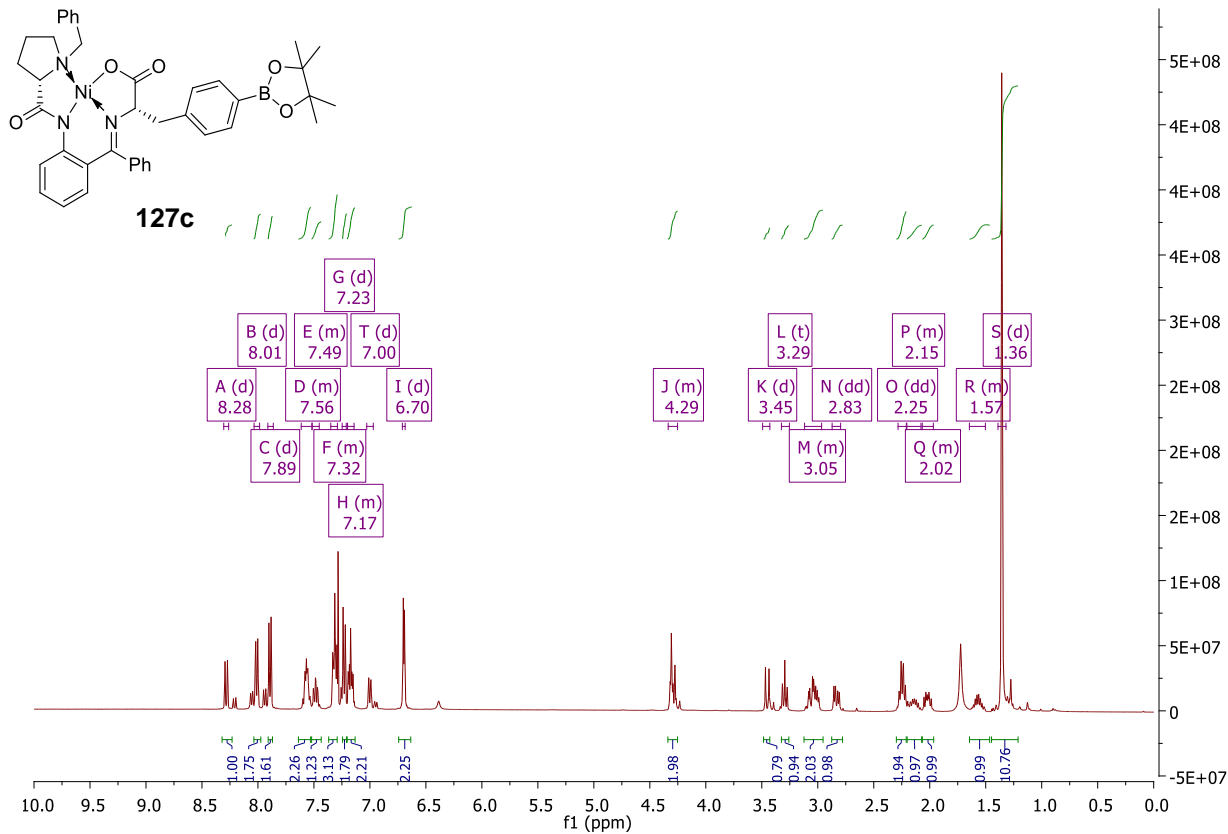


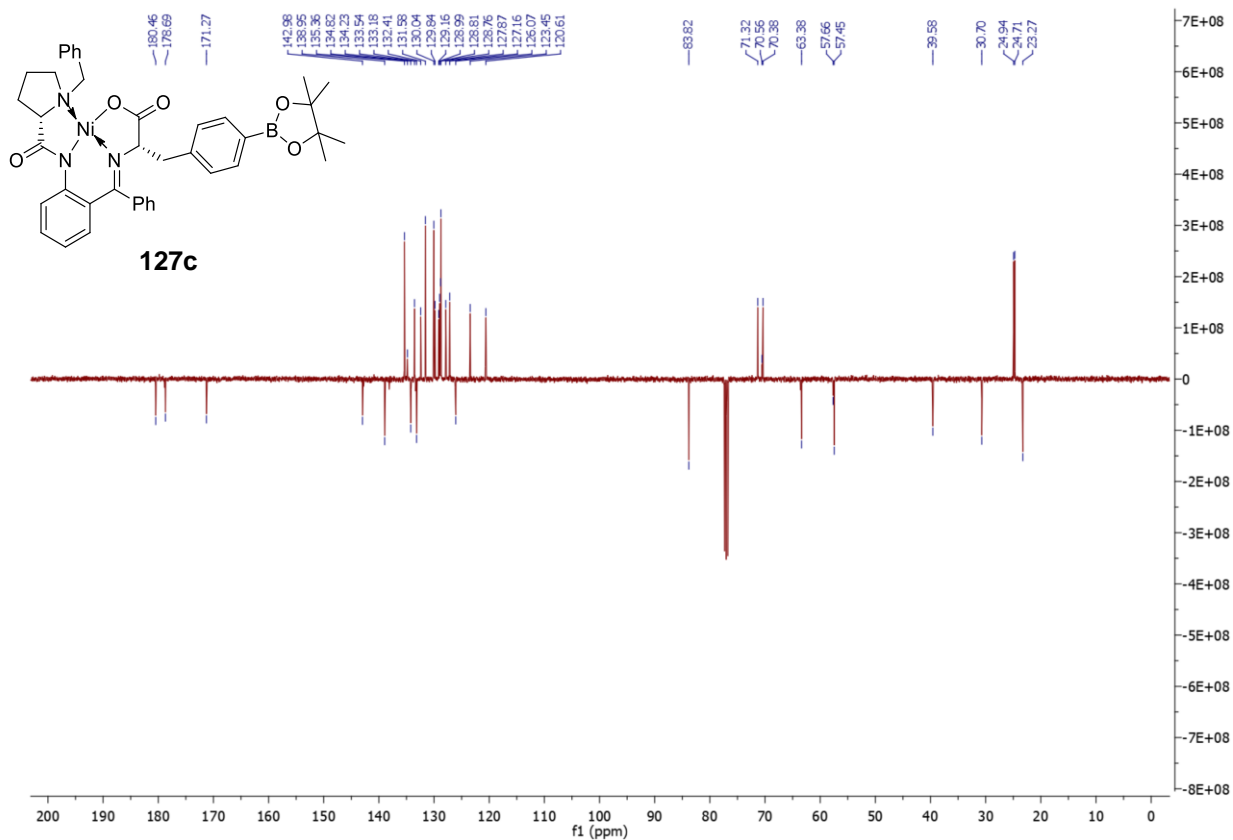
**(*S,S*)-Ni-BPB-3-BpinPhe (127b) (Following RP Purification) (CDCl<sub>3</sub>) <sup>1</sup>H NMR (400 MHz) <sup>13</sup>C NMR (101 MHz)**



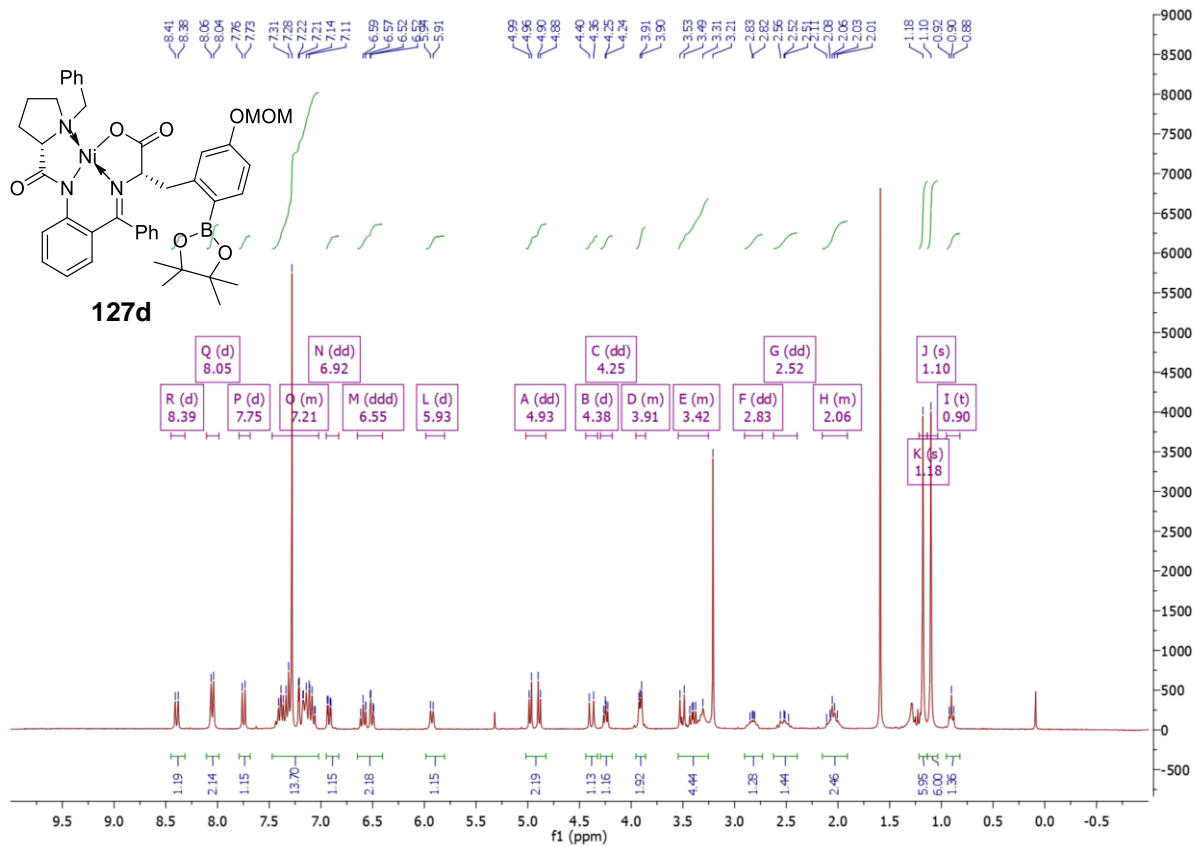


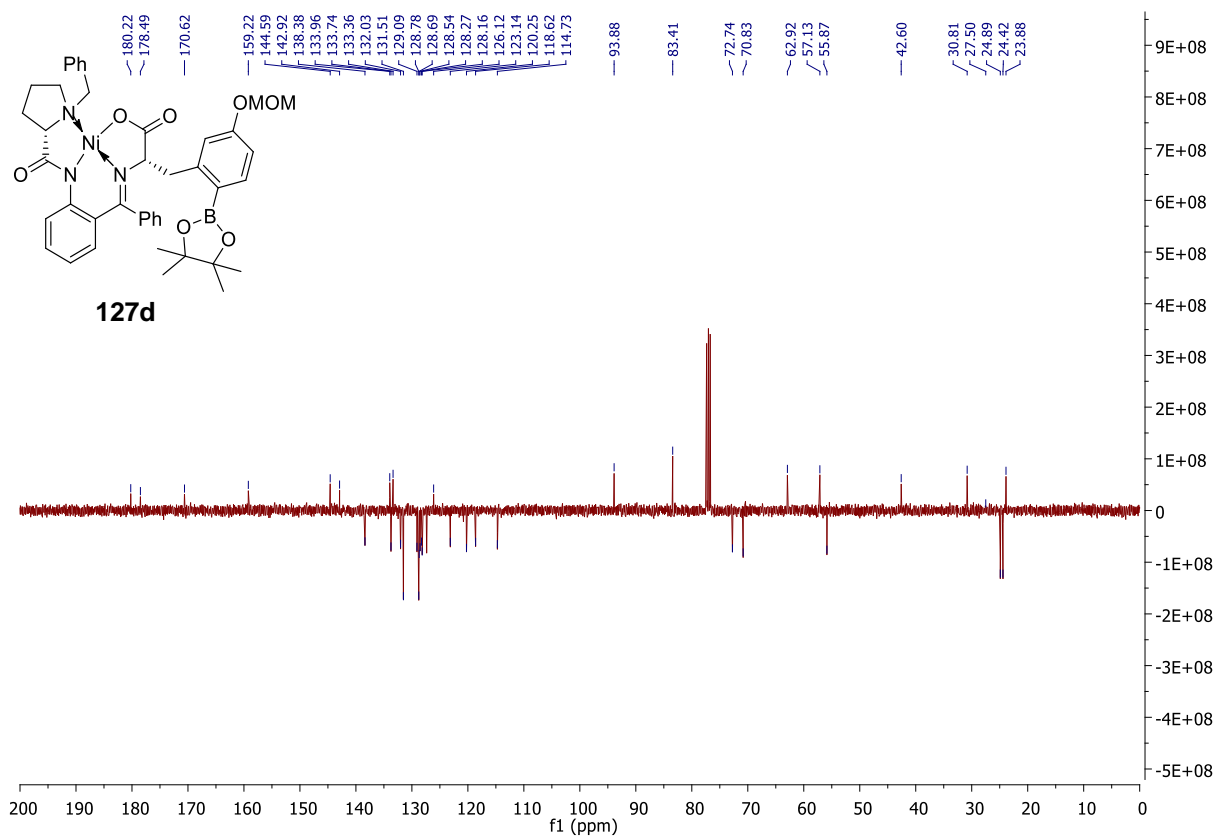
**(*S,S*)-Ni-BPB-4-BpinPhe (127c) (CDCl<sub>3</sub>) <sup>1</sup>H NMR (400 MHz) <sup>13</sup>C NMR (101 MHz)**



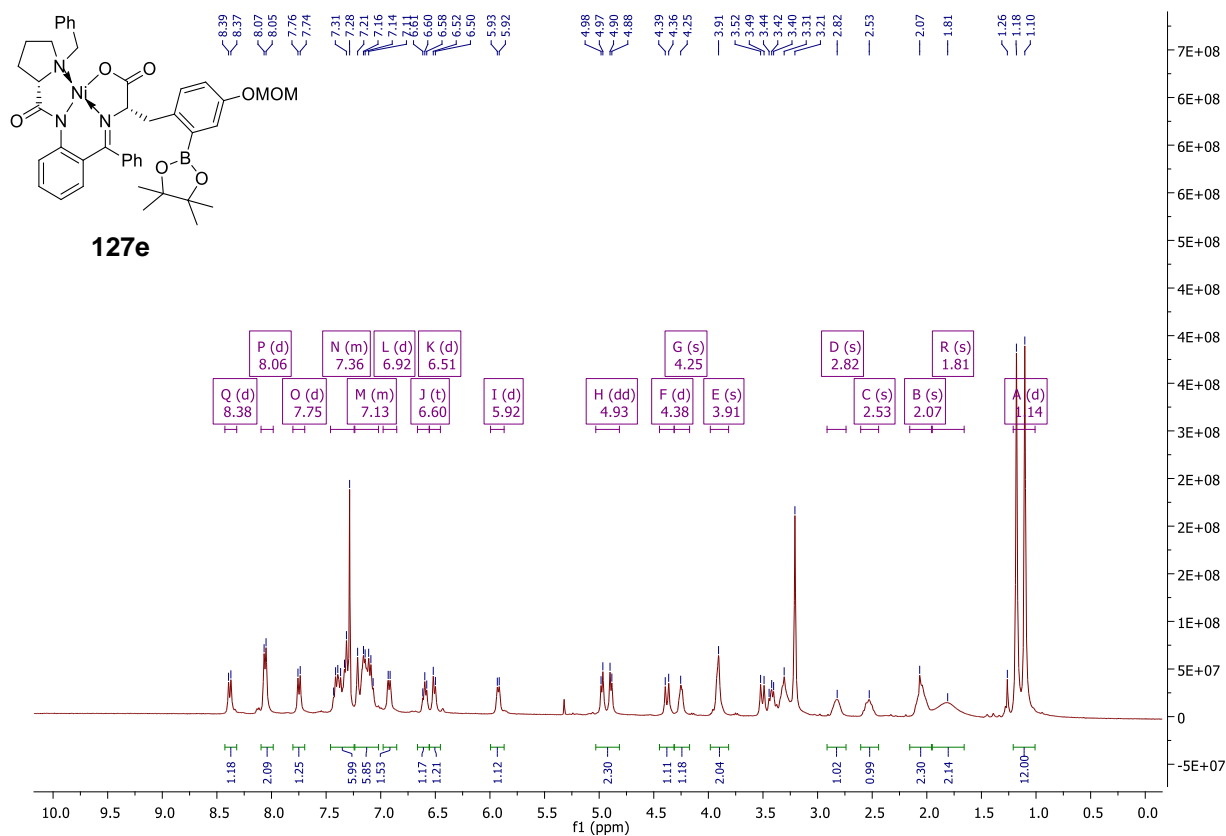


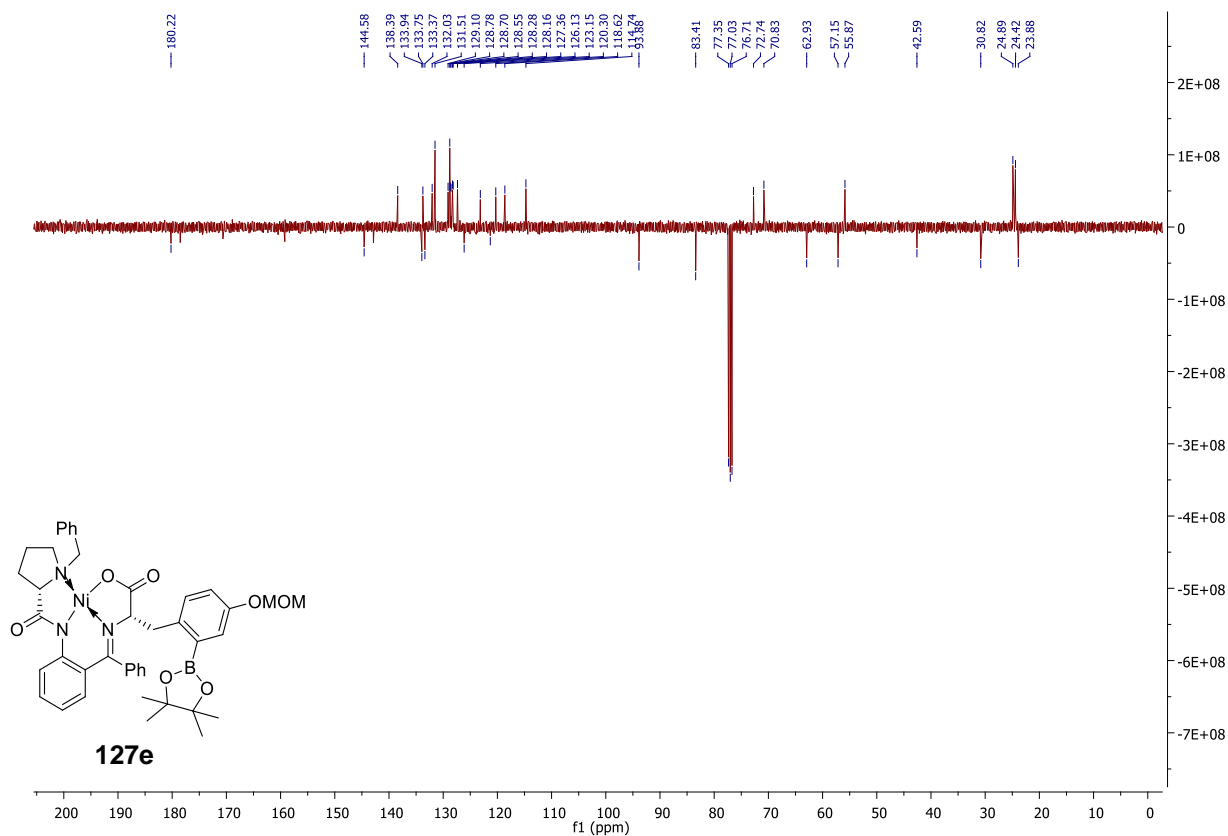
**(*S,S*)-Ni-BPB-2-Bpin-5-MOMO-Phe (127d)** (CDCl<sub>3</sub>) <sup>1</sup>H NMR (400 MHz) <sup>13</sup>C NMR (101 MHz)



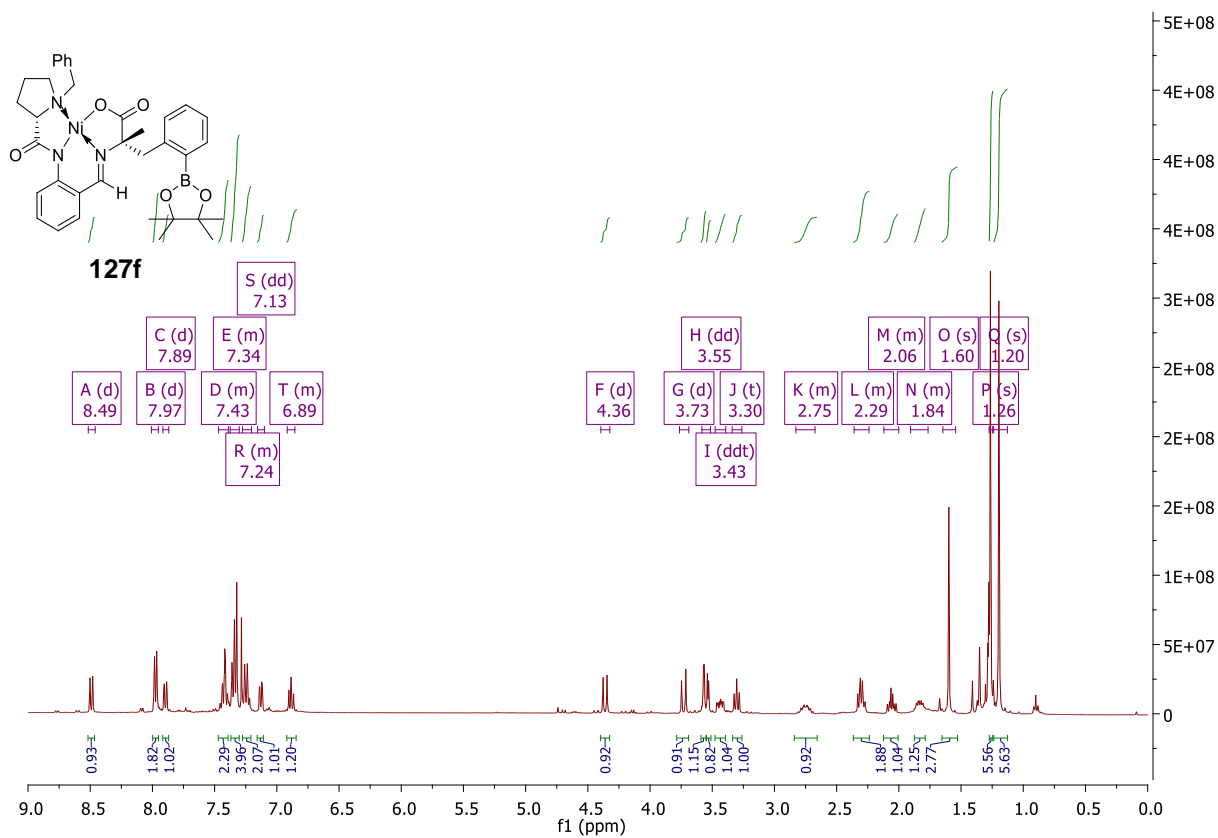


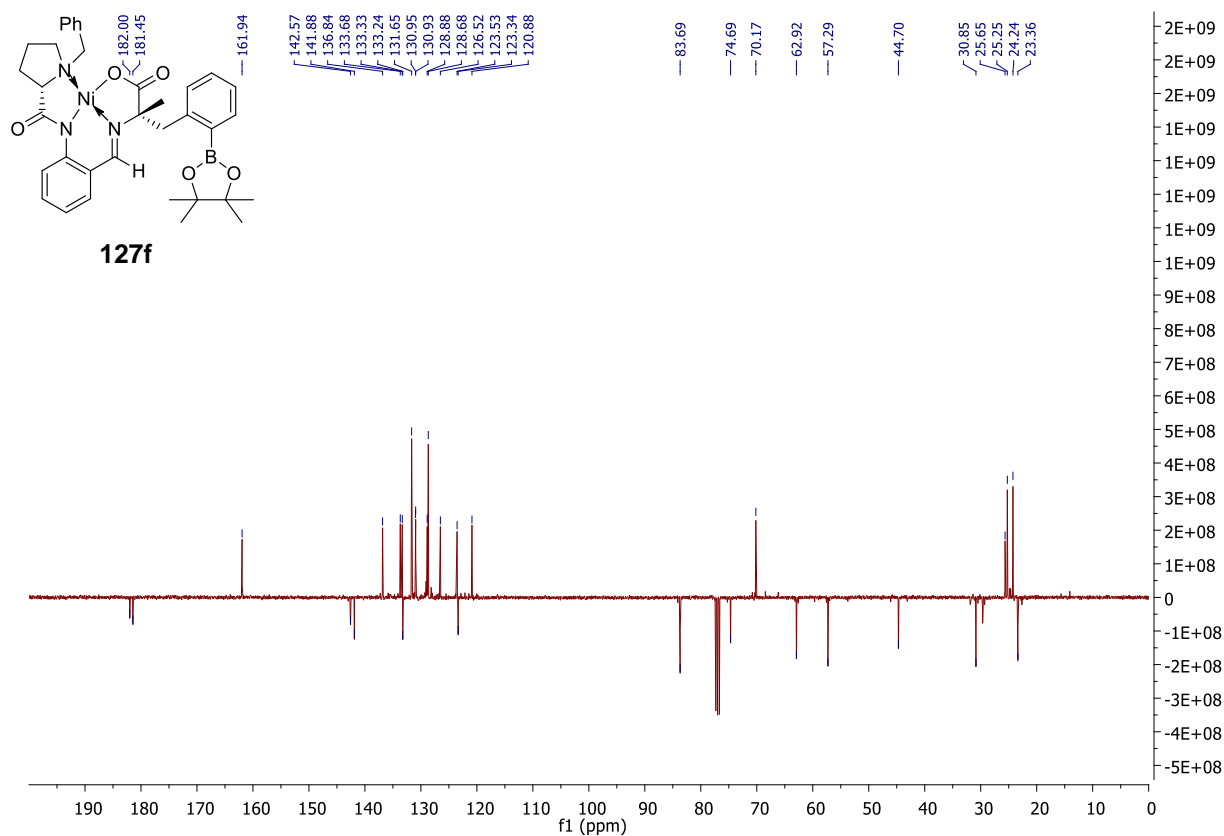
**(S,S)-Ni-BPB-2-Bpin-OMOM-Tyr (127e)** (CDCl<sub>3</sub>) <sup>1</sup>H NMR (400 MHz) <sup>13</sup>C NMR (101 MHz)



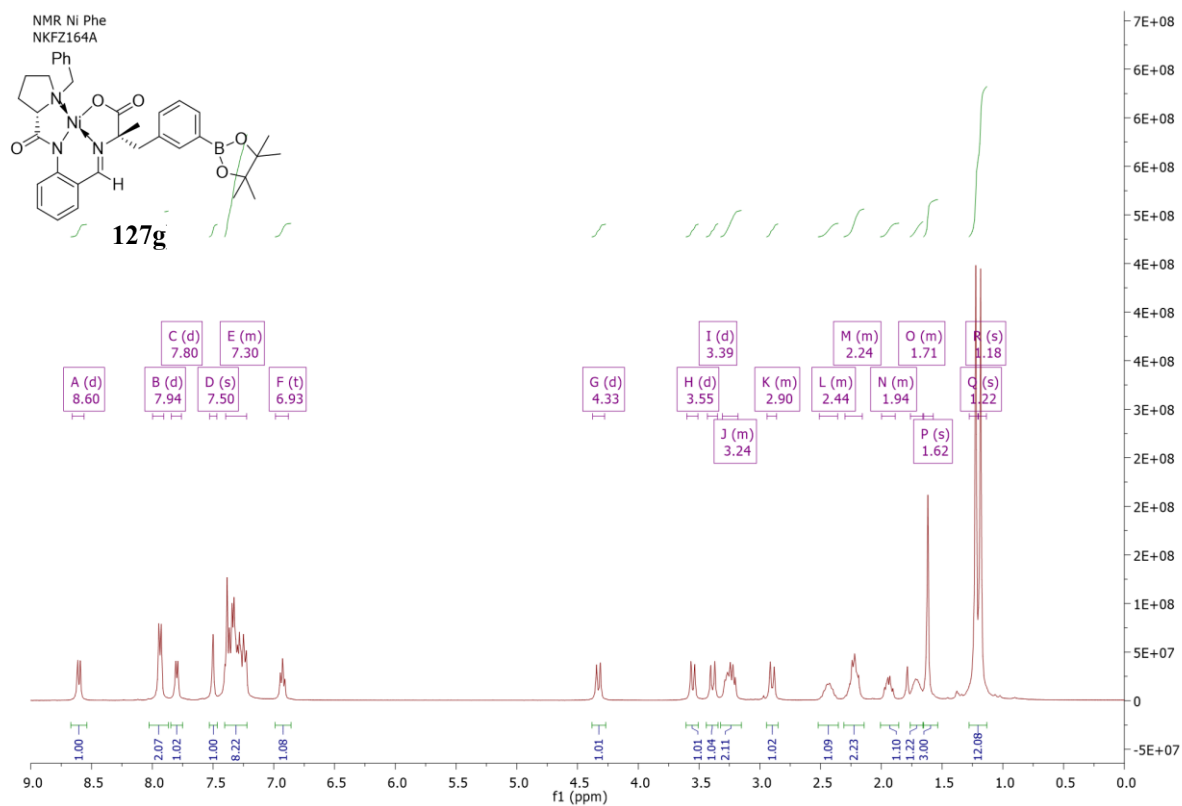


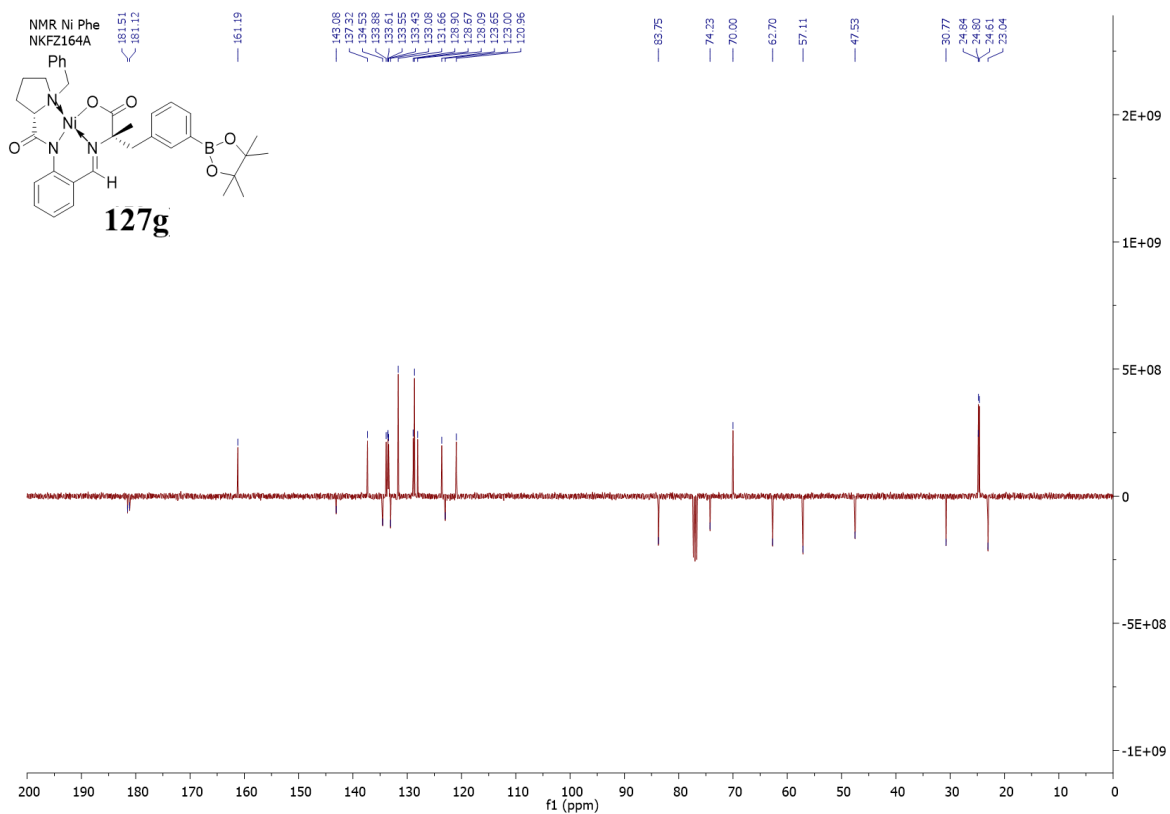
**(S,S)-Ni-BPA-2-BpinPhe (127f) (CDCl<sub>3</sub>) <sup>1</sup>H NMR (400 MHz) <sup>13</sup>C NMR (101 MHz)**



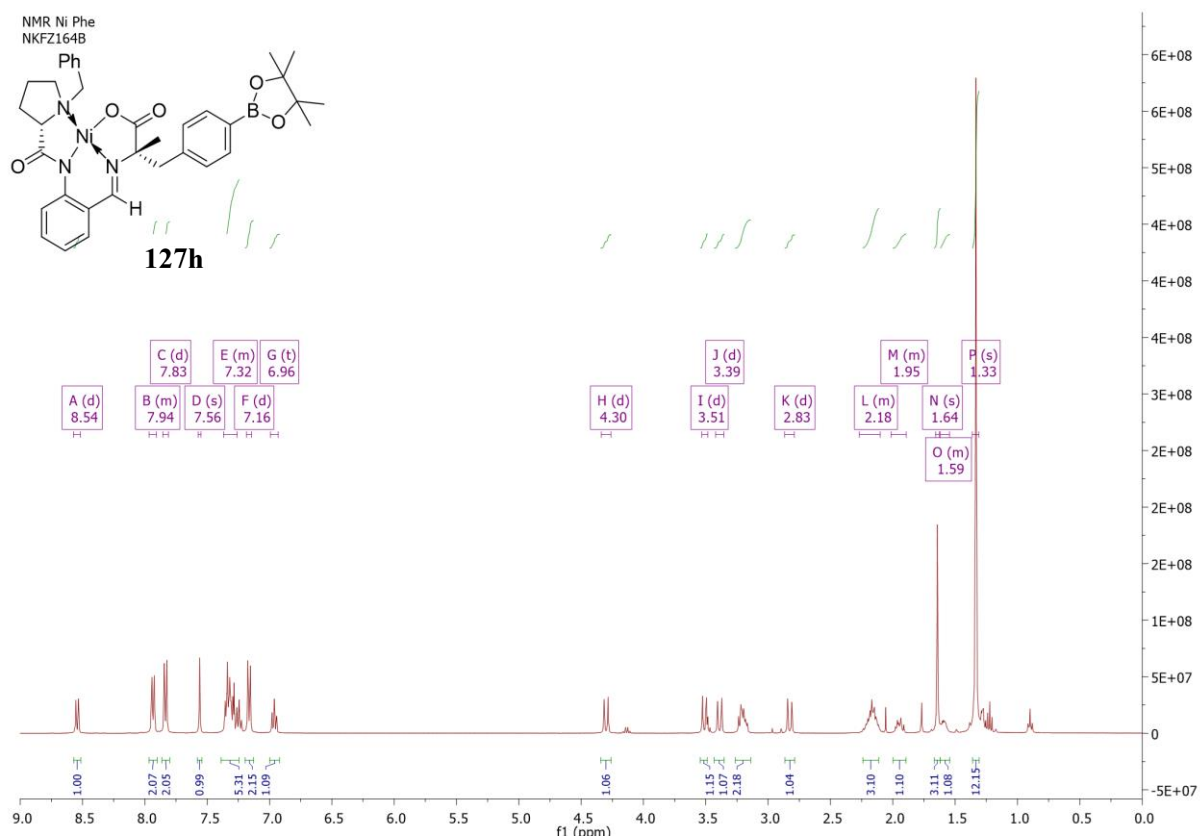


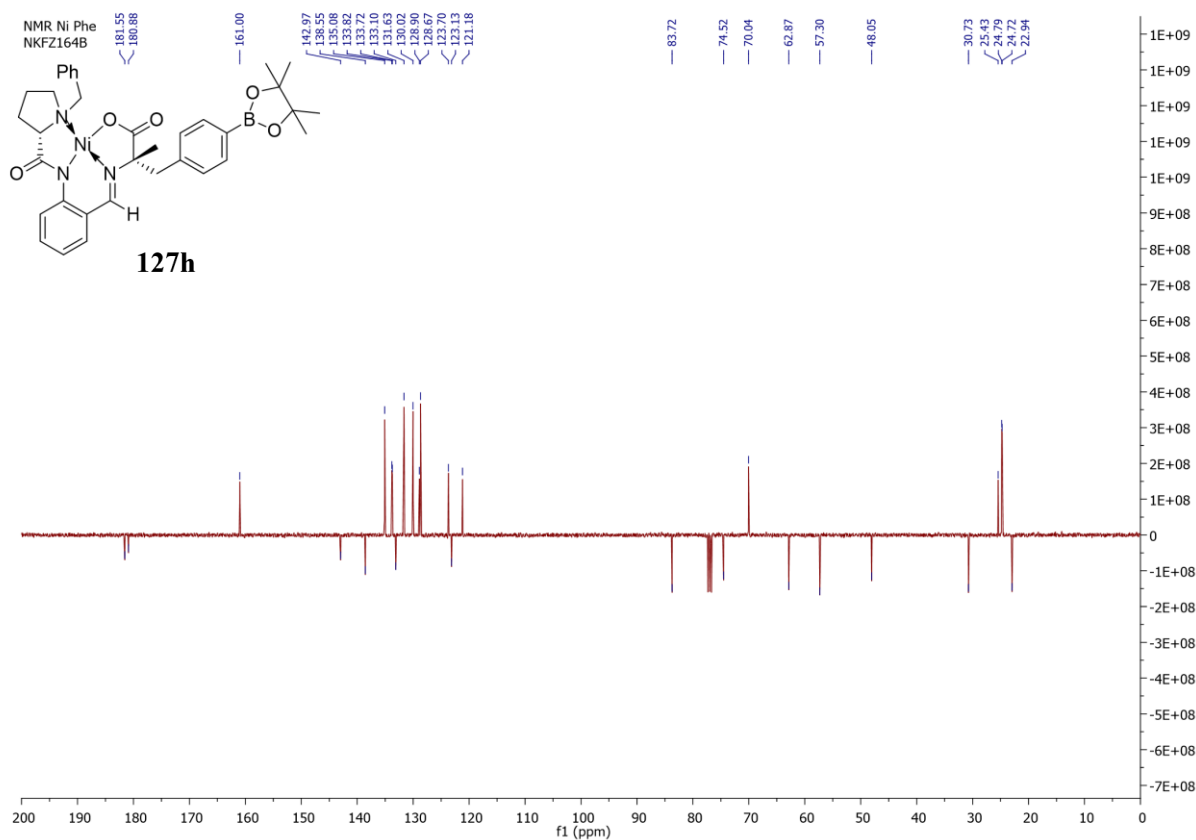
**(*S,S*)-Ni-BPA-3-BpinPhe (127g)** (CDCl<sub>3</sub>) <sup>1</sup>H NMR (400 MHz) <sup>13</sup>C NMR (101 MHz)



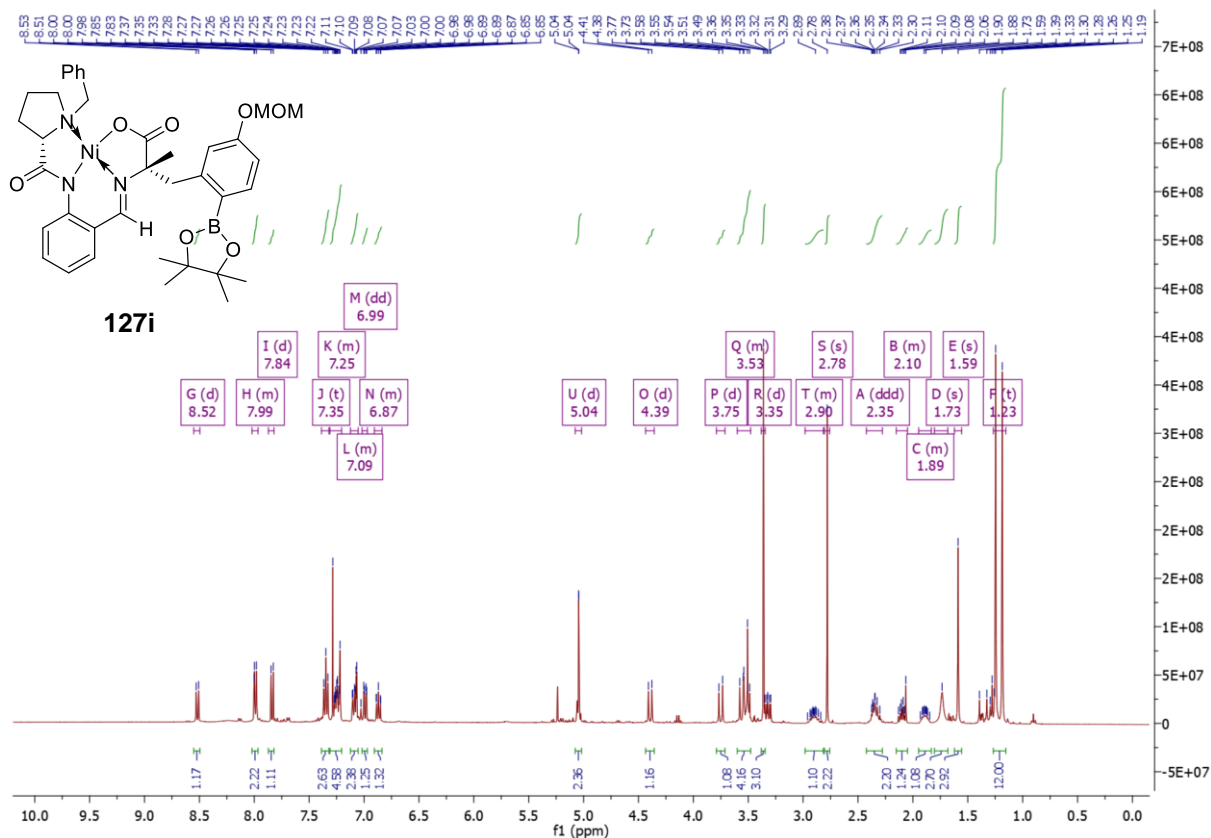


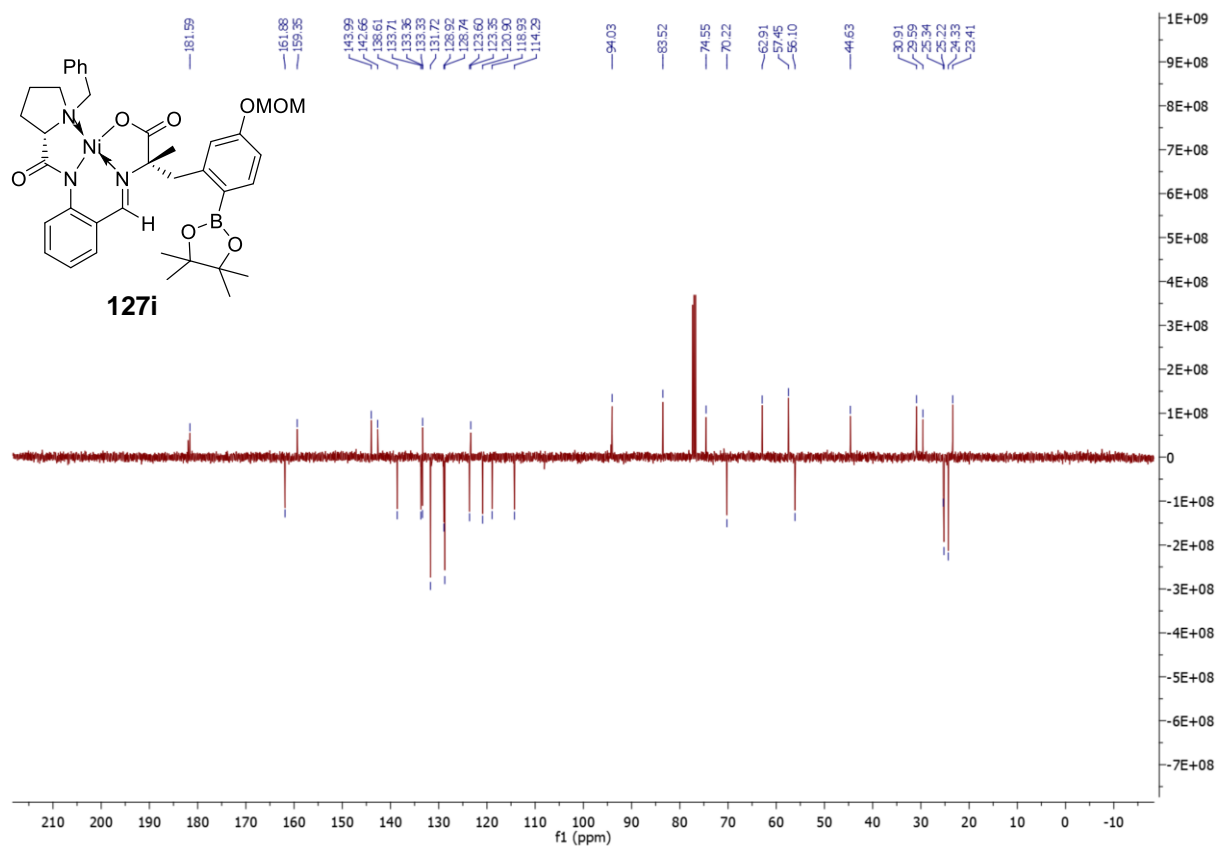
**(*S,S*)-Ni-BPA-4-BpinPhe (127h) (CDCl<sub>3</sub>) <sup>1</sup>H NMR (400 M Hz) <sup>13</sup>C NMR (101 MHz)**



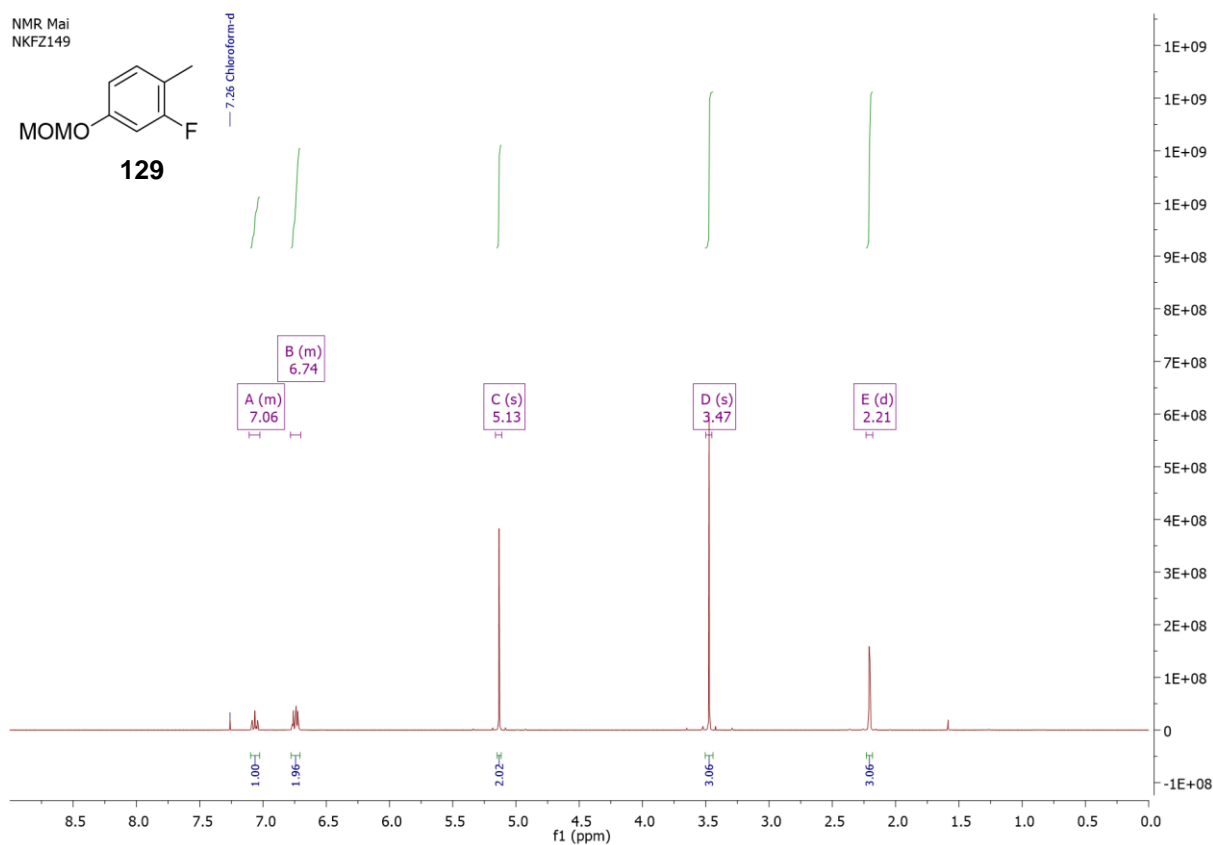


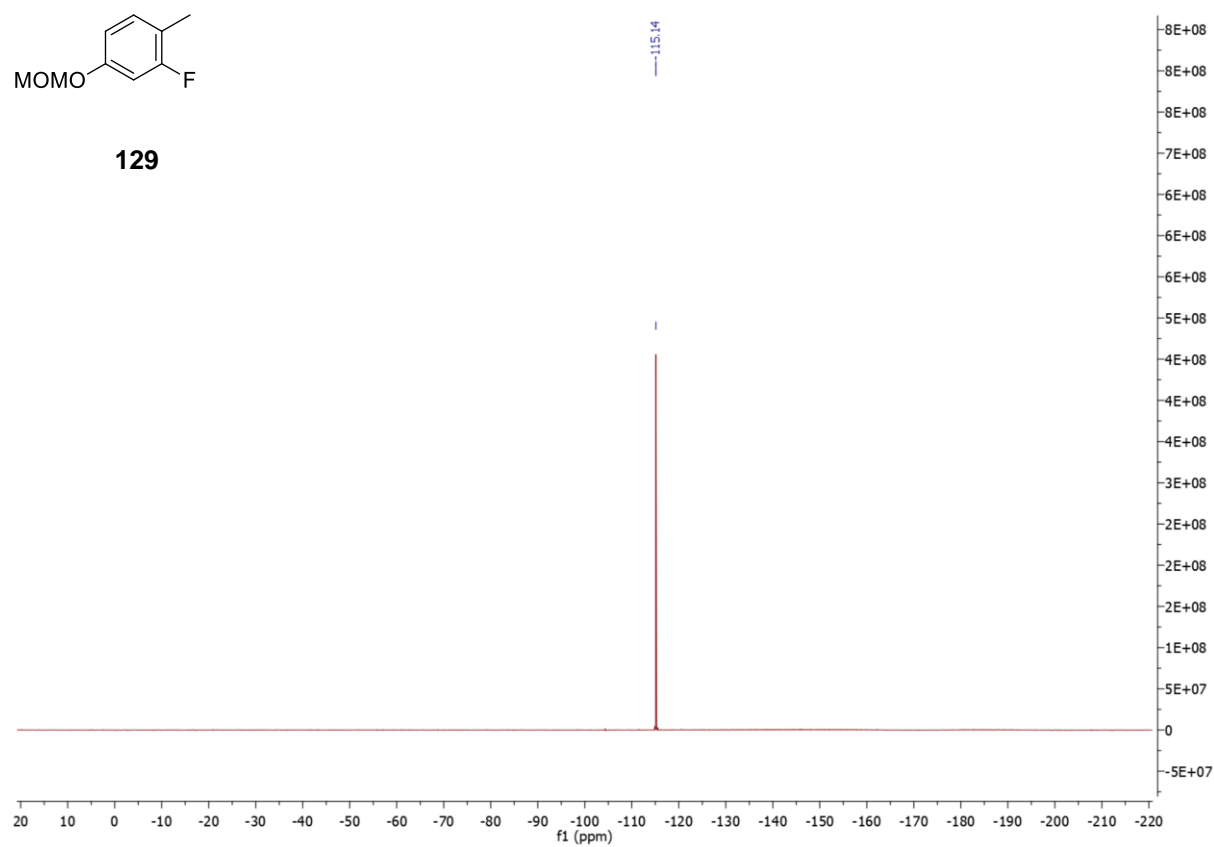
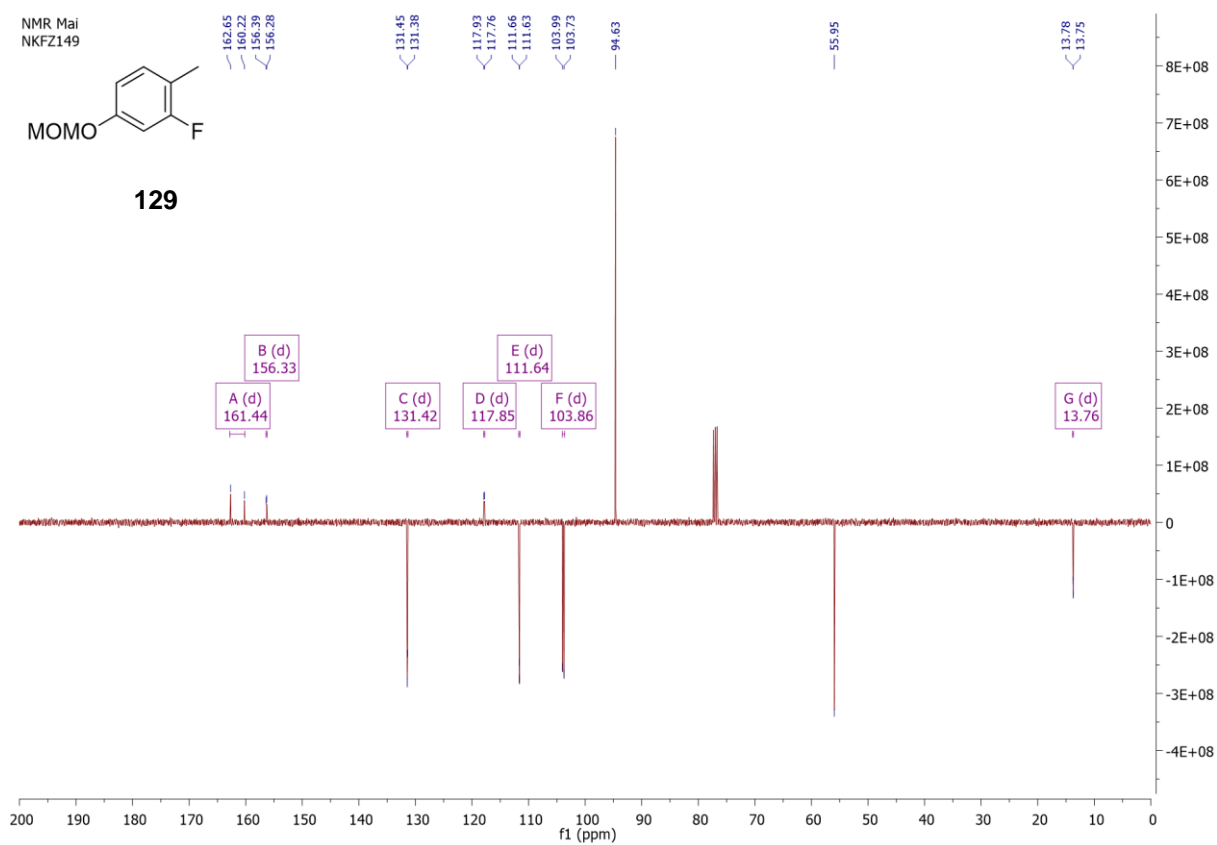
**(S,S)-Ni-BPA-2-Bpin-5-MOMO-Phe (127i)** (CDCl<sub>3</sub>) <sup>1</sup>H NMR (400 MHz) <sup>13</sup>C NMR (101 MHz)





**1-Fluoro-4-(methoxymethoxy)-2-methylbenzene (129)** ( $\text{CDCl}_3$ )  $^1\text{H}$  NMR (400 MHz),  $^{13}\text{C}$  NMR (101 MHz),  $^{19}\text{F}$  NMR (376 MHz)





**134a**

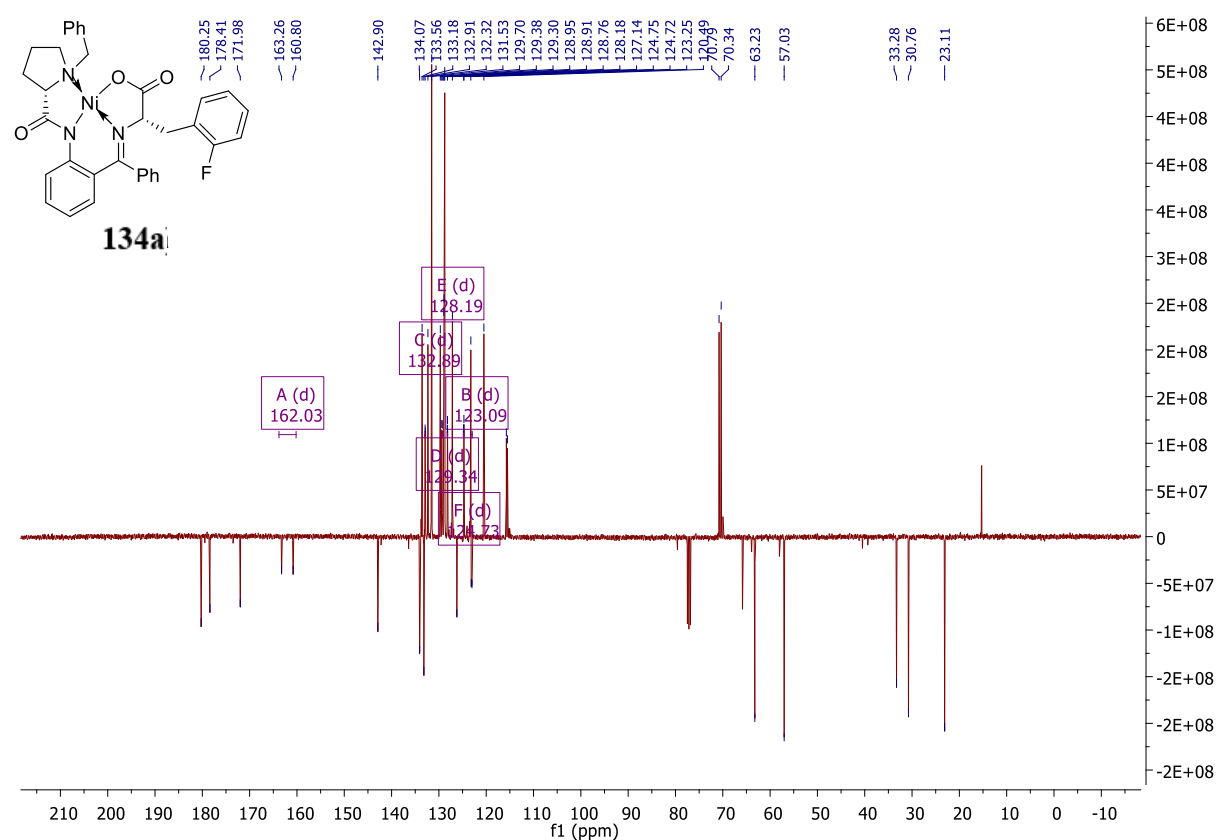
Chemical structure of **134a** is shown. The spectrum displays peaks from 0 to 10 ppm with corresponding integrations and peak labels.

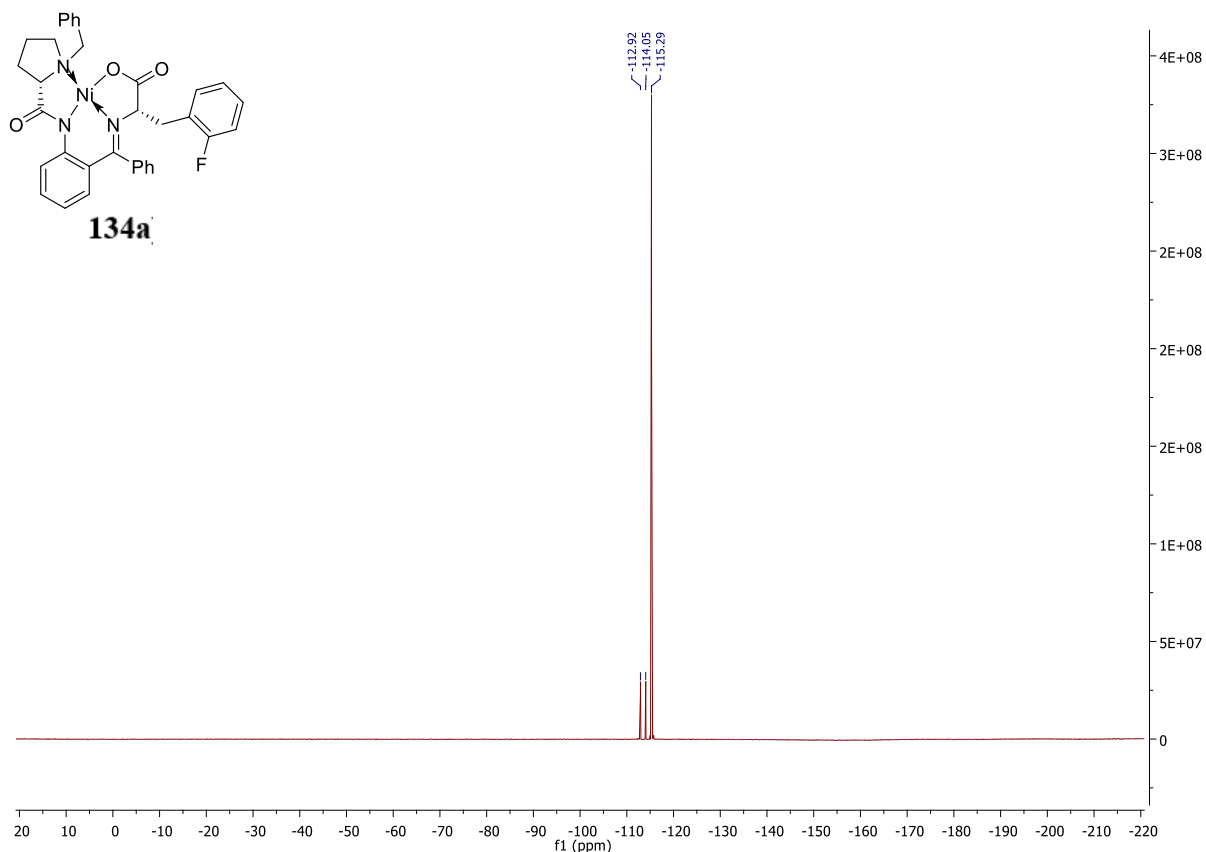
Chemical shifts (ppm): 8.29, 8.27, 8.00, 7.98, 7.54, 7.52, 7.51, 7.49, 7.45, 7.44, 7.43, 7.41, 7.40, 7.38, 7.36, 7.35, 7.32, 7.30, 7.28, 7.27, 7.25, 7.19, 7.17, 7.15, 7.14, 7.13, 7.12, 7.11, 6.99, 6.97, 6.66, 6.65, 4.30, 4.29, 4.28, 4.27, 3.51, 3.50, 3.48, 3.46, 3.45, 3.43, 3.31, 3.29, 3.19, 3.18, 3.16, 3.15, 3.12, 3.11, 3.09, 3.08, 2.98, 2.97, 2.94, 2.93, 2.92, 2.37, 2.35, 2.34, 2.33, 1.96, 1.95, 1.93, 1.69, 1.68, 1.67, 1.22, 1.20, 1.18.

Peak labels and integrations:

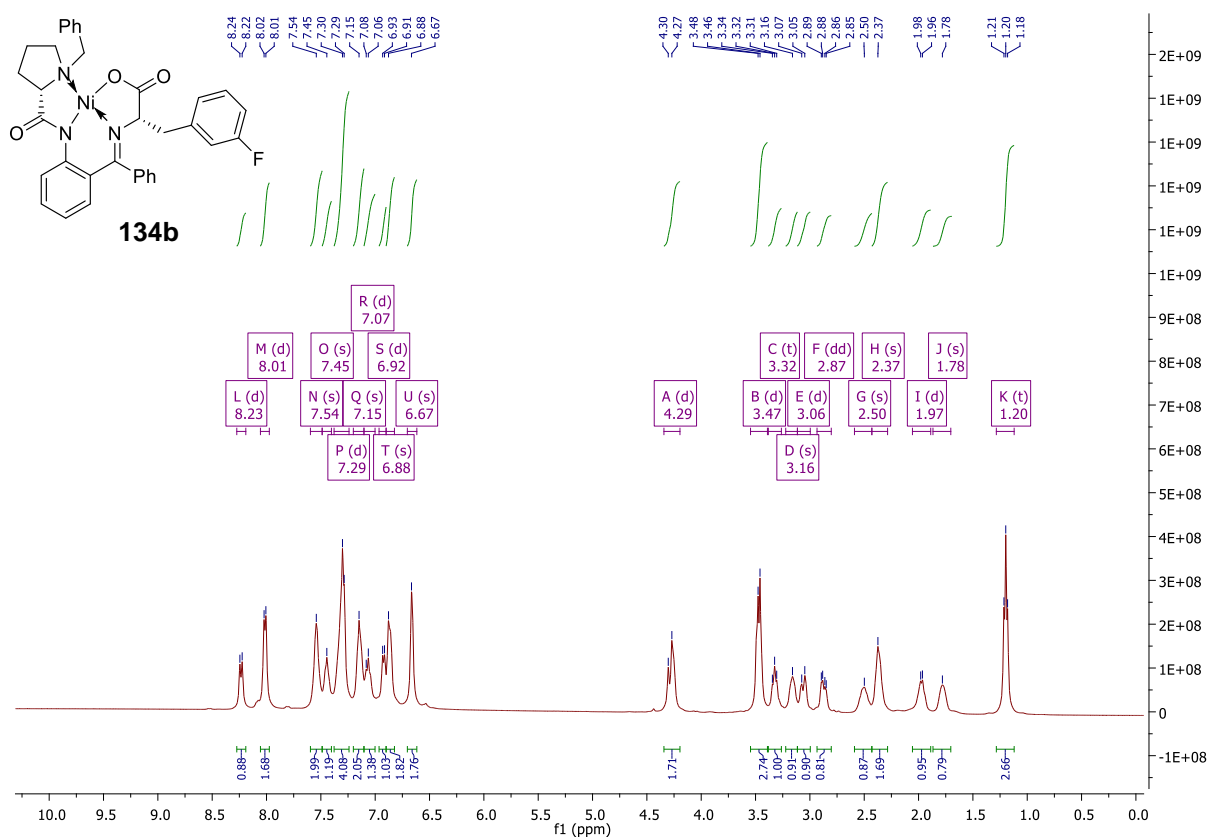
- J (d) 8.28
- K (d) 7.99
- L (m) 7.52
- M (m) 7.42
- N (m) 7.36
- O (m) 7.29
- P (ddd) 7.15
- Q (d) 6.98
- R (d) 6.65
- A (dd) 4.29
- B (dt) 3.48
- C (t) 3.31
- D (m) 3.13
- E (dd) 2.95
- F (m) 2.34
- G (dd) 1.94
- H (m) 1.69
- I (t) 1.20

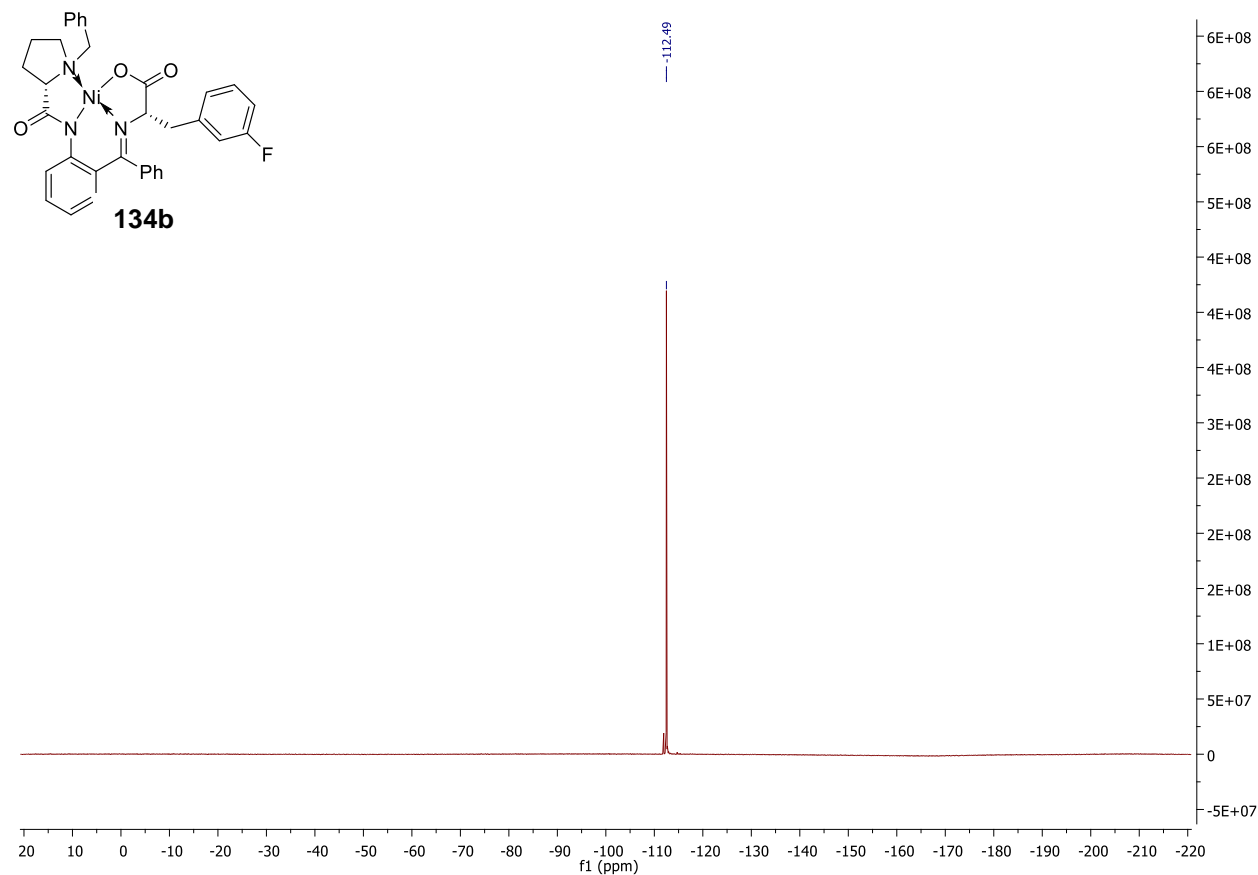
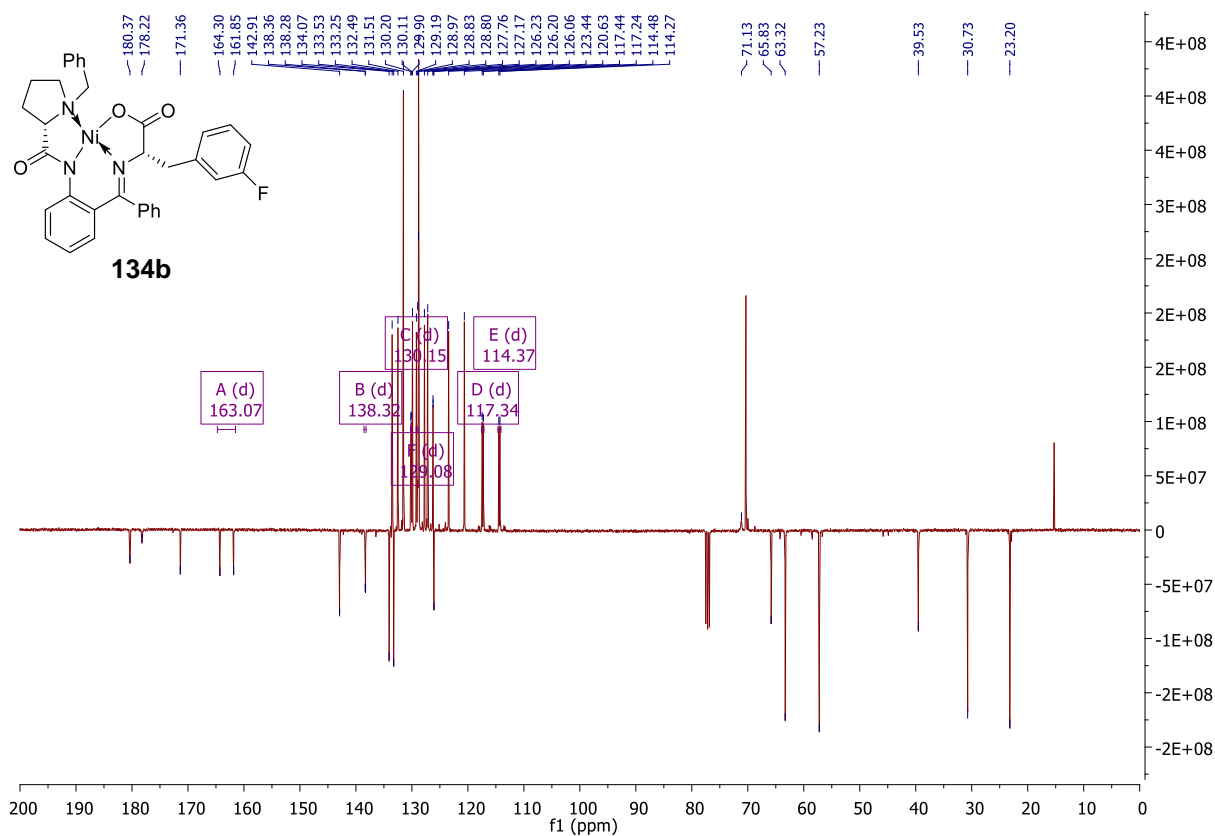
Integrations (from left to right): 1.13, 2.25, 2.42, 1.60, 1.34, 5.17, 5.10, 1.19, 2.14, 2.21, 2.97, 1.17, 2.33, 1.05, 3.18, 1.00, 1.03, 2.75.



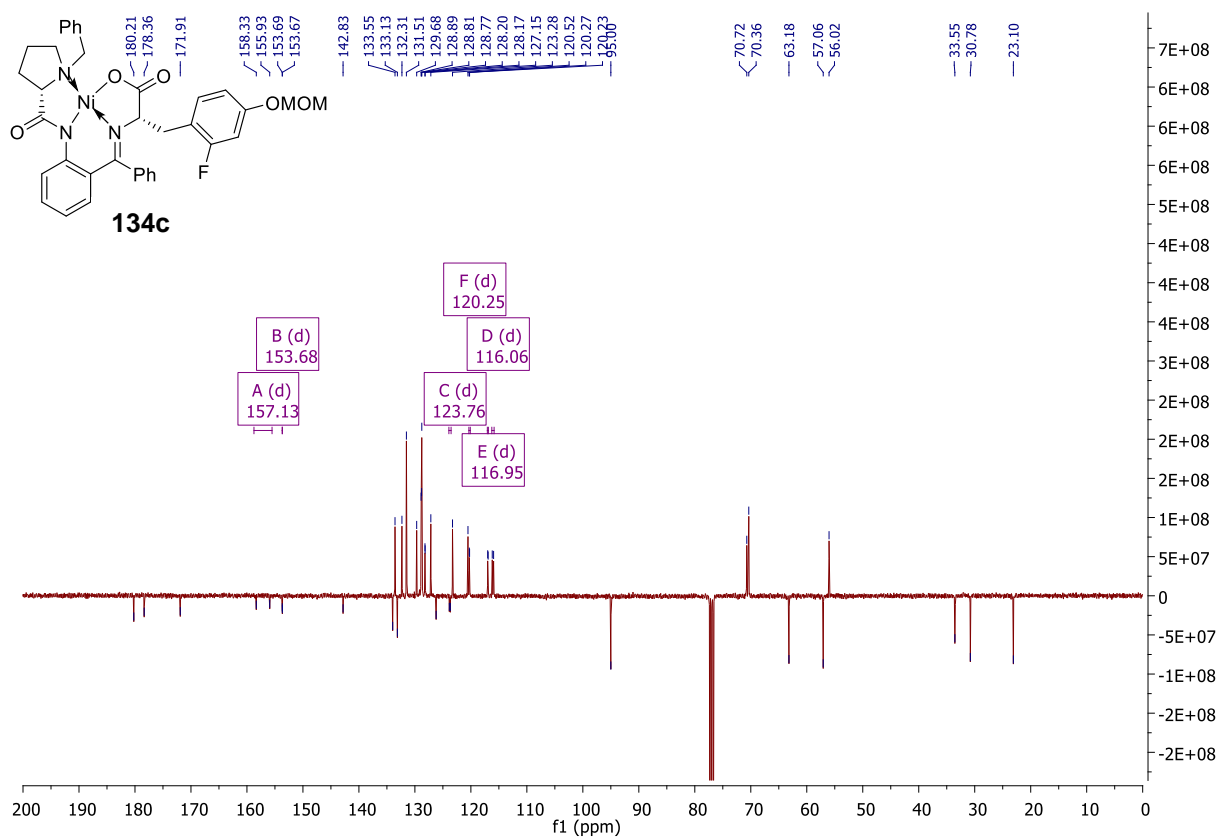
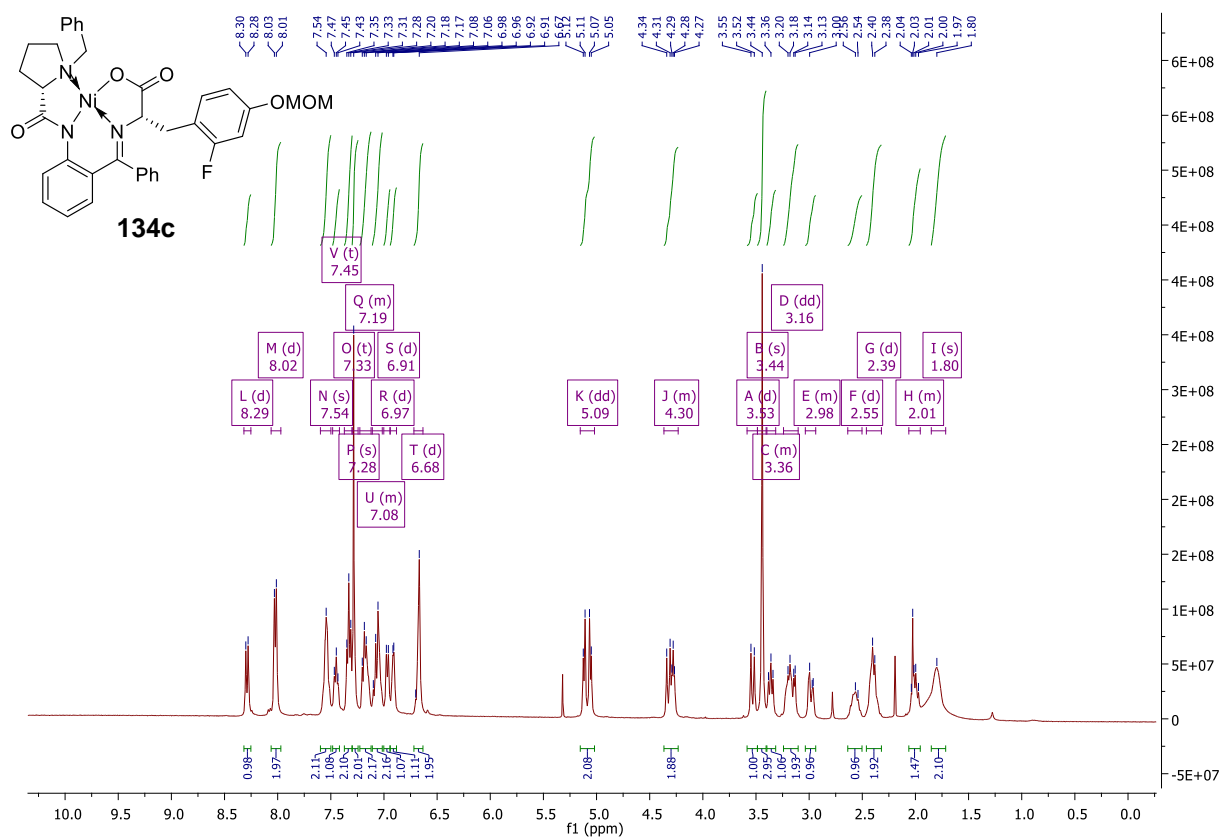


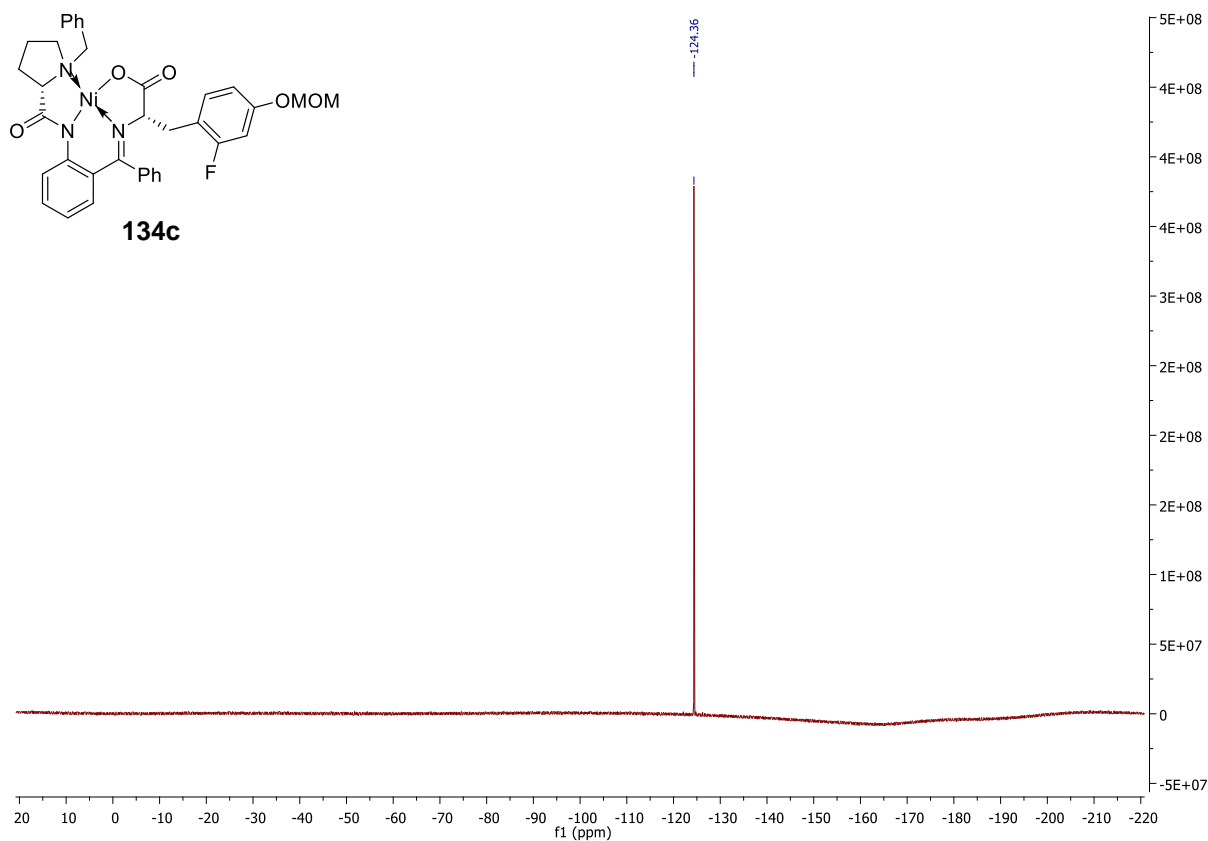
**(*S,S*)-Ni-BPB-3-FPhe (134b)** ( $\text{CDCl}_3$ )  $^1\text{H}$  NMR (400 MHz),  $^{13}\text{C}$  NMR (101 MHz),  $^{19}\text{F}$  NMR (376 MHz)



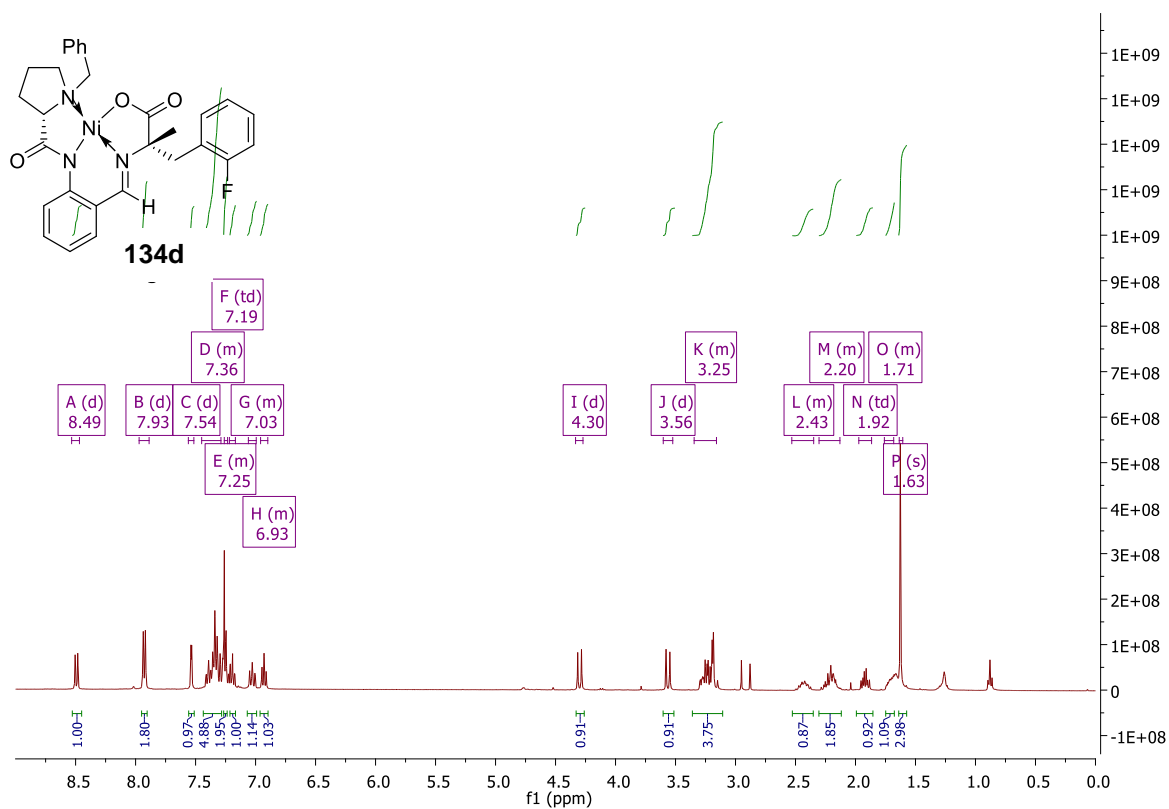


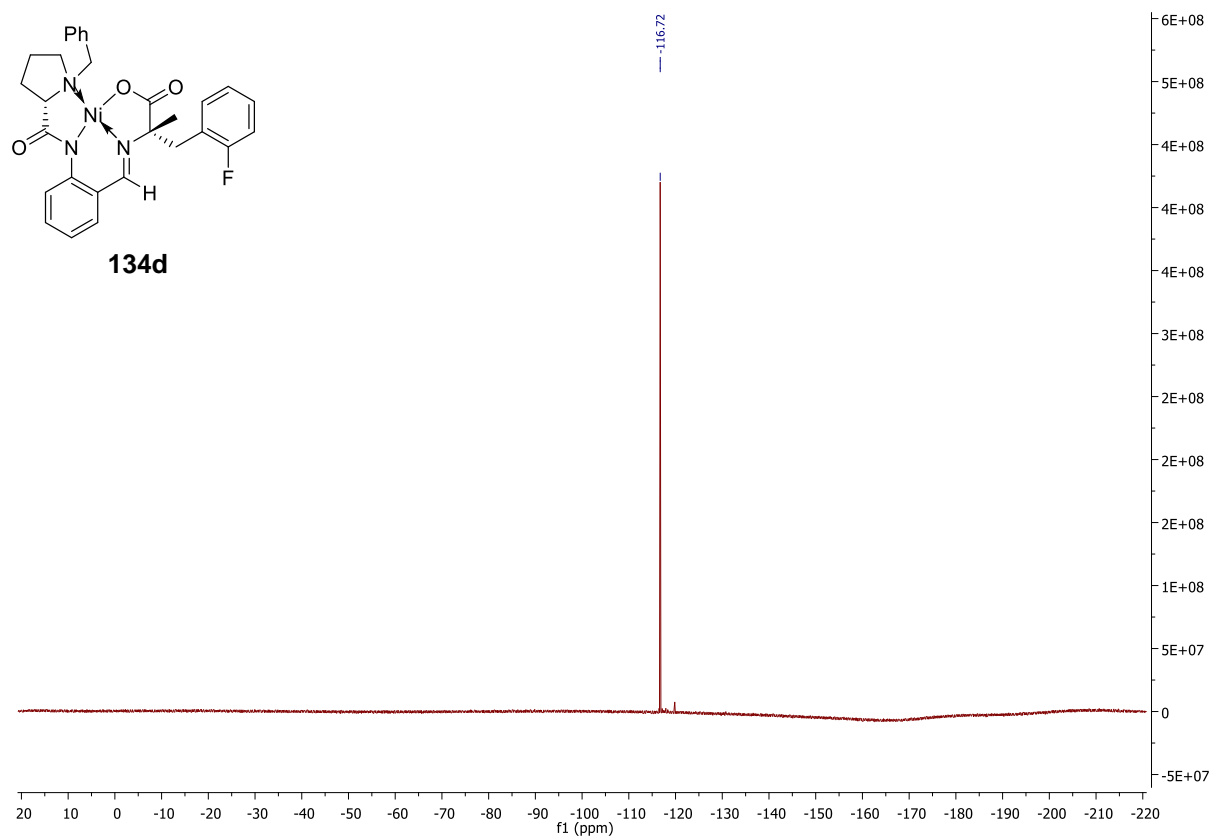
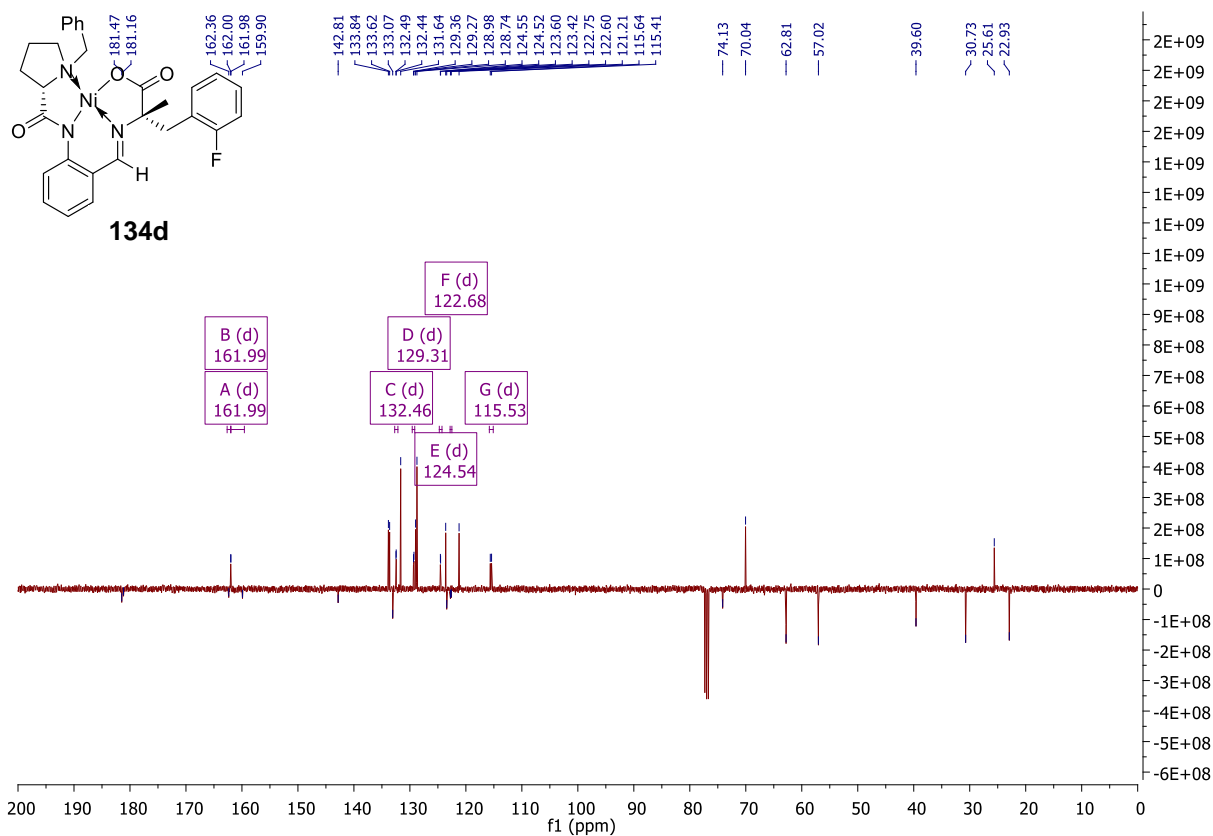
**(*S,S*)-Ni-BPB-2-F-OMOM-Tyr (134c)** (CDCl<sub>3</sub>) <sup>1</sup>H NMR (400 MHz), <sup>13</sup>C NMR (101 MHz), <sup>19</sup>F NMR (376 MHz)



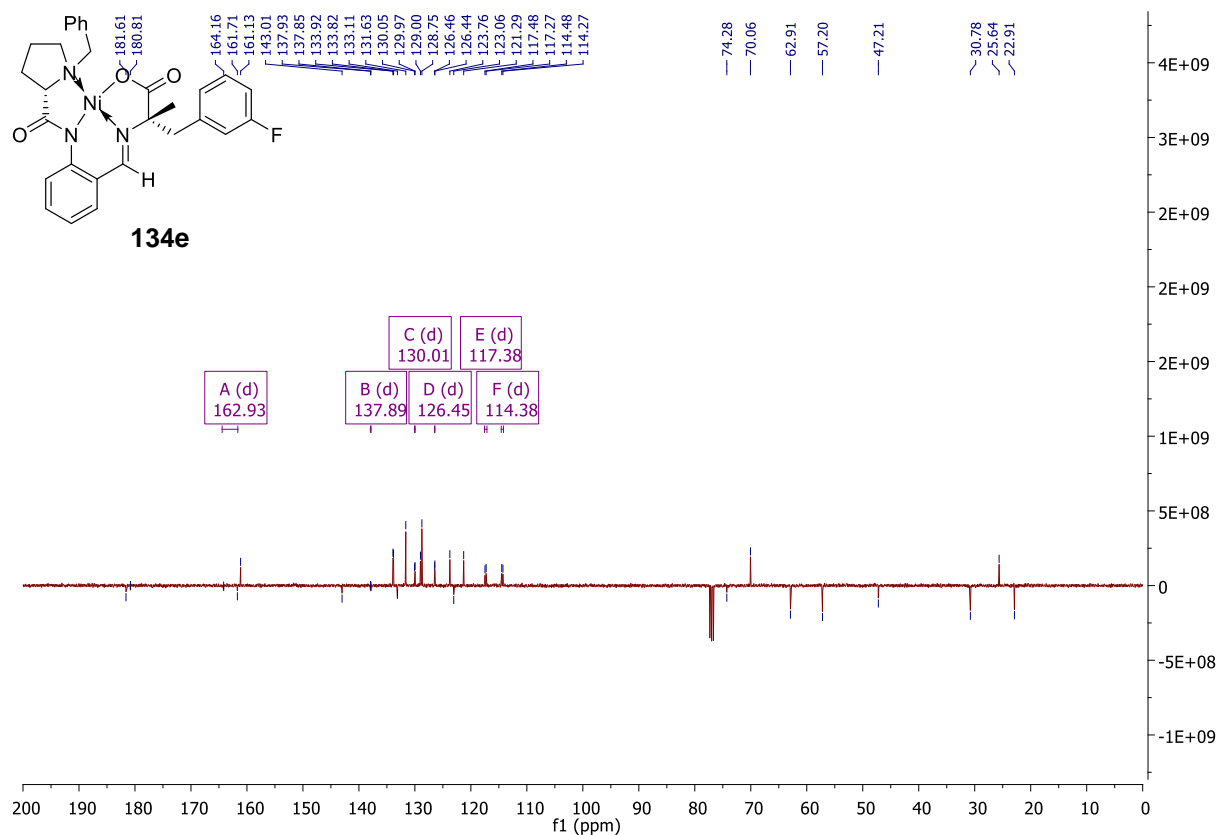
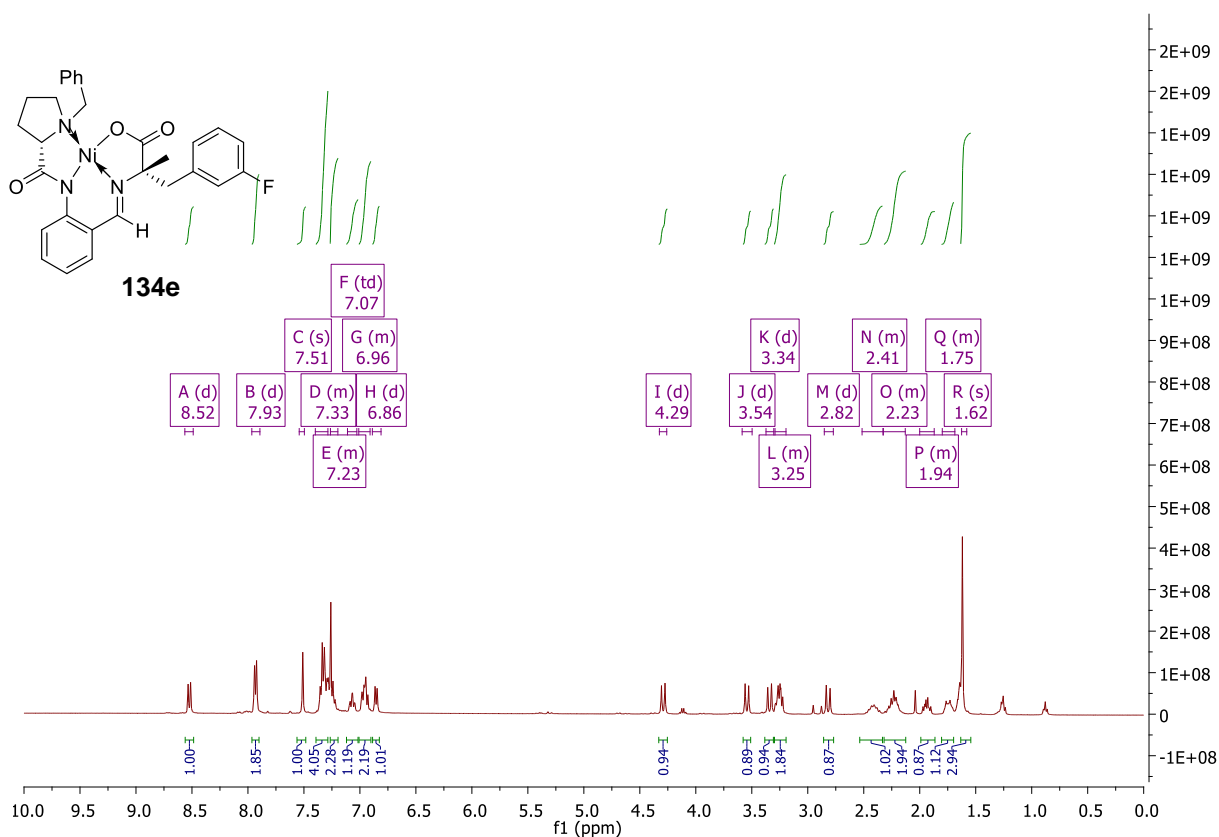


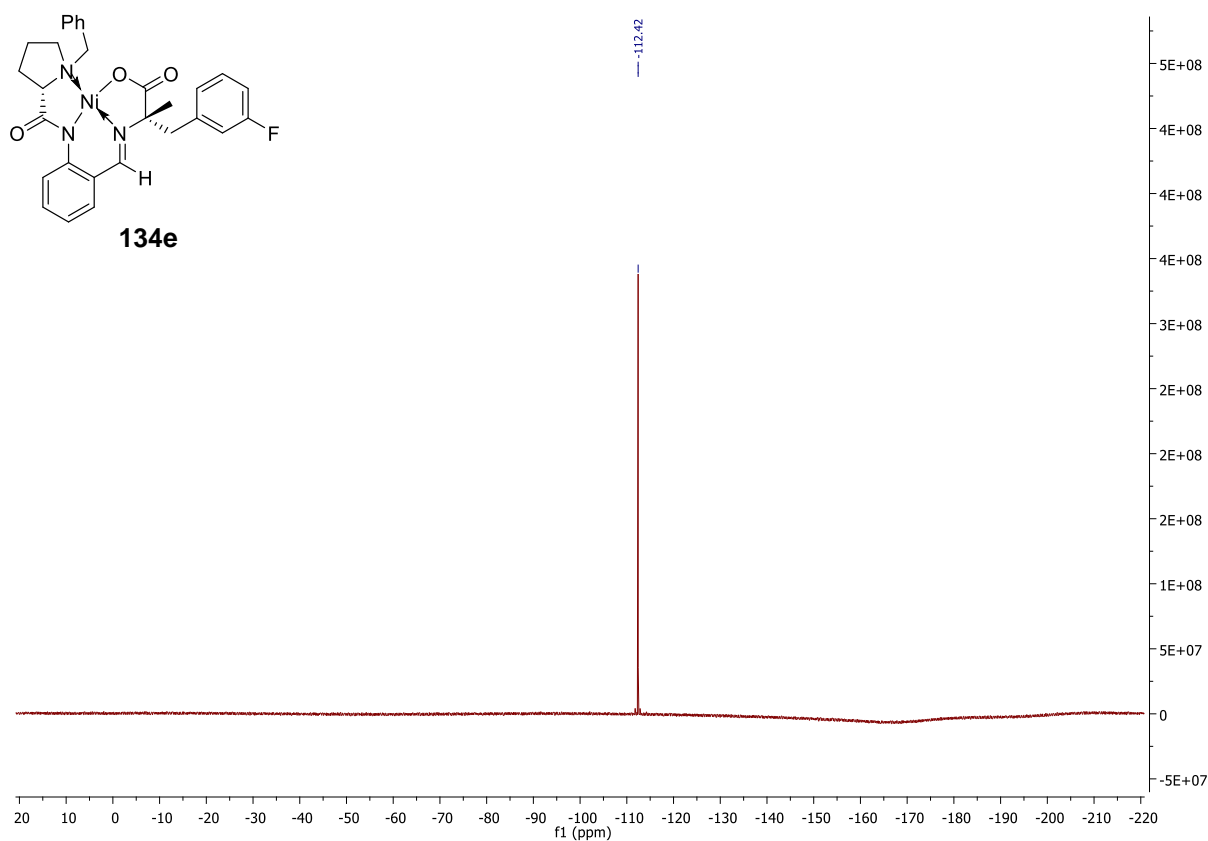
**(S,S)-Ni-BPA-2-FPhe (134d)** (CDCl<sub>3</sub>) <sup>1</sup>H NMR (400 MHz), <sup>13</sup>C NMR (101 MHz), <sup>19</sup>F NMR (376 MHz)



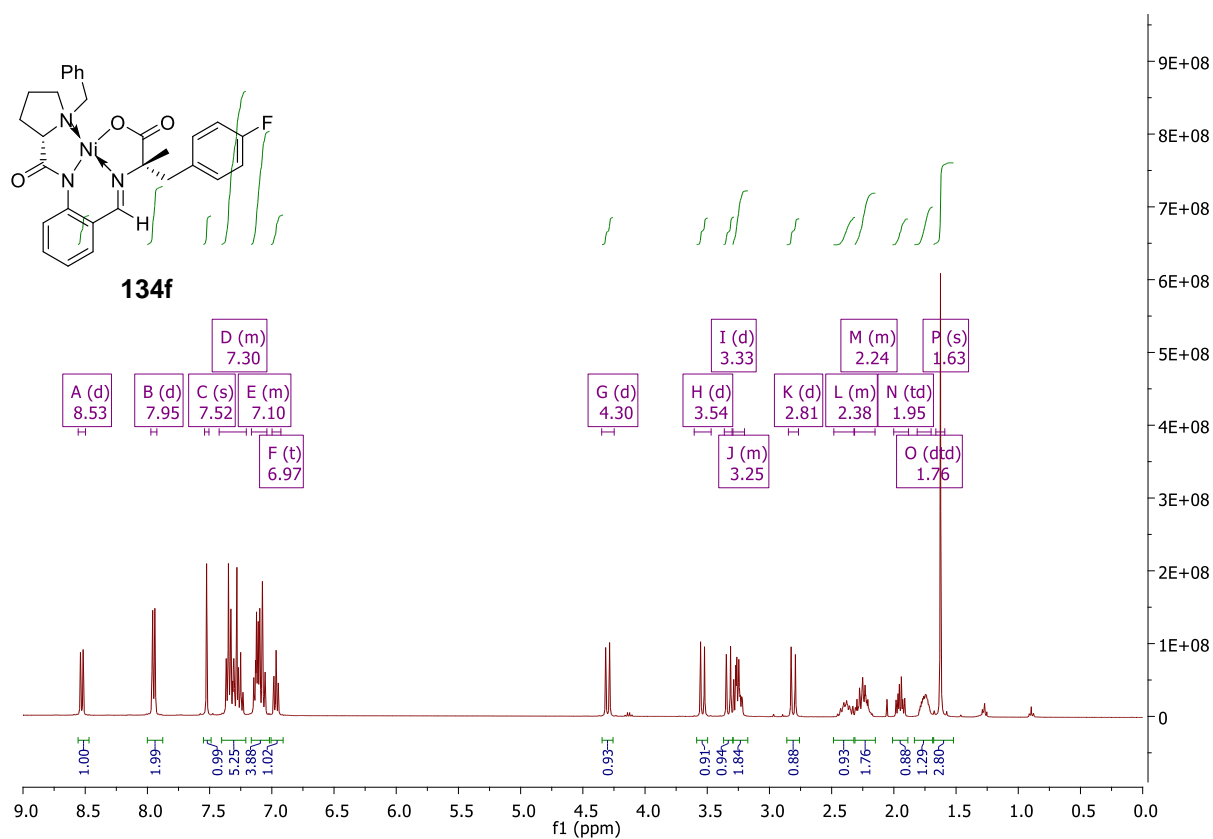


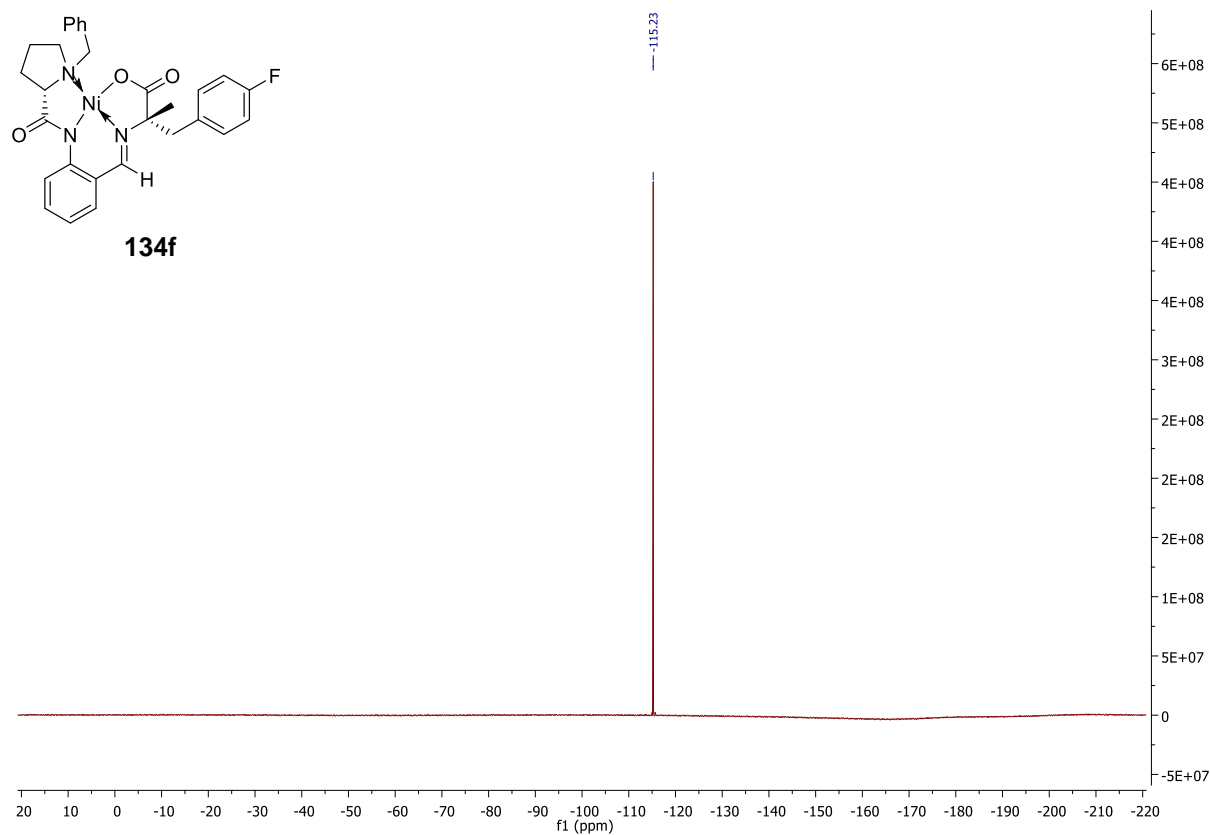
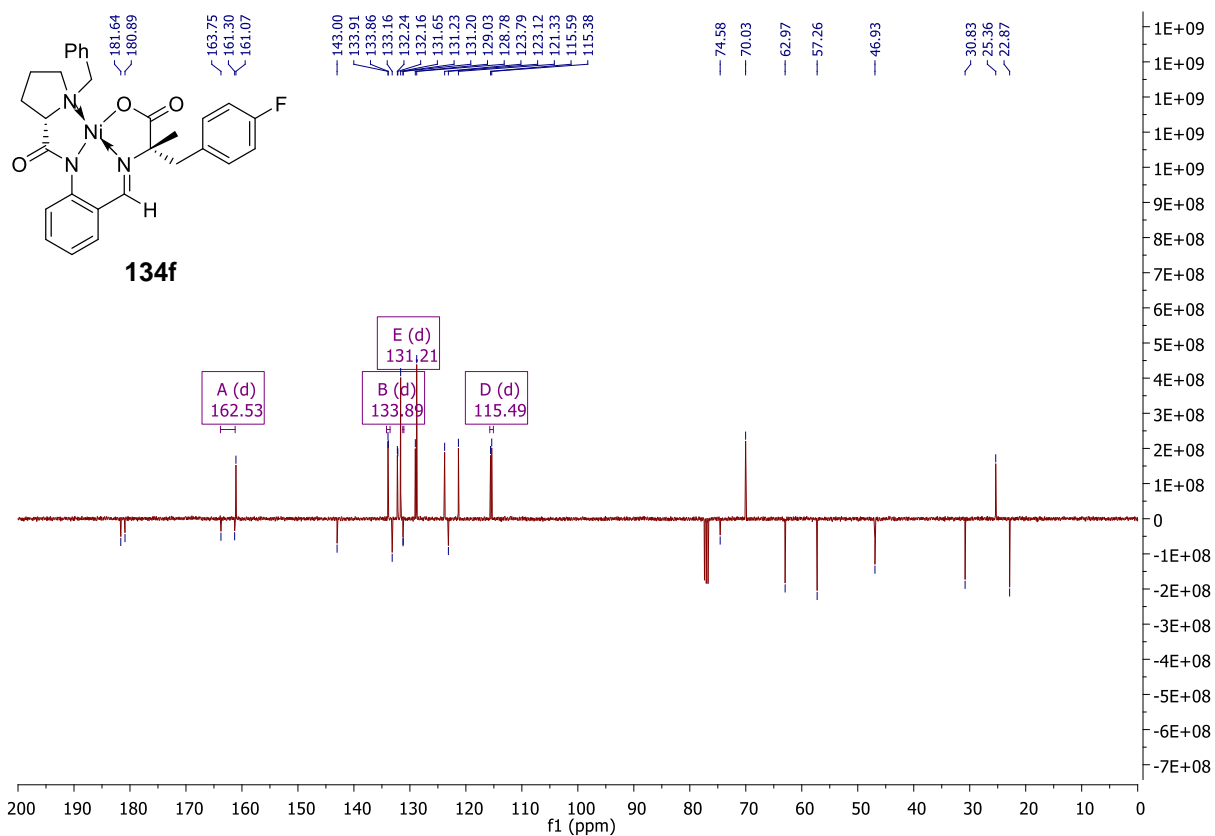
**(*S,S*)-Ni-BPA-3-FPhe (134e)** (CDCl<sub>3</sub>) <sup>1</sup>H NMR (400 MHz), <sup>13</sup>C NMR (101 MHz), <sup>19</sup>F NMR (376 MHz)





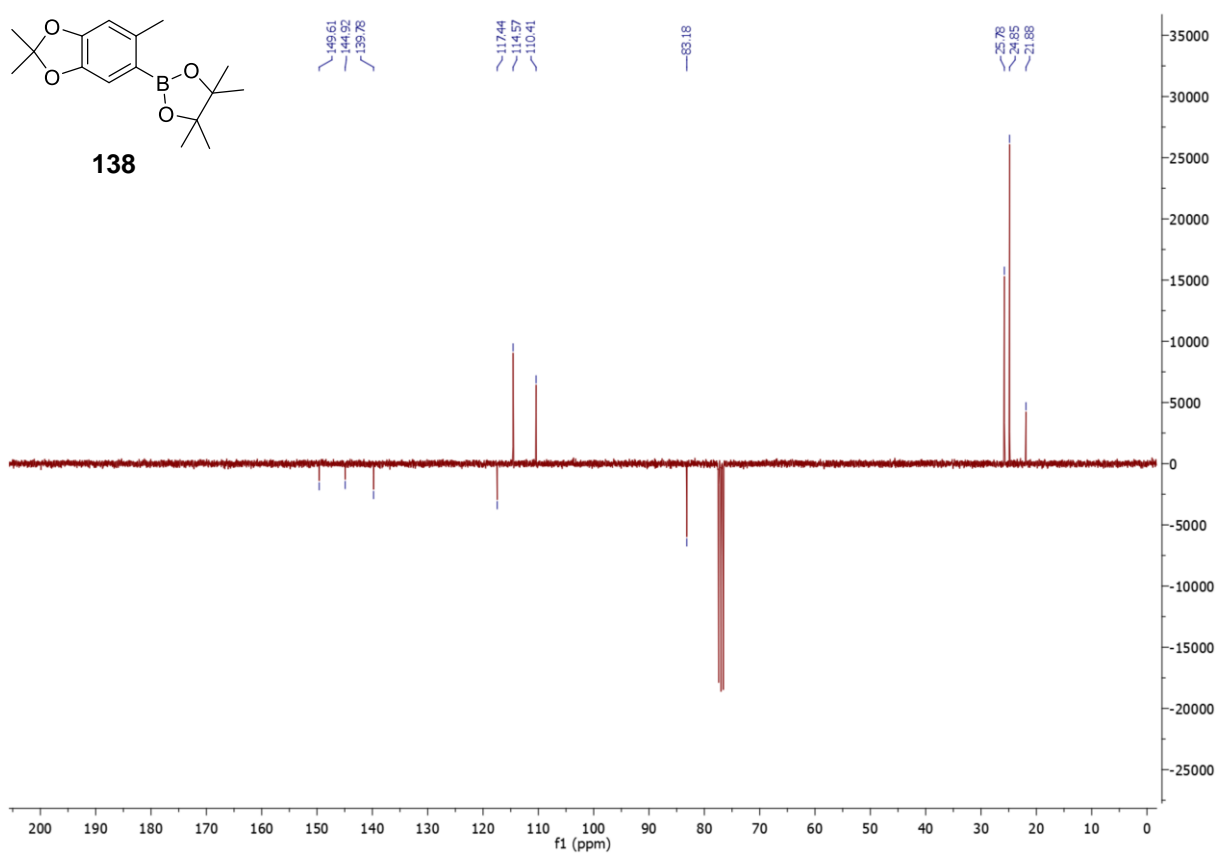
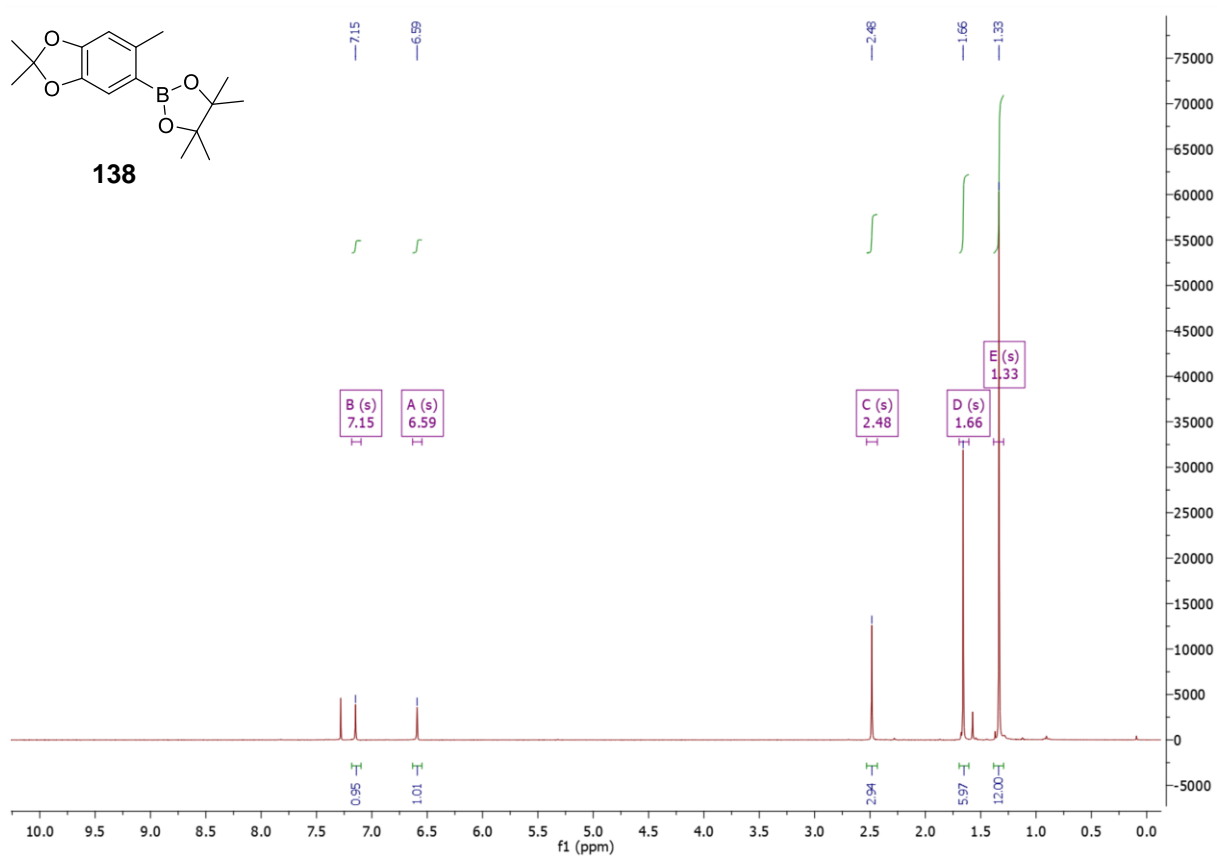
**(S,S)-Ni-BPA-4-FPhe (134f)** ( $\text{CDCl}_3$ )  $^1\text{H}$  NMR (400 MHz),  $^{13}\text{C}$  NMR (101 MHz),  $^{19}\text{F}$  NMR (376 MHz)



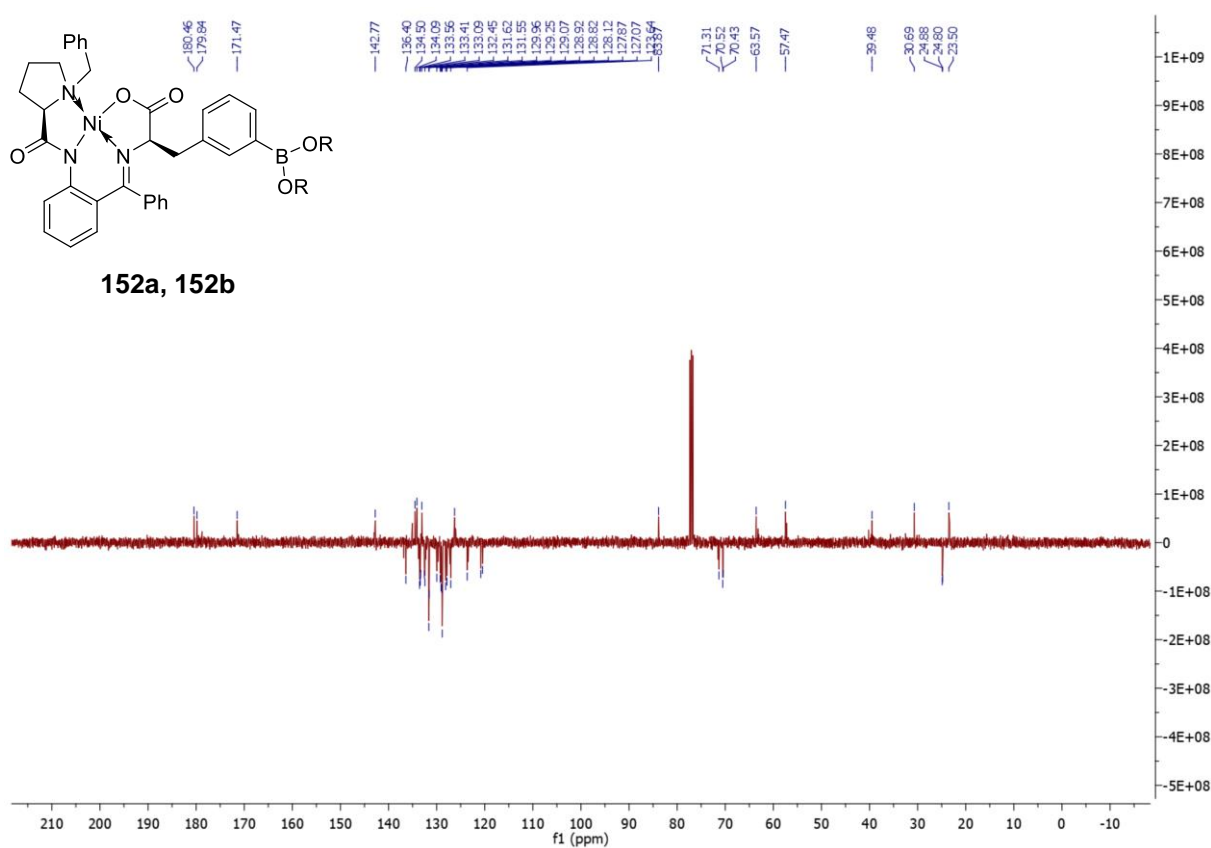
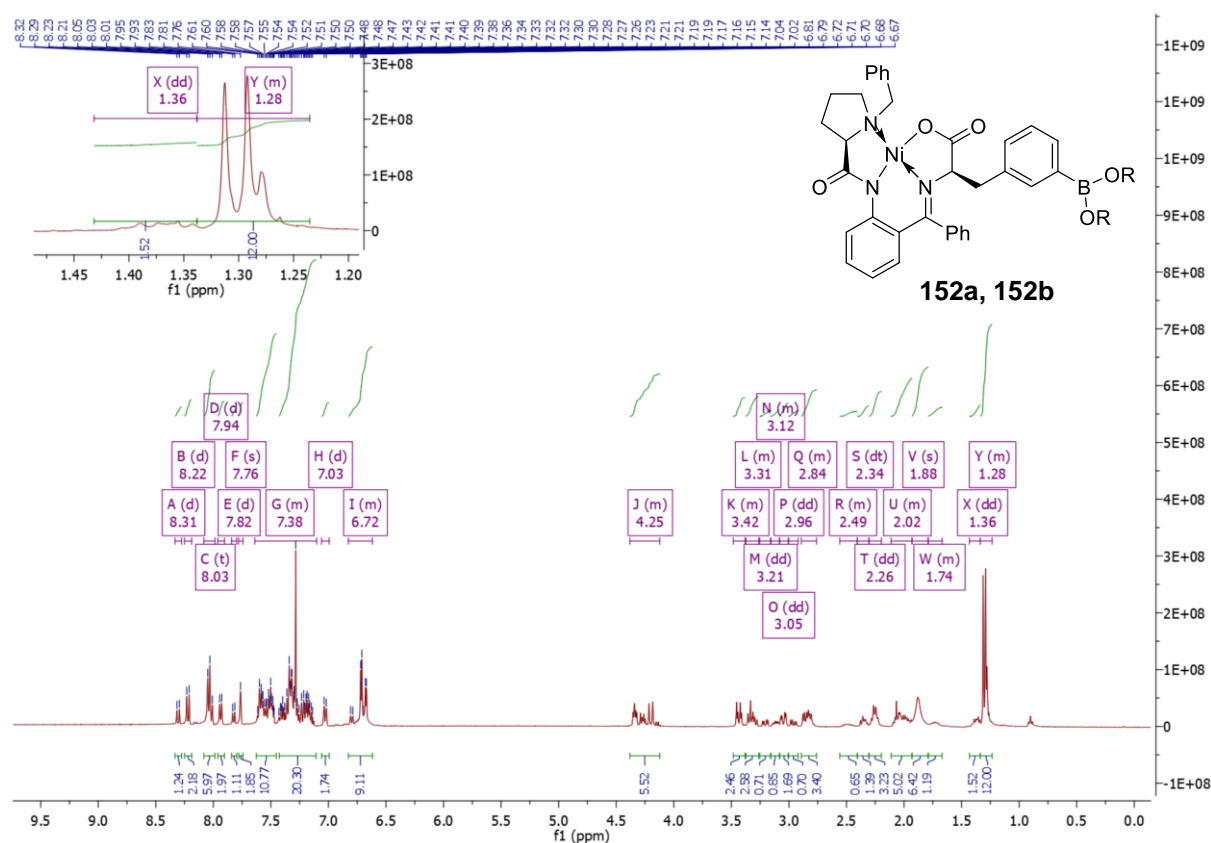


**4,4,5,5-Tetramethyl-2-(2,2,6-trimethylbenzo[d][1,3]dioxol-5-yl)-1,3,2-dioxaborolane**

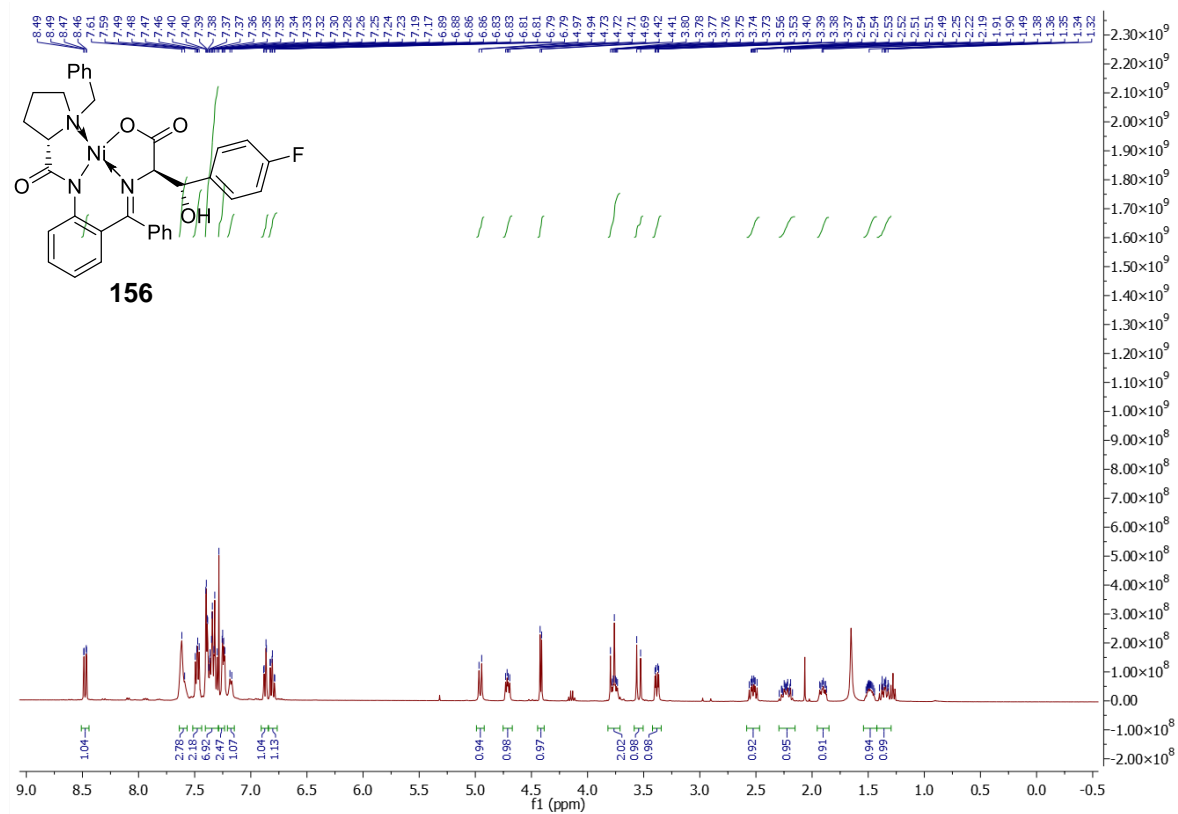
**(138)** (CDCl<sub>3</sub>) <sup>1</sup>H NMR (400 MHz) <sup>13</sup>C NMR (101 MHz)

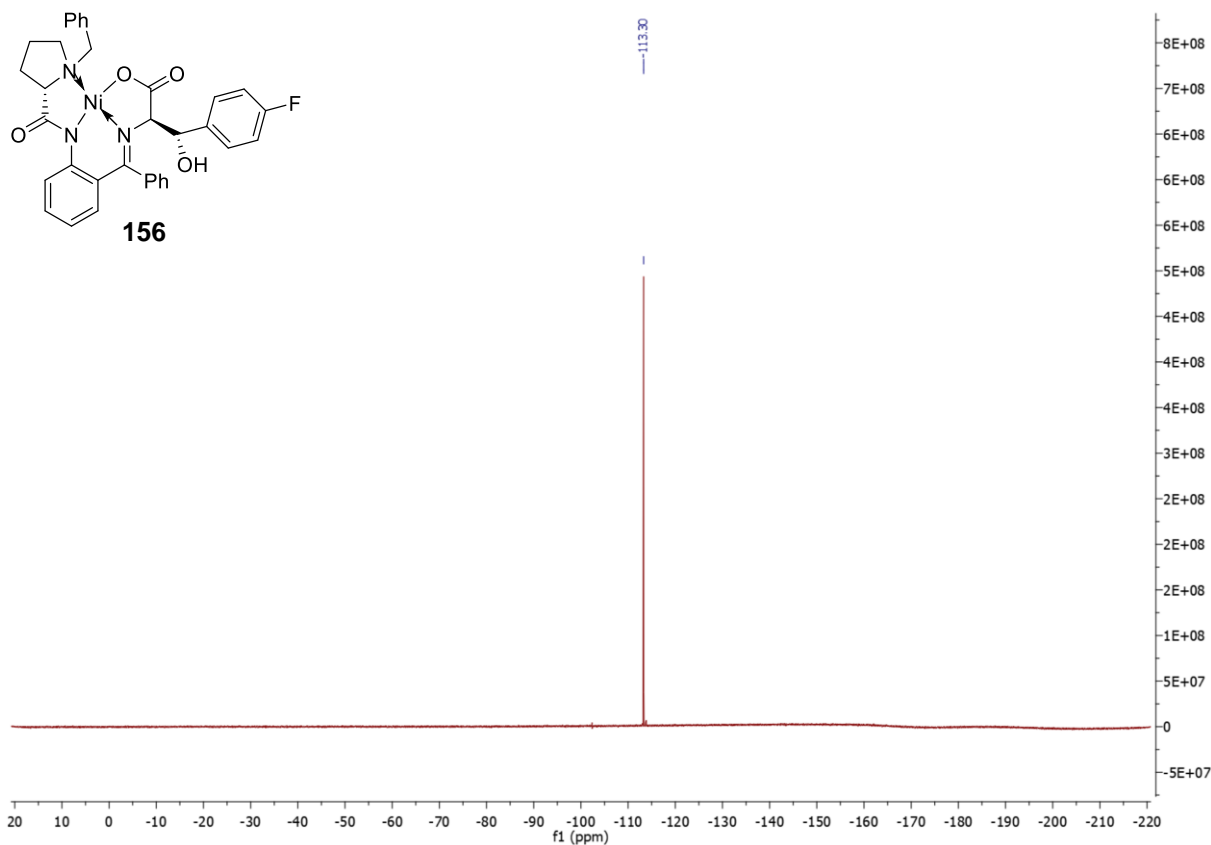


**(*R,R*)-Ni-BPB-3-Bpin-Phe (152a, 152b) (CDCl<sub>3</sub>) <sup>1</sup>H NMR (400 MHz) <sup>13</sup>C NMR (101 MHz)**

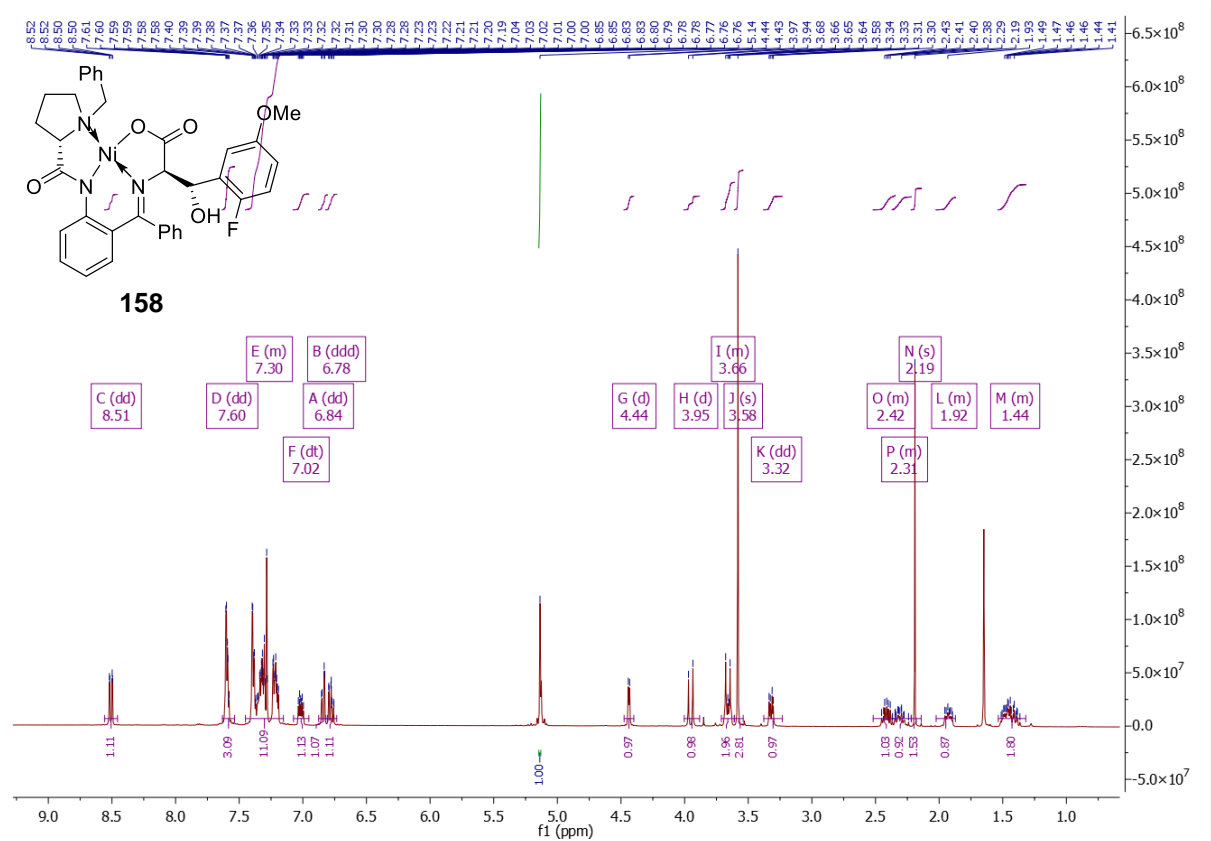


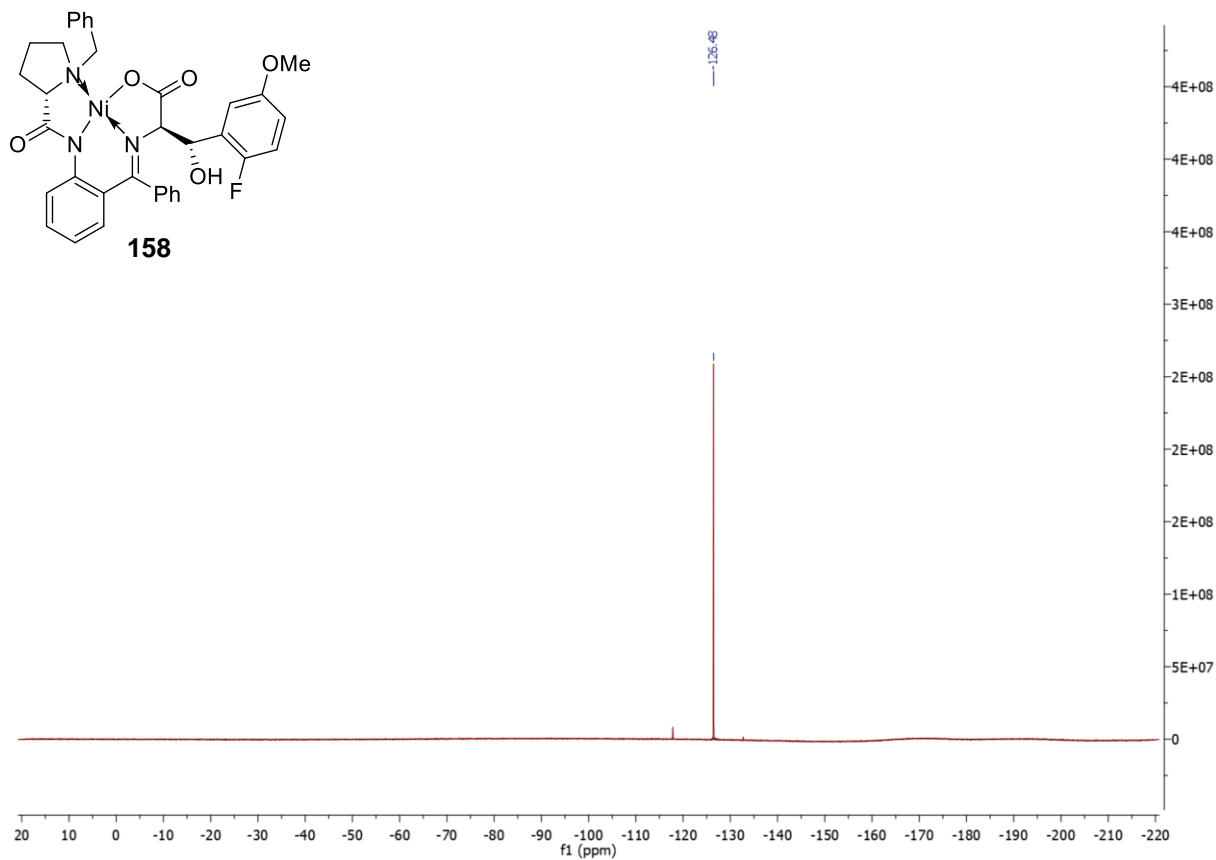
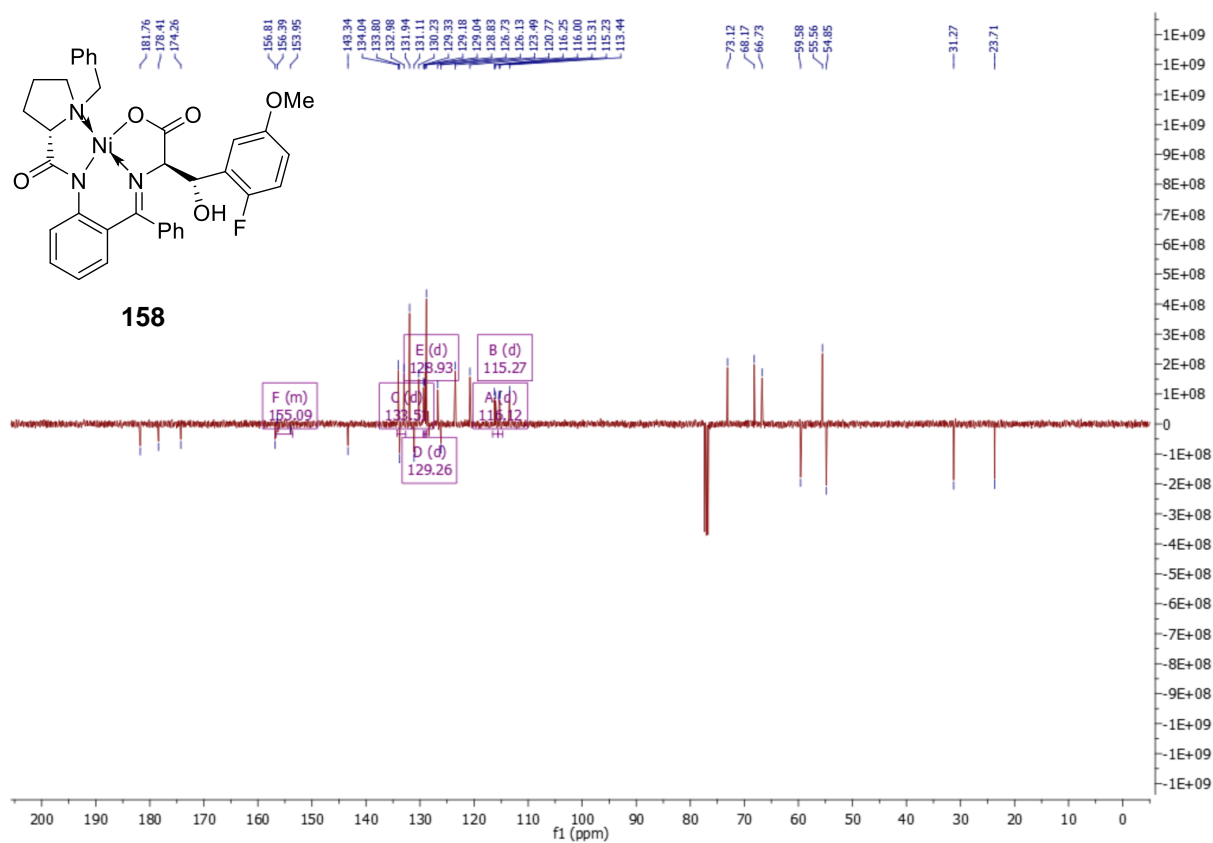
**(*S,S*)-Ni-BPB-4-F-PheSer (156)** (CDCl<sub>3</sub>) <sup>1</sup>H NMR (400 MHz) <sup>13</sup>C NMR (101 MHz) <sup>19</sup>F NMR (376 MHz)





**(*S,S*)-Ni-BPB-2-F-5-MeO-PheSer (158)** ( $\text{CDCl}_3$ )  $^1\text{H}$  NMR (400 MHz)  $^{13}\text{C}$  NMR (101 MHz)  $^{19}\text{F}$  NMR (376 MHz)





**160**

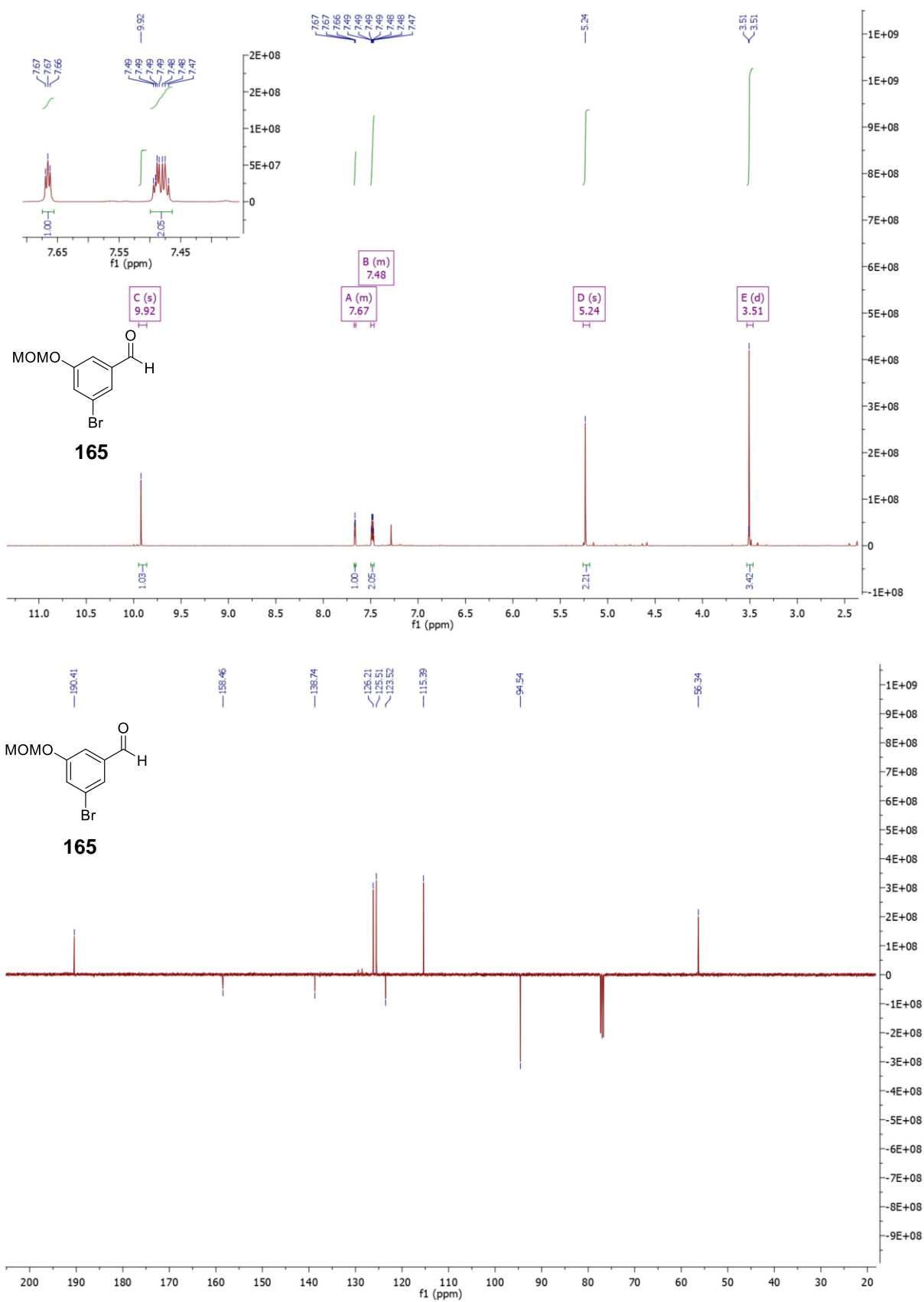
<sup>1</sup>H NMR spectrum (CDCl<sub>3</sub>) of compound **160**. The spectrum shows peaks from 0 to 10.5 ppm. Key peaks are labeled with letters A through N, corresponding to the following chemical shifts (ppm): A (d) 8.65, B (d) 7.84, C (s) 7.61, D (m) 7.31, E (m) 6.86, F (s) 4.94, G (s) 4.65, H (d) 4.37, I (d) 3.99, J (d) 3.58, K (dd) 3.39, L (m) 2.37, M (m) 1.95, and N (dd) 1.45. Integration values are provided below the baseline for each group of peaks.

**163**

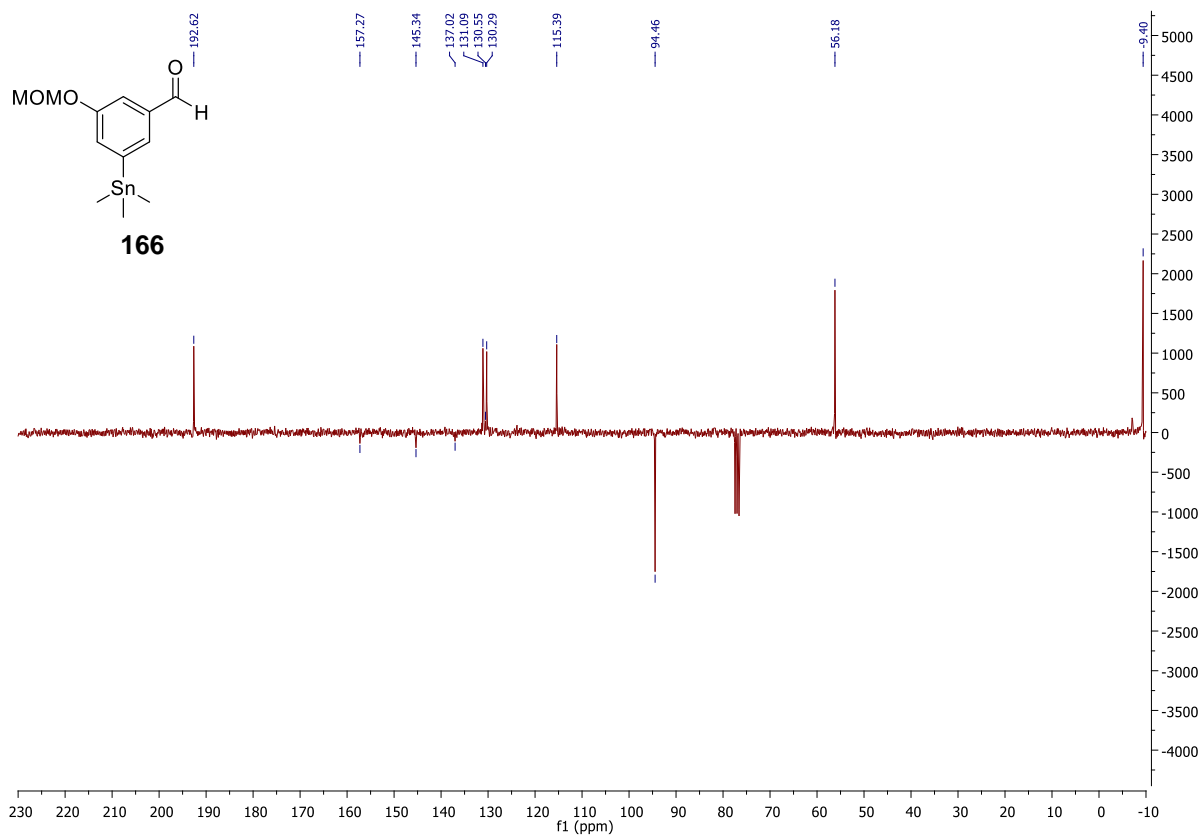
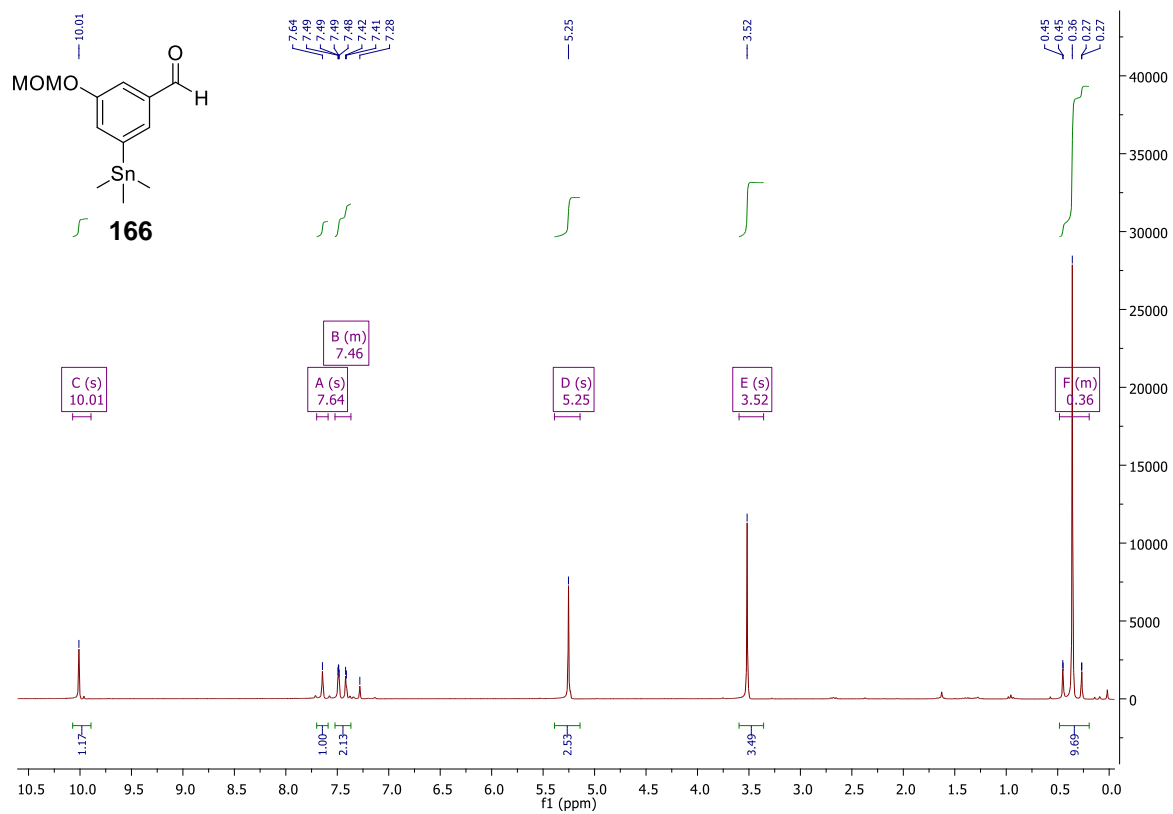
C[Sn](C)(C)c1ccc(C=O)cc1

<sup>1</sup>H NMR spectrum (CDCl<sub>3</sub>) of compound **163**. The spectrum shows peaks at 10.00 ppm (s, 1H), 7.69 ppm (d, 2H), 7.82 ppm (d, 2H), and 0.36 ppm (s, 6H). Integration values are 1.14, 2.28, 1.80, and 9.00 respectively.

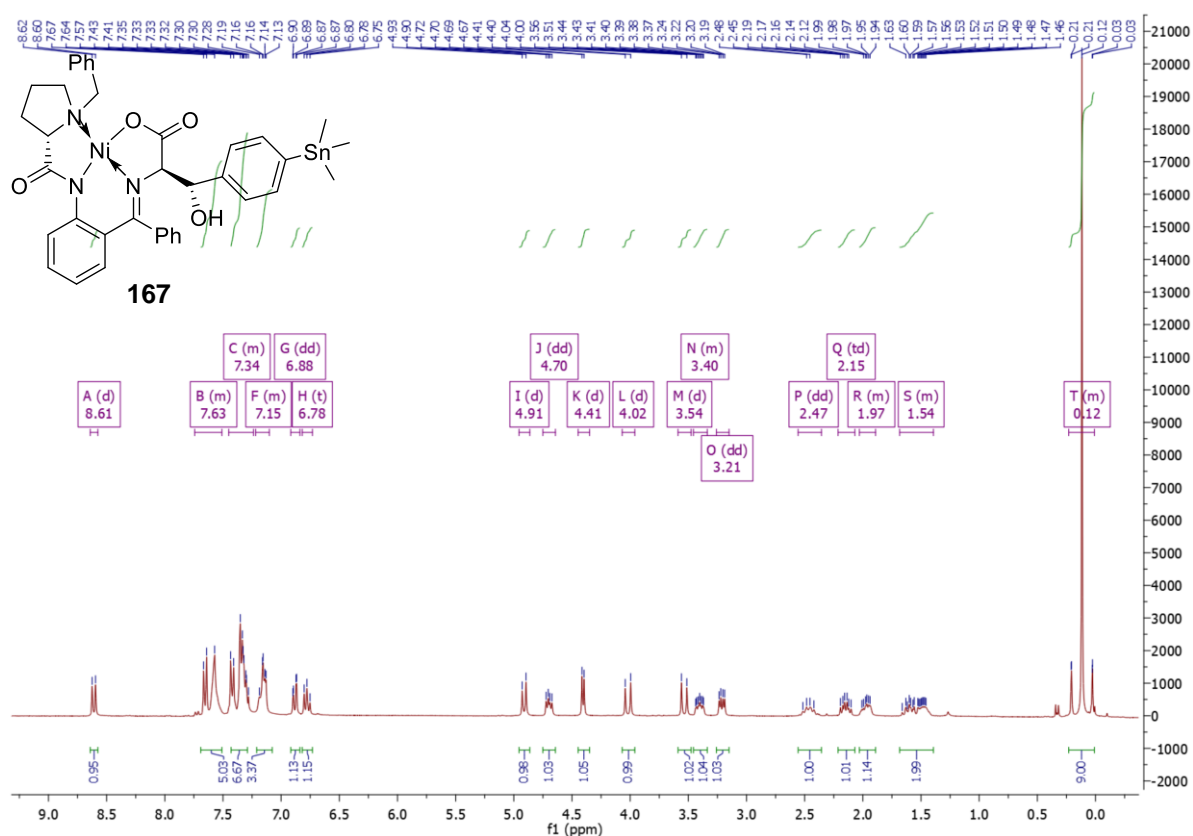
**3-Bromo-5-(methoxymethoxy)benzaldehyde (165)** (CDCl<sub>3</sub>) <sup>1</sup>H NMR (400 MHz) <sup>13</sup>C NMR (101 MHz)



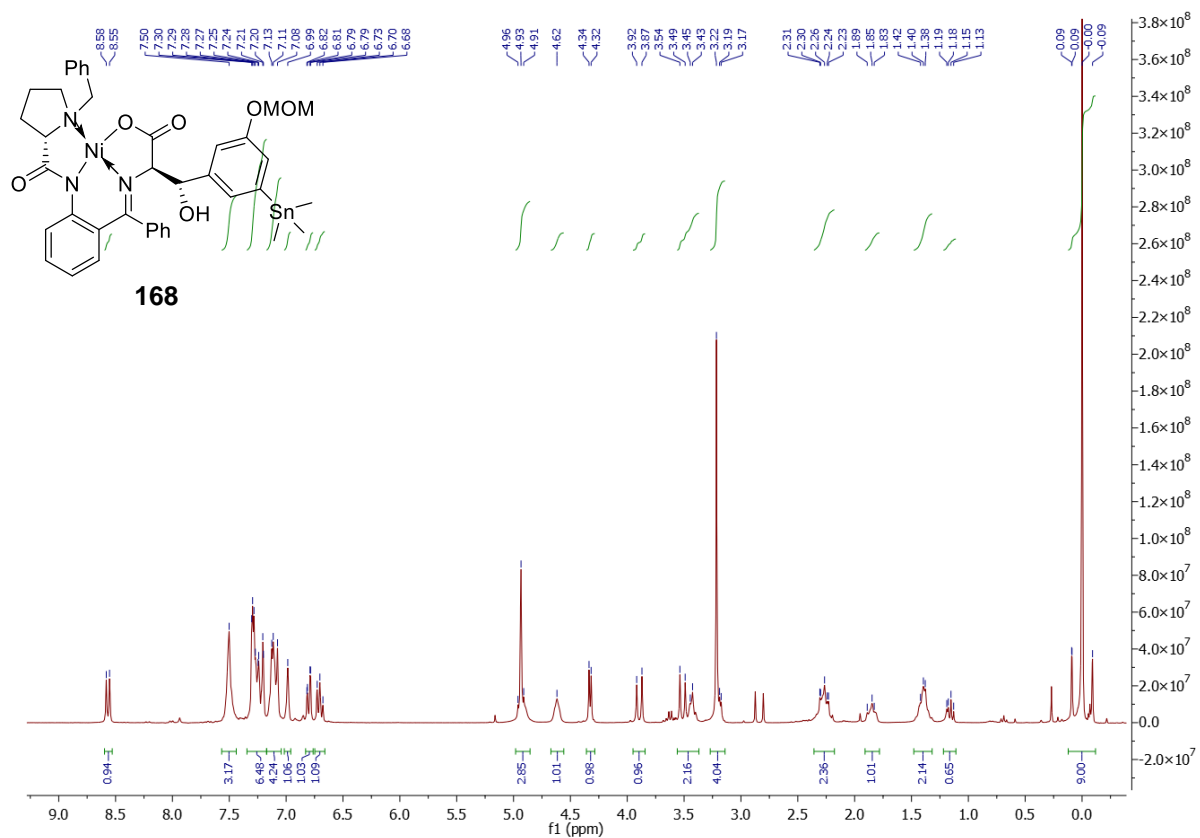
**3-(Methoxymethoxy)-5-(trimethylstannyl)benzaldehyde (166)** (CDCl<sub>3</sub>) <sup>1</sup>H NMR (400 MHz) <sup>13</sup>C NMR (101 MHz)

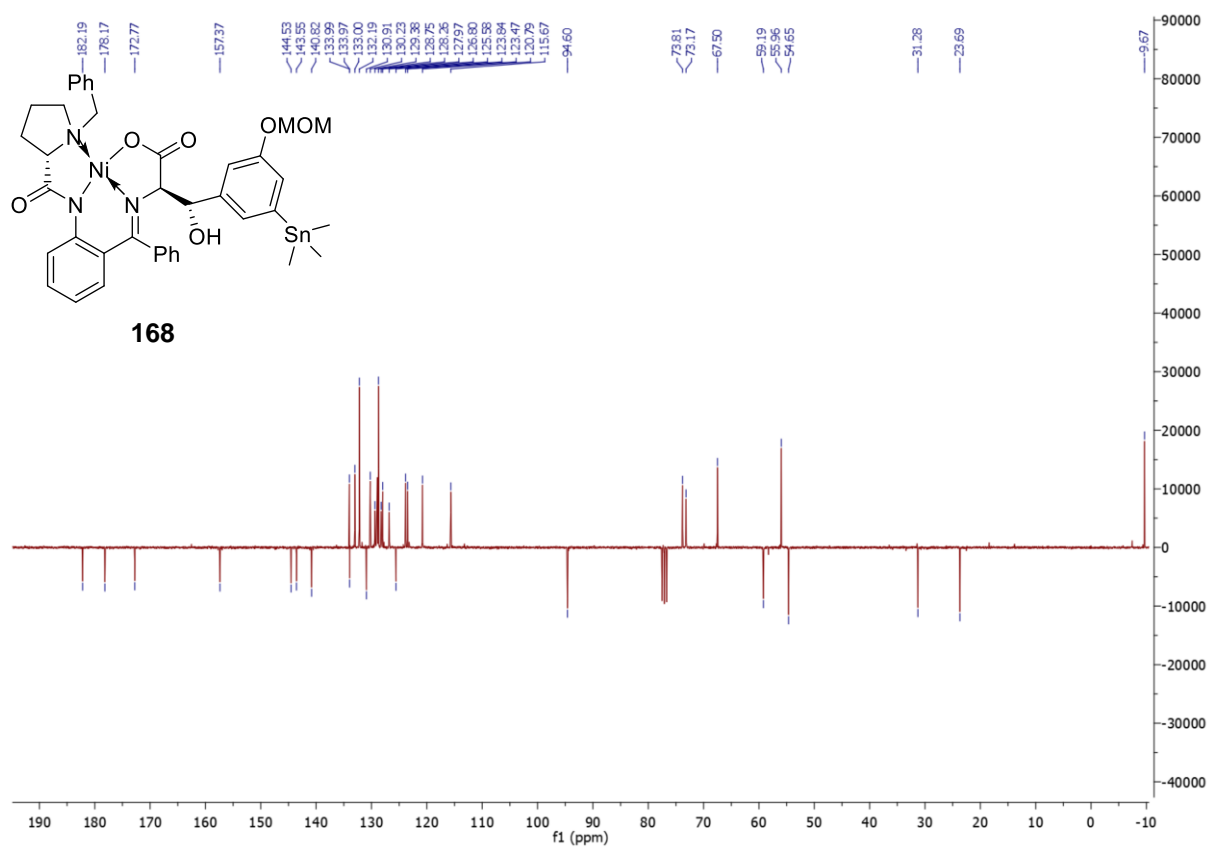


**(*S,S*)-Ni-BPB-4-trimethylstannyl-PheSer (167)** (CDCl<sub>3</sub>) <sup>1</sup>H NMR (400 MHz) <sup>13</sup>C NMR (101 MHz)



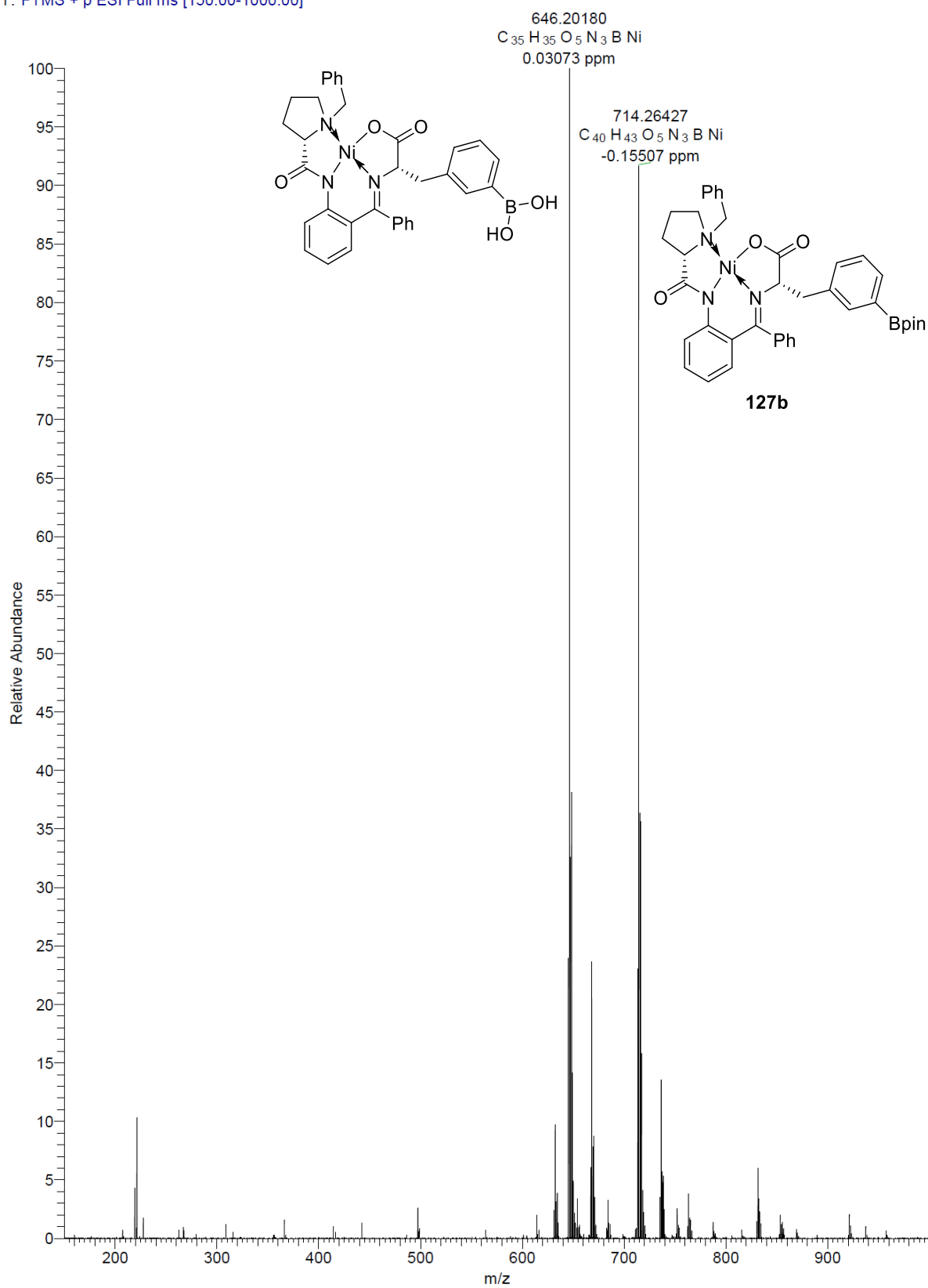
**(*S,S*)-Ni-BPB-3-trimethylstannyl-5-MOMO-PheSer (168)** (CDCl<sub>3</sub>) <sup>1</sup>H NMR (400 MHz) <sup>13</sup>C NMR (101 MHz)



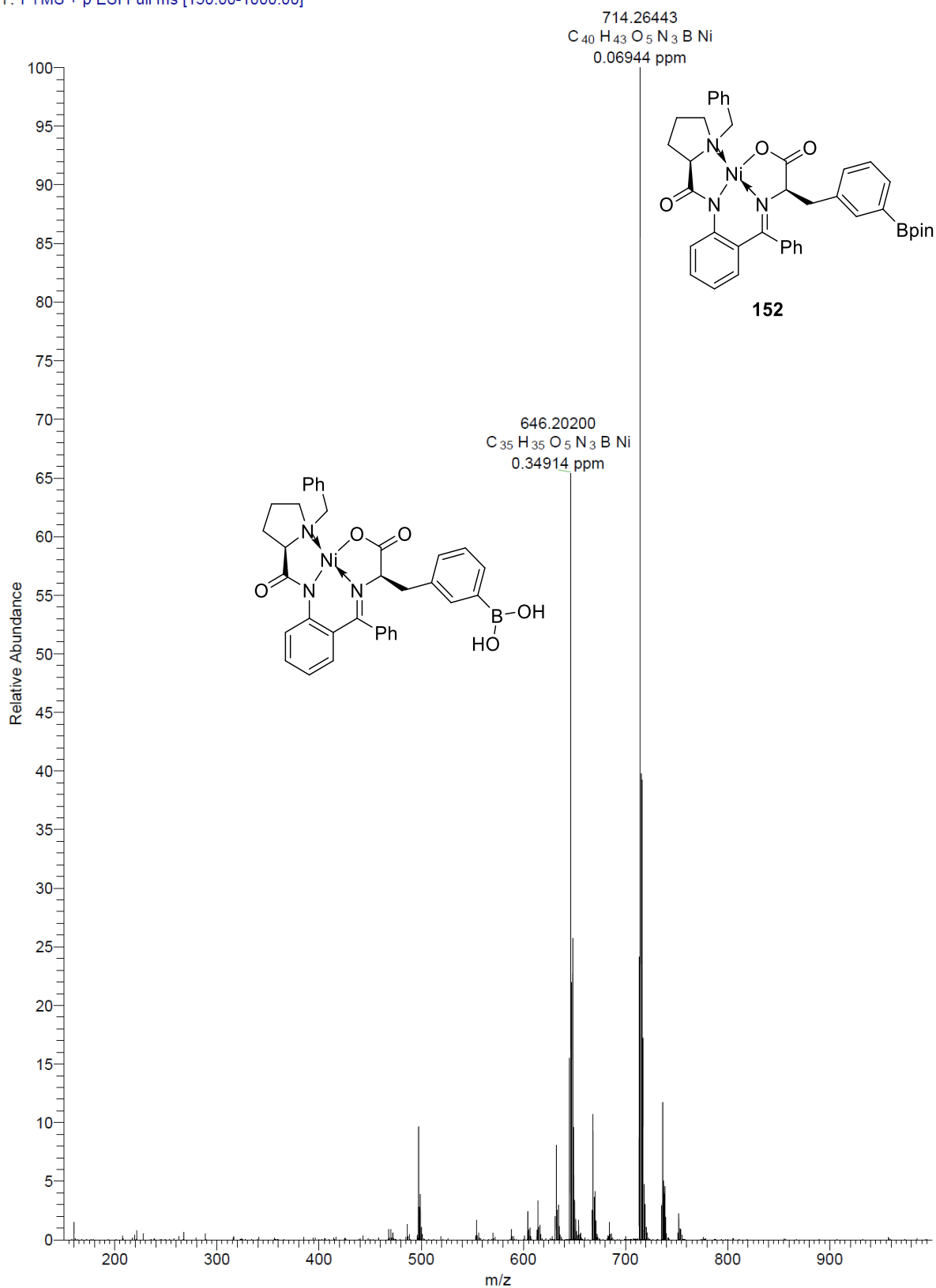


## 6.1.2. Mass Spectra

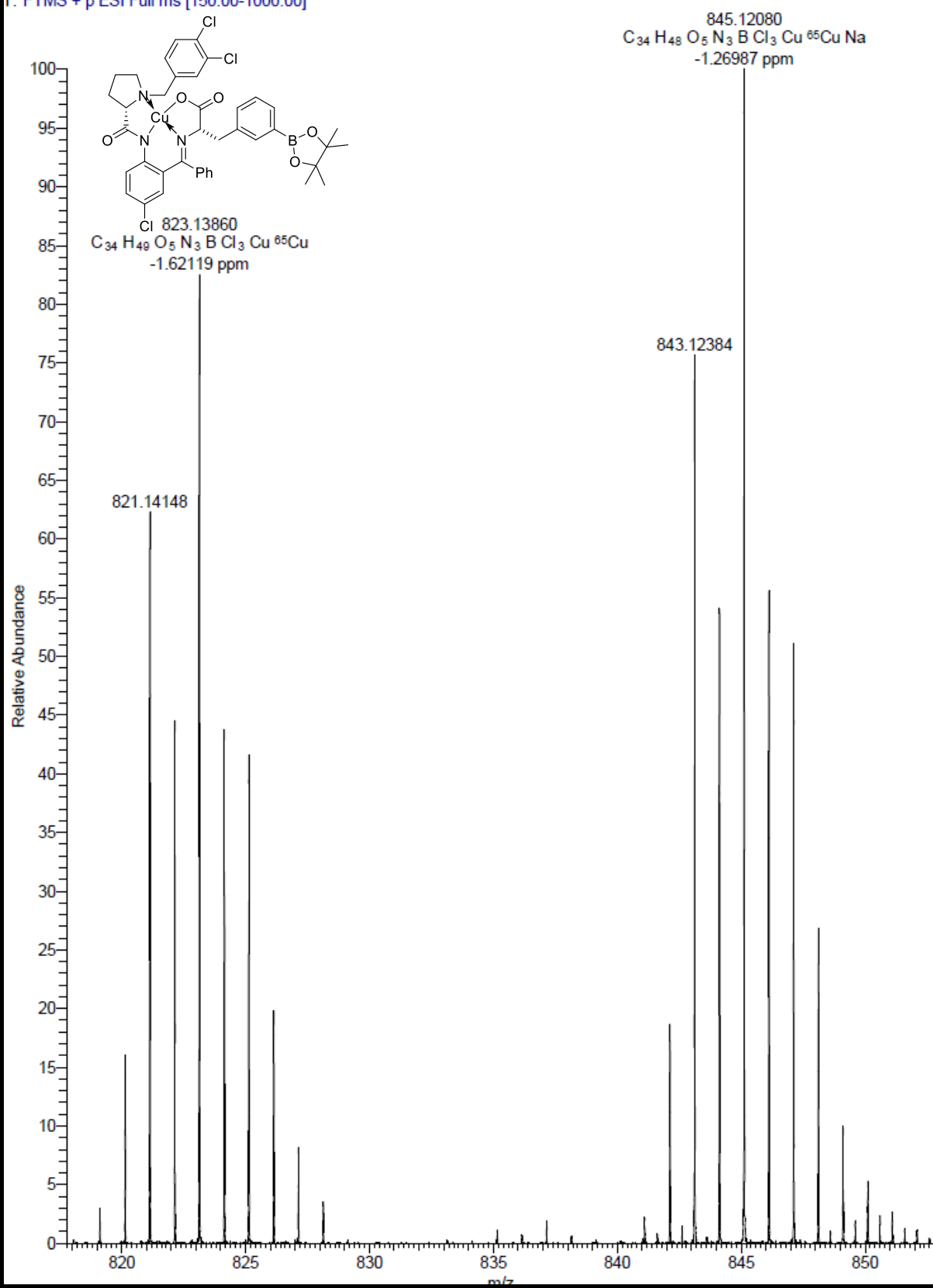
#191079\_FTICRMS\_3-FPhe\_pos #1-10 RT: 0.00-0.27 AV: 10 NL: 1.41E7  
T: FTMS + p ESI Full ms [150.00-1000.00]



#191079\_FTICRMS\_ACX\_3-D-FPhe\_pos #1-10 RT: 0.01-0.28 AV: 10 NL: 3.33E7  
T: FTMS + p ESI Full ms [150.00-1000.00]



#191079 FTICRMS Cu-BPB3-FPhe pos #1-10 RT: 0.01-0.28 AV: 10 NL: 4.77E6  
T: FTMS + p ESI Full ms [150.00-1000.00]



## 7. Radiochemistry

### 7.1.1. Radiochemical Terminology and Nomenclature

#### **Radiochemical Yield**

The radiochemical yield (RCY) is defined as “the amount of activity in the product expressed as the percentage (%) of starting activity used in the corresponding process (e.g., synthesis, separation, etc.). The quantity of both must be decay corrected to the same point in time before the calculation is made.”<sup>125</sup>

#### **Enantiomeric Excess**

Enantiomeric excess (*ee*) is a purity measurement for chiral molecules. The *ee* indicates the relative presence of one enantiomer with respect to the other enantiomer in a percentage value (Equation 1.). An *ee* value of over 95% is desired for final AAA tracer products.

$$ee\ (\%) = ((R - S)/(R + S) \times 100)$$

*Equation 1. Enantiomeric excess equation.*

Chiral HPLC columns were used to determine the *ee* of the AAA tracers, providing adequate separation between the L- and D- enantiomers (Fig. 37). The co-injection of the AAA tracers with a suitable reference compound can provide clear information regarding the enantiomeric configuration (L or D) of the product and the *ee*.

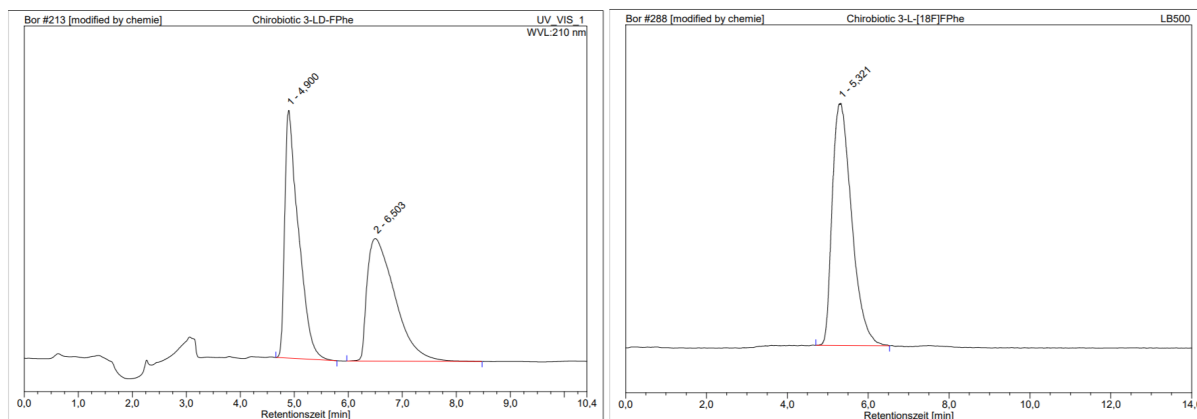


*Figure 37. HPLC chromatographs of racemic reference compound 3-FPhe and final product 3-(S)-[<sup>18</sup>F]FPhe tracer. Chirobiotic T column: 60% EtOH 1 mL/min isocratic conditions.*

### 7.2. General Information and Procedures

[<sup>18</sup>F]Fluoride was produced by bombardment of enriched [<sup>18</sup>O]H<sub>2</sub>O by 16.5 MeV protons via <sup>18</sup>O(p,n)<sup>18</sup>F reaction using BC1710 cyclotron (The Japan Steel Works Ltd., Shinagawa, Japan) at the INM-5 (Forschungszentrum Jülich).

All radiosyntheses were carried out using anhydrous *n*-BuOH and DMA stored over molecular sieves in AcroSeal<sup>®</sup> flasks (Thermo-Fisher Scientific, Acros, Germany) and under ambient air. Cu(OTf)<sub>2</sub>(py)<sub>4</sub> was prepared according to the literature procedure<sup>9</sup> and stored under ambient conditions. Sep-Pak Accell Plus QMA light carbonate cartridges (46 mg) and Oasis Wax 1cc cartridges were purchased from Waters GmbH (Eschborn, Germany).

#### 7.2.1. Preprocessing of [<sup>18</sup>F]Fluoride

[<sup>18</sup>F]Fluoride was processed prior to radiosynthesis as follows: A solution of aqueous [<sup>18</sup>F]fluoride was loaded onto a QMA light carbonate (anion-exchange cartridge) from the male side. Washing and flushing were also carried out from the male side. The [<sup>18</sup>F]fluoride was eluted from the female to the male side.

#### 7.2.2. Synthesis of FET

[<sup>18</sup>F]FET was prepared at the cyclotron facility of INM-5 (Forschungszentrum, Jülich GmbH) as previously reported.<sup>22</sup>

### 7.3. General Procedure for the <sup>18</sup>F-Labeling of Ni-BPB-AAAs (RGP1)

The radiosynthesis commenced with the loading of [<sup>18</sup>F]fluoride (500–5000 MBq) onto a QMA<sup>®</sup> light carbonate cartridge (preconditioned with 1 mL H<sub>2</sub>O) followed by subsequent elution with Et<sub>4</sub>NHCO<sub>3</sub> (3 mg, 15.7 μmol) in MeOH (0.75 mL). Thereafter, all volatiles were removed under reduced pressure at 80 °C for 5 minutes, a solution of the corresponding precursor (10 μmol) and Cu(OTf)<sub>2</sub>(py)<sub>4</sub> (20 μmol) in DMA/*n*BuOH 2:1 (0.75 mL) added and the reaction mixture was stirred at 110 °C for 15 min. The mixture was then concentrated under reduced pressure at 110 °C for 10 min. 12 M HCl (1 mL) was added, the reaction mixture was stirred at 110 °C for 15 min and concentrated at the same temperature under reduced pressure. Thereafter, the residue was taken up in 6% EtOH (1 mL) and purified using high-performance liquid chromatography (HPLC). Unless otherwise stated, all columns were fitted with a precolumn protector (Phenomenex, SecurityGuard Cartridge System).

### 7.4. Preparation of [<sup>18</sup>F]FPBA (RGP2)

In a similar manner to a literature protocol, the radiosynthesis commenced with the loading of [<sup>18</sup>F]fluoride (50–500 MBq) onto an Oasis<sup>®</sup> Wax 1cc cartridge (preconditioned with 5 mL of 0.5 M NaHCO<sub>3</sub> and 10 mL H<sub>2</sub>O) from the male side. Thereafter, the cartridge was washed with 1 mL *i*-PrOH in the same direction and dried using compressed air. [<sup>18</sup>F]Fluorine was eluted with DMAPOTf (6.7 mg, 25 μmol) in 0.5 mL DMA from the female side into the reaction vessel containing 1,4-benzenediboronic acid (3.3 g, 20 μmol) and Cu(OTf)<sub>2</sub>(py)<sub>4</sub> (3.6 mg, 5.3

μmol) in DMA (0.5 mL). The mixture was heated (110 °C, 15 min) under aerobic conditions. The <sup>18</sup>F-incorporation was determined using HPLC.

### 7.5. HPLC

Gradient A1: H<sub>2</sub>O/MeCN, 2 mL/min, Chromolith SpeedROD®, 50 × 4.6 mm (Merck Millipore); gradient: 0–2 min: 5% MeCN, 2–2.5 min 5→20% MeCN, 2.5–6 min: 20% MeCN, 6–7 min 20→70% MeCN, 7–9 min: 70% MeCN, 9–12 min 70→5% MeCN.

Gradient A2: H<sub>2</sub>O/MeCN, 3 mL/min, Chromolith SpeedROD®, 50 × 4.6 mm (Merck Millipore); gradient: 0–2 min: 5% MeCN, 2–2.5 min: 5→70% MeCN, 2.5–7 min: 70% MeCN, 7–8 min: 70→5% MeCN, 8–9 min: 5% MeCN.

Gradient B1: 1.3 mL/min 0.2% H<sub>3</sub>PO<sub>4</sub> in 6% EtOH (v/v), Synergi Hydro-RP, 4 μm, 80 Å, 250 mm × 4.6 mm (Phenomenex, Aschaffenburg, Germany).

Gradient B2: 1.3 mL/min 0.2% H<sub>3</sub>PO<sub>4</sub> in 4% EtOH (v/v), Synergi Hydro-RP, 4 μm, 80 Å, 250 mm × 4.6 mm (Phenomenex, Aschaffenburg, Germany). These conditions were used for the isolation of 6-[<sup>18</sup>F]FMT and 2-[<sup>18</sup>F]FTyr.

Gradient B3: 1.0 mL/min 10% EtOH Synergi Hydro-RP, 4 μm, 80 Å, 250 mm × 4.6 mm (Phenomenex, Aschaffenburg, Germany).

Gradient B4: 6 mL/min 0.1% TFA in 10% EtOH (v/v), Hydro RP Synergi 250 mm × 10 mm Synergi Hydro-RP, 4 μm, 80 Å, 250 mm × 4.6 mm (Phenomenex, Aschaffenburg, Germany), isocratic. These conditions were used for the isolation of 2–4-[<sup>18</sup>F]Phes and 2–4-αMe-[<sup>18</sup>F]Phes.

Gradient B5: 6 mL/min 0.1% TFA in 15% EtOH (v/v), Hydro RP Synergi 250 mm × 10 mm Synergi Hydro-RP, 4 μm, 80 Å, 250 mm × 4.6 mm (Phenomenex, Aschaffenburg, Germany). These conditions were used for the isolation of 4-[<sup>18</sup>F]FTTrp.

Gradient C: 1 mL/min 60% EtOH Chirobiotic T column (Astec®), 5 μm, 100 Å isocratic 1–12 min. A precolumn protector was not utilized in this case.

HPLC analyses were carried out on a Dionex Ultimate 3000 HPLC system and a DAD UV detector coupled in series with a Berthold NaI detector or on a homemade HPLC system consisting of a Knauer 80-P pump, a Knauer K-2500 UV/vis detector (Knauer, Berlin, Germany), and a Rheodyne manual injector coupled in series with a NaI(Tl) well-type scintillation detector model 276 photomultiplier base with an ACE mate amplifier and BIAS supply (EG&G Ortec Ametek, Meerbusch, Germany). Semipreparative HPLC separations were carried out using the same HPLC systems or a homemade HPLC system equipped with a

Hitachi L-6000 pump (Merck, Darmstadt), a Knauer K-2500 UV/vis detector (Knauer, Berlin, Germany), and a Rheodyne manual injector (5 mL loop) coupled in series with a NaI(Tl) well-type scintillation detector model 276 photomultiplier base with an ACE mate amplifier and BIAS supply (EG&G Ortec Ametek, Meerbusch, Germany). The unselective adsorption of  $^{18}\text{F}$  onto HPLC columns was determined to be  $< 10\%$  in each case. The UV and radioactivity detectors were connected in sequence, giving a time delay of 0.1–0.9 min between the corresponding responses, depending on the flow rate. The identity of the  $^{18}\text{F}$ -labeled products was confirmed by the co-injection of the respective non-radioactive reference compound. All radiosyntheses were carried out at least three times. In most cases, the standard deviation (SD) of RCCs did not exceed 10% of the mean values.

## 7.6. Automated Synthesis of Radiofluorinated Amino Acids

All automated radiosyntheses were carried out in a home-made synthesis module. FFKM valves (Christian Bürkert GmbH&Co. KG, Ingelfingen, Germany) were applied. All connections between the valves were made using PTFE tubes and PEEK fittings. The flow scheme for the preparation of radiolabeled amino acids is depicted in (Fig. 38). Synthetic air and He (Westfalen AG, Muenster, Germany) were used as operating gases.

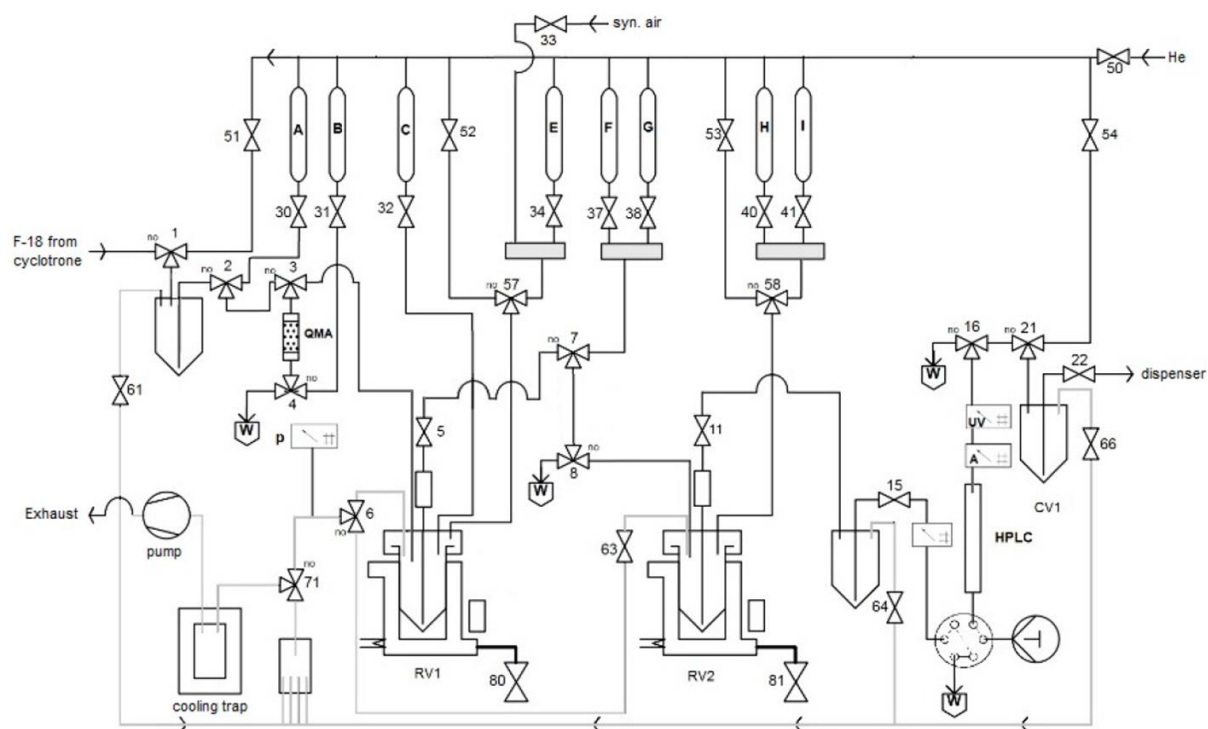


Figure 38. Process flow diagram (PFD) for the automated radiosynthesis of  $^{18}\text{F}$ -labeled AAAs. A: MeOH (2 mL); B:  $\text{Et}_4\text{NHCO}_3$  (3 mg, 15.7  $\mu\text{mol}$ ) in MeOH (0.75 mL); C:  $\text{Cu}(\text{OTf})_2(\text{py})_4$  (13.6 mg, 20  $\mu\text{mol}$ ) and radiolabeling precursor (10  $\mu\text{mol}$ ) in DMA/*n*-BuOH (3:1) (0.75 mL); E: 37% HCl (1 mL); F: 6% EtOH<sub>aq</sub> (1 mL).

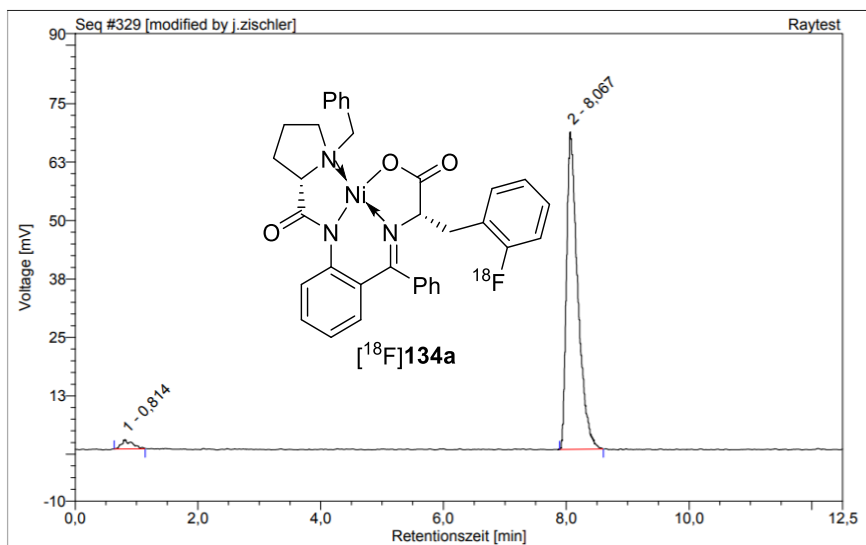
1. Loading of [ $^{18}\text{F}$ ]fluoride onto a QMA ion exchange cartridge;
2. Washing of the QMA with MeOH (2 mL);
3. Closing air valve (50), and system venting;
4. Elution of [ $^{18}\text{F}$ ]fluoride from the ion-exchange cartridge with a methanolic solution of  $\text{Et}_4\text{NHCO}_3$  into RV 1;
5. Open air valve (50) to transfer methanolic solution from QMA to RV 1 completely;
6. Evaporation of MeOH in RV1 at 80 °C for 3–5 min using a flow of synthetic air under reduced pressure;
7. Addition of a solution of the radiolabeling precursor (10  $\mu\text{mol}$ ) and  $\text{Cu}(\text{OTf})_2(\text{py})_4$  (20  $\mu\text{mol}$ ) in *n*-BuOH/DMA 1:3 (0.75 mL);
8. Heating of the reaction mixture in RV1 at 110 °C for 15 min;
9. Evaporation of reaction mixture in RV1 at 110 °C for 10 min;
10. Addition of 37% HCl (1 mL) and heating at 110 °C for 15 min;
11. Evaporation of reaction mixture in RV1 at 130 °C for 10 min;
12. Addition of 6%  $\text{EtOH}_{\text{aq}}$  (1 mL) in RV1;
13. Injection of the loop content onto the HPLC column and elution with 6%\*  $\text{EtOH}_{\text{aq}}$  (0.2%  $\text{H}_4\text{PO}_3$ ) at 1.3 mL/min;
14. Manual collection of the product fraction in a collection vial (CV1).

\*Depending on the desired  $^{18}\text{F}$ -labeled AAA.

As previously described, the aforementioned radiosynthetic protocol was not robust.

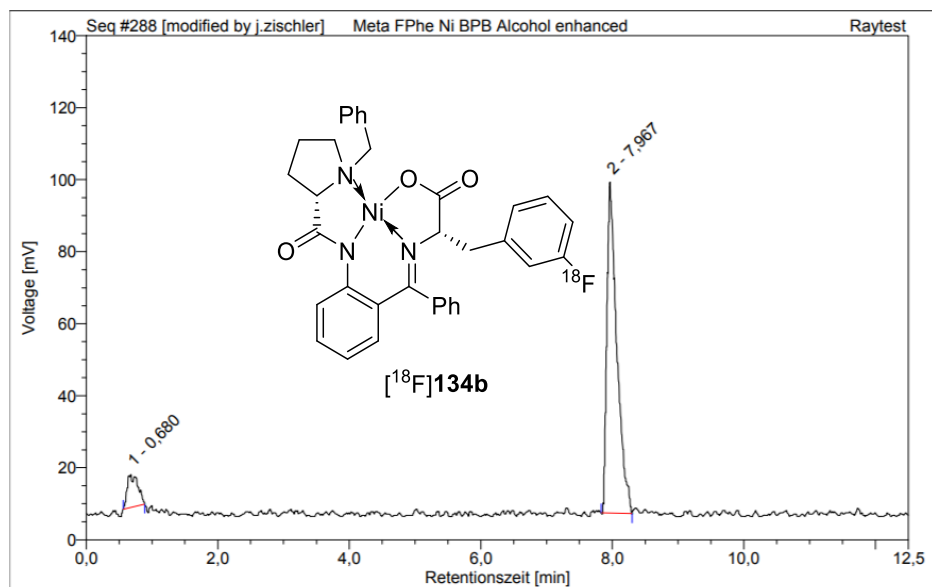
## 8. Radio HPLC Traces and RCC Data for $^{18}\text{F}$ -Labeled Products

### $^{18}\text{F}$ 134a (Gradient A1)



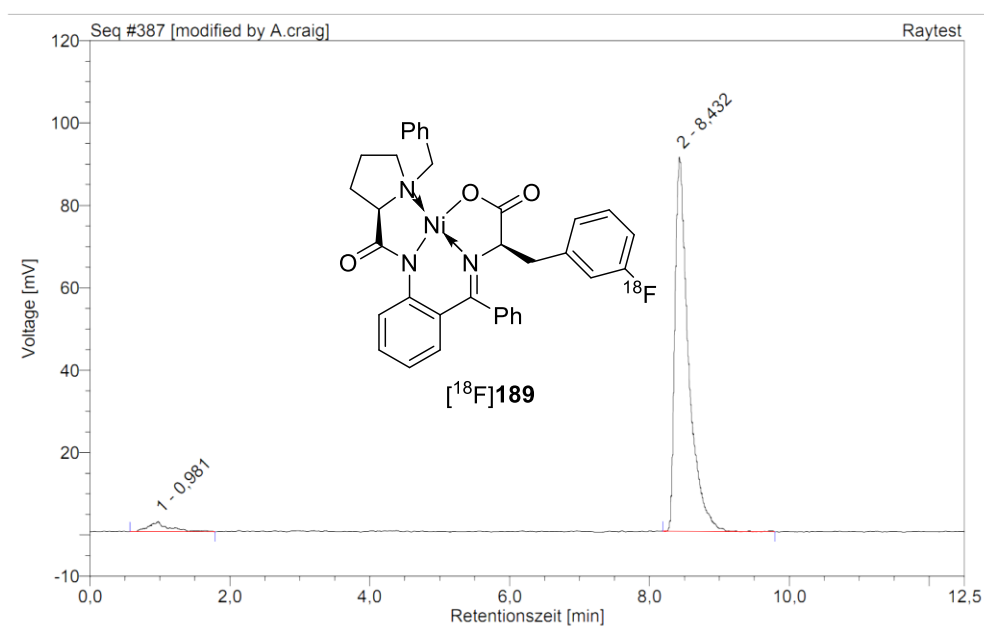
Nr.	Retentionszeit min	Intensität mAU	Integral %
1	0,81	1,965	2,76
2	8,07	67,890	97,24
Total:		69,855	100,00

### $^{18}\text{F}$ 134b (Gradient A1)

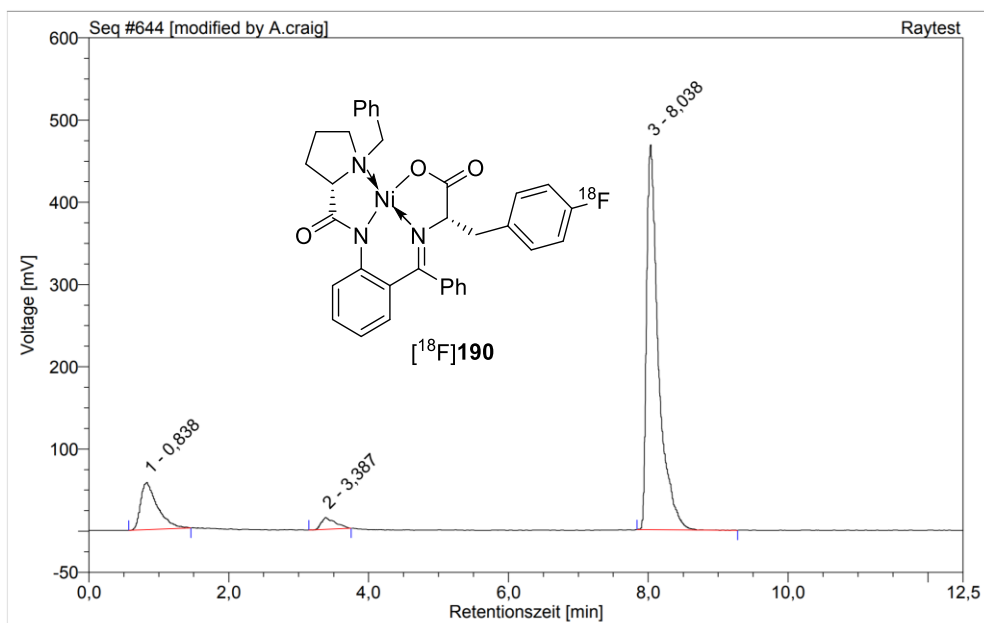


Nr.	Retentionszeit min	Intensität mAU	Integral %
1	0,68	9,128	9,45
2	7,97	91,921	90,55
Total:		101,048	100,00

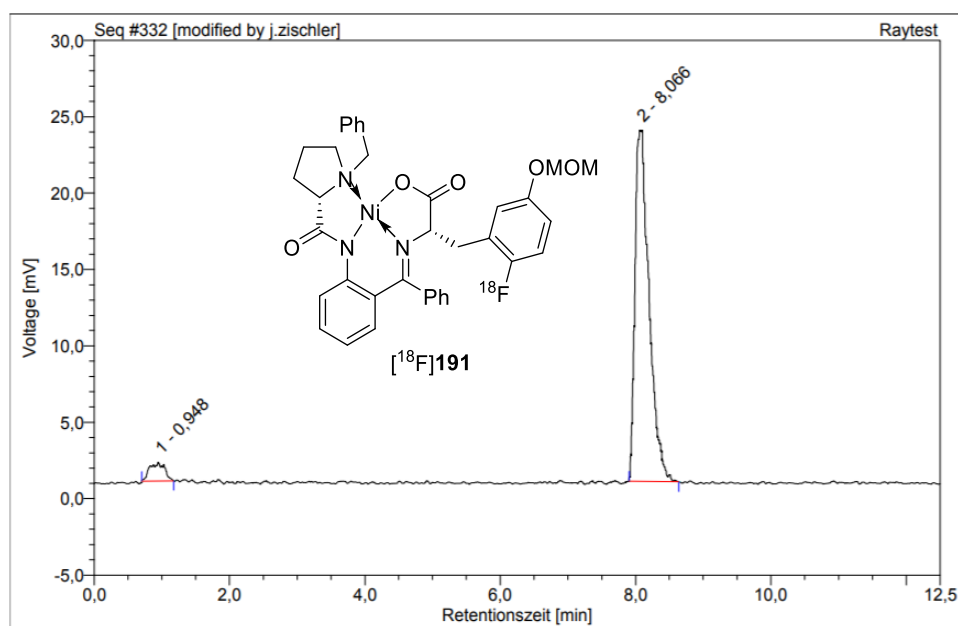
# **[<sup>18</sup>F]189 (Gradient A1)**



# **[<sup>18</sup>F]190 (Gradient A1)**

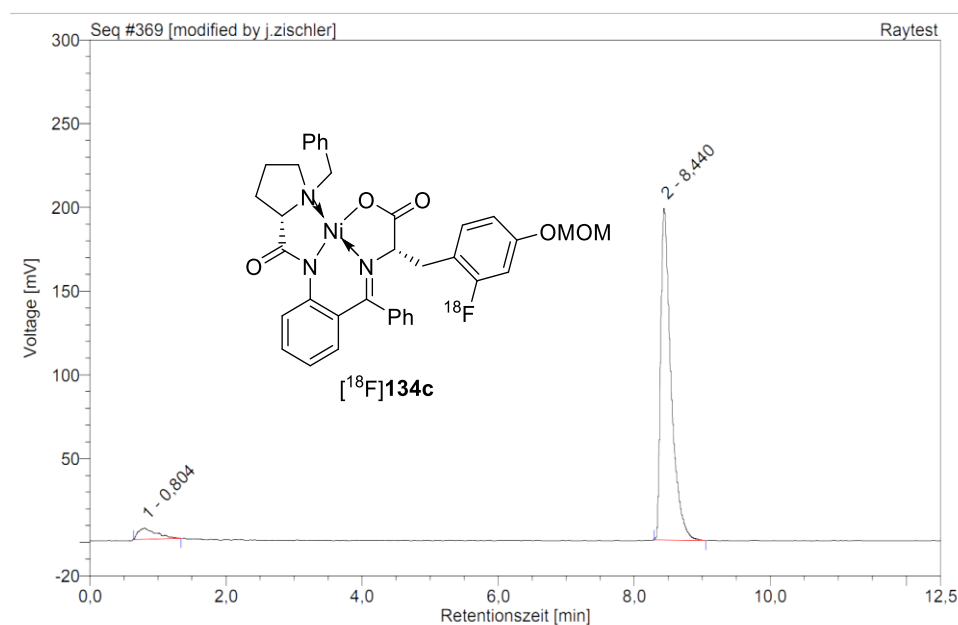


**[<sup>18</sup>F]191 (Gradient A1)**



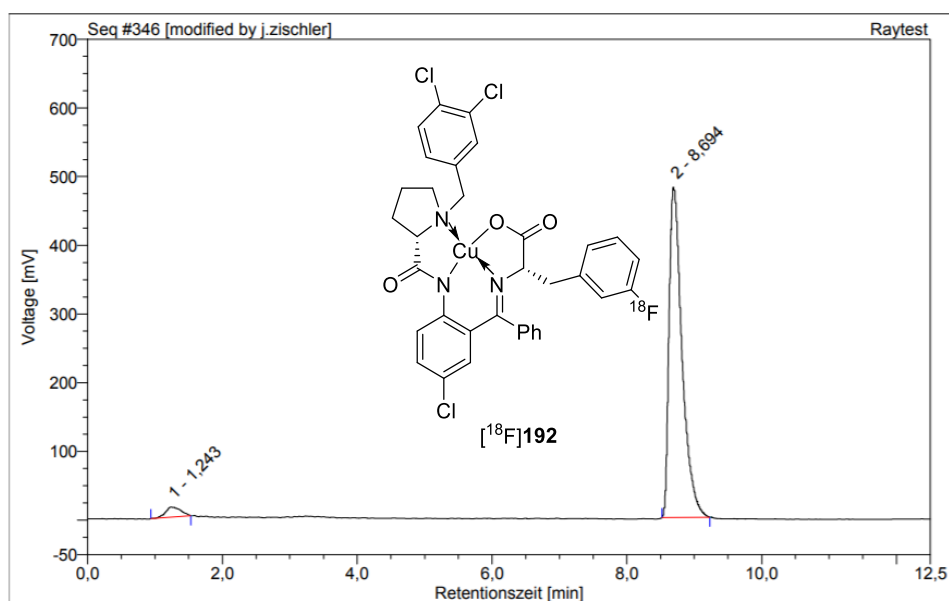
Nr.	Retentionszeit min	Intensität mAU	Integral %
1	0,95	1,222	5,28
2	8,07	22,987	94,72
Total:		24,209	100,00

**[<sup>18</sup>F]134c (Gradient A1)**



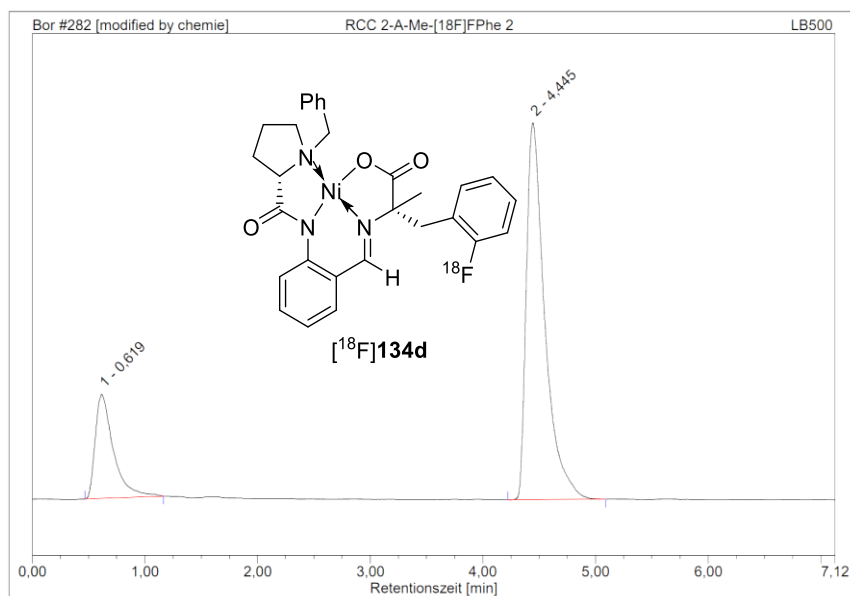
Nr.	Retentionszeit min	Intensität mAU	Integral %
1	0,80	6,724	5,48
2	8,44	198,105	94,52
Total:		204,829	100,00

# **[<sup>18</sup>F]192 (Gradient A1)**



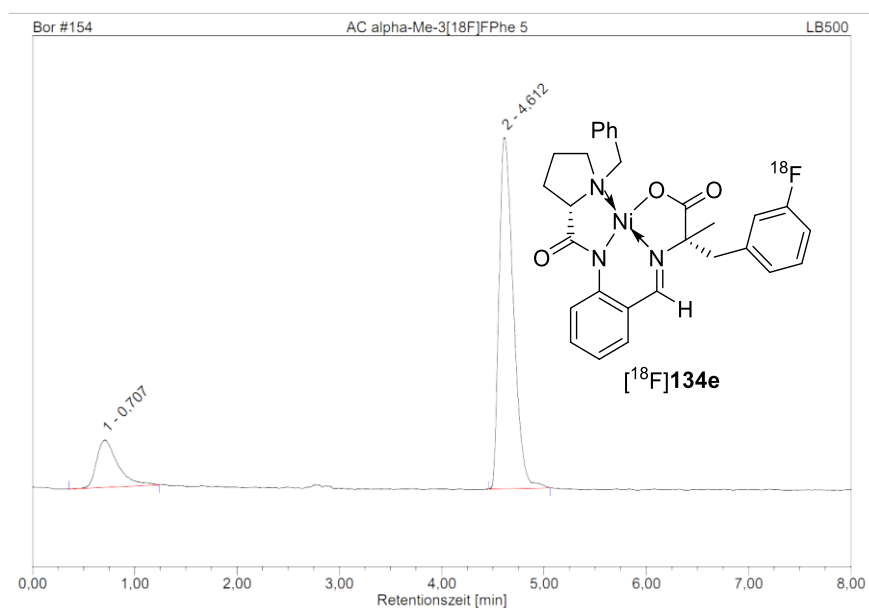
Nr.	Retentionszeit min	Intensität mAU	Integral %
1	1,24	14,748	3,41
2	8,69	480,914	96,59
Total:		495,662	100,00

# **[<sup>18</sup>F]134d (Gradient A1)**



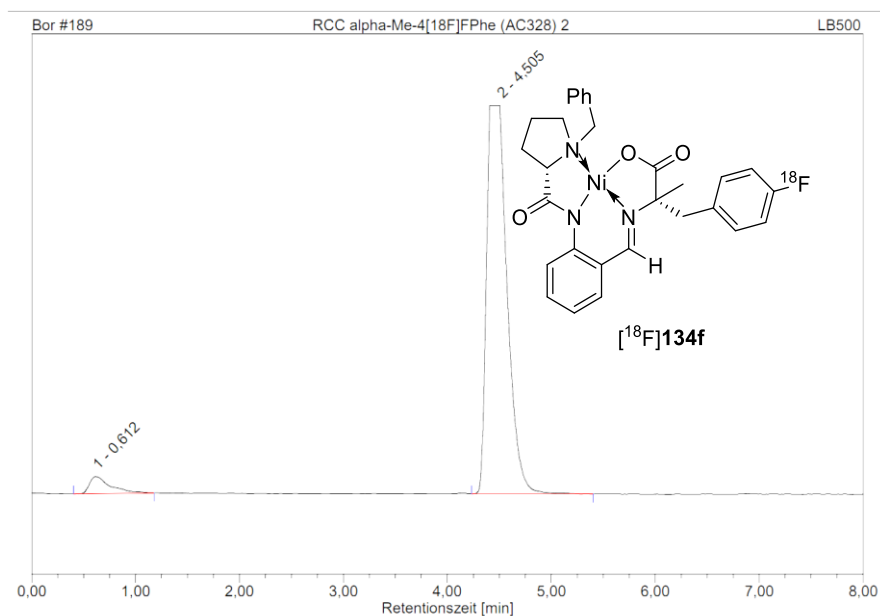
Nr.	Retentionszeit min	Intensität mAU	Integral %
1	0,62	198,870	21,28
2	4,45	722,458	78,72
Total:		921,328	100,00

# **[<sup>18</sup>F]134e (Gradient A1)**



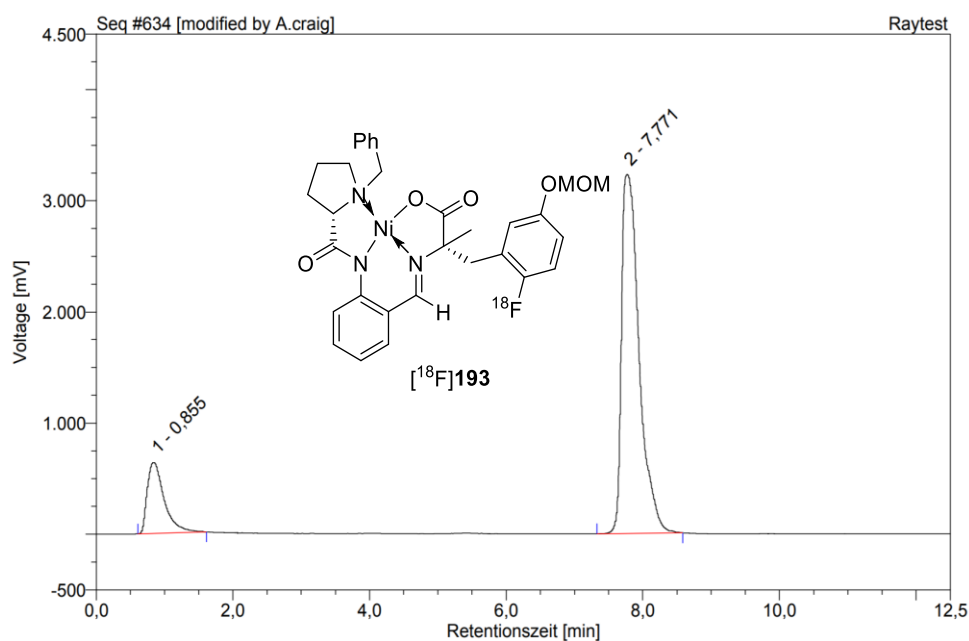
Nr.	Retentionszeit min	Intensität mAU	Integral %
1	0,71	71,571	16,76
2	4,61	529,945	83,24
Total:		601,516	100,00

# **[<sup>18</sup>F]134f (Gradient A1)**



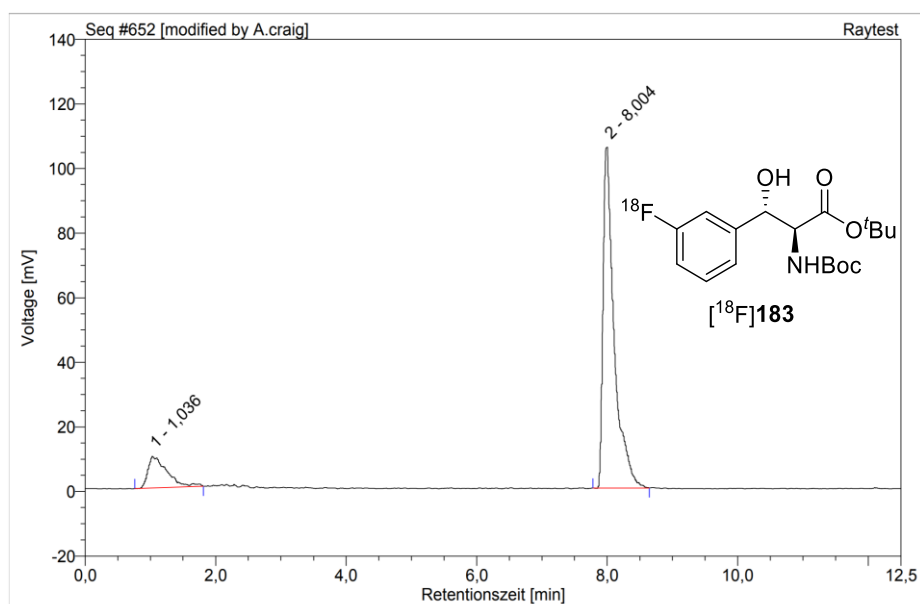
Nr.	Retentionszeit min	Intensität mAU	Integral %
1	0,61	44,688	4,31
2	4,50	1006,396	95,69
Total:		1051,084	100,00

# **[<sup>18</sup>F]193 (Gradient A1)**



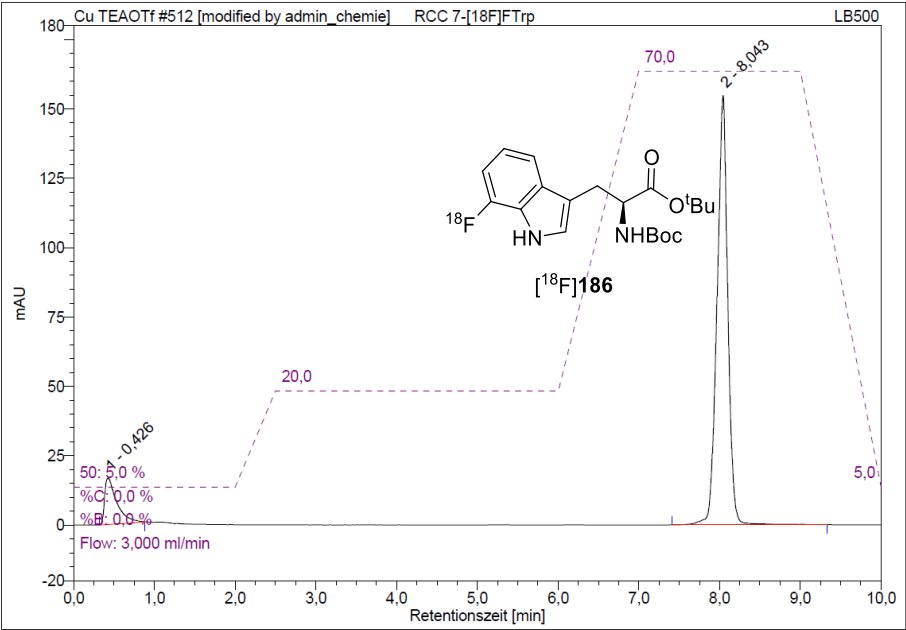
Nr.	Retentionszeit min	Intensität mAU	Integral %
1	0,85	639,907	16,13
2	7,77	3230,428	83,87
Total:		3870,335	100,00

# **[<sup>18</sup>F]183 (Gradient A2)**



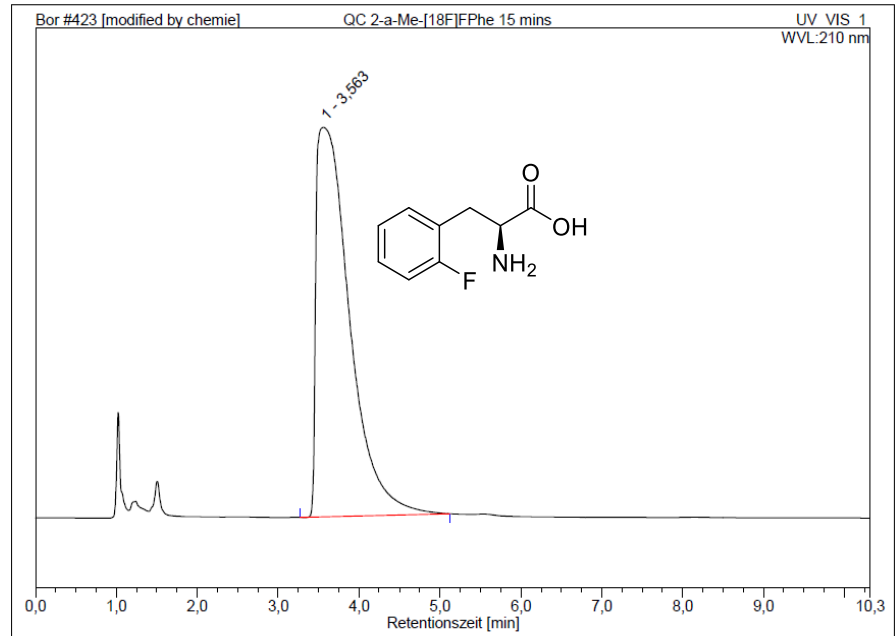
Nr.	Retentionszeit min	Intensität mAU	Integral %
1	1,04	9,850	13,78
2	8,00	105,556	86,22
Total:		115,406	100,00

[<sup>18</sup>F]186 (Gradient A1)

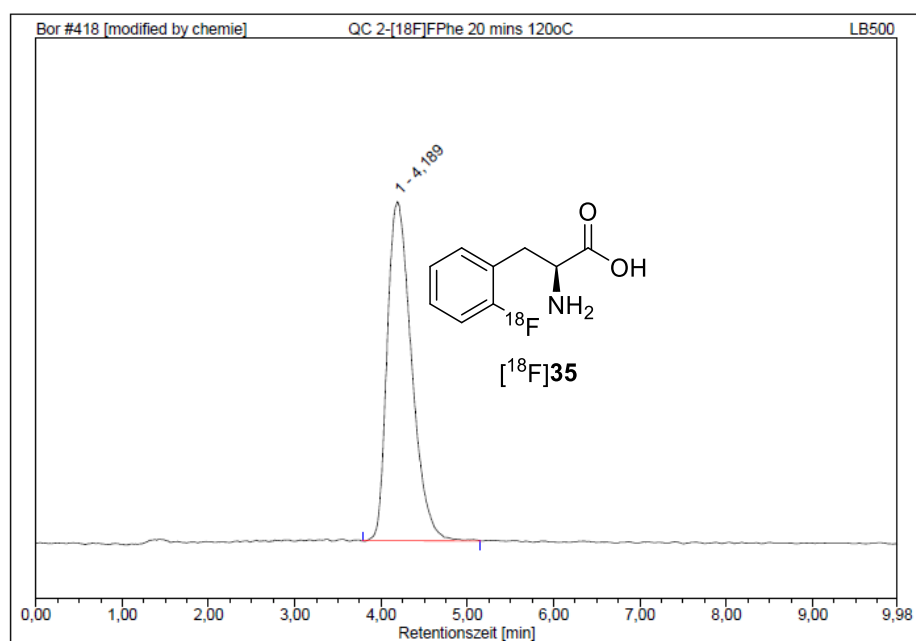


9. Quality Control of Products

2-FPhe (Gradient B1)

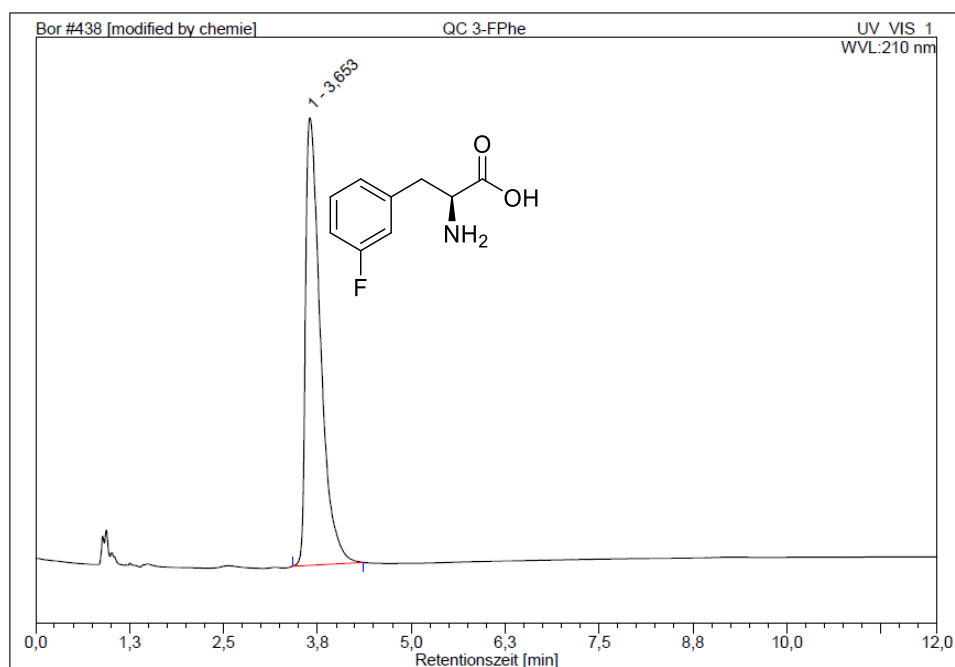


## 2-[<sup>18</sup>F]FPhe ([<sup>18</sup>F]35) (Gradient B1)



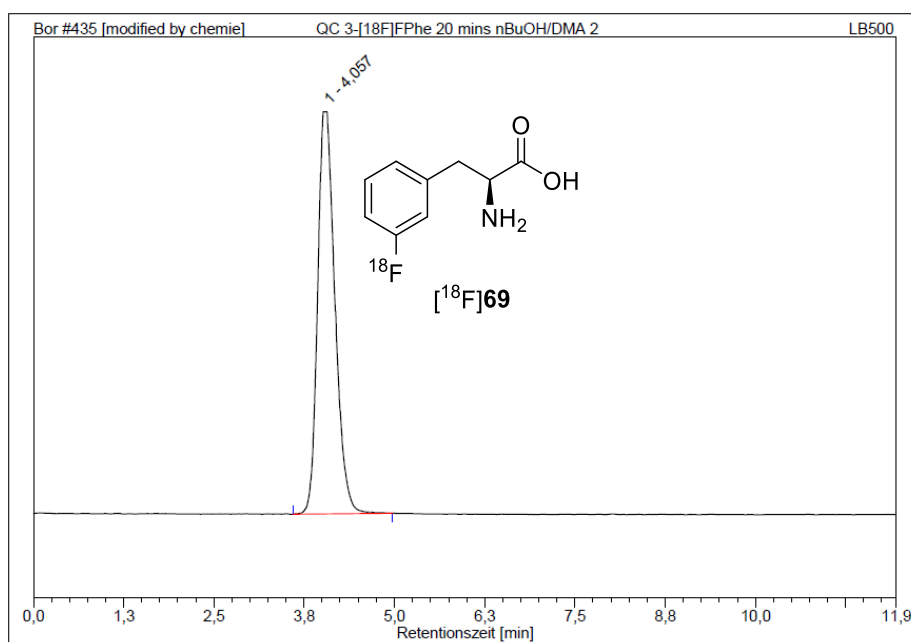
Nr.	Retentionszeit min	Intensität mAU	Integral %
1	4.19	163,696	100,00
Total:		163,696	100,00

## 3-FPhe (Gradient B1)



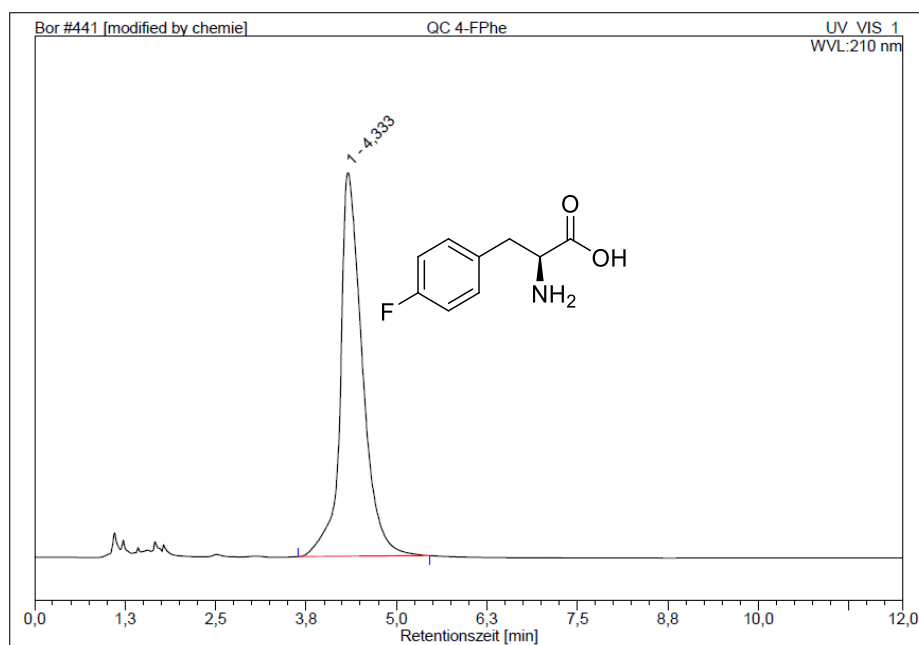
Nr.	Retentionszeit min	Intensität mAU	Integral %
1	3.65	687,692	100,00
Total:		687,692	100,00

### 3-[<sup>18</sup>F]FPhe ([<sup>18</sup>F]68) (Gradient B1)



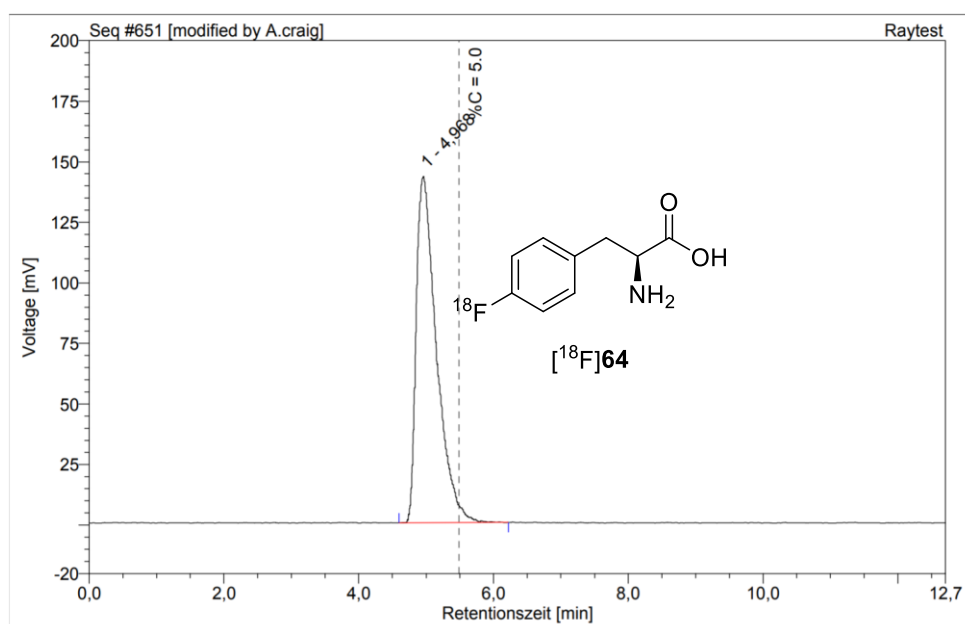
Nr.	Retentionszeit min	Intensität mAU	Integral %
1	4.06	1004,256	100,00
Total:		1004,256	100,00

### 4-FPhe (Gradient B1)



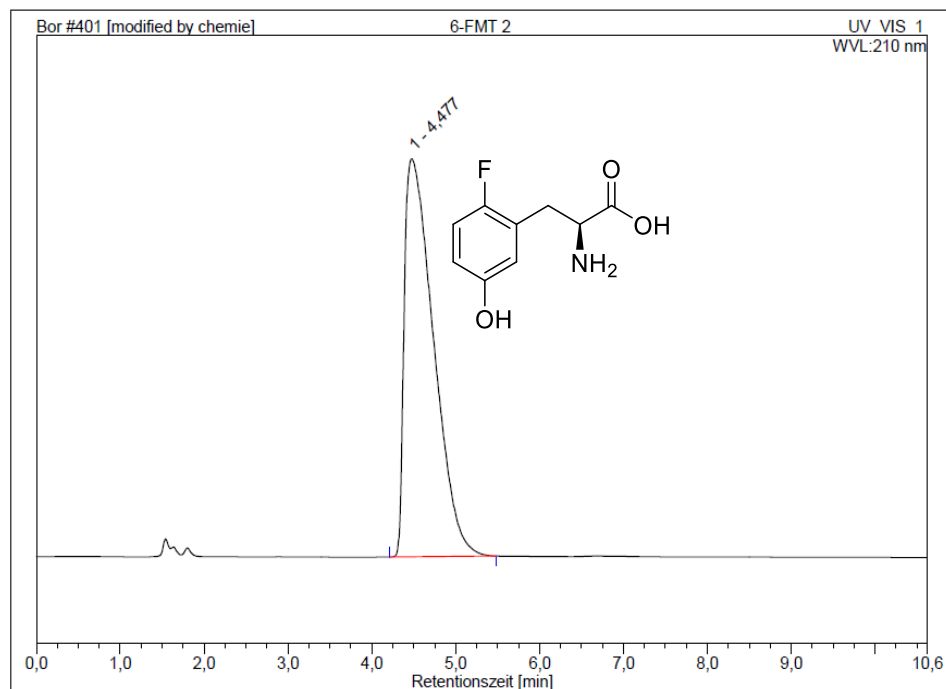
Nr.	Retentionszeit min	Intensität mAU	Integral %
1	4.33	441,810	100,00
Total:		441,810	100,00

#### 4-<sup>18</sup>F]Phe ([<sup>18</sup>F]64) (Gradient B1)



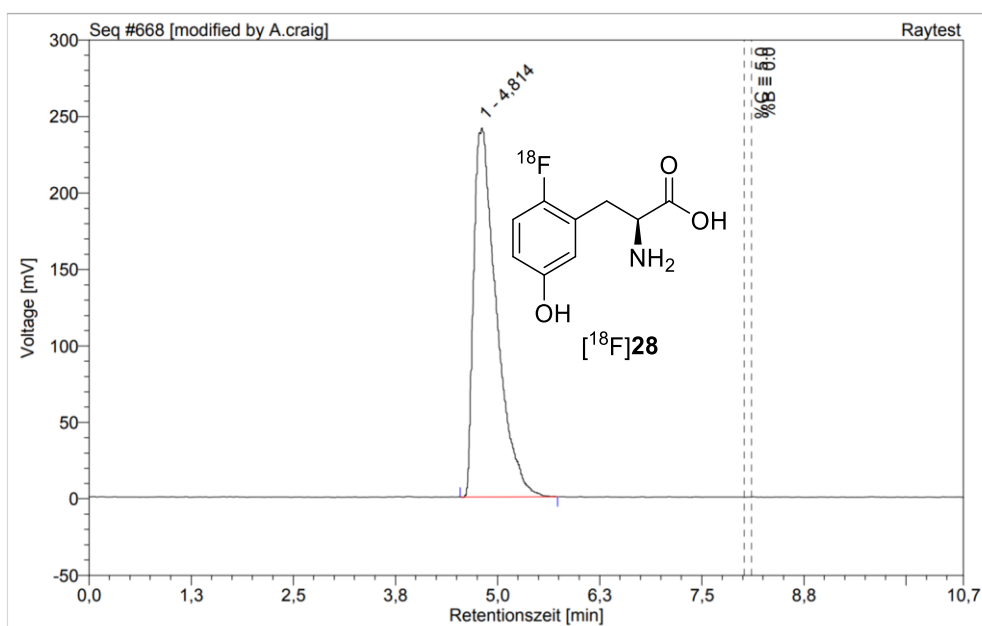
Nr.	Retentionszeit min	Intensität mAU	Integral %
1	4.97	143,092	100,00
Total:		143,092	100,00

#### 6-FMT (Gradient B2)



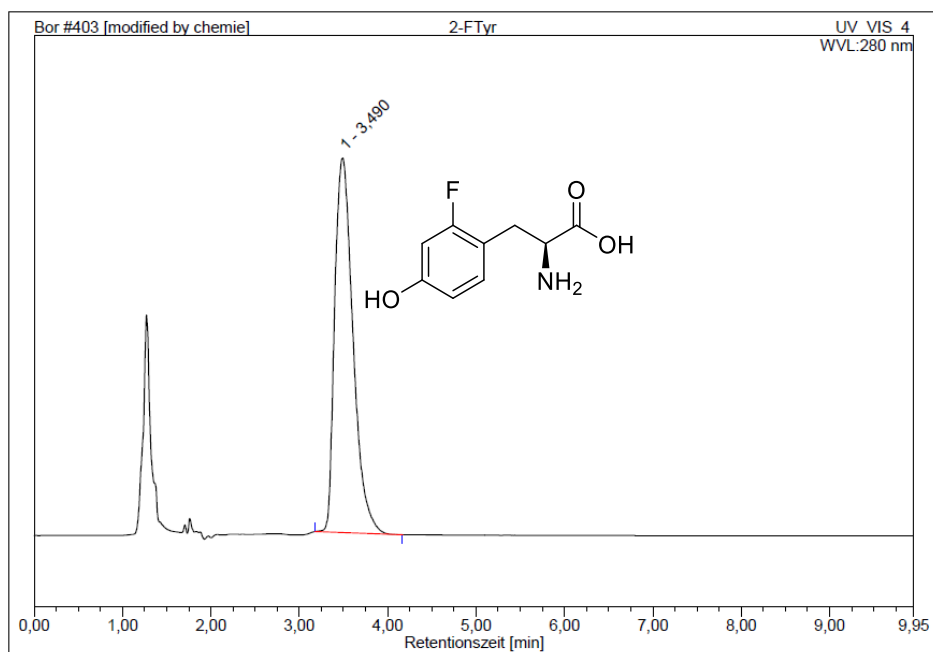
Nr.	Retentionszeit min	Intensität mAU	Integral %
1	4.48	2291,784	100,00
Total:		2291,784	100,00

## 6-<sup>18</sup>F]FMT ([<sup>18</sup>F]28) (Gradient B2)



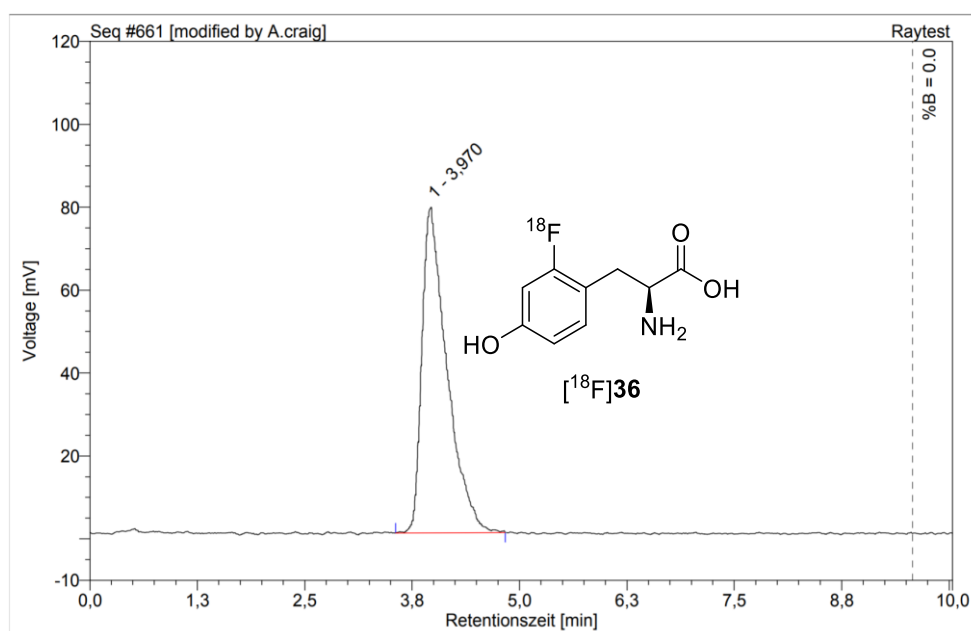
Nr.	Retentionszeit min	Intensität mAU	Integral %
1	4,81	241,305	100,00
Total:		241,305	100,00

## 2-F<sup>18</sup>Tyr (Gradient B2)



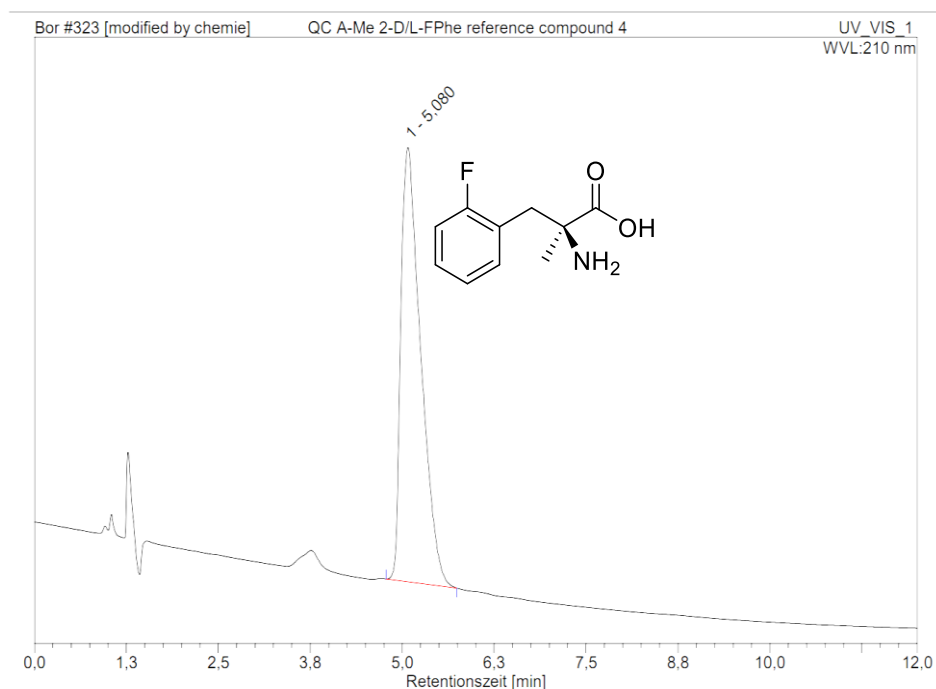
Nr.	Retentionszeit min	Intensität mAU	Integral %
1	3,49	104,956	100,00
Total:		104,956	100,00

## 2- $^{18}\text{F}$ ]FTyr ( $^{18}\text{F}$ ]36) (Gradient B2)



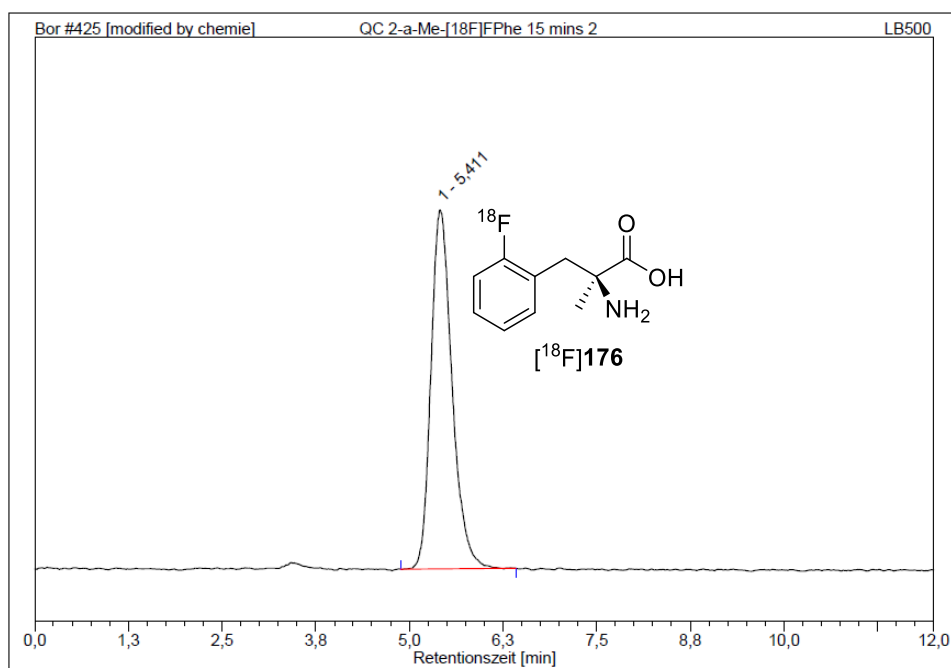
Nr.	Retentionszeit min	Intensität mAU	Integral %
1	3,97	78,543	100,00
Total:		78,543	100,00

## $\alpha$ -Methyl-2-FPhe (Gradient B1)



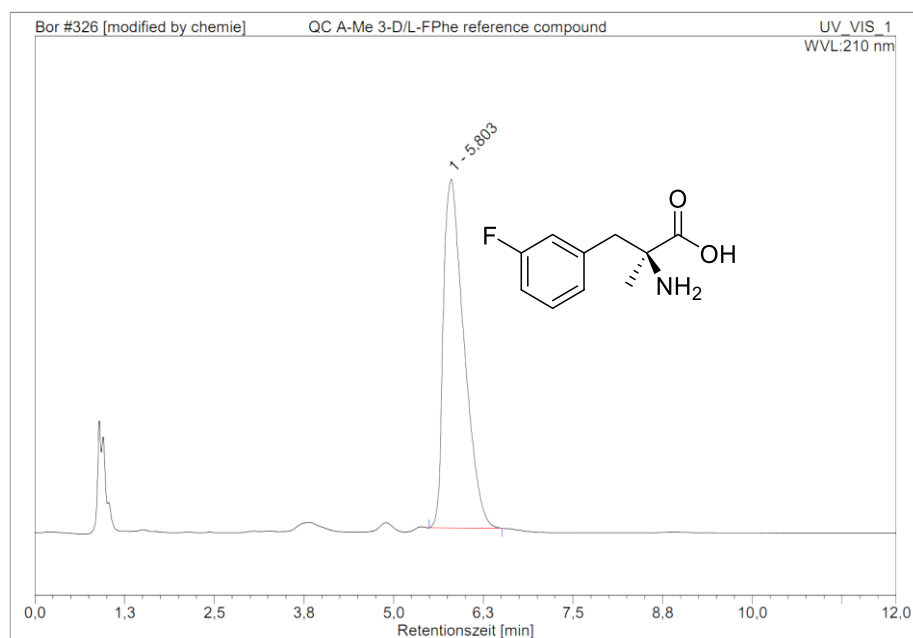
Nr.	Retentionszeit min	Intensität mAU	Integral %
1	5,08	358,252	100,00
Total:		358,252	100,00

### $\alpha$ -Methyl-2-[ $^{18}\text{F}$ ]FPhe ([ $^{18}\text{F}$ ]176) (Gradient B1)



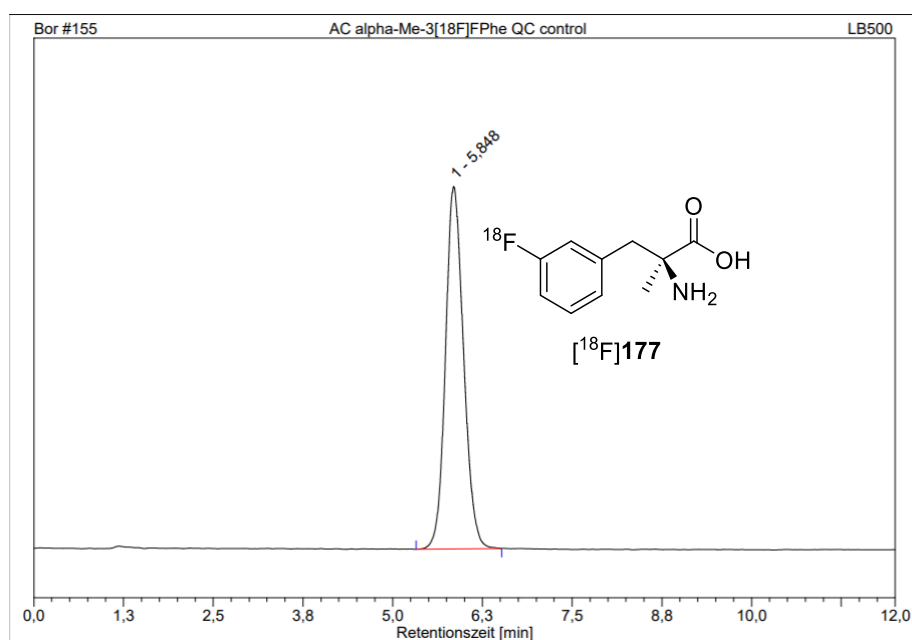
Nr.	Retentionszeit min	Intensität mAU	Integral %
1	5.41	196,987	100,00
Total:		196,987	100,00

### $\alpha$ -Methyl-3-FPhe (Gradient B1)



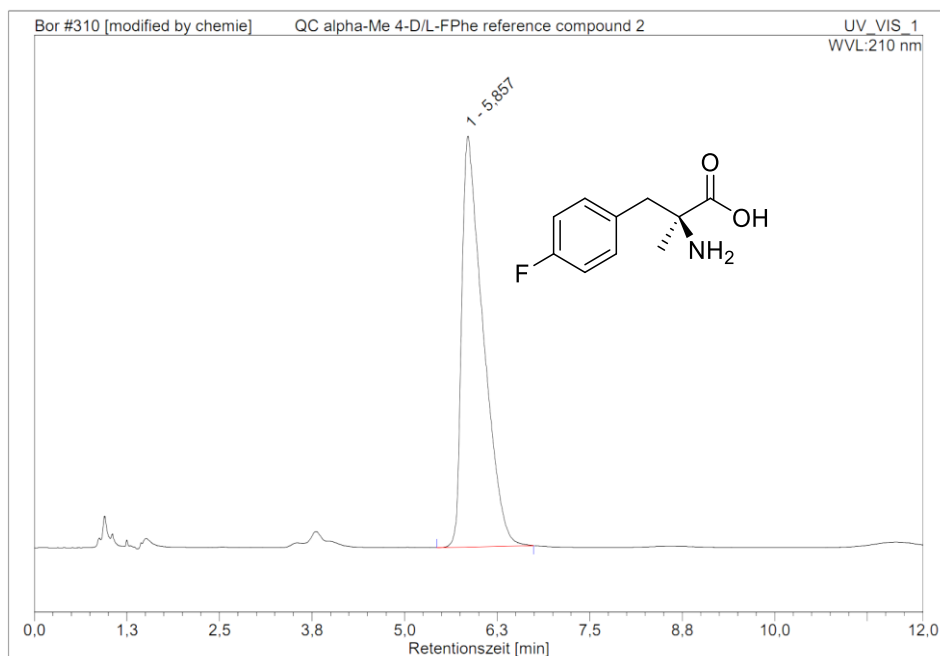
Nr.	Retentionszeit min	Intensität mAU	Integral %
1	5.80	280,639	100,00
Total:		280,639	100,00

### $\alpha$ -Methyl-3- $^{18}\text{F}$ FPhe ( $^{18}\text{F}$ ]177) (Gradient B1)



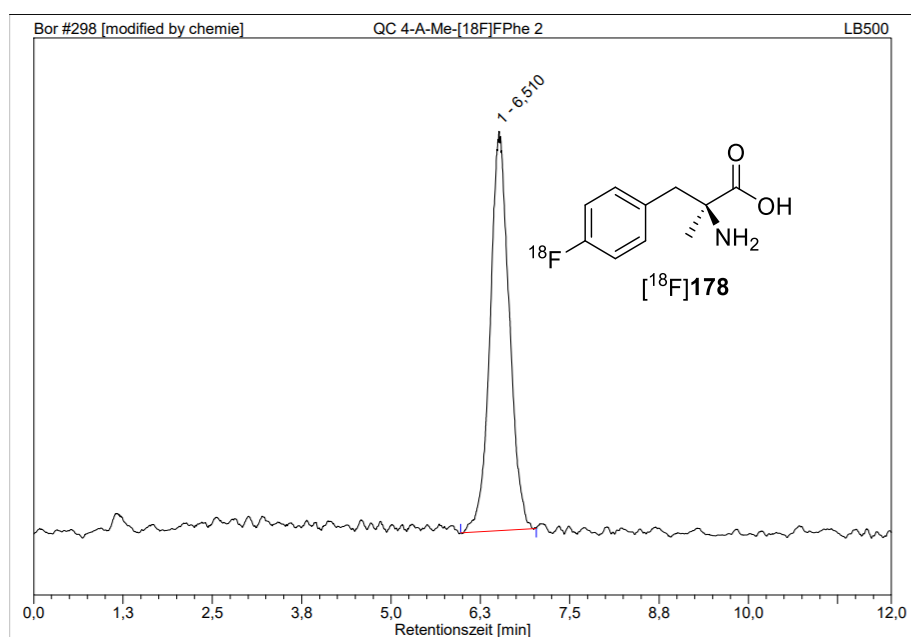
Nr.	Retentionszeit min	Intensität mAU	Integral %
1	5.85	842,027	100,00
Total:		842,027	100,00

### $\alpha$ -Methyl-4-FPhe (Gradient B1)



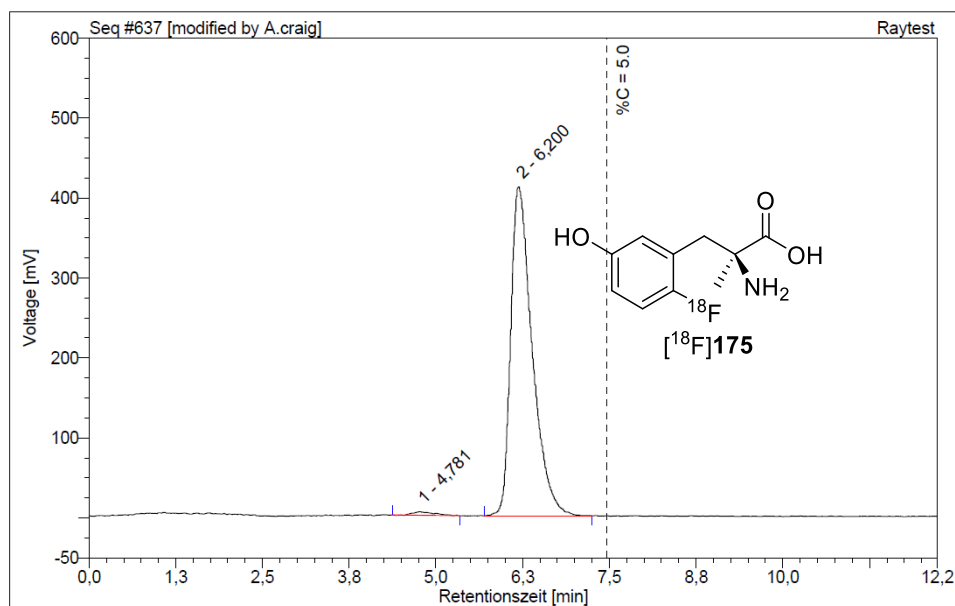
Nr.	Retentionszeit min	Intensität mAU	Integral %
1	5.86	320,770	100,00
Total:		320,770	100,00

**$\alpha$ -Methyl-4-[ $^{18}\text{F}$ ]FPhe ([ $^{18}\text{F}$ ]196) (Gradient B1)**



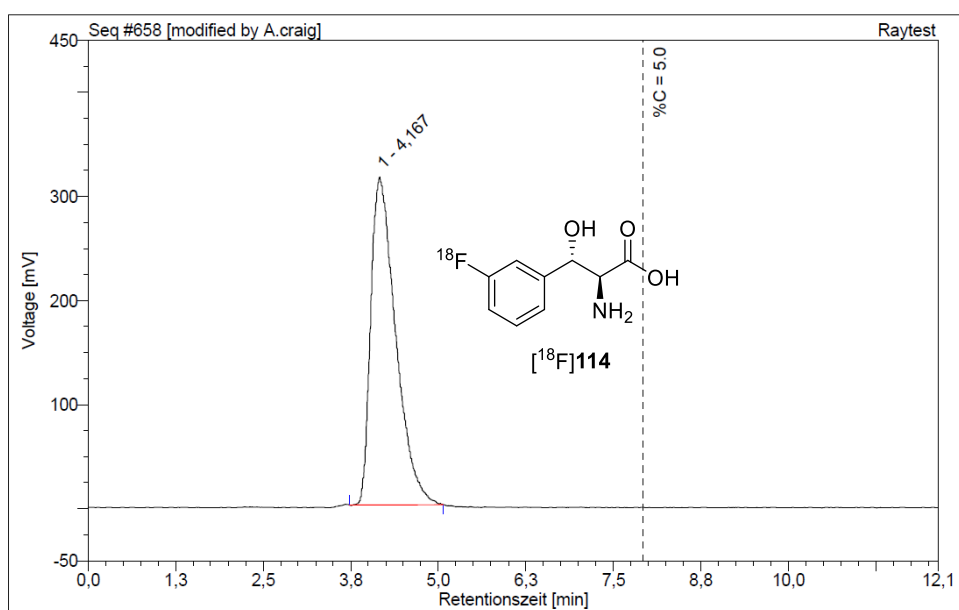
Nr.	Retentionszeit min	Intensität mAU	Integral %
1	6.51	35,846	100,00
Total:		35,846	100,00

**$\alpha$ -Methyl-6-[ $^{18}\text{F}$ ]FMT ([ $^{18}\text{F}$ ]175) (Gradient B1)**



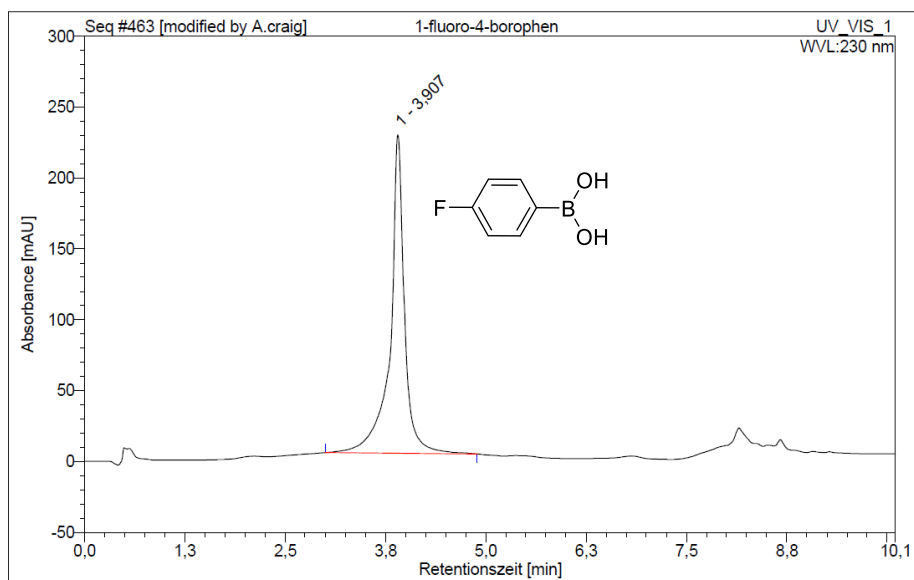
Nr.	Retentionszeit min	Intensität mAU	Integral %
1	4.78	4,369	1,04
2	6.20	411,247	98,96
Total:		415,616	100,00

### 3- $^{18}\text{F}$ FPheSer ( $^{18}\text{F}$ 114) (Gradient B3)



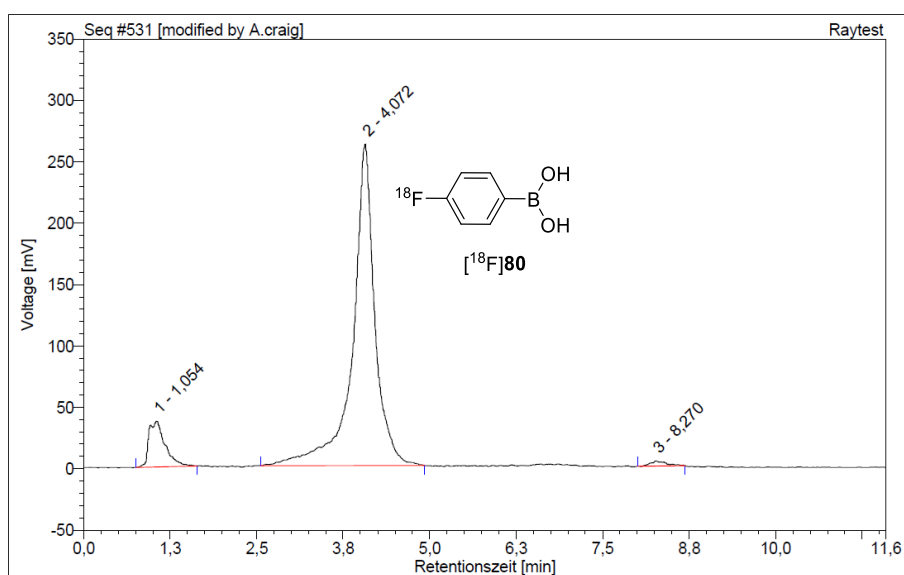
Nr.	Retentionszeit min	Intensität mAU	Integral %
1	4,17	314,812	100,00
Total:		314,812	100,00

### FPBA (Gradient A1)



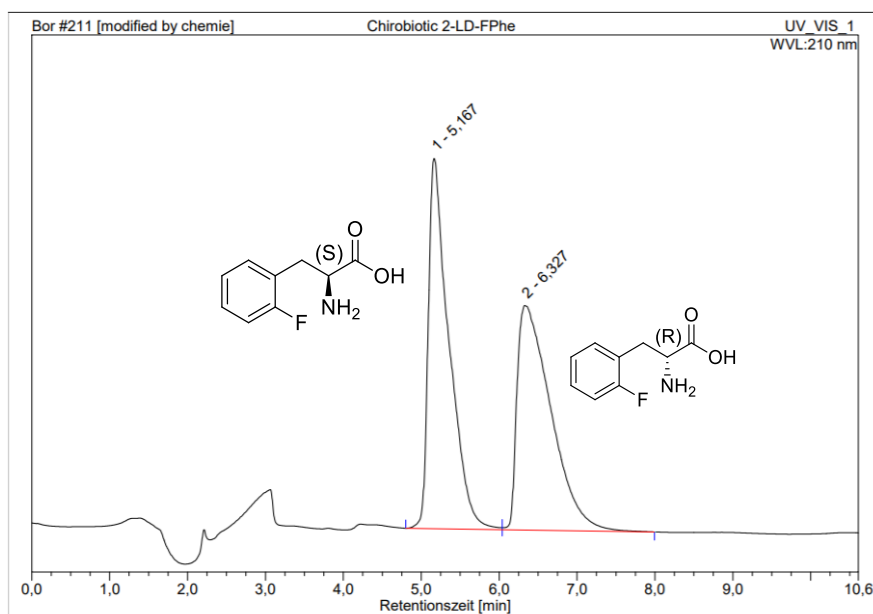
Nr.	Retentionszeit min	Intensität mAU	Integral %
1	3,91	224,830	100,00
Total:		224,830	100,00

## **[<sup>18</sup>F]FPBA ([<sup>18</sup>F]80) (Gradient A1)**



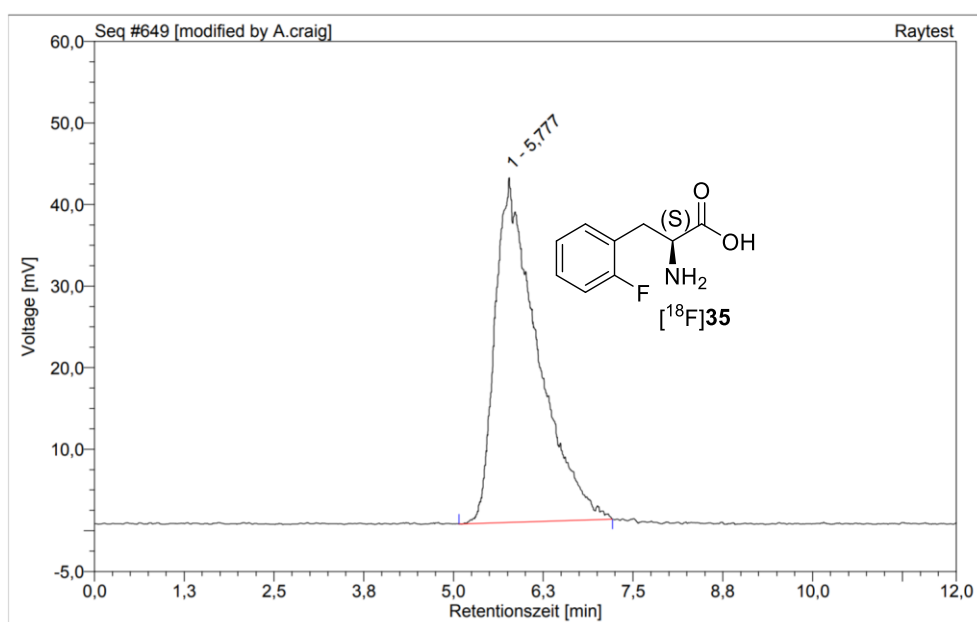
Nr.	Retentionszeit min	Intensität mAU	Integral %
1	1,05	37,504	9,33
2	4,07	262,105	89,69
3	8,27	4,075	0,98
Total:		303,683	100,00

## 10. Determination of Enantiomeric Excess for AAA PET Tracers *rac*-2-FPhe (35) (Gradient C)



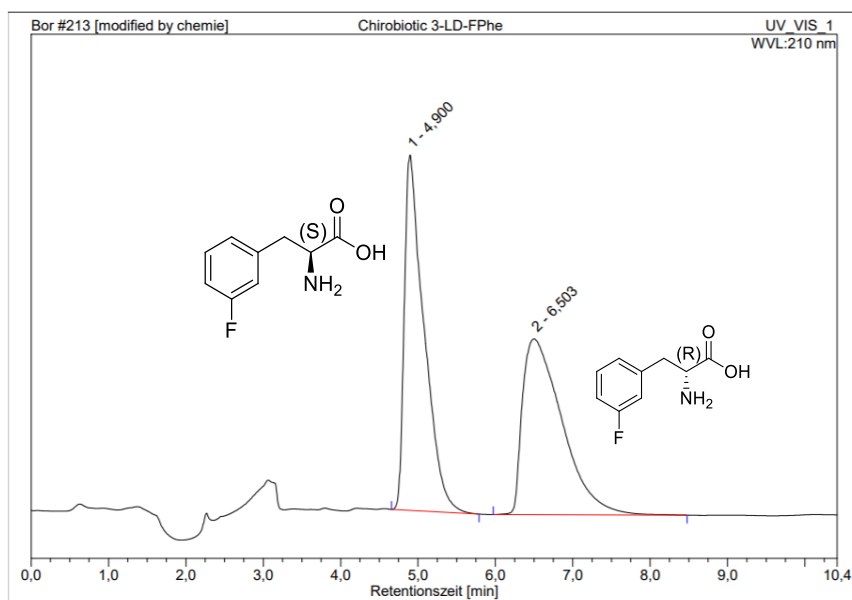
Nr.	Retentionszeit min	Intensität mAU	Integral %
1	5,17	379,213	50,19
2	6,33	230,063	49,81
Total:		609,276	100,00

## 2-[<sup>18</sup>F]FPhe ([<sup>18</sup>F]35) (Gradient C)



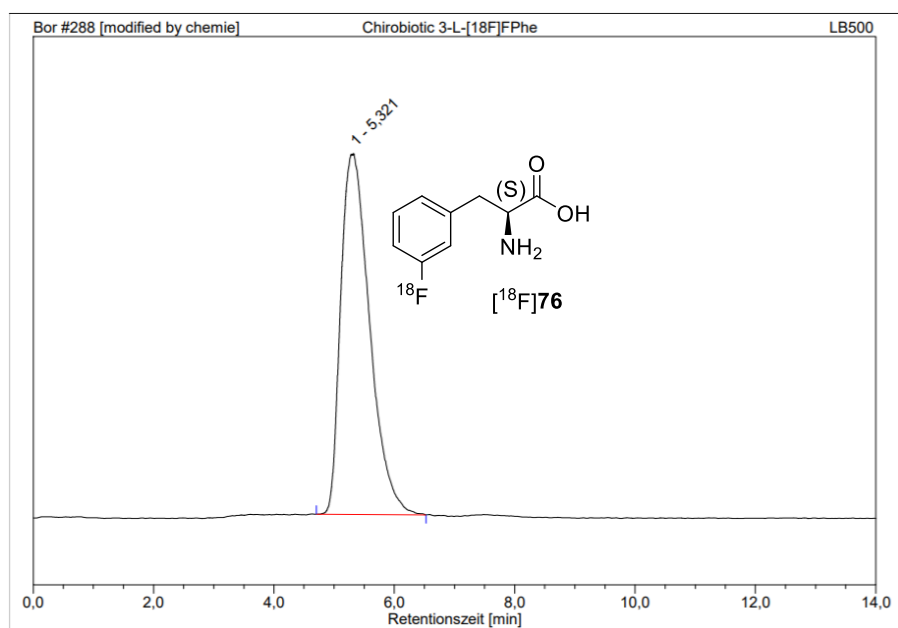
Nr.	Retentionszeit min	Intensität mAU	Integral %
1	5,78	42,251	100,00
Total:		42,251	100,00

## rac-3-FPhe (Gradient C)



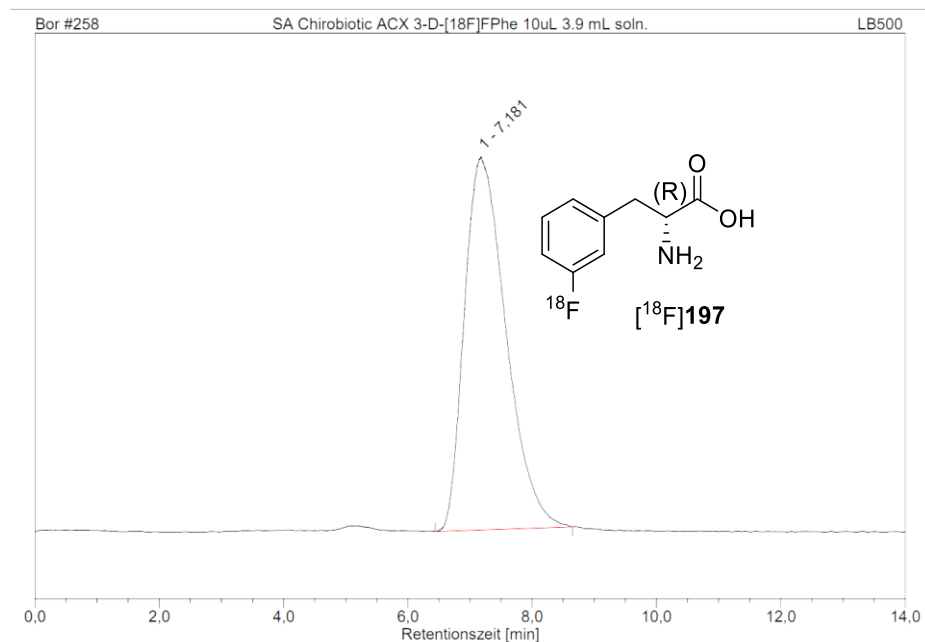
Nr.	Retentionszeit min	Intensität mAU	Integral %
1	4,90	373,068	50,00
2	6,50	184,506	50,00
Total:		557,574	100,00

### 3-<sup>18</sup>F]Phe ([<sup>18</sup>F]68) (Gradient C)



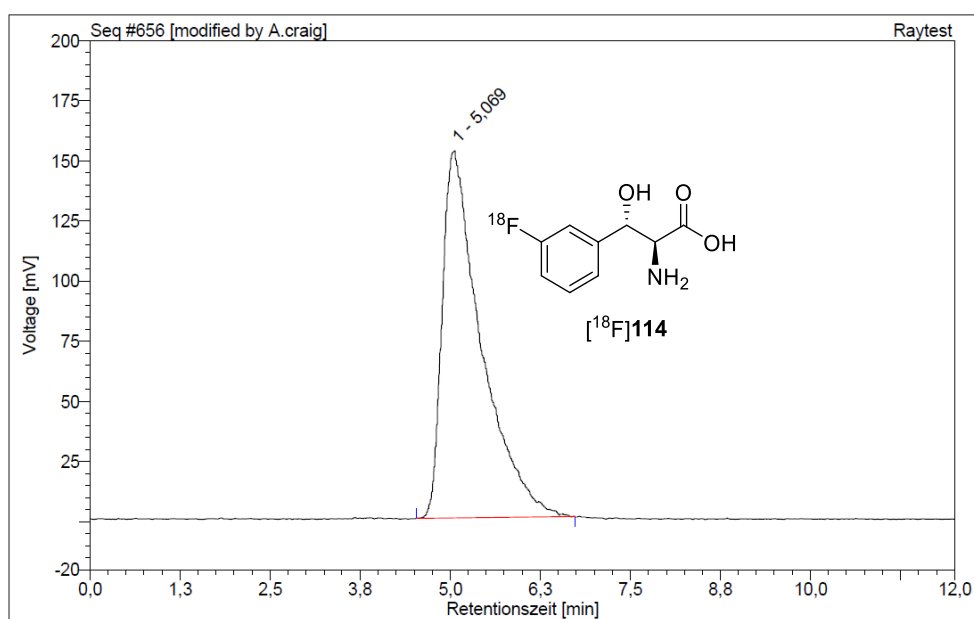
Nr.	Retentionszeit min	Intensität mAU	Integral %
1	5,32	592,219	100,00
Total:		592,219	100,00

### 3-(*R*)-<sup>18</sup>F]Phe ([<sup>18</sup>F]197) (Gradient C)



Nr.	Retentionszeit min	Intensität mAU	Integral %
1	7,18	593,283	100,00
Total:		593,283	100,00

### 3-<sup>18</sup>F]PheSer (<sup>18</sup>F]114) (Gradient C)



Nr.	Retentionszeit min	Intensität mAU	Integral %
1	5.07	152,784	100,00
Total:		152,784	100,00

## 11. Supplementary Information: PET Evaluation

All images and graphs courtesy of Prof. apl. Heike Endepols, Mr. Lukas Vieth and Mrs. Maximiliane-Felicia Krämer.

### 11.1.1. 2- $^{18}\text{F}$ FPhe in Healthy Rats with/without Benserazide

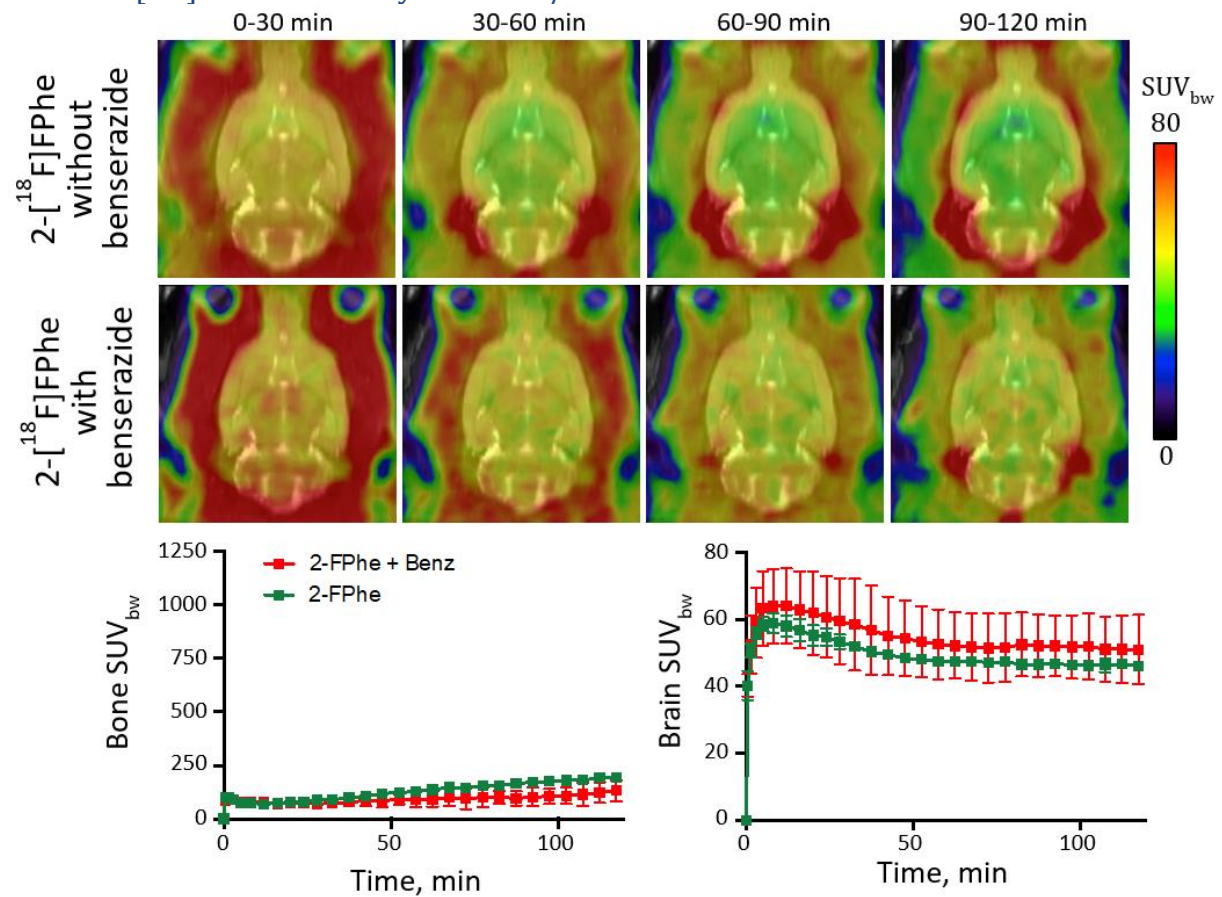


Figure 39. 2- $^{18}\text{F}$ FPhe in healthy rats with/without benserazide.

### 11.2.2. 3- $^{18}\text{F}$ FPhe in Healthy Rats with/without Benserazide

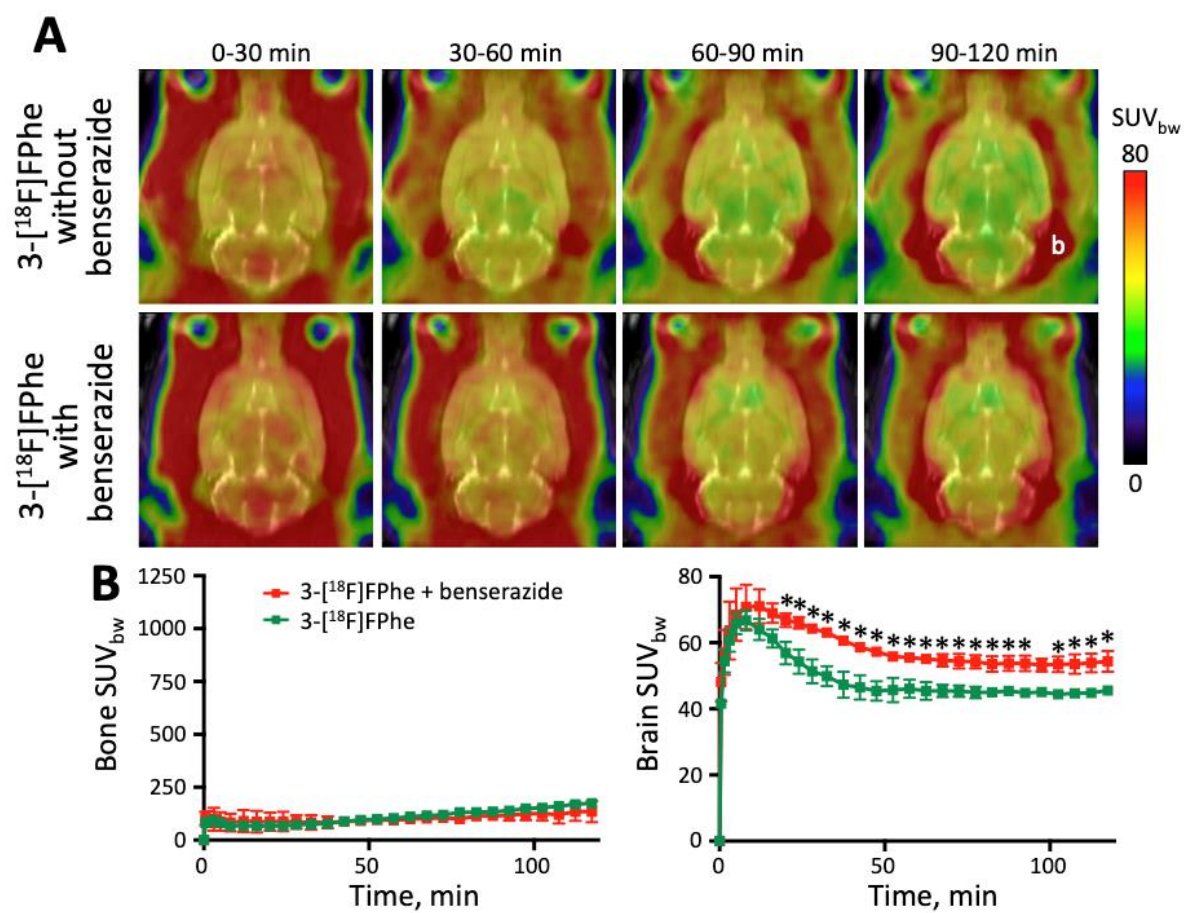


Figure 40. 3- $^{18}\text{F}$ FPhe in healthy rats with/without benserazide.

### 11.2.3. 3-(S)-[ $^{18}\text{F}$ ]FPhe in Healthy Rats with/without Benserazide

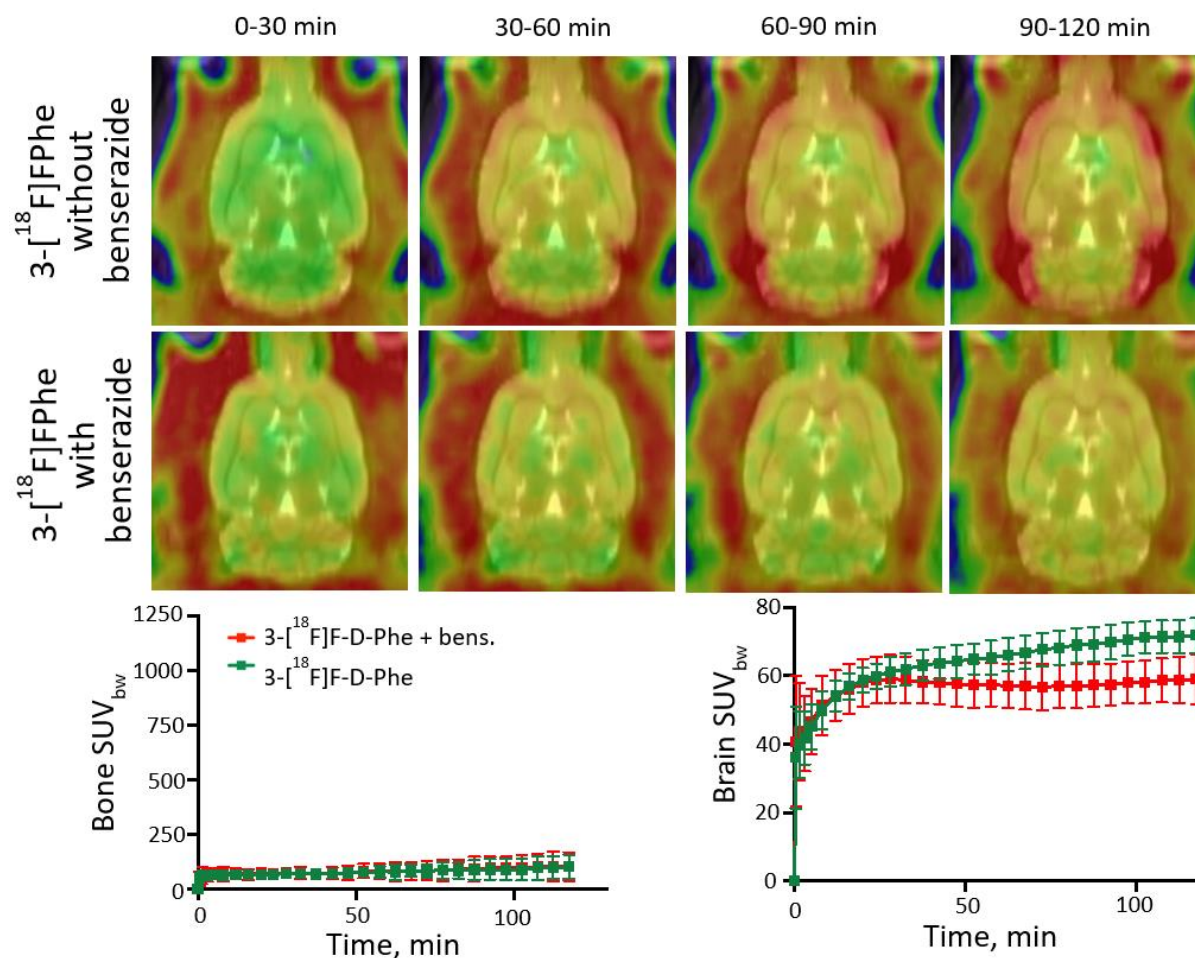


Figure 41. 3-(S)-[ $^{18}\text{F}$ ]FPhe in healthy rats with/without benserazide.

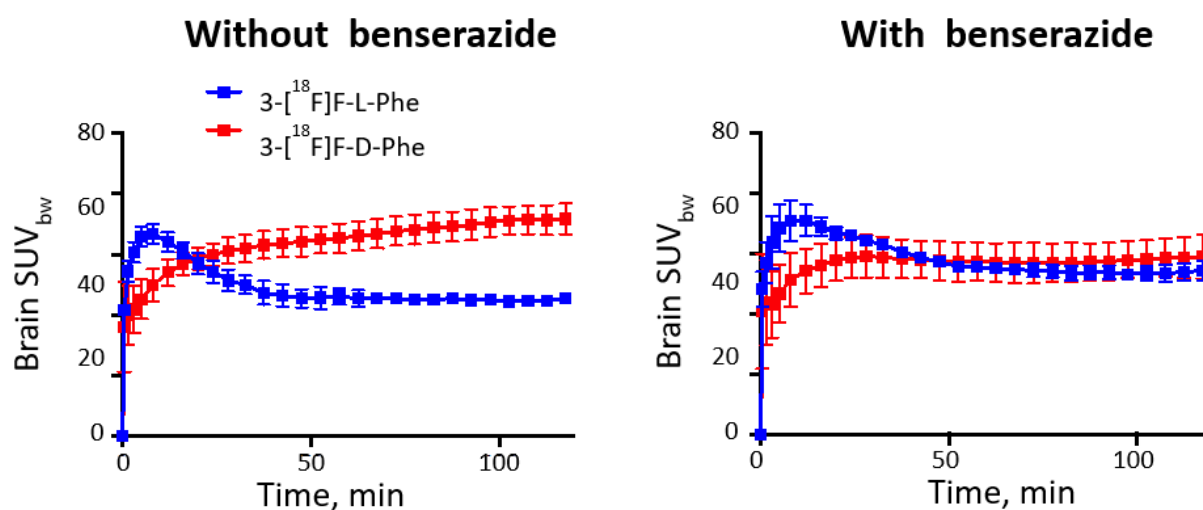


Figure 42. Comparison of 3-[ $^{18}\text{F}$ ]F-L/D-Phe and in healthy rats with/without benserazide.

#### 11.2.4. 4- $^{18}\text{F}$ FPhe in Healthy Rats without Benserazide

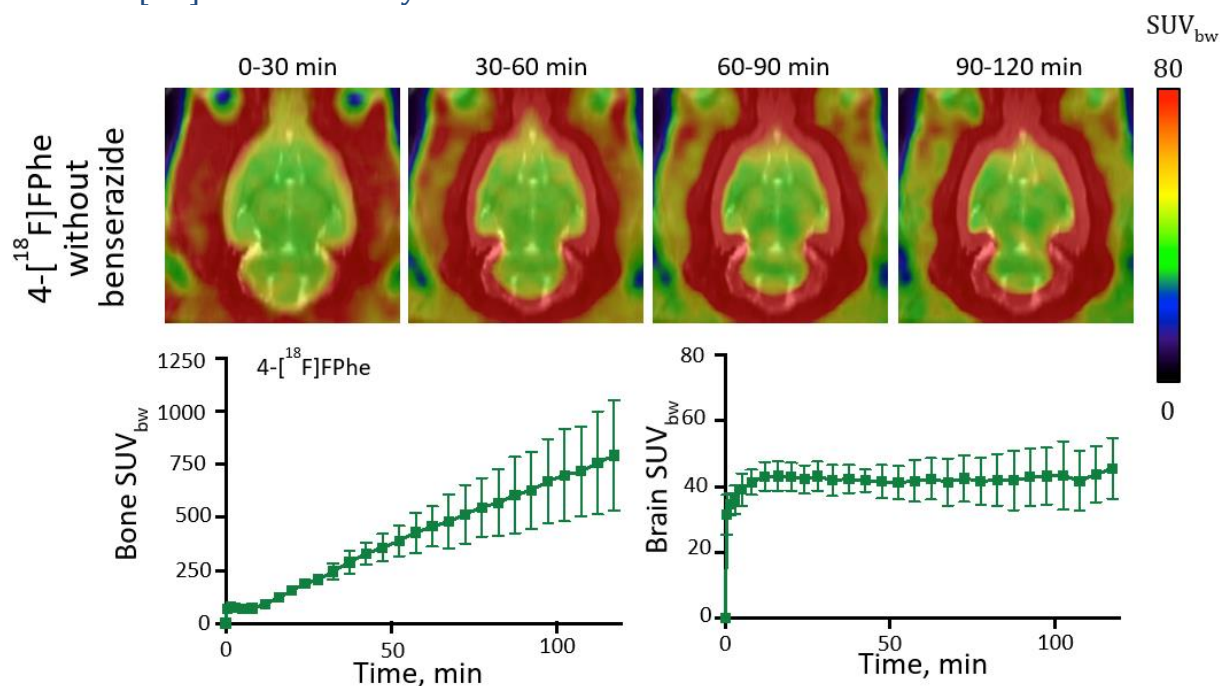


Figure 43. 4- $^{18}\text{F}$ FPhe in healthy rats with/without benserazide.

#### 11.2.5. $\alpha$ -Methyl-2- $^{18}\text{F}$ FPhe in Healthy Rats with/without Benserazide

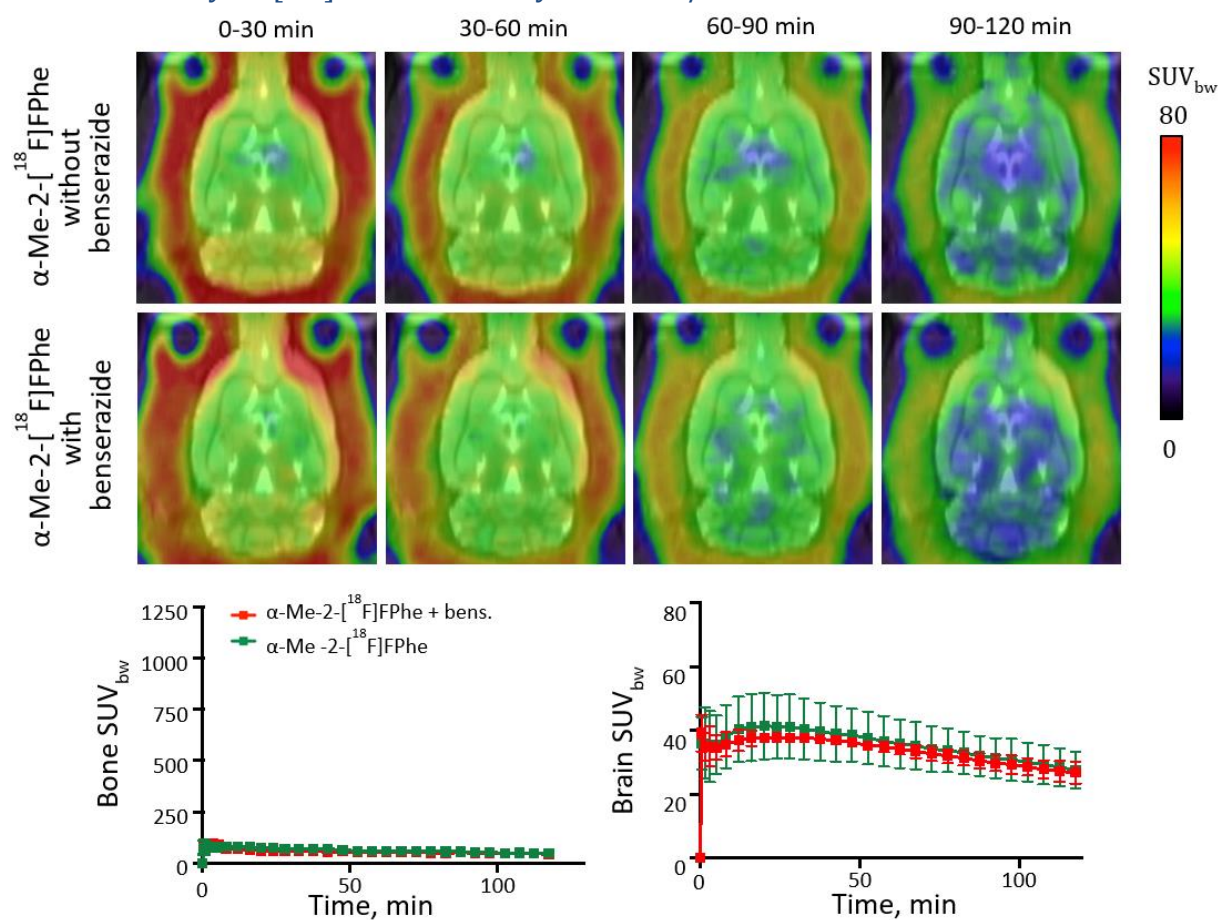


Figure 44.  $\alpha$ -Methyl-2- $^{18}\text{F}$ FPhe in healthy rats with/without benserazide.

### 11.2.6. $\alpha$ -Methyl-3- $^{18}\text{F}$ FPhe in Healthy Rats with/without Benserazide

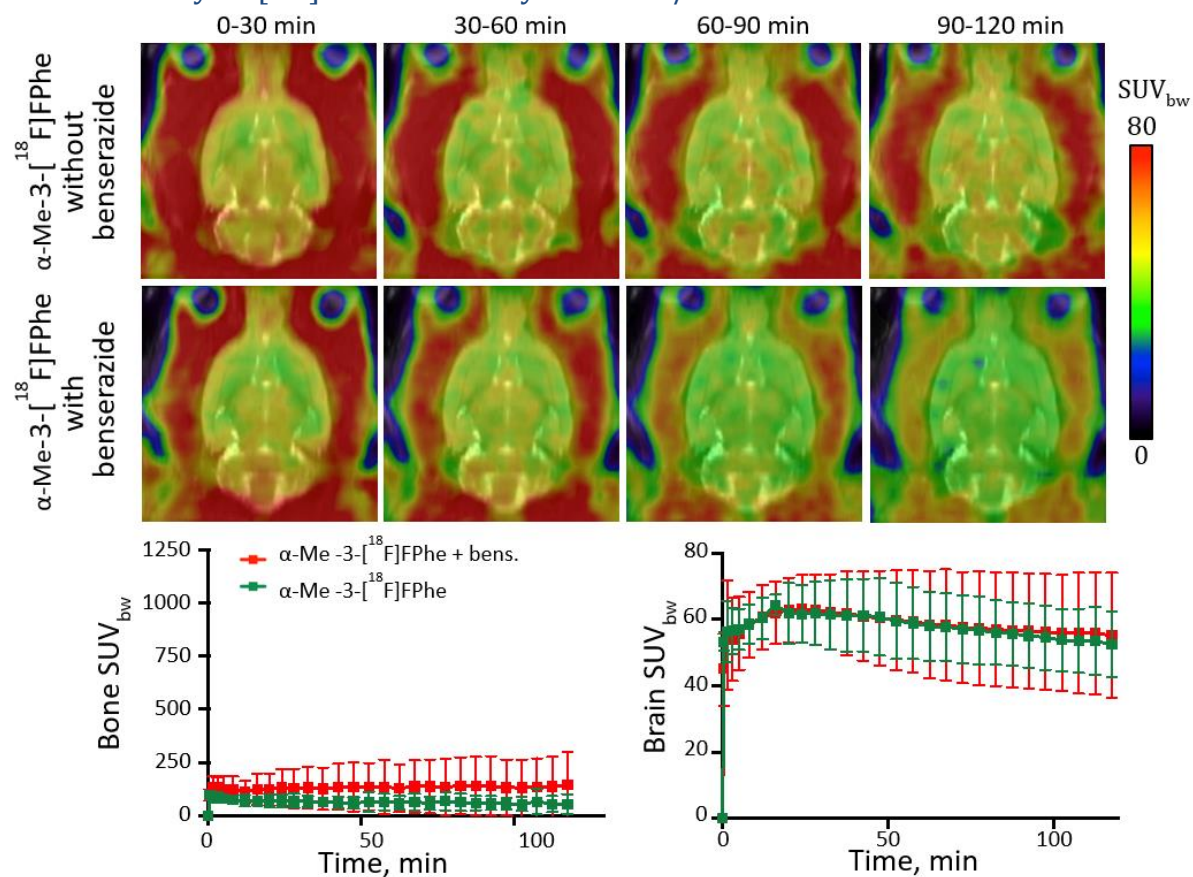


Figure 45.  $\alpha$ -Methyl-3- $^{18}\text{F}$ FPhe in healthy rats with/without benserazide.

### 11.2.7. $\alpha$ -Methyl-4- $^{18}\text{F}$ FPhe in Healthy Rats with/without Benserazide

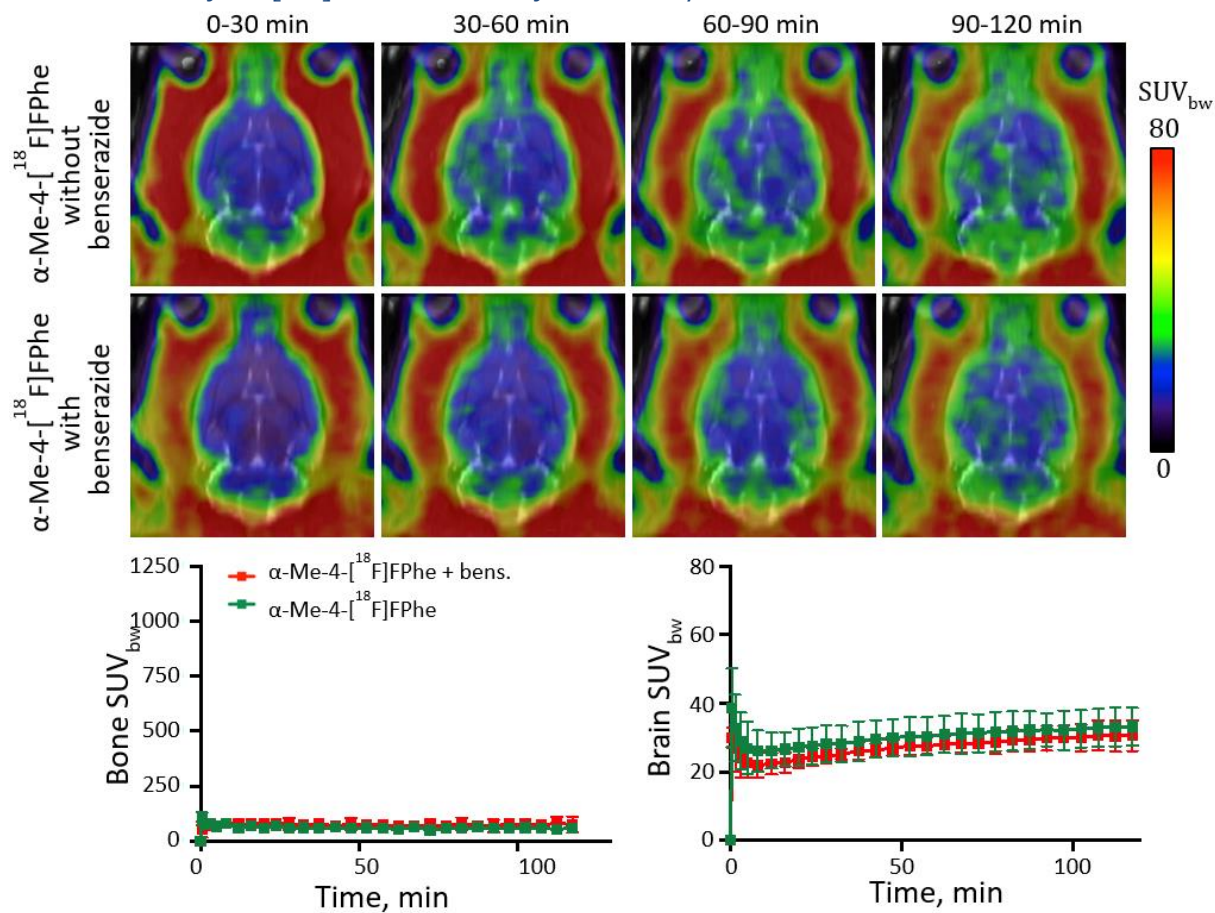
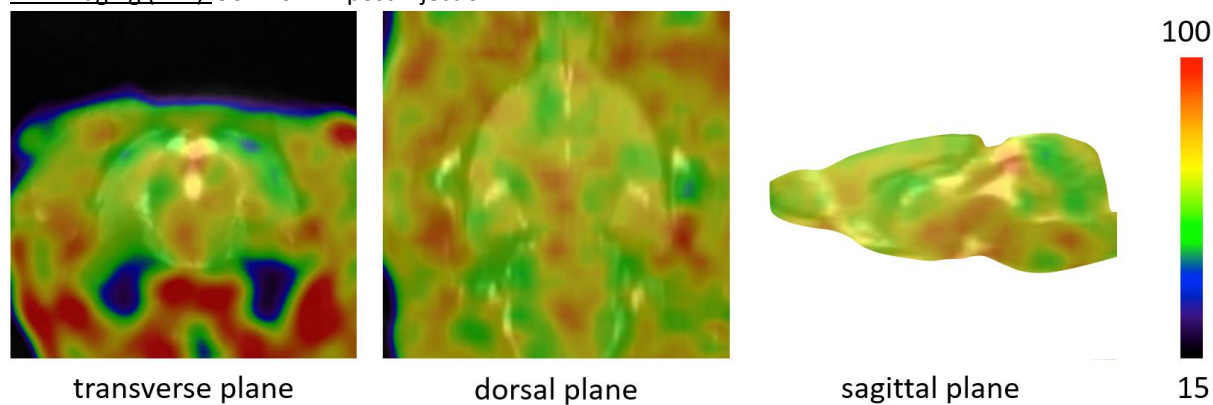


Figure 46.  $\alpha$ -Methyl-4- $^{18}\text{F}$ FPhe in healthy rats with/without benserazide..

### 11.2.8. 7- $^{18}\text{F}$ FTrp in Healthy Rats with Benserazide

PET imaging (n=1): 90-120 min post injection



Time activity curves (n = 3)

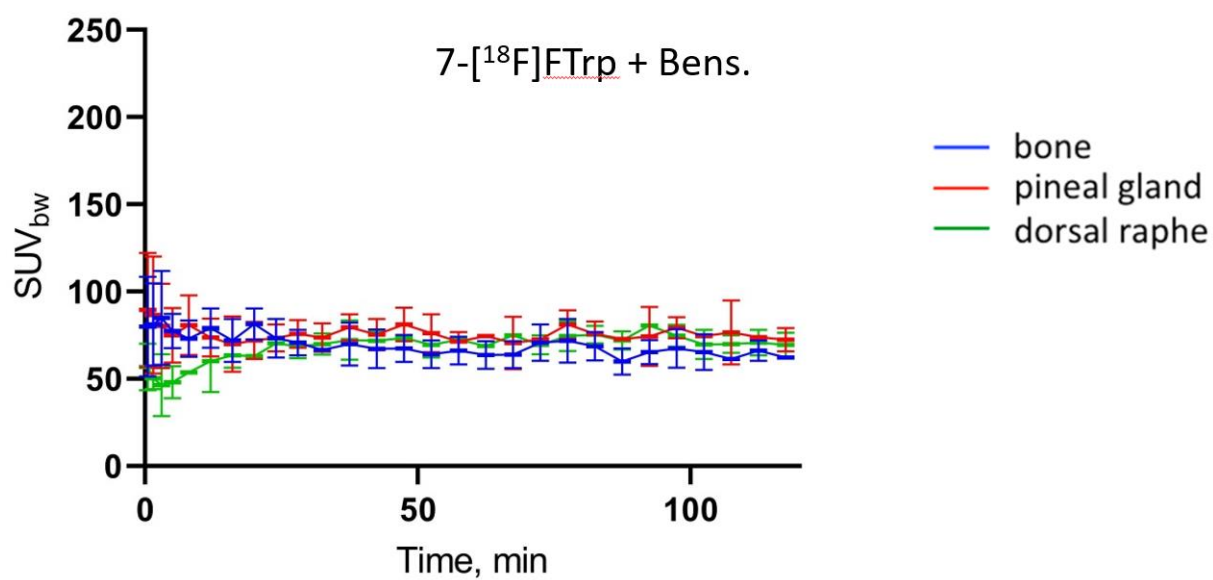
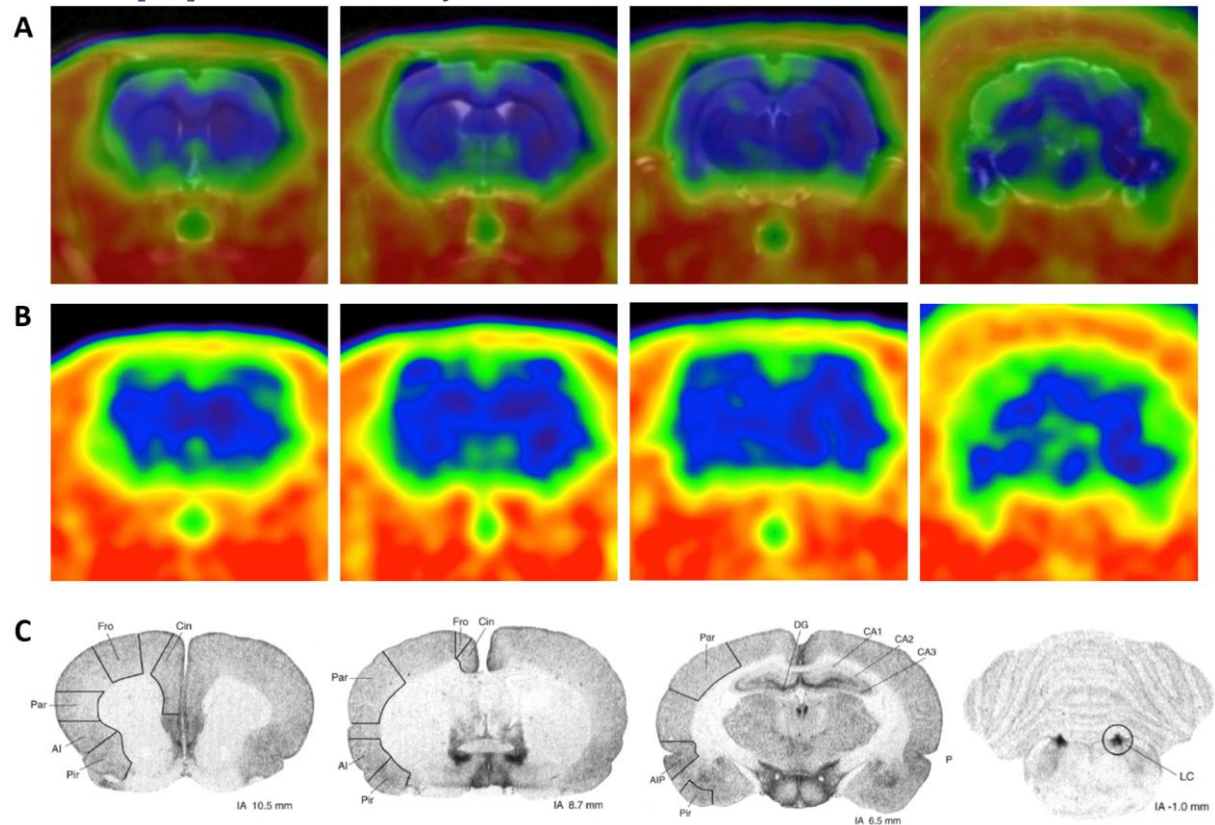


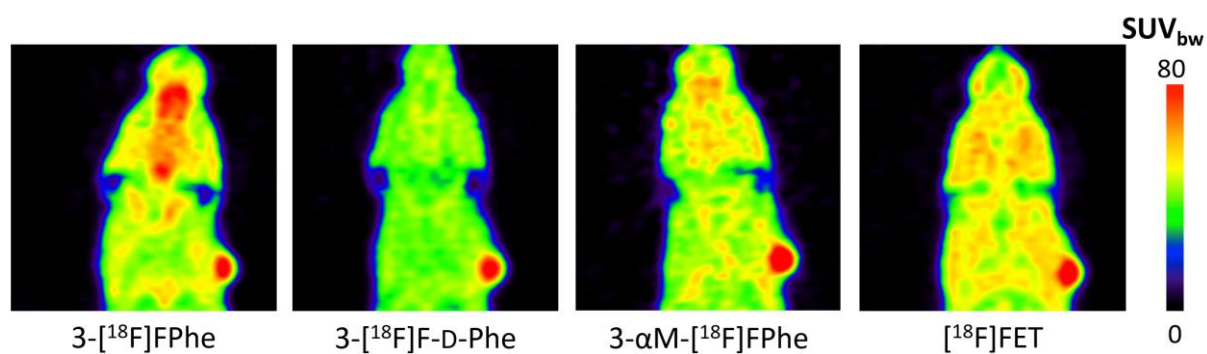
Figure 47. 7- $^{18}\text{F}$ FTrp in healthy rats with/without benserazide.

### 11.2.9. 3- $^{18}\text{F}$ FPheSer in Healthy Rats



### 11.2.10. Tumor Model Mice

#### MCF-7



#### PC-3

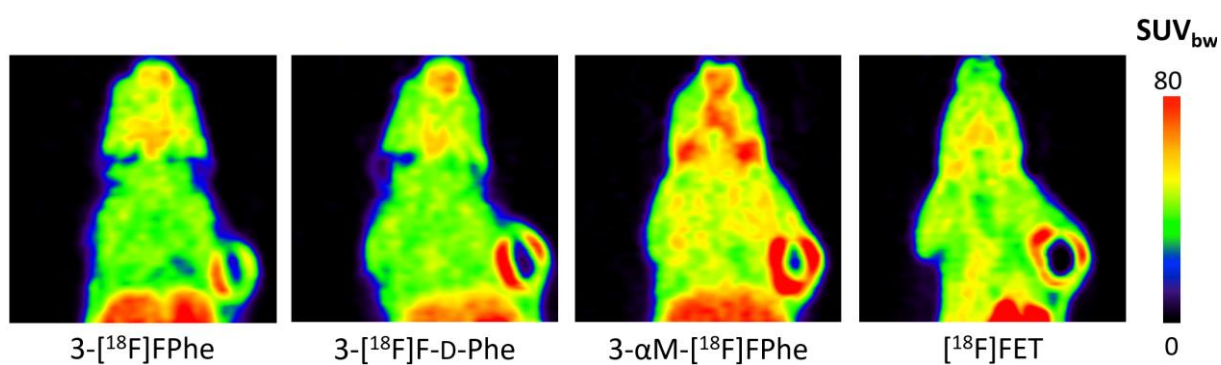
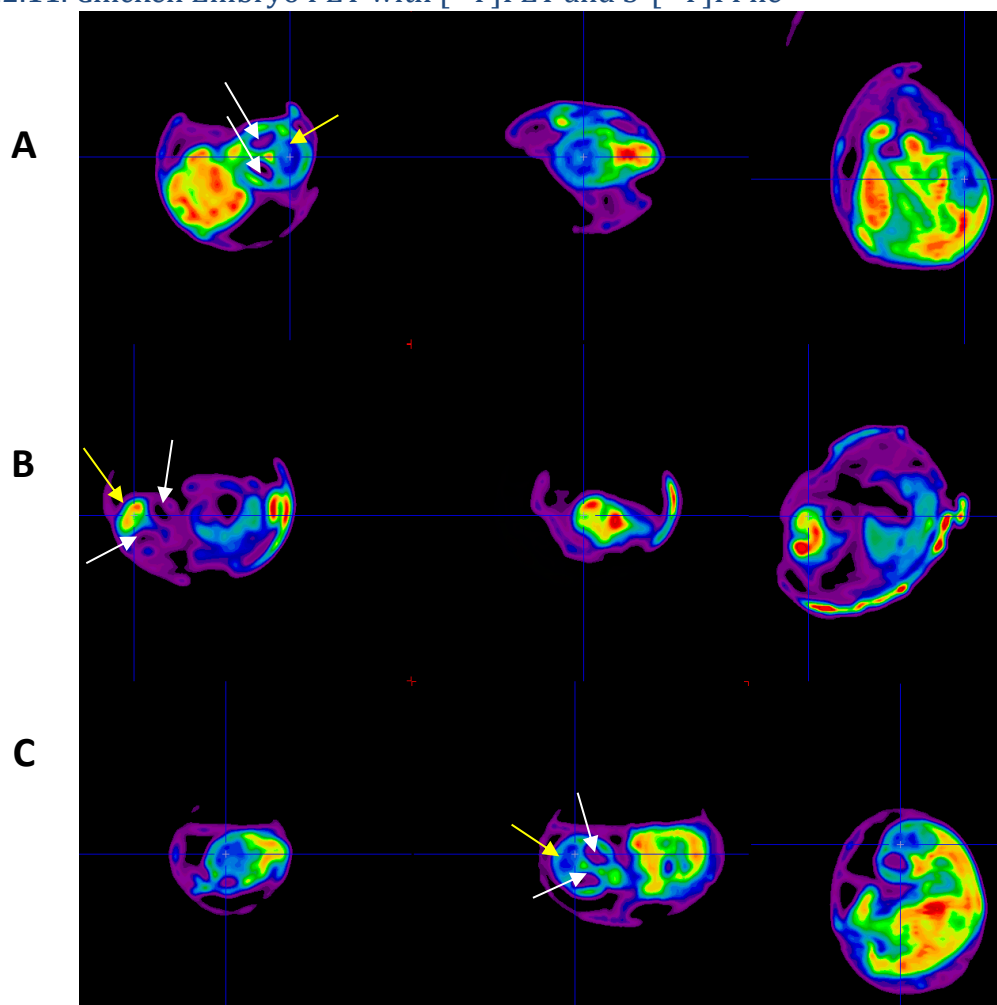
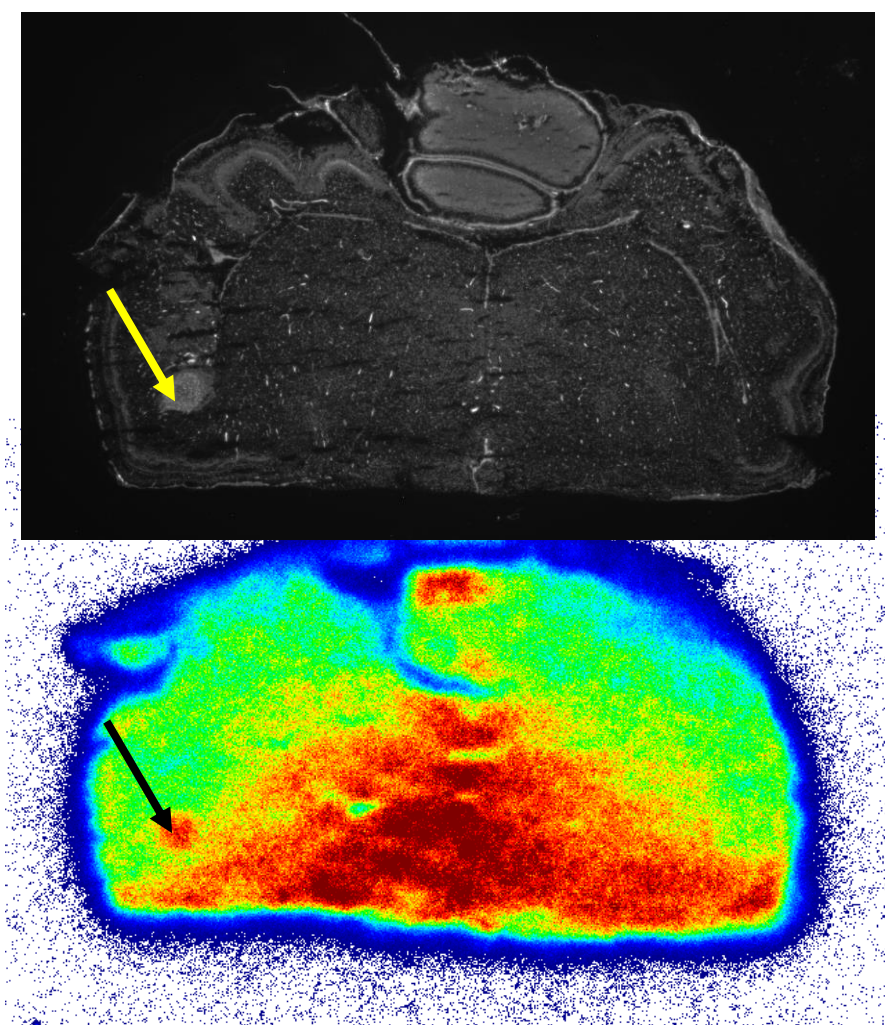


Figure 49.  $^{18}\text{F}$ -labeled AAAs in tumor model mice with/without Benseraazide.

### 11.2.11. Chicken Embryo PET with [ $^{18}\text{F}$ ]FET and 3- $^{18}\text{F}$ ]FPhe



*Figure 50. Chicken embryo PET experiments with [ $^{18}\text{F}$ ]FET (A, C) and 3- $^{18}\text{F}$ ]FPhe (B). The yellow arrows indicate the chicken embryo's brain, and the white arrows indicate the chicken embryo's eyes.*



*Figure 51. Chicken Embryo PET experiments showing 3- $^{18}\text{F}$ FPhe tracer uptake in the tumor.*

*Chicken embryo PET and MRI images courtesy of Mrs. Carina Stegmayr.*

## 12. Appendix

### Abbreviations

°C	Degrees Celsius
Å	Ångström
A	Adrenaline
AA	Amino acid
AAA	Aromatic amino acid
AAAH	Aromatic amino acid hydroxylase
AADC	Aromatic amino acid decarboxylase
Ac	Acetyl
AcOH	Acetic acid
AD	Alzheimer's disease
AIBN	Azobisisobutyronitrile
APT	Attached proton test
aq	Aqueous
A <sub>s</sub>	Specific activity
A <sub>m</sub>	Molar activity
BBB	Blood-brain barrier
Boc	<i>tert</i> -butoxy-carbonyl
Bn	Benzyl
BPB	<i>N</i> -Benzylproline benzophenone
Bpin	Boronic acid pinacol ester
B <sub>2</sub> pin <sub>2</sub>	Bis(pinacolato)diboron
BPX	( <i>S</i> )- <i>O</i> -[( <i>N</i> -benzylpropyl)amino]-phenone-derivative
Bq	Becquerel
Bu	Butyl
<i>c.a.</i>	Carrier added

Calcd	Calculated
cat	catalytic
cod	Cyclooctadiene
COMT	Catechol- <i>O</i> -methyltransferase
CT	Computed tomography
Cu-BPB	Cu-[(Benzylpropyl)amino]benzophenone
d	Days
DA	Dopamine
<i>de</i>	Diastereomeric excess
DIPEA	<i>N,N</i> -Diisopropylethylamine
DMA	Dimethylacetamide
DMAP	4-Dimethylaminopyridine
DMAPOTf	4-Dimethylaminopyridine-triflate
DMF	Dimethylformamide
DMSO	Dimethylsulfoxide
E	Energy
<i>ee</i>	enantiomeric excess
Eq	Equivalents
ESI	Electrospray ionization
Et	Ethyl
EtOH	Ethanol
EWG	Electron-withdrawing group
[ <sup>18</sup> F]FDG	2-[ <sup>18</sup> F]Fluoro-2-desoxy-D-glucose
[ <sup>18</sup> F]FDOPA	6-[ <sup>18</sup> F]Fluoro-3,4-dihydroxyphenylalanine
[ <sup>18</sup> F]FET	<i>O</i> -(2-[ <sup>18</sup> F]Fluoroethyl)-tyrosine
[ <sup>18</sup> F]FPBA	4-[ <sup>18</sup> F]fluorophenylboronic acid
2-FPhe	2-Fluorophenylalanine

2-[ <sup>18</sup> F]FPhe	2-[ <sup>18</sup> F]Fluorophenylalanine
4-FPhe	4-Fluorophenylalanine
4-[ <sup>18</sup> F]FPhe	4-[ <sup>18</sup> F]Fluorophenylalanine
Fig.	Figure
6-FMT	6-Fluoro - <i>meta</i> -tyrosine
6-[ <sup>18</sup> F]FMT	6-[ <sup>18</sup> F]Fluoro- <i>meta</i> -tyrosine
FTyr	2-Fluorotyrosine
FZJ	Forschungszentrum Jülich GmhH
g	Gram
GBq	Gigabecquerel
GC	Gas Chromatography
Gly	Glycine
h	Hour
HPLC	High-performance liquid chromatography
HTP	5-Hydroxytryptophan
hν	light
HVZ	Hell-Volhard-Zelinsky
Hz	Hertz
ICP-MS	Inductively coupled plasma mass spectrometry
INM	Institute for Nuclear Medicine
IR	Infrared
<i>J</i>	Coupling constant
K <sub>222</sub>	Kryptofix <sup>®</sup> 222
kJ	Kilojoules
L	Liter
LAT1	L-Amino acid transporter 1
LC	<i>Locus coeruleus</i>

LG	Leaving group
LOR	Line of response
<i>m</i> -	<i>meta</i> -
M	Molar
mAU	Milli-atomic units
MAO	Monoamine oxidase
max	Maximum
Me	Methyl
MeCN	Acetonitrile
MeOH	Methanol
Mes	Mesityl-
MeV	Mega electronvolt
mg	milligrams
min	Minutes
MOM	Methoxy- <i>O</i> -methyl
mol	Mole
MRI	Magnetic resonance imaging
MS	Mass spectroscopy
Ms	Mesylate
NA	Noradrenaline
NBS	<i>N</i> -bromosuccinimide
<i>n.c.a.</i>	No carrier-added
Ni-BPB	Ni-[(Benzylpropyl)amino]benzophenone
Ni-BPX	Ni-[(Benzylpropyl)amino]phenone-derivative
NMR	Nuclear magnetic resonance
<i>o</i> -	<i>ortho</i> -
<i>p</i> -	<i>para</i> -

PD	Parkinson's disease
Pd(dppf)Cl <sub>2</sub>	[1,1'-Bis(diphenylphosphino)ferrocene]dichloropalladium(II)
PET	Positron emission tomography
Ph	Phenyl
Phe	Phenylalanine
PG	Protecting group
pKa	Acid dissociation constant
ppm	Parts per million
Pr	Propyl
Ps	Positronium
py	Pyridine
RCC	Radiochemical conversion
RCP	Radiochemical purity
RCY	Radiochemical yield
R <sub>f</sub>	Relation to front
RP	Reversed-phase
rt	Room temperature
s	Seconds
sat.	Saturated
SMB	Suzuki-Miyaura borylation
SMC	Suzuki-Miyaura coupling
S <sub>N</sub> Ar	Nucleophilic aromatic substitution
sol.	Solution
SPE	Solid Phase Extraction
SPECT	Single photon emission computed tomography
t	Time
t <sub>1/2</sub>	Half life

TEA	Tetraethylammonium
<i>tert-</i>	<i>tertiary-</i>
Tf	Triflate
TFA	Trifluoroacetic acid
THF	Tetrahydrofuran
TLC	Thin layer chromatography
Trp	Tryptophan
Ts	Tosylate
UV	Ultraviolet
V	Volt
v	Volume

## 13. References

1. G. Hevesy, *Biochemical Journal*, **1923**, 17, 439–445.
2. Royal Society: Anniversary Address by Sir Robert Robinson, O.M., F.R.S", *Nature*, **1949**, 164 (4181), 1023–1030.
3. K. A. Herrmann, A. A. Kohan, M. C. Gaeta, C. Rubbert, J. L. Vercher-Conejero, R. M. Paspulati, B. Mansoori, P. F. Faulhaber, N. Avril, P. R. Ros, *Curr Radiol Rep*, **2013**, 1, 161–176.
4. C. D. Anderson, *Physical Review*, **1933**, 43 (6), 491–494.
5. The Nobel Prize in Physics, **1936**.
6. J. Shapiro, *Radiation Protection*, Harvard University Press, Cambridge MA, **1981**, 2.
7. D. L. Bailey, D. W. Townsend, P. E. Valk, M. N. Maisey, NJ: Springer-Verlag, **2005**.
8. M. Conti, L. Eriksson, *EJNMMI Phys.*, **2016**, 3 (1), 8.
9. S. M. Ametamey, M. Honer, P. A. Schubiger, *Chem. Rev.*, **2008**, 108, 1501–1516.
10. S. R. Banerjee, M. G. Pomper, *Appl. Radiat. Isot.*, **2013**, 76, 2–13.
11. E. O. Lawrence, *U.S. Patent* 1,948,384, **1934**.
12. Department of Energy - This media is available in the holdings of the National Archives and Records Administration, *cataloged under the National Archives Identifier* (NAID) 558593.
13. S. M. Qaim, J. C. Clark, C. Crouzel, M. Guilleme, H. J. Helmeke, B. Nebeling, V. W. Pike, G. Stocklin, *Radiopharmaceuticals for positron emission tomography – methodological aspects. Dordrecht: Springer Netherlands*, **1993**, 1–42.
14. J. Bergmann, O. Solin, *Nuclear Medicine and Biology*, **1997**, 24, 677–683.
15. T. Ido, C.-N. Wan, V. Casella, J. S. Fowler, A. P. Wolf, M. Reivich, D. E. Kuhl, *J. Label. Compounds Radiopharm.*, **1978**, 14, 171–183.
16. H. H. Coenen, *Ernst Schering Res. Found. Workshop*, **2007**, 64, 15–50.
17. H. Teare, E. G. Robins, E. Arstad, S. K. Luthra, V. Gouverneur, *Chem. Commun.*, **2007**, 2330–2332.
18. H. Teare, E. G. Robins, A. Kirjavainen, S. Forsback, G. Sandford, O. Solin, S. K. Luthra, V. Gouverneur, *Angew. Chem., Int. Ed. Engl.*, **2010**, 49, 6821–6824.
19. I. S. Stenhagen, A. K. Kirjavainen, S. J. Forsback, C. G. Jorgensen, E. G. Robins, S. K. Luthra, O. Solin, V. Gouverneur, *Chem. Commun.*, **2013**, 49, 1386–1388.
20. J.-H. Chun, V. W. Pike, *Chem. Commun.*, **2012**, 48, 9921–9923.
21. K. Hamacher, H. H. Coenen, G. Stocklin, *J. Nucl. Med.*, **1986**, 27 (2), 235–238.

22. K. Hamacher, H. H. Coenen, *Appl. Radiat. Isot.*, **2002**, 57, 853.
23. G. Balz, G. Schiemann, *Ber. Dtsch. Chem. Ges.*, **1927**, 60, 1186–1190.
24. A. Knochel, O. Zwernemann, *Appl. Radiat. Isot.*, **1991**, 42, 1077–1080.
25. O. Wallach, *Justus Liebigs Ann. Chem.*, **1886**, 235, 242–255.
26. C. Picherit, F. Wagner, D. Uguen, *Tetrahedron Lett.*, **2004**, 45, 2579–2583.
27. N. N. Ryzhikov, N. Seneca N, R. N. Krasikova, N. A. Gomzina, E. Shchukin, O. S. Fedorova, D. A. Vassiliev, B. Gulyás, H. Hall, I. Savic, C. Halldin, *Nucl. Med. Biol.* **2005**, 32 (2), 109–116.
28. B. H. Rotstein, L. Wang, R. Y. Liu, J. Patteson, E. E. Kwan, N. Vasdev, S. H. Liang, *Chem. Sci.*, **2016**, 7, 4407.
29. F. M. Wagner, J. Ermert, H. H. Coenen, *J. Nucl. Med.*, **2009**, 50, 1724.
30. J.-C. Meleán, J. Ermert, H. H. Coenen, *Org. Biomol. Chem.*, **2011**, 9 (3), 765–769.
31. P. S. Weiss, J. Ermert, J.-C. Meleán, D. Schäfer, H. H. Coenen, *Bioorganic & Medicinal Chemistry*, **2015**, 23 (17), 5856–5869,
32. J.-C. Meleán, S. Humpert, J. Ermert, H. H. Coenen, *Journal of Fluorine Chemistry*, **2015**, 178, 202–207.
33. Y.-S. Ding, F. Liang, J. S. Fowler, M. J. Kuhar, F. I. Carroll, *J. Label. Compd. Radiopharm.*, **1997**, 39, 827–832.
34. L. Mu, C. R. Fischer, J. P. Holland, J. Becaude, P. A. Schubiger, R. Schibli, S. M. Ametamey, K. Graham, T. Stellfeld, L. M. Dinkelborg, L. Lehmann, *Eur. J. Org. Chem.*, **2012**, 889–892.
35. V. W. Pike, F. I. Aigbirhio, *J. Chem. Soc., Chem. Commun.*, **1995**, 2215–2216.
36. F. Basuli, H. Wu, G. L. Griffiths, *J. Labelled Compd. Radiopharm.*, **2011**, 54, 224–228.
37. B. C. Lee, K. C. Lee, H. Lee, R. H. Mach, J. A. Katzenellenbogen, *Bioconjugate Chem.*, **2007**, 18, 514–523.
38. M. Tredwell, V. Gouverneur, *Angew. Chem., Int. Ed. Engl.*, **2012**, 51, 11426–11437.
39. T. L. Ross, J. Ermert, C. Hocke, H. H. Coenen, *J. Am. Chem. Soc.*, **2007**, 129, 8018–8025.
40. R. Gail, C. Hocke, H. H. Coenen, *J. Labelled Compd. Radiopharm.*, **1997**, 40, 50–52.
41. K. M. Lancer, G. H. Wiegand, *Journal of Organic Chemistry*, **1976**, 41 (21), 3360–3364.
42. W.-J. Kuik, I. P. Kema, A. H. Brouwers, R. Zijlma, K. D. Neumann, R. A. J. O. Dierckx, S. G. DiMaggio, P. H. Elsinga, *J. Nucl. Med.*, **2015**, 56 (1), 106.
43. R. Richarz, P. Krapf, F. Zarrad, E. A. Urusova, B. Neumaier, B. D. Zlatopolskiy, *Organic & Biomolecular Chemistry*, **2014**, 12, 8094–8099.

44. E. Lee, A. S. Kamlet, D. C. Powers, C. N. Neumann, G. B. Boursalian, T. Furuya, D. C. Choi, J. M. Hooker, T. Ritter, *Science*, **2011**, 334, 639–642.
45. E. Lee, J. M. Hooker, T. Ritter, *J. Am. Chem. Soc.*, **2012**, 134, 17456–17458.
46. J. Zischler, N. Kolks, D. Modemann, B. Neumaier, B. D. Zlatopolskiy, *Chem. Eur.*, **2017**, 23, 3251–3256.
47. A. V. Mossine, A. F. Brooks, V. Bernard-Gauthier, J. J. Bailey, N. Ichiishi, R. Schirmacher, M. Sanford, P. J. H. Scott, *J. Label. Compd. Radiopharm.*, **2018**, 61, 228–36.
48. B. D. Zlatopolskiy, J. Zischler, E. A. Urusova, H. Endepols, E. Kordys, H. Frauendorf, F. M. Mottaghy, B. Neumaier, *ChemistryOpen*, **2015**, 4, 457.
49. N. Ichiishi, A. F. Brooks, J. J. Topczewski, M. E. Rodnick, M. S. Sanford, P. J. H. Scott, *Organic Letters*, **2014**, 16, 3224–3227.
50. M. Tredwell, S. M. Preshlock, N. J. Taylor, S. Gruber, M. Huiban, J. Passchier, J. Mercier, C. Génicot, V. Gouverneur, *Angewandte Chemie International Edition*, **2014**, 53, 7751–7755.
51. A. V. Mossine, A. F. Brooks, K. J. Makaravage, J. M. Miller, N. Ichiishi, M. S. Sanford, P. J. H. Scott, *Org. Lett.*, **2015**, 17, 5780–5783.
52. K. J. Makaravage, A. F. Brooks, A. V. Mossine, M. S. Sanford, P. J. H. Scott, *Organic Letters*, **2016**, 18 (20), 5440–5443.
53. S. J. Lee, K. J. Makaravage, A. F. Brooks, P. J. H. Scott, and M. S. Sanford, *Angew. Chem. Int. Ed.*, **2019**, 58, 3119.
54. L. S. Sharninghausen, A. F. Brooks, W. P. Winton, K. J. Makaravage, P. J. H. Scott, M. S. Sanford, *Journal of the American Chemical Society*, **2020**, 142 (16), 7362–7367.
55. B. D. Zlatopolskiy, J. Zischler, P. Krapf, F. Zarrad, E. A. Urusova, E. Kordys, H. Endepols, B. Neumaier, *Chem. Eur. J.*, **2015**, 21, 5972–5979.
56. B. D. Zlatopolskiy, J. Zischler, D. Schäfer, E. A. Urusova, M. Guliyev, O. Bannykh, H. Endepols, B. Neumaier, *Journal of Medicinal Chemistry*, **2018** 61 (1), 189–206.
57. F. Zarrad, B. D. Zlatopolskiy, P. Krapf, J. Zischler, B. Neumaier, *Molecules*, **2017**, 22 (12), 2231.
58. D. J. Modemann, B. D. Zlatopolskiy, E. A. Urusova, J. Zischler, A. Craig, J. Ermert, M. Guliyev, H. Endepols, B. Neumaier, *Synthesis*, **2019**, 51 (03), 664–676.
59. V. V. Orlovskaya, D. J. Modemann, O. F. Kuznetsova, O. S. Fedorova, E. A. Urusova, N. Kolks, B. Neumaier, R. N. Krasikova, B. D. Zlatopolskiy, *Molecules*, **2019**, 24 (17), 3197.

60. D. Antuganov, M. Zykov, K. Timofeeva, Y. Antuganova, V. Orlovskaya, R. Krasikova, *ChemistrySelect*, **2017**, 2, 7909.
61. D. Antuganov, M. Zykov, V. Timofeev, K. Timofeeva, Y. Antuganova, V. Orlovskaya, O. Fedorova, R. Krasikova, *Eur. J. Org. Chem.*, **2019**, 918–922.
62. R. Schirmacher, B. Wängler, J. Bailey, V. Bernard-Gauthier, E. Schirmacher, C. Wängler, *Seminars in Nuclear Medicine*, **2017**, 47 (5), 474–492,
63. D. Y. Chi, M. R. Kilbourn, J. A. Katzenellenbogen, J. W. Brodack, M. J. Welch, *Int. J. Rad. Appl. Instrum. A.*, **1986**, 37 (12), 1173–1180.
64. J. Marik, J. L. Sutcliffe, *Tetrahedron Lett.*, **2006**, 47 (37), 6681–6684.
65. H. C. Kolb, M. G. Finn, K. B. Sharpless, *Angew Chem Int Ed Engl.*, **2001**, 40 (11), 2004–2021.
66. C. Wängler, R. Schirmacher, P. Bartenstein, B. Wängler, *Curr. Med. Chem.*, **2010**, 17 (11), 1092–1116.
67. B. D. Zlatopolskiy, R. Kandler, F. M. Mottaghy, B. Neumaier, *Appl Radiat Isot.* **2012**, 70 (1), 184–92.
68. B. D. Zlatopolskiy, P. Krapf, R. Richarz, H. Frauendorf, F. M. Mottaghy, B. Neumaier, *Chem. Eur. J.*, **2014**, 20, 4697–4703.
69. Z. Gao, V. Gouverneur, B. G. Davis, *Journal of the American Chemical Society*, **2013**, 135 (37), 13612–13615.
70. A. B. Housh, M. S. Matthes, A. Gerheart, S. L. Wilder, K.-E Kil, M. Schueller, J. M. Guthrie, P. McSteen, R. Ferrieri, *Int. J. Mol. Sci.*, **2020**, 21, 976.
71. A. Strecker, *Ann. Chem. Pharm.* **1850**, 75, 27–45.
72. W. C. Tobie, G. B. Ayres, *Journal of the American Chemical Society*, **1937**, 59 (5), 950.
73. C. M. von Hell, *Berichte*, **1881**, 14, 891–893.
74. J. Volhard, *Annalen der Chemie*, **1887**, 242, 1–2, 141–163.
75. N. Zelinsky, *Berichte*, **1887**, 20, 2026.
76. Y. N. Belokon, V. I. Bakmutov, N. I. Chernoglazova, K. A. Kochetkov, S. V. Vitt, N. S. Garbalinskaya, V. M. Belikov, *J. Chem. Soc., Perkin Trans. I*, **1988**, 305–312.
77. Y. N. Belokon, A. G. Bulychev, S. V. Vitt, Y. T. Struchkov, A. S. Batsanov, T. V. Timofeeva, V. A. Tsiryapkin, M. G. Ryzhov, L. A. Lysova, *J. Am. Chem. Soc.*, **1985**, 107, 4252–4259.
78. D. J. Smith, G. P. Yap, J. A. Kelley, J. P. Schneider, *J. Org. Chem.*, **2011**, 76 (6), 1513–1520.

79. T. Li, S. Zhou, J. Wang, J. L. Acena, V. A. Soloshonok, H. Liu, *Chem. Commun.*, **2015**, 51, 1624–1626.
80. V. A. Larionov, T. F. Savel'yeva, M. G. Medvedev, N. V. Stoletova, A. F. Smol'yakov, Z. T. Gugkaeva, T. Cruchter, V. I. Maleev, *Eur. J. Org. Chem.*, **2019**: 3699–3703.
81. R. N. Krasikova, O. F. Kuznetsova, O. S. Fedorova, V. I. Maleev, T. F. Saveleva, Y. N. Belokon, *Bioorganic & Medicinal Chemistry*, **2008**, 16(9), 4994–5003.
82. R. N. Krasikova, O. S. Fedorova, O. F. Kuznetsova, I. K. Mosevich, V. I. Maleev, Y. N. Belokon, *Eur. J. Nucl. Med. Molec. Imaging.*, **2004**, 31, 381.
83. R. N. Krasikova, Y. N. Belokon, *unpublished results*.
84. E. Marcos, B. Basanta, T. M. Chidyausiku, Y. Tang, G. Oberdorfer, G. Liu, G. V. T. Swapna, R. Guan, D.-A. Silva, J. Dou, J. H. Pereira, R. Xiao, B. Sankaran, P. H. Zwart, G. T. Montelione, D. Baker, *Science*, **2017**, 355, 201–206.
85. K. J. Broadley, *Pharmacol Ther.*, **2010**, 125(3), 363–75.
86. L. Lindemann, M. C. Hoener, *Trends Pharmacol. Sci.*, **2005**, 26 (5), 274–281.
87. R. Daneman, A. Prat, *Cold Spring Harbor Perspectives in Biology*, **2015**, 7(1), a020412.
88. R. E. Yee, D. W. Cheng, S. C. Huang, M. Namavari, N. Satyamurthy, J. R. Barrio, *Biochem Pharmacol.*, **2001**, 15, 62(10), 1409–15.
89. H. Shen, K. Kannari, H. Yamato, A. Arai, M. Matsunaga, *The Tohoku journal of experimental medicine*, **2003**, 199 (3), 149–59.
90. R. M. Weinshilboum, D. M. Otterness, C. L. Szumlanski, *Ann Rev Pharmacol Toxicol.*, **1999**, 39, 19–52.
91. B. T. Zhu, A. H. Conney, *Carcinogenesis*, **1998**, 19, 1–27.
92. C. Worda, M. O. Sator, C. Schneeberger, T. Jantschev, K. Ferlitsch, J. C. Huber, *Hum. Reproduct.*, **2003**, 18 (2), 262–266.
93. A. J. Shield, B. A. Thomae, B. W. Eckloff, E. D. Wieben, R. M. Weinshilboum, *Mol. Psychiatry*, **2004**, 9 (2), 151–160.
94. M. B. M. van Duursen, J. T. Sanderson, P. C. de Jong, M. Kraaij, M. van der Berg, *Toxicol Sci.*, **2004**, 81, 316–324.
95. C. Zarow, S. A. Lyness, J. A. Mortimer, H. C. Chui, *Arch. Neurol.*, **2003**, 60, 337–341.
96. H. Braak, K. Del Tredici, *Acta Neuropathol.*, **2011**, 121, 171–181.
97. M. Iba, J. D. McBride, J. L. Guo, B. Zhang, J. Q. Trojanowski, V. M.-Y. Lee, *Acta Neuropathol.*, **2015**, 130, 349–362.
98. F. R. López-Picón, A. K. Kirjavainen, S. Forsback, J. S. Takkinen, D. Peters, M. Haaparanta-Solin, and O. Solin, *Theranostics*, **2019**, 9, 1.

99. M. Dunn, A. Henkel, S. Clark, Y. Kovalyova, K. A. Kempadoo, R. J. Karpowicz Jr., E. R. Kandel, D. Sulzer, and D. Sames, *Nat. Commun.*, **2018**, 9, 2838.
100. Y. S. Ding, K. S. Lin, J. Logan, H. Benveniste, P. Carter, *J. Neurochem.*, **2005**, 94, 337–351.
101. Y. S. Ding, K. S. Lin, J. Logan, *Curr Pharm Des.*, **2006**, 12, 3831–3845.
102. J. D. Gallezot, D. Weinzimmer, N. Nabulsi, S.-F. Lin, K. Fowles, C. Sandiego, T. J. McCarthy, R. P. Maguire, R. E. Carson, Y.-S. Ding, *Neuroimage*, **2011**, 56, 268–279.
103. M. Schou, C. Halldin, V. W. Pike, P. D. Mozley, D. Dobson, R. B. Innis, L. Farde, Håkan Hall, *European Neuropsychopharmacology*, **2005**, 15 (5), 517–520.
104. N. Seneca, B. Gulyas, A. Varrone, M. Schou, A. Airaksinen, J. Tauscher, F. Vandenhende, W. Kielbasa, L. Farde, R. B. Innis, C. Halldin, *Psychopharmacology (Berl.)*, **2006**, 188, 119–127.
105. F. Zeng, J. Mun, N. Jarkas, J. S. Stehouwer, R. J. Voll, G. D. Tamagnan, L. Howell, J. R. Votaw, C. D. Kilts, C. B. Nemeroff, M. M. Goodman, *J. Med. Chem.*, **2009**, 52, 62–73.
106. "Tumor Types". *National Brain Tumor Society*. Retrieved 2019-06-28.
107. A. M. Najjar, J. M. Johnson, D. Schellingerhout, *Bioengineering*, **2018**, 5, 104.
108. Z. Fleischmann, D. Unterrainer, M. Bartenstein, P. Belka, C. Albert, M. Niyazi, *Journal of Neuro-Oncology*, **2017**, 132 (2), 277–286.
109. S. Sveinbjornsdottir, *Journal of Neurochemistry*, **2016**, 139 (1), 318–324.
110. L. V. Kalia, A. E. Lang, *Lancet.*, **2015**, 386 (9996), 896–912.
111. K. A. Jellinger, *Acta Neuropathologica.*, **2007**, 114 (3), 299–303.
112. Disease Injury Incidence Prevalence Collaborators, *Lancet.*, **2016**, 388 (10053), 1545–1602.
113. L. M. de Lau, M. M. Breteler, *Lancet Neurol.*, **2006**, 5, 525–535.
114. C. E. Leyton, L. I. Golbe, *Neurology*, **2018**, 91 (22), 991–992.
115. <https://clipground.com/nereis-diversicolor-clipart.html> (Accessed 23/10/19, 17.44)
116. M. A. Berliner, K. Belecki, *J. Org. Chem.* **2005**, 70, 23, 9618.
117. E. K. M. Zangana, Synthesis of Amino Acids from Chiral NiII Schiff Base Complexes for Novel Stapled Peptides, *PhD thesis*, University of Leicester, **2019**, 199.
118. T. W. Green, P. G. M. Wuts, *Protective Groups in Organic Synthesis*, Wiley-Interscience, New York, **1999**, 27–33, 708–711.
119. J. M. Keith, *Tetrahedron Letters*, **2004**, 45, 13, 2739–2742.
120. H. C. Chien, C. Colas, K. Finke, S. Springer, L. Stoner, A. A. Zur, B. Venteicher, J. Campbell, C. Hall, A. Flint, E. Augustyn, C. Hernandez, N. Heeren, L. Hansen, A.

- Anthony, J. Bauer, D. Fotiadis, A. Schlessinger, K. M. Giacomini, A. A. Thomas, *J. Med. Chem.*, **2018**, 23, 61 (16), 7358–7373.
121. A. S. Saghiyan, S. A. Dadayan, S. G. Petrosyan, L. L. Manasyan, A. V. Geolchanyan, S. M. Djamgaryan, S. A. Andreasyan, V. I. Maleev, V. N. Khrustalev, *Tetrahedron: Asymmetry*, **2006**, 17 (3), 455–467.
122. E. Flöistrup, P. Goede, R. Strömberg, J. Malm, *Tetrahedron Letters*, **2011**, 52 (2), 209–211,
123. N. Kolks, *Master thesis*, University of Cologne, **2019**.
124. SmithKline Beecham p.l.c.US6048852, **2000**, A.
125. H. H. Coenen, A.D. Gee, M. Adam, G. Antoni, C. S. Cutler, Y. Fujibayashi, J. M. Jeong, R. H. Mach., T. L. Mindt, V. W. Pike, A. D. Windhorst, Consensus nomenclature rules for radiopharmaceutical chemistry – setting the record straight, *U.S. Department of Energy*, **2017**.

## 14. Declaration

Hiermit versichere ich an Eides statt, dass ich die vorliegende Dissertation selbstständig und ohne die Benutzung anderer als der angegebenen Hilfsmittel und Literatur angefertigt habe. Alle Stellen, die wörtlich oder sinngemäß aus veröffentlichten und nicht veröffentlichten Werken dem Wortlaut oder dem Sinn nach entnommen wurden, sind als solche kenntlich gemacht. Ich versichere an Eides statt, dass diese Dissertation noch keiner anderen Fakultät oder Universität zur Prüfung vorgelegen hat; dass sie - abgesehen von unten angegebenen Teilpublikationen und eingebundenen Artikeln und Manuskripten - noch nicht veröffentlicht worden ist sowie, dass ich eine Veröffentlichung der Dissertation vor Abschluss der Promotion nicht ohne Genehmigung des Promotionsausschusses vornehmen werde. Die Bestimmungen dieser Ordnung sind mir bekannt. Darüber hinaus erkläre ich hiermit, dass ich die Ordnung zur Sicherung guter wissenschaftlicher Praxis und zum Umgang mit wissenschaftlichem Fehlverhalten der Universität zu Köln gelesen und sie bei der Durchführung der Dissertation zugrundeliegenden Arbeiten und der schriftlich verfassten Dissertation beachtet habe und verpflichte mich hiermit, die dort genannten Vorgaben bei allen wissenschaftlichen Tätigkeiten zu beachten und umzusetzen. Ich versichere, dass die eingereichte elektronische Fassung der eingereichten Druckfassung vollständig entspricht.

Teilpublikationen:

1. Preparation of Labeled Aromatic Amino Acids via Late-Stage  $^{18}\text{F}$ -Fluorination of Chiral Nickel and Copper Complexes, A. Craig, N. Kolks, E. A. Urusova, J. Zischler, M. Brugger, H. Endepols, B. Neumaier, B. D. Zlatopolskiy, *Chemical Communications*, **2020**, 56, 9505–9508.
2. The Efficient Preparation of Aromatic Amino Acids via Cu-Mediated radiofluorination of Ni- and Cu-complexes, A. Craig, N. Kolks, E. Urusova, B. D. Zlatopolskiy, B. Neumaier, *Nuklearmedizin*, **2019**, 58 (2) (Conference paper).
3. 2- $^{18}\text{F}$ Fluorophenylalanine: Synthesis by Nucleophilic  $^{18}\text{F}$ -Fluorination and Preliminary Biological Evaluation, D. J. Modemann, B. D. Zlatopolskiy, E. A. Urusova, J. Zischler, A. Craig, J. Ermert, M. Guliyev, H. Endepols, B. Neumaier, *Synthesis*, **2019**, 51 (03), 664–676.

Datum, Name und Unterschrift



08.02.2021, Austin Craig

## 15. Curriculum Vitae

### Personal Details

Name: Austin Craig

Date of birth: 15.08.1991

Nationalities: Irish & American

### Employment History

10.2020 – present	<b>Postdoctoral Researcher</b> Helmholtz Center Dresden-Rossendorf (HZDR), Dresden, Germany
05.2020 – 09.2020	<b>CMC Manager</b> PentixaPharm GmbH, Berlin, Germany
08.2017 – 04.2020	<b>Radiochemist</b> Jülich Research Centre, Jülich, Germany
01.2017 – 04.2020	<b>Radiochemist</b> University Clinic Cologne, Cologne, Germany
04.2019	<b>Radiochemist</b> University of Michigan, Michigan, USA
10.2018	<b>Radiochemist</b> Russian Academy of Sciences, St. Petersburg, Russian Federation
01.2017 – 05.2018	<b>Organic Chemist</b> Max-Planck Institute for Metabolism Research, Cologne, Germany
10.2016 – 12.2016	<b>Inorganic Chemist</b> Trinity College Dublin, Dublin, Ireland
01.2016 – 08.2016	<b>Science Teacher</b> Sogang Language Program (SLP), Pyeongtaek, South Korea
01.2015 – 10.2015	<b>Trainees Officer &amp; Local Committee Member</b> International Association for the Exchange of Students for Technical Experience (IAESTE), Dublin, Ireland
05.2014 – 01.2015	<b>Research &amp; Development - Polymer Chemist</b> Dynea AS, Lillestrøm, Norway
10.2009 – 05.2014	<b>Infantry Soldier</b> Defence Forces Ireland, Dublin, Ireland
06.2013 – 08.2013	<b>Organic Chemist</b> Institute of Organic Chemistry and Biochemistry (IOCB), Prague, Czechia

### Education

01.2017 – 07.2020	<b>Doctorate Nuclear Chemistry</b> University of Cologne, Cologne, Germany
09.2015 – 09.2016	<b>Masters in Chemistry</b> National University of Ireland, Galway, Ireland
01.2013 – 06.2013	<b>Bachelor of Science (Honours) Medicinal Chemistry &amp; Chemical Biology</b> University College Dublin, Ireland & University of California, Los Angeles, USA

## **Publications**

1. A. Craig, N. Kolks, E. A. Urusova, J. Zischler, M. Brugger, H. Endepols, B. Neumaier, B. D. Zlatopolskiy, *Chemical Communications*, **2020**, 56, 9505–9508.
2. D. Conboy, S. Mirallai, A. Craig, P. McArdle, A. A. Al-Kinani, S. Barton, F. Aldabbagh, *J. Org. Chem.*, **2019**, (15), 9811–9818.
3. A. Craig, N. Kolks, E. Urusova, B. D. Zlatopolskiy, B. Neumaier, *Nuklearmedizin*, **2019**, 58(2) (Conference paper).
4. D. J. Modemann, B. D. Zlatopolskiy, E. A. Urusova, J. Zischler, A. Craig, J. Ermert, M. Guliyev, H. Endepols, B. Neumaier, *Synthesis*, **2019**, 51 (03), 664–676.

## **Conference Oral Presentations**

- 2019 International Society of Radiopharmaceutical Sciences (ISRS), Beijing, China Deutsche Gesellschaft für Nuklearmedizin (DGN), Bremen, Germany
- 2018 Jahrestagung Arbeitsgemeinschaft Radiochemie & Radiopharmazie (AGRR), Aachen, Germany Institut für Nuklearchemie (INM-5) Retreat, Jülich, Germany
- 2017 European Association for Nuclear Medicine (EANM), Vienna, Austria

## **Awards**

- 2019 Collaborative Research Internship (DAAD) stipend
- 2018 German Academic Exchange Service (DAAD) IPaK Travel Funding Grant  
Poster Presentation Prize - University of Cologne Chemistry Graduate School
- 2017 DFG funded Ph.D. studentship – Deutsche Forschungsgemeinschaft (DFG)
- 2016 Gold Medal for MSc. Chemistry highest grade- National University of Ireland, Galway
- 2014 IAESTE funded Traineeship with Dynea AS Award
- 2013 IAESTE Trainee of the Year Award (Third Prize)  
IAESTE funded Traineeship with the Institute of Organic Chemistry & Biochemistry  
University of California Exchange Abroad Program (UCEAP) Scholarship
- 2010 Galileo Thermometer Award (Science Student of the Year) - St. Conleth's College